Universidad de Concepción
Dirección de Postgrado
Facultad de Ciencias Naturales y Oceanográficas-Programa de Doctorado en Oceanografía

Dinámica de procesos y factores físico-biológicos en la zona sur del Sistema de Corrientes de Humboldt: un enfoque basado en modelación

Tesis para optar al grado de Doctor en Oceanografía

ODETTE ALEJANDRA VERGARA SOTO

CONCEPCIÓN-CHILE 2018

Profesor guía: Renato Quiñones Bergeret
Departamento de Oceanografía
Facultad de Ciencias Naturales y Oceanográficas
Universidad de Concepción

Universidad de Concepción

Dirección de Postgrado

La Tesis de Doctorado en Oceanografía titulada "Dinámica de procesos y factores físico-biológicos en la zona sur del Sistema de Corrientes de Humboldt: un enfoque basado en modelación", de la Srta. Odette Vergara Soto y realizada bajo la Facultad de Ciencias Naturales y Oceanográficas, Universidad de Concepción, ha sido aprobada por la siguiente Comisión de Evaluación:

Dr. Renato A. Quiñones
Profesor Guía
Departamento de Oceanografía
Universidad de Concepción _____

Dr. Vincent Echevin
Miembro Comité de Tesis
LOCEAN
Universidad Pierre et Marie Curie, Paris _____

Dr. Héctor Hito Sepúlveda
Miembro Comité de Tesis
Departamento de Geofísica
Universidad de Concepción _____

Dr. Marcus Sobarzo
Miembro Comité de Tesis
Departamento de Oceanografía
Universidad de Concepción _____

Dra. Beatriz Yannicelli
Miembro Comité de Tesis
Centro de Estudios Avanzados de Zonas Áridas _____

Dr. José Luis Iriarte M.
Evaluador externo
Centro IDEAL
Universidad Austral de Chile _____

Dr. Rubén Escribano
Director Programa de Doctorado en Oceanografía
Departamento de Oceanografía
Universidad de Concepción _____

Dedicada a Samuel y al bello hogar que hemos formado

AGRADECIMIENTOS

El desarrollo de esta Tesis Doctoral fue posible gracias al financiamiento del Centro Interdisciplinario para la Investigación Acuícola (INCAR; proyecto FONDAP Nº15110027; CONICYT), el Programa de Investigación Marina de Excelencia (PIMEX) de la Facultad de Ciencias Naturales y Oceanográficas de la Universidad de Concepción, este último financiado por Celulosa Arauco y Constitución S.A. y la Red Doctoral en Ciencia, Tecnología y Ambiente (REDOC.CTA), el cual es un Convenio de Desempeño de MINEDUC, adjudicado por la Universidad de Concepción.

Mi manutención, así como el financiamiento de los gastos de matrícula, fueron posibles gracias a la Beca Doctoral del Programa de Formación de Capital Humano Avanzado de CONICYT y a la Escuela de Postgrado de la Universidad de Concepción.

Quisiera comenzar agradeciendo de manera especial al Dr. Renato Quiñones Bergeret por su excepcional dirección académica, por el incondicional apoyo profesional y por contribuir con gran dedicación al desarrollo de esta Tesis Doctoral. Sus innovadoras ideas, su forma de hacer ciencia y su temple para enfrentar la vida, han contribuido sin dudar a mi formación académica y personal.

También agradezco al Dr. Vincent Echevín por apoyarme incondicionalmente en el desarrollo de la metodología de esta Tesis, por su tiempo dedicado y por las veces en las que me recibió en LOCEAN, oportunidades que me permitieron llegar a esta etapa de finalización.

Quisiera agradecer al Dr. Héctor H. Sepúlveda, miembro del comité de esta Tesis por sus importantes aportes para el desarrollo de los artículos publicados en los capítulos 2 y 3 de esta Tesis y por otorgarme un lugar en su oficina por tiempo ilimitado. También agradezco al Dr. Marcus Sobarzo por sus fundamentales contribuciones en el desarrollo de una parte importante de este trabajo, quiero destacar especialmente su gran calidad humana, su paciencia y filosofía de vida, las cuales me han inspirado en el camino a seguir, no solo como científica, sino como ser humano, infinitas gracias por eso. Agradezco a la Dra. Beatriz Yaniccelli por recibirme en su laboratorio en el centro de

Estudios de Zonas Áridas (CEAZA) y por su gran voluntad al momento de requerir su apoyo académico.

Quiero reconocer de forma especial a mi exgrupo de trabajo PLAMZ (Pelagic Laboratory and Mesozooplankton). El tiempo en cual trabajé junto a ellos en la Estación de Biología Marina de Dichato, me inspiró para continuar en el camino de la ciencia es por eso que no puedo dejar de mencionar al Dr. Rubén Escribano por apoyarme para ingresar al Doctorado, a Marcelo Fuentes, a Anahí Jorquera, a Katty Donoso, a Claudia Pérez, a Paula Mendoza, a Valentina Valdés y a Pamela Hidalgo, por haber sido parte de este gran equipo.

Deseo expresar mi más sentida gratitud a la secretaria del Programa de Postgrado en Oceanografía, Fabiola Gaete, quien siempre estuvo dispuesta a ayudarme. También de manera muy especial quiero agradecer a la secretaria de INCAR, la Srta. Susana Llanca por su gran apoyo, confianza y profesionalismo, siempre dispuesta a colaborar.

Agradezco infinitamente a mi familia por la contención en este proceso de investigación, gracias a mi compañero de vida Samuel Soto, a mis padres Aurelio Vergara y María Raquel Soto, a mi hermano Marco Antonio y a Valentina. No puedo dejar de mencionar a mi sobrino Joel Herrera por su gran amistad, a mis suegros, cuñados y a mi segunda madre Guillermina, por estar siempre presentes con su incondicional cariño.
A mis amigos, Priscila, Karina, Marcelo, Karen, Javiera, Fabiola, Juan José, Juan, Carlos, Gabriela, Bárbara y Gisela, por participar de esta etapa de mi vida animándome constantemente a continuar este proceso.

Finalmente doy las gracias a mis compañeros de generación del Programa de Postgrado por la ayuda otorgada y por la amistad formada; gracias Marcelo Fuentes, Dernis Mediavilla, Susannah Buchan, Francisca Bown, Montserrat Aldunate, Leslie Abarzúa y Paulina Vásquez.

CURRICULUM VITAE

Odette A. Vergara Soto

Nacida el 20 de marzo de 1980, en Curanilahue, Chile.

2000-2005: Licenciatura en Biología Marina, Universidad de Concepción, Chile.
2006 : Bióloga Marina, Universidad de Concepción, Chile.
2010-2017: Doctor en Oceanografía, Universidad de Concepción, Chile.

PUBLICACIONES

Valdés, V., Escribano, R., Vergara, O. 2017. Scaling copepod grazing in a coastal upwelling system: the importance of community size structure for phytoplankton C flux. Lat. Am. J. Aquat. Res., 45(1): 41-54.

Vergara, O., Echevín, V., Sepúlveda, H.H., Quiñones, R., 2017**.** Controlling factors of the seasonal variability of productivity in the southern Humboldt Current System (30°S-40°S): a biophysical modeling approach. Manuscrito aceptado en Continental Shelf Research (https://doi.org/10.1016/j.csr.2017.08.013).

Hernández-Miranda, E., Betancourt, I., Sobarzo, M., Vergara, O., Quiñones, R. 2017. E. Bio-physical coupling explains spatial distribution of zooplankton in a channel intensely used by aquaculture farms. Manuscrito enviado a Aquaculture.

Vergara, O., Quiñones, R., Montes, R., Hernández-Miranda, E, Sobarzo, M. 2017. Year-round variability of upwelling and downwelling favorable events off central-southern Chile. Manuscrito en preparación para Progress in ocenography.

Vergara, O., Echevín, V., Sepúlveda, H.H., Colas, F., Quiñones, R., 2016**.** Modelling the seasonal dynamics of the Peru-Chile Undercurrent off Central Chile (30–40°S). Continental Shelf Research 123, 61-79.

Hidalgo, P., Escribano, R., Fuentes, M., Jorquera, E., Vergara, O. 2012. How coastal Upwelling influences spatial patterns of size- structured diversity of copepods off central-southern Chile (summer 2009). Progress in Oceanography 92-95, 134-145.

ÁREAS DE INVESTIGACIÓN

Oceanografía Biológica

Oceanografía Física

EXPERIENCIA DOCENTE

Año 2010: Ecología de sistemas acuáticos para Ingeniería en Biotecnología Marina, UdeC

Año 2011: Oceanografía Física para Biología Marina, ayudante en curso de oceanografía UdeC

Año 2011: Zooplancton para Biología Marina, Profesor Invitado a una clase UNAB

Año 2012: Zooplancton para Biología Marina, Profesor Invitado a una clase, UNAB

Año 2012: Oceanografía física para Biología marina, ayudante en curso de oceanografía UdeC

ESTADIAS DE INVESTIGACIÓN

Noviembre 2011-Enero 2012, pasantía Universidad Pierre et Marie Curie, Francia. Beca de la Embajada de Francia. Avance en Proyecto de Tesis doctoral con el Dr. Vincent Echevín.

Enero 2014-Marzo 2014, pasantía Universidad Pierre et Marie Curie, Francia. Beca REDOC_UDEC, Avance Tesis Doctoral con el Dr. Vincent Echevín.

Enero 2015-Febrero 2015, pasantía Universidad Pierre et Marie Curie, Francia. Beca LIA-MORFUN, Avance Tesis Doctoral con el Dr. Vincent Echevín.

Tabla de Contenidos

ÍNDICE DE FIGURAS

ÍNDICE DE TABLAS

Resumen

Dinámica de procesos y factores físico-biológicos en la zona sur del Sistema de Corrientes de Humboldt: un enfoque basado en modelación

Odette Alejandra Vergara Soto
Doctorado en Oceanografía
Universidad de Concepción, 2017
Dr. Renato Quiñones Bergeret, Profesor Guía

En la zona sur del Sistema de Corrientes de Humboldt (SCH), el proceso de surgencia, el Agua Ecuatorial Subsuperficial rica en nutrientes transportada por la Corriente Subsuperficial Chile-Perú (PCUC), y la dinámica de advección de los nutrientes, son factores cruciales para la generación de la alta productividad biológica del ecosistema costero. En este contexto, esta Tesis Doctoral desarrolla los siguientes objetivos específicos: (i) Determinar la evolución temporal de los eventos favorables a surgencia en la zona centro-sur de Chile durante los últimos 25 años, junto con evaluar si los vientos Sur-oeste durante la estación de invierno, presentan una intensidad, frecuencia y duración similares a los presentes en primavera-verano; (ii) Determinar la evolución temporal de los eventos de viento favorables a hundimiento en la zona centro-sur de Chile durante los últimos 25 años, junto con evaluar si los vientos norte durante la estación de primavera-verano, presentan una intensidad, frecuencia y duración similares a los presentes en otoño-invierno; (iii) Caracterizar la dinámica física en la zona sur del SCH utilizando un modelo físico de alta resolución y describir la variabilidad estacional e interanual de la Corriente Subsuperficial Chile-Perú (PCUC), en términos de transporte y velocidad a lo largo de la plataforma continental de Chile; y (iv) Caracterizar la variabilidad espacial y temporal de los nutrientes potencialmente limitantes del crecimiento del fitoplancton en la zona sur del SCH, mediante modelación biogeoquímica/física acoplada. La zona de estudio de la Tesis se encuentra delimitada entre 30-40ºS y 70º-80ºW. Para responder los Objetivos Específicos 1 y 2 se realizó el análisis de una serie de tiempo de vientos (1988-2013) de una estación meteorológica localizada en el Aeropuerto Carriel Sur, Talcahuano (36º47'S, 73º04'W). Los Objetivos Específicos 3 y 4 se desarrollaron mediante la utilización del modelo hidrodinámico ROMS (Regional Oceanic

Modeling System) acoplado a un modelo biogeoquímico (Pelagic-Interactions Scheme for carbon and Ecosystem Studies; PISCES). Los resultados de la serie de tiempo de vientos (Objetivos Específicos 1 y 2, Capítulo 1) mostraron una notable disminución ($p<0.05$) de la intensidad de la surgencia y su duración los últimos 25 años. A pesar de esto, la frecuencia en el número de eventos aumentó, es decir, los eventos son cada vez menos intensos, más cortos, pero más frecuentes. Por otro lado, el hundimiento exhibió cambios considerables solamente en su intensidad, la cual al igual que la surgencia, disminuyó los últimos 25 años. La frecuencia y duración de los eventos de hundimiento, no han experimentado cambios significativos ($p>0.05$). El conocimiento generado en esta tesis sobre la evolución temporal del hundimiento, proceso escasamente estudiado en el SCH, es un aporte para entender la dinámica física de este ecosistema altamente productivo, en el tiempo. La modelación hidrodinámica desarrollada (ROMS; Objetivo Especifico 3, Capítulo 2) representa de forma realista la variabilidad detectada en el nivel del mar, así como también a las variables físicas tales como temperatura y salinidad. El transporte promedio máximo de la PCUC fue de 0.8 Sv en 30°S, lo cual es consistente antecedentes previos, tanto de modelación como de estimaciones derivadas de observaciones *in situ*. También se detectó una reducción de la fuerza de la PCUC hacia el sur generada, en parte, por la disminución del rotor del estrés del viento hacia el polo y por la formación de un jet cerca de 35°S, asociado con la propagación de remolinos hacia el oeste. Un análisis lagrangiano virtual de las masas de agua transportadas por la PCUC, muestra que sólo el 14-20% de los flotadores subsuperficiales son advectados a superficie dentro de los siguientes seis meses después de su liberación. Finalmente, los resultados de la modelación acoplada ROMS/PISCES (Objetivo Específico 4, Capítulo 3), mostraron una potencial co-limitación del crecimiento del fitoplancton cerca de la costa, asociada en otoño e invierno a la intensidad de la luz, y a la concentración de silicato en primavera y verano, mientras que otros nutrientes (N, P, Fe) podrían ser limitantes fuera de la costa, entre enero y abril. Por otro lado, se observó que aquellas áreas que presentaron alta advección vertical se asociaron a zonas históricamente descritas como de surgencia costera. Estas zonas fueron compensadas parcialmente por procesos horizontales relacionados con el transporte inducido por remolinos desde la costa hacia el océano abierto. Se demostró que la mezcla vertical juega un rol clave en la reposición de nutrientes en la capa superficial y, por consiguiente, en la productividad biológica de la zona sur del SCH.

Abstract

Dynamics of processes and physical-biological factors in the southern zone of the Humboldt Current System: a modelling approach

Odette Alejandra Vergara Soto
Doctorate in Oceanography
Universidad de Concepción, 2017
Dr. Renato Quiñones Bergueret, Advisor

In the southern zone of the Humboldt Current System (HCS), the upwelling process, the nutrient-rich Equatorial Subsurface Water transported by the Peru-Chile Subsurface Current (PCUC), and the nutrient advection dynamics are known to be crucial factors to generate the high biological productivity of the coastal ecosystem. This Doctoral Thesis aims at accomplishing the following Specific Objectives: (i) To determine the temporal evolution of the wind events favorable to upwelling in the southern zone of the HCS in the last 25 years, and to evaluate whether the south-west winds during winter have an intensity, frequency and duration similar to those winds present in spring-summer; (ii) To determine the temporal evolution of the wind events favorable to downwelling in the southern zone of the HCS in the last 25 years, and to evaluate whether the north winds during spring-summer have an intensity, frequency and duration similar to those winds present in autumn-winter (iii) To characterize the physical dynamics in the southern zone of the HCS using a physical model of high resolution and describe the seasonal and inter-annual variability of the PCUC in terms of transport and velocity, along the continental shelf off Chile; and (iv) To characterize, using coupled biogeochemical/physical modelling, the spatial and temporal variability of nutrients that can potentially be a limiting factor for phytoplankton growth in the southern zone of the HCS. The specific study zone of this Thesis is located between 30-40ºS and 70º-80ºW. To accomplish objectives 1 and 2, a 25-year time series time-series (1988-2013) of wind data from a meteorological station located at Carriel Sur Airport (Talcahuano; 36º47'S, 73º04'W) was analyzed. The objectives 3 and 4 were approached using the ROMS hydrodynamic model (Regional Oceanic Modeling System) coupled with a biogeochemical model (Pelagic-Interactions Scheme for Carbon and Ecosystem Studies; PISCES). The analysis of the wind time series (Objectives 1 and 2, Chapter 1) shows a decrease over the last 25 years

($p<0.05$) in the intensity and duration of upwelling-favorable events. However, the frequency of these events has increased. In fact, according to our analysis the upwelling-favorable events are progressively less intense and shorter, but more frequent. On the other hand, the intensity of downwelling events has also experienced significant change, decreasing in the last 25 years. The frequency and duration of downwelling events have not changed significantly ($p>0.05$).

The knowledge generated in this Thesis on the temporal evolution of downwelling-favorable events, a process scarcely studied in the HCS, is a contribution for the understanding of the temporal physical dynamics of this highly productive ecosystem. The hydrodynamic modelling (ROMS; Specific objective 3, Chapter 2) provides a realistic representation of the variability observed in sea level and physical variables like temperature and salinity. The average maximum of the PCUC transport was 0.8 Sv at 30°S, which is consistent with previous estimations from modelling and in situ observations. A reduction in the southward force of the PCUC was observed, partly owing to the decrease in poleward wind stress curl and to the formation of a westward jet near 35°S associated with westward-propagating eddies. A Lagrangian virtual analysis of water masses transported by the PCUC shows that only 14-20% of the subsurface floats were advected to the surface within six months after their release. Finally, the results of the coupled ROMS/PISCES model (Specific Objective 4, Chapter 3) shows a potential co-limitation of phytoplankton growth, in autumn and winter, by light intensity and by silicate concentration in spring and summer, while other nutrients (N, P, Fe, etc.) may be limiting offshore areas between January and April. It was observed that areas with high degree of vertical advection are associated with what are historically described as coastal upwelling areas. These areas are partially offset by horizontal eddy-induced transport from the coast to the open ocean. The results of this investigation show that vertical mixing plays a key role in nutrient repositioning in the surface layer, and consequently, in the biological productivity of the southern HCS.

1.- INTRODUCCIÓN

1.1. Características generales del SCH

El Sistema de Corrientes de Humboldt (SCH), también descrito por algunos autores como el Sistema de Corrientes Chile-Perú (PCCS), se extiende desde ~42ºS hasta el ecuador (Montecino et al., 2005). Este sistema está formado por distintas corrientes, las cuales tienen diversos orígenes.

El límite sur del SCH se asocia a la Deriva de los Vientos del Oeste (WWDC) la cual forma parte del giro subtropical del Pacífico Sur (Quiñones et al., 2010). WWDC incide en el continente sudamericano alrededor de 42º-48ºS bifurcándose en dos ramas principales (Orsi et al., 1995; Reid, 1999). La rama que se dirige al norte es conocida como la Corriente de Humboldt (CH), la cual transporta Agua Superficial Subantártica (ASAA) hacia el ecuador. La otra rama que se desplaza hacia el sur es denominada Corriente del Cabo de Hornos (CHC), la cual es una corriente costera que se alimenta de los ríos locales y se vuelve más fuerte durante invierno austral y que también transporta SAAW, la cual es mezclada posteriormente con aguas provenientes de los fiordos (Silva y Neshyba, 1977; Strub et al., 1998). Otros componentes de este sistema son la Contracorriente Chile-Perú (PCCC) la cual fluye hacia el sur entre 100-300 km costa afuera y la Corriente Subsuperficial Chile-Perú (PCUC), la cual transporta Agua Ecuatorial Subsuperficial (AESS) (Wooster y Gilmartin, 1961; Gunther, 1936; Wyrtki, 1963; Silva and Konow, 1975; Strub et al., 1998) y se traslada como una corriente costera hasta el Golfo de Penas (48ºS) (Silva and Neshyba, 1979). Ambas corrientes provienen de la Corriente Ecuatorial Subsuperficial (EUC), la cual se divide en la Isla Galápagos (Lucas, 1986). Un brazo alcanza Sudamérica cerca del ecuador y gira hacia el sur formando la PCUC y otro brazo dobla al sudeste de las Galápagos y se acerca a la costa formando la PCCC (Strub et al., 1995, 1998). Por otro lado, cerca de la plataforma principalmente fluyendo hacia el ecuador, se encuentran la Corriente Costera Chile (CCC) y la Corriente Costera Perú (PCC), ambas están influenciadas por vientos locales y por la surgencia costera (Wyrtki, 1966, 1967; Aiken et al., 2008). La circulación de gran escala del Sistema de Corrientes de Humboldt se presenta en la Figura 1.1.

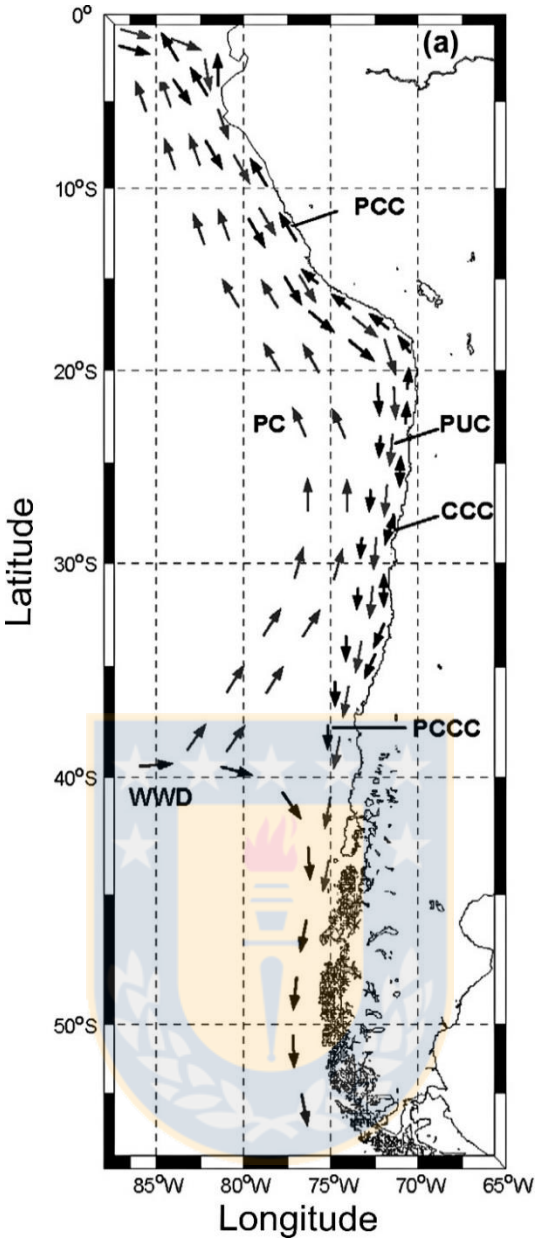

Figura 1.1: Sistema de corrientes de Humboldt (Parada et al., 2012, modificado de Strub et al., 1998): Corriente Costera Perú (PCC), Corriente Costera Chile (CCC), Corriente Perú-Chile o Corriente de Humboldt (PC), Contra-Corriente Costera Perú-Chile (PCCC), Corriente Subsuperficial Chile-Perú (PUC o PCUC), Deriva de los vientos del oeste (WWD).

El límite costa afuera del SCH ha sido ampliamente discutido por Quiñones et al. (2010) destacando diferentes criterios para establecer esta definición. Por ejemplo, considerando solo el dominio físico, la extensión de este sistema es de 120 km de costa, con un área total de 182.000 km2 desde 4º- 18ºS (Chávez y Barber, 1987). Demarcq (2009) considera como margen externo, la principal área de surgencia biológicamente activa donde Chl-a > 1 mg de Chl-a/m^3. Nixon and Thomas (2001), utilizando el mismo criterio de Demarcq

(2009), estiman un área total de 220.000 km^2 durante un período la Niña (1998/1999) y de 120.000 km^2 durante el Niño (1997/1998) para la costa peruana.

La relevancia del SCH radica en que es uno de los sistemas de surgencia de borde oriental (SSBO) más extensos del mundo (Chávez et al., 2009), el cual sostiene importantes pesquerías pelágicas y bentónicas (Cubillos et al., 1998; Cubillos *et al*., 1999; Cubillos *et* al., 2007; Quiñones et al., 2009; Hernández et al., 2011). Se caracteriza por presentar altas tasas de producción primaria (10-20 g C/m^2 día, Fossing et al., 1995; Daneri et al., 2000; Montero et al., 2007), una extensa Zona Mínima de Oxígeno asociada a altas tasas de producción procarionte (Troncoso et al., 2003; Levipán et al., 2007) y a procesos de pérdida de nitrógeno (De Pol-Holz et al., 2009; Galán et al., 2009; Cornejo y Farías, 2012; Farías et al., 2015) y presenta además, alta variabilidad temporal de la abundancia y diversidad de ictio, meso y macrozooplancton (Claramunt et al., 2014; González et al., 2015; Escribano et al., 2016; Riquelme et al., 2016). Las altas tasas de materia orgánica generadas por este sistema son aprovechadas por diversos grupos taxonómicos incluyendo los hongos filamentosos, que participan activamente en su descomposición (Gutiérrez et al., 2011; Fuentes et al., 2015).

En el SCH, como en otros SSBO (i.e. California, Benguela, Canarias), la surgencia impulsada por el viento es el proceso de transporte que más incide en la variabilidad espacio-temporal de la costa (Strub et al., 1998, 2013). Este mecanismo local recibe la influencia de fenómenos de gran escala como las ondas atrapadas a la costa (CTW) forzadas por fluctuaciones del Pacífico ecuatorial (Shaffer et al., 1997, 1999; Hormazábal et al., 2002) y la influencia de remolinos y meandros (Grob et al., 2003; Correa-Ramírez et al., 2007, 2012; Hormazábal et al., 2004, 2013) (Figura 1.2).

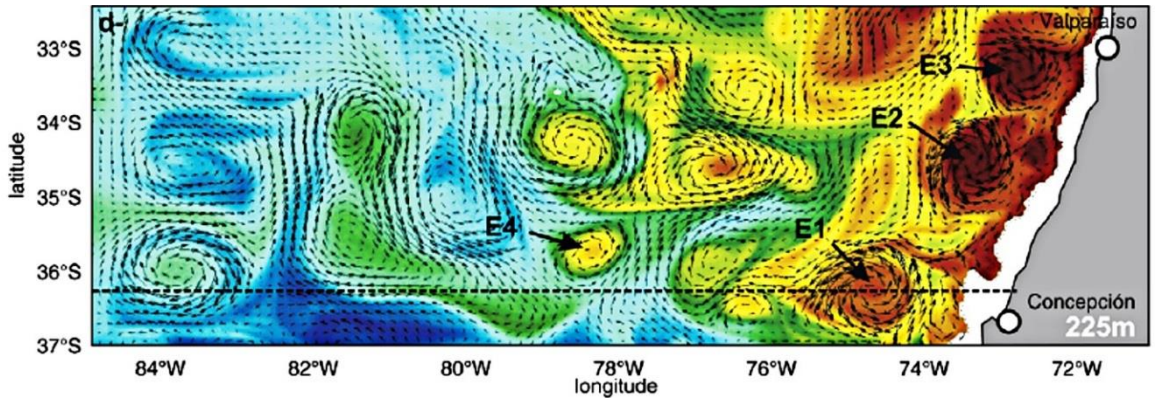

Figura 1.2: Remolinos intratermoclina en 225 metros de profundidad señalados por E1, E2, E3 y E4 (Hormazábal et al., 2013).

Las características físicas y biológicas descritas anteriormente, están sujetas a una fuerte variabilidad interanual promovida por el ciclo ENOS (El Niño Oscilación del Sur). Se ha observado que durante las fases cálidas de ENOS, i.e. El Niño, el transporte de nutrientes hacia la superficie se reduce, generando disminución en la producción primaria (Barber y Chávez, 1983) y consecuencias negativas para el ecosistema marino en su conjunto (Artnz y Farhbach, 1996). Estudios más recientes indican que tales impactos pueden variar ampliamente dependiendo del área y componente biológico a considerar (Ulloa et al., 2001; Iriarte y González, 2004).

La dinámica estacional e interanual de la interacción físico/biológica abarca, por lo tanto, una gran variedad de factores. No obstante, esta Tesis se focalizará en el estudio de la surgencia/hundimiento, en la variabilidad estacional e interanual de la PCUC y en el transporte de nutrientes en las dimensiones zonal, meridional y vertical y como se correlacionan estos últimos procesos con la distribución de la clorofila *a*, en la zona centro sur de Chile (30º-40ºS).

1.2. Surgencia y hundimiento costero en Chile centro-sur (30º-40ºS)

1.2.1. Surgencia costera en Chile centro-sur (30º-40ºS)

El forzamiento del viento en el Pacífico sudeste es dominado principalmente por el Anticiclón del Pacífico Sur (APS) y los centros atmosféricos de baja presión en altas latitudes y el continente (Saavedra, 1980).

Dada la presencia de los bordes costeros en los SSBO, los vientos a lo largo de la costa son más intensos sobre el océano que en la tierra, ya que la fricción superficial sobre el continente es mayor por la presencia de orografía y vegetación. Esto crea un gradiente horizontal en la intensidad del viento a lo largo de la costa, donde se reduce el viento costero, en una zona que ha sido llamada de "disminución" ("drop-off"; Capet et al., 2004).

Por otra parte, los cambios estacionales del viento a lo largo de la costa oeste de América del Sur también están relacionados a cambios en el forzamiento estacional promedio, los cuales se encuentran asociados al gradiente de presión a lo largo de la costa en escalas de tiempo sinópticas (Garreaud y Muñoz, 2005; Rahn y Garreaud, 2009).

En la zona centro-sur de Chile, los vientos presentan un marcado ciclo estacional (Garreaud y Muñoz, 2005), los cuales modulan la variabilidad de la surgencia y de los diferentes flujos superficiales y subsuperficiales observados en esta región (Strub et al., 1998). Este ciclo estacional está sujeto al desplazamiento meridional del APS el cual en

primavera y verano austral, impone un régimen de circulación de vientos anticiclónicos (vientos Sur-Oeste favorables a surgencia costera). Durante esta época, el APS facilita con su migración, la reducción de las precipitaciones y descargas de ríos favoreciendo aún más el ascenso de aguas por la disminución de la estratificación vertical (Sobarzo et al., 2007). Junto con esto, la migración del APS durante el verano, intensifica el rotor del estrés del viento y el transporte hacia el norte, acelerando como consecuencia, la rama oceánica del SCH (Fuenzalida et al., 2008). Se han observado, además, entre 30°S-35°S durante la primavera y verano austral, intensos episodios de vientos a lo largo de la costa conocidos como jets o chorros de bajos niveles (Garreaud y Muñoz, 2005; Muñoz y Garreaud, 2005), los que tienen consecuencias directas en la surgencia costera. Durante invierno en cambio, el APS se mueve hacia el norte permitiendo la llegada de bajas atmosféricas con circulación de vientos ciclónicos, favoreciendo el hundimiento, la precipitación y la descarga de ríos, con lo cual aumenta la estratificación en la columna de agua en la zona costera (Sobarzo et al., 2007 (b)). La relocalización de un intenso núcleo de rotor del estrés del viento producto del desplazamiento del APS en la época invernal, favorece el incremento de la velocidad de la rama costera del SCH en 3 cm/s (Fuenzalida et al., 2008). El movimiento del APS se representa en la Figura 1.3 a través del estrés y rotor del viento durante el verano e invierno austral.

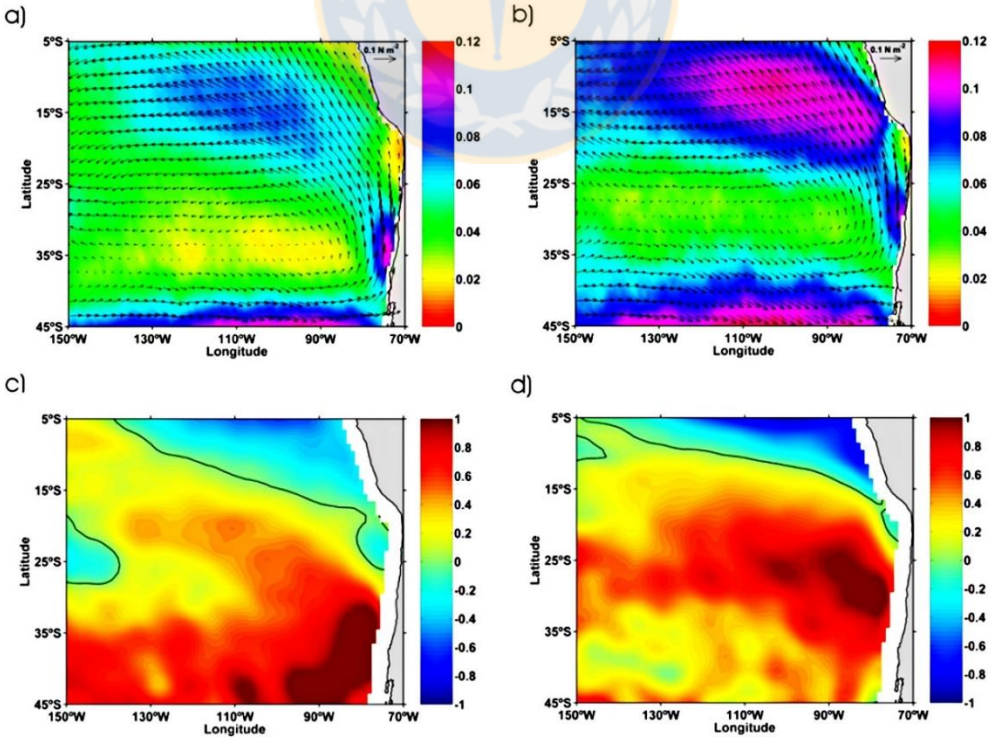

Figura 1.3: a) Estrés del viento durante verano, b) Estrés del viento durante invierno, c) rotor del viento en verano y d) rotor del viento durante invierno. Climatología desde 1993 hasta 2000, basado en ERS I+II (Fuenzalida et al., 2008).

El proceso de surgencia ha sido descrito innumerables veces, tanto en el SCH (ej. Strub et al., 1998; Shaffer et al., 1999; Valle-Levinson et al., 2003) como en otros SSBO (ej. Smith, 1981; Huyer, 1983; Lentz, 1992). Dinámicamente, la surgencia costera resulta de la transferencia de momentum desde el viento hacia el océano y del efecto de la rotación terrestre. El resultado es la deriva horizontal de la capa de agua superficial costera (Capa de Ekman) en 90°, a la izquierda en el hemisferio sur, de la dirección del viento (Yoshida, 1959; Gill, 1982). Este movimiento vertical, o surgencia, genera cambios físicos y químicos en la zona eufótica, tales como disminución de la temperatura, del oxígeno y del pH y aumento de los nutrientes y de la salinidad. El posterior aumento de la productividad primaria es un complejo proceso de interacción físico-biológica (Mann y Lazier, 1991). En la zona centro-sur de Chile, la surgencia traslada hacia superficie el Agua Ecuatorial Subsuperficial (AESS) (Gunther, 1936) la cual se caracteriza por un máximo salino (34.9), bajas concentraciones de oxígeno disuelto (4.4-44 µM) y alta concentración de nutrientes (10-40 µM nitrato, 2.6-3 µM fosfato, 25-40 µM silicato) (Silva et al., 2009). Gracias al aporte de nutrientes de esta masa de agua a la zona eufótica, el SCH de la zona centro-sur de Chile es uno de los sistemas más productivos del mundo, con tasas de producción diaria de hasta 15 g C/m^2 durante eventos de surgencia activa (Montero et al., 2007).

Se han reconocido 5 principales focos de surgencia en el centro-sur de Chile (Fonseca y Farías, 1987). Entre ellos destaca el área localizada entre 35º y 38ºS que se caracteriza por presentar una compleja y amplia batimetría con un quiebre cerca de 150 m de profundidad y un área de 3066 km^2. Esta área se encuentra limitada por los cañones submarinos de los ríos Itata y Biobío, los cuales pueden modificar la circulación local de manera significativa (Sobarzo et al., 2001; Sobarzo y Djurfeldt, 2004; Sobarzo et al., 2016). Dentro de esta zona, se encuentra el Golfo de Arauco (36.7º-37.1ºS; 73.2-73.5ºW), relevante por constituir un centro de desove y de retención de larvas de especies pelágicas (Arcos et al., 1987; Castillo et al., 1991; Arcos et al., 1996; Castro et al., 1997). Bahías semicerradas de cara al ecuador como el Golfo de Arauco y la Bahía de Monterrey en California por ejemplo, que se constituyen al lado de corrientes de borde oriental, se ven favorecidas por cambios de orientación de la costa, los cuales contribuyen a aumentar la productividad (Figueroa y Moffat, 2000). El Golfo de Arauco es importante no tan solo por recibir la influencia de vientos favorables a surgencia en la época estival, los cuales pueden ser >17 m/s, sino también por la profundización de la picnoclina, cuyas oscilaciones tienen amplitudes de 5 metros y se propagan hacia el polo a lo largo de la

costa contribuyendo a la mezcla de aguas ricas en nutrientes y de bajo oxígeno en la zona eufótica, realzando aún más la producción de este lugar (Valle-Levinson et al., 2003). Por otro lado, la formación de remolinos superficiales e intratermoclina de rotación ciclónica/anticiclónica (Leth y Middleton, 2004; Morales et al., 2012; Hormazábal et al., 2013) y de filamentos y meandros que contribuyen a exportar aguas ricas en nutrientes fuera de la costa (Cáceres, 1992; Mesías et al., 2001; Grob et al., 2003), integran los complejos mecanismos que se desarrollan en el Golfo de Arauco.

En la mayoría de los estudios de interacciones físico-biológicas en SSBO, las estadísticas de surgencia se calculan en escalas de tiempo mensuales, estacionales y anuales (Black et al., 2011; Landaeta y Castro, 2012; Cropper et al., 2014), mientras que la surgencia se produce de forma natural en altas frecuencias (días o semanas) con una duración entre 3-15 días (Largier et al., 1993). La surgencia por lo tanto, presenta un ciclo gobernado por la escala de tiempo sinóptica (Jury et al., 1985; Sobarzo et al., 2010; García-Reyes et al., 2014), frecuencia que se acopla a la dinámica biológica en los SSBO (Montecino et al., 2004; Botsford et al., 2006; Jacob et al., 2011; García-Reyes et al., 2014). El período de tiempo sinóptico y la posibilidad que los vientos del suroeste estén presentes durante todo el año, pueden incitar el desarrollo de eventos surgencia no tan solo en primavera-verano, sino también durante en otoño e invierno, tópico que en general ha sido poco estudiado en Chile.

En otros SSBO, como el de California, se ha reportado que la "surgencia de invierno", incluso cuando es de corta duración o de débil magnitud, proporciona a la región los nutrientes suficientes para realzar la productividad y la disponibilidad de alimento para aves marinas, generando como consecuencia una población adulta saludable y un inicio más temprano de la temporada de reproducción (Schroeder et al., 2009). Por otro lado, en este mismo sistema, Black et al. (2011) encontraron que algunas especies de peces se ven favorecidas por la surgencia en invierno, la cual a su vez se encontró fuertemente ligada a ENOS y a la presión del nivel del mar. En la península Ibérica se han llevado a cabo numerosos estudios que señalan a la surgencia invernal como un componente relevante en la formación de afloramientos fitoplanctónicos tan importantes como en primavera-verano (Ribeiro et al., 2004; Prego et al., 2007; Varela et al., 2010), que el promedio de días de surgencia al mes durante invierno es entre 8-10, favoreciendo al nanofitoplancton, ciliados y nanoflagelados (Álvarez et al., 2009) y que la surgencia invernal favorece la retención de larvas y huevos de peces pelágicos (Santos et al., 2004).

Junto con estudiar la relación entre la interacción de procesos físicos/biológicos con la surgencia en otoño-invierno, es importante considerar si estos "eventos anómalos" están ligados al aumento de la surgencia a través del tiempo (Álvarez et al., 2003; de Castro et al., 2008), asociada al cambio en el régimen de vientos (Sydeman et al., 2003; García-Reyes y Largier, 2010). La mayoría de las investigaciones al respecto, sugieren que los eventos de surgencia están cambiando de una manera consistente con las predicciones que se realizaron sobre el efecto que el cambio climático tendría sobre los vientos (Bakun, 1990; Diffenbaugh et al., 2004; Bakun et al., 2010), volviéndose dichos eventos de surgencia cada vez menos frecuentes, más fuertes y de mayor duración (Iles et al., 2011).

1.2.2. Hundimiento costero en Chile centro-sur (30º-40ºS)

La circulación atmosférica de gran escala que domina la cuenca del Pacífico Sur es conducida, por el Anticiclón del Pacífico Sur (APS), que está limitado en el norte por la Zona de Convergencia Inter-Tropical (ZCIT), en el sur por el frente polar y hacia el este por la costa y la cordillera de los Andes (Strub et al. 1998). El APS tiene ciclos estacionales, interanuales e interdecadales (Montecino et al., 2006; Ancapichún y Garcés-Vargas, 2015), siendo los ciclos estacionales los más ampliamente estudiados (Saavedra y Fopiano, 1992; Montecino et al., 2006; Schneider et al., 2017). En verano, el APS se desplaza hacia el polo (centro en ~35°S) favoreciendo la surgencia costera desde 40°S hacia el ecuador, mientras que en otoño-invierno, el APS se mueve hacia el norte (centro en ~27°S), debilitando los vientos en Chile central e incrementándolos en Perú (Bakun y Nelson, 1991).

Durante el invierno austral la llegada de bajas atmosféricas con circulación de vientos ciclónicos favorecen el hundimiento, la precipitación y la descarga de ríos, con lo cual aumenta la estratificación en la columna de agua (Sobarzo et al., 2007 (b)). En esta época, la variabilidad sinóptica (3-15 días) de los vientos norte más fuertes (favorables a hundimiento), es muy pronunciada al sur de 35°S debido al paso de perturbaciones atmosféricas de baja presión (Garreaud et al., 2002; Garreaud y Muñoz, 2005). Esta variabilidad del viento de alta frecuencia está todavía presente en verano (Sobarzo et al., 2010) debido a la presencia de episodios cuasi semanales de jet costeros (low-level jet) hacia el sur, lo cuales se caracterizan por presentar máximas velocidades que pueden superar los 15 m/s (Garreaud y Muñoz, 2005; Renault et al., 2009).

En oposición a la surgencia, el hundimiento es el movimiento vertical descendente de agua desde el fondo de la capa superficial hacia aguas más profundas producido por una

convergencia en la superficie (Tomczak y Godfrey, 2001). El hundimiento en zonas de surgencia costera de borde oriental, ocurre cuando soplan vientos norte, forzando un patrón de circulación constante a través de la plataforma, generando un flujo que se moviliza hacia la costa (favoreciendo los procesos de retención de agua dentro de la plataforma) y un flujo compensatorio que se dirige fuera de la costa cerca del fondo (Ekman 1905). Este patrón de circulación descrito por Ekman (1905) que se presenta en épocas de hundimiento en SSBO, ha podido ser confirmado a través de estudios observacionales (Winant, 1980) y de modelación (Allen et al., 1995; Austin and Lentz, 2002) en la costa central de Oregon, que es parte del Sistema de la Corriente de California (CCS).

Algunos estudios han explorado la respuesta de plumas de ríos a eventos favorables a surgencia y a hundimiento (Lentz et al., 2004; Whitney et al., 2005; Gan et al., 2008; Liu et al., 2008; Moffat y Lentz, 2012), destacando que los vientos pueden influir en la circulación de las plumas a través y a lo largo de la plataforma de zonas costeras. Los vientos favorables a hundimiento, inducen mezcla en las plumas, generando una profundización significativa de su estructura y un estrechamiento en la superficie, así como un aumento en el transporte a lo largo de la costa (Moffat et al., 2012). En las costas de Chile-central (34°-38°S), Saldías et al. (2012) han señalado que durante otoño-invierno el viento Norte favorable a hundimiento, sumado al efecto de Coriolis, induce a que las plumas de los ríos Mataquito, Maule, Itata, Biobío y Valdivia sean atrapadas en la costa y que rápidamente se propaguen hacia el sur, fusionándose y formando una sola gran pluma. Adicionalmente en esta época del año los ríos se encuentran en su máximo de descarga formando un amplia área de turbidez que supera los 1000 km^2 (Saldías et al., 2012).

Desde el punto de vista biológico, algunos autores han reportado la importancia del hundimiento sobre la dinámica del transporte de larvas planctónicas, e.j. larvas de bivalvos y de gastrópodos (Garland et al. 2002; Shanks et al. 2002). Varios autores destacan que durante periodos de hundimiento producto del transporte de Ekman hacia la plataforma, las larvas que se encuentran en la capa superficial, son trasladadas hacia la costa generando alto asentamiento (Farrel et al., 2001). En este escenario, las larvas planctónicas se comportarían como partículas pasivas que son transportadas junto con el flujo debido a que las velocidades de natación de muchos tipos de larvas (mm/s) son más bajas que las tasas de velocidad en la capa de Ekman (cm/s) (Barber y Smith 1981; Chia et al., 1984). A pesar de esto, algunas larvas de invertebrados intermareales, son capaces

de nadar y permanecer en la costa o fuera de ella sin que la surgencia y el hundimiento ejerzan efecto en su distribución (Shanks y Brink, 2005; Shanks y Shearman, 2009).

En otras regiones de surgencia, como la costa Nor-oeste de la península Ibérica (Ría de Vigo), eventos de hundimiento generan aumento en las concentraciones de fitoplancton, incluyendo las especies potencialmente dañinas (Floraciones Algales Nocivas; FAN), como resultado de la advección hacia la costa, la subducción y la capacidad de los dinoflagelados asociados a FAN (*G. catenatum, D. acuta*, y *D. acuminata*) para mantener su posición en la columna de agua nadando (Figueiras et al., 1994; Sordo et al., 2001; Barton et al., 2016).

En las costas de Chile, se ha reportado que estadios de vida temprana de poblaciones de peces que desovan en invierno, pueden beneficiarse de la circulación costera inducida por vientos favorables a hundimiento (Arcos y Navarro, 1986), este es el caso de la anchoveta, la cual presenta mayor reproducción durante el invierno austral (entre Julio y Septiembre; Mujica y Rojas, 1980). Castro et al. (2000), han encontrado alta densidad de microplancton en la columna de agua en sincronización a una máxima densidad de huevos y larvas de anchoveta en condiciones de hundimiento invernal frente a las costas de Talcahuano (36.5°S). Los autores destacan que aunque la estabilidad general de la columna de agua en esta época es baja, se observaron parches de alimento larval distribuyéndose a lo largo de múltiples estructuras frontales (hialinas y termales) en el área total de estudio.

Por otra parte, en la costas de, Chile central (33°30’S, 71°40’W), Narváez et al. (2006) han encontrado que vientos favorables a hundimiento se asocian a “grandes eventos de calentamiento”, los cuales ocurren algunas veces en primavera y verano. Durante estos característicos eventos, los autores observaron una sincronía significativa en el reclutamiento de varios taxa de invertebrados (decápodos, gastrópodos, poliquetos, mejillones y erizos), sugiriendo que las larvas podrían ser “arrastradas” en estos frentes advectivos y ser liberadas en la costa.

Se ha demostrado también en el SCH, que en épocas de vientos favorables a hundimiento frente a Concepción (36°S), el microzooplancton ejerce una importante remoción (>100%) de la producción primaria (Böttjer y Morales, 2004), lo cual revela que no tan solo durante primavera-verano la presión de pastoreo sobre el fitoplancton es significativa.

El hundimiento puede acoplarse también a otros procesos físicos remotos que se observan en la costa de Chile centro-sur. Por ejemplo, Hormazábal et al. (2006) relacionan las

ondas Rossby con condiciones de hundimiento y surgencia. Destacan que el paso de ondas Rossby junto a la fase de hundimiento (surgencia) genera isotermas más profundas (superficiales), aumentando (disminuyendo) el espesor de la Zona de Mínimo Oxígeno (ZMO), incrementando (disminuyendo) la concentración media de silicato, y disminuyendo (aumentando) el déficit de nitrato en la ZMO. De acuerdo a sus resultados, las propiedades de la capa superficial en el sistema de surgencia de Chile central, podrían estar influenciadas significativamente por ondas Rossby forzadas remotamente. Este sistema podría estar modulado por el paso de estas ondas de baja frecuencia, de modo que la capa superficial tendería a ser más caliente y pobre en nutrientes en asociación a la fase de hundimiento de estas ondas.

En algunas regiones de otros SSBO, como el Sistema de la Corriente de California (CCS), se ha observado que la productividad puede verse afectada por el "preacondicionamiento" del invierno, principalmente a través de hundimientos anormalmente intensos que reducen los inventarios de nutrientes en la plataforma afectando también la productividad durante la primavera y el verano siguientes (Ianson y Allen, 2002; Tortell et al., 2012). Los vientos hacia el polo que dominan durante la época invernal en el CCS, pero que también están presentes a lo largo del año aunque en menor frecuencia, producen junto con el hundimiento, una “depresión o profundización de la picnoclina” en la costa y un forzamiento de las aguas superficiales hacia la plataforma (Smith et al., 1994). El movimiento descendente de la picnoclina empuja estas aguas subsuperficiales las cuales son ricas en carbono y nutrientes limitantes para el desarrollo del fitoplancton desde la plataforma costera hacia otras cuencas oceánicas adyacentes (Hales et al., 2005). El presupuesto neto anual de carbono, por lo tanto, está influenciado directamente por la surgencia y el hundimiento, así como por las características batimétricas de la plataforma costera (Ianson et al., 2009).

Se ha demostrado que la intensidad del hundimiento durante invierno, ha aumentado los últimos 50 años en el límite norte de la CCS (Foreman et al., 2011). Algunos modelos han pronosticado un incremento en los vientos favorables a hundimiento durante el año 2100; sin embargo, estas predicciones no han evidenciado ser estadísticamente significativas (Merryfield et al., 2009). Existe una variedad de indicadores que han sido utilizados para estimar el inicio y desarrollo de la surgencia, estos incluyen la clorofila superficial (Henson y Thomas, 2007), la temperatura (Tapia et al., 2009; Benazzouz et al., 2014) y los nutrientes (García-Reyes et al., 2014). Sin embargo, la sincronización (inicio, duración y término) de la "estación de hundimiento", solo ha sido evaluada por

algunos autores (ej. Bograd et al., 2009; Foreman et al., 2011; Bylhouwer et al., 2013). En este aspecto, es necesario profundizar en el conocimiento de la dinámica del hundimiento en el centro-sur de Chile en distintas escalas temporales y espaciales, lo cual permitirá avanzar en la predicción de los efectos del cambio climático en esta región.
Sumado a lo anterior, estudiar los eventos de surgencia durante otoño-invierno y compararlos con los típicos eventos de primavera-verano, así como evaluar los eventos de hundimiento en primavera-verano y compararlos con los típicos eventos de hundimiento de otoño invierno, es un tópico relevante para la comprensión del ecosistema en esta zona.

1.3. El Sistema de Corrientes de Humboldt y la Corriente Subsuperficial Chile-Perú (PCUC) en Chile centro-sur (30°-40°S)

Las corrientes subsuperficiales hacia los polos (PUC) se presentan comúnmente en SSBO de latitudes medias (Fonseca, 1989; Neshyba, 1989; Hill et al., 1998). Estas corrientes viajan sobre la plataforma continental en dirección opuesta al flujo superficial hacia el ecuador (Pierce et al., 2000), localizando su núcleo entre 100-300 metros de profundidad, con velocidades entre 0.1-0.3 m/s (Neshyba et al., 1989; Warren, 1990). Las PUC generalmente se profundizan y pierden su fuerza hacia el polo (McCreary y Chao, 1985; Clarke, 1989; Thomson y Krassovski, 2010).
En el SCH, la Corriente Subsuperficial Chile-Perú (PCUC) se origina en las costas de Perú cerca de 5°S y fluye hasta el Golfo de Penas (48°S; Wooster y Gilmartin, 1961; Wooster y Reid, 1963; Silva y Neshyba, 1979). Esta corriente proviene de la Corriente subsuperficial Ecuatorial (EUC) (Lucas, 1986) y de dos ramas de la SSCC (Contracorriente Subsuperficial Sur; Montes et al. 2010; Czeschel et al. 2011). Mediciones directas sobre esta corriente se han efectuado a lo largo de las costas de Perú y Chile, concluyendo que está presente durante todo el año, que es posible distinguirla desde la superficie hasta 600 metros de profundidad, que su núcleo de máxima velocidad se encuentra entre 100 y 250 metros y que se localiza principalmente entre la costa y 200 km mar adentro (Woster y Gilmarti, 1961; Silva y Neshyba, 1979; Johnson, 1980; Silva y Fonseca, 1983; Huyer et al., 1987; Shaffer et al,.1997,1999; Pizarro et al., 2002; Chaigneau et al., 2013). Se ha reportado que la velocidad promedio de este flujo adquiere diferentes valores dependiendo de la zona y época del año (Tabla I). El transporte promedio estimado para esta corriente es de 0.3-0.5 Sv entre 12°-16°S (Chaigneau et al.,

2013), de 1.8 Sv en 10°S (Huyer et al., 1991) y de 1-1.3 Sv en 30°S (Huyer, 1987; Shaffer et al., 1999, 2004).

Tabla I: Velocidad (cm/s) reportada para la PCUC

Velocidad PCUC (cm/s)	Localización	Referencia
5-10	5º-12ºS	Huyer et al. (1991)
5-10	10º-15ºS	Silva y Neshybat (1977) (calculado desde Wooster y Gilmarti, 1961)
0-5	15º-18ºS	Silva y Neshybat (1977) (calculado desde Wooster y Gilmarti, 1961)
5-10	20º-30ºS	Silva y Neshybat (1977) (calculado desde Siever y Silva, 1977)
12.8	30ºS	Shaffer et al. (1999)
10	30ºS	Leth et al. (2004)
0-5	32º-37ºS	Silva y Neshybat (1977) (calculado desde Chin, 1970)
0-5	40º-45ºS	Silva y Neshybat (1977) (calculado desde Silva, 1977)

Por otra parte, la PCUC es modulada fuertemente por el rotor del estrés del viento a través de la dinámica de Sverdrup (Marchesiello et al., 2003; Albert et al., 2010; Chaigneau et al., 2013) y por el forzamiento tropical remoto (Pizarro et al., 2002; Ramos et al., 2006). En periodos estacionales e interanuales, la PCUC recibe la influencia de ondas Rossby forzadas por ondas Kelvin ecuatoriales (IEKW; Belmadani et al., 2012) que arriban a las costas de Sudamérica y explican más de un 50% de la variabilidad de la PCUC (Pizarro et al., 2002). Estas IEKW se propagan como ondas atrapadas a la costa (CTW), las cuales modifican el cizalle vertical (vertical shears) entre la PCUC y la Corriente costera Chile-Perú, modulando las inestabilidades baroclínicas y, por lo tanto, la generación de remolinos de mesoescala que se propagan desde la costa al oeste (Echevin et al., 2011).
Es un factor común de los SSBO, que la presencia de un jet costero hacia el ecuador fluyendo sobre una corriente subsuperficial que se dirige al polo genere inestabilidades baroclínicas, producto de gradientes horizontales de densidad (Allen et al., 1991; Barth et al., 2000). Así, el jet que se desarrolla en el frente de surgencia, se fortalece y se mueve fuera de la costa desarrollando meandros y remolinos (Strub et al., 1991; Strub y James, 2000; Aristegui et al., 2009). Por ejemplo, se ha encontrado que remolinos anticiclónicos intratermoclina (ITEs) se desprenden de la PCUC en la temporada de surgencia, propagándose fuera de la costa y transportando aguas ricas en nutrientes y bajo oxígeno, propiedades características de la AESS (Hormazábal et al., 2004, 2013).

La PCUC es importante además, porque inyecta a la superficie, en periodos de surgencia, la masa de Agua Ecuatorial Subsuperficial (AESS). La AESS aporta nutrientes, concentraciones bajas de oxígeno, alta salinidad y baja temperatura a la zona eufótica, favoreciendo a la productividad primaria (promedio anual de 10- 20 g C.m-2.day-1; Daneri et al., 2000; Montero et al., 2007). Si los vientos favorables a surgencia son altamente persistentes, el ecosistema puede verse afectado negativamente como consecuencia de bajas concentraciones de oxígeno provenientes de la AESS, llegando incluso a presentar eventos severos de hipoxia que conllevan varazones y mortandades de biota costera (Hernández-Miranda et al., 2010; 2012a, b; 2017).

Por lo tanto, es relevante estudiar la dinámica estacional e interanual la PCUC en la plataforma continental de Chile centro-sur considerando la influencia que ejerce esta corriente sobre el transporte de la AESS (meridional y zonal), la cual sostiene las altas tasas de productividad en el SCH de Chile.

1.4. Dinámica de nutrientes y fitoplancton en la zona centro-sur de Chile

Como se ha mencionado anteriormente, los SSBO son regiones marinas biológicamente productivas las cuales cubren < 1% del océano, pero que proporcionan hasta el 20% de las pesquerías en el mundo (Pauly y Christensen, 1995). Los altos niveles de productividad de los SSBO son el resultado de vientos con dirección al ecuador a lo largo de la costa, los cuales en combinación con el efecto Coriolis, transportan aguas superficiales fuera de la costa. Como consecuencia de la conservación de masa, aguas profundas con alta concentración de nutrientes y CO_2 y baja concentración de oxígeno y pH, son advectadas hacia la zona eufótica (Huyer, 1983).

La advección vertical de nutrientes sumada a la dinámica de la capa de mezcla y de la radiación solar, favorece las altas tasas de producción nueva en los SSBO, con proporciones f (f-ratios) fluctuando entre 0.21 y 0.75 (e.g. Dugdale, 1985; Minas et al. 1986; Chávez y Toggweiler, 1995; Clark et al., 2016).

En el SCH, pulsos de Agua Ecuatorial Subsuperficial (AESS) seguidos por períodos de relajación del estrés del viento, representan probablemente las mejores condiciones para estimular el crecimiento fitoplanctónico y obtener altas tasas de producción de materia orgánica (Marín et al., 1993; Daneri et al., 2012).

La dinámica de las variables biológicas como oxígeno, clorofila y nutrientes en el SCH ha sido ampliamente investigada. En la zona centro-sur de Chile, se ha estudiado su distribución espacial mediante la ejecucíon de cruceros bio-oceanográficos financiados

por el Fondo de Investigación Pesquera y de Acuicultura (FIPA; Subsecretaría de Pesca, Ministerio de Economía, Fomento y Turismo, Gobierno de Chile) y en la dimensión temporal a través de la serie de tiempo de la estación 18, localizada en la plataforma Continental de la zona centro sur (36°31'S; 73°08'W) (Figura 1.4) (Anabalón et al., 2007; Morales et al., 2007; Sobarzo et al., 2007; Quiñones et al., 2009; Gutiérrez et al., 2010; Hernández et a., 2012; Escribano et al., 2015).

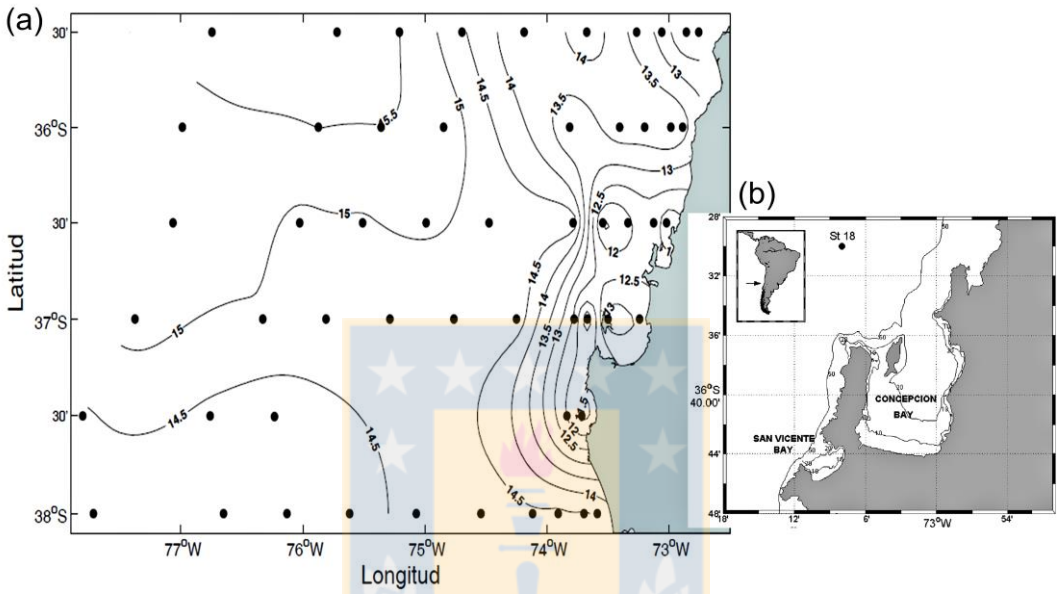

Figura 1.4: (a) Localización de las estaciones oceanográficas correspondientes al Crucero MOBÍOBÍO (FIP 2004-20) y (b) Localización de la Estación 18 (36°31'S; 73°08'W) (Cornejo et al., 2007).

Algunos resultados de los cruceros FIP durante primavera (FIP 2004-20; FIP 2005-01), revelan que el nitrato y el fosfato han presentado patrones similares, con dos núcleos de máximos valores en superficie en la zona costera, uno en 36ºS y otro frente a Punta Lavapié (37º30' S). La mayor concentración de silicato también se ha localizado en la zona costera, especialmente entre 35°S y 36°S. Se ha observado, además, que los nutrientes pueden presentar altas concentraciones hasta 100 km fuera de la costa.

Las concentraciones de nutrientes medidos en la serie de tiempo (Estación 18), especialmente nitrato y fosfato, no presentan grandes diferencias estacionales los primeros metros de la columna de agua, como consecuencia de la surgencia y del aporte de agua dulce al ecosistema durante la época invernal (Anabalón et al., 2007; Montero et al., 2007; Iriarte et al., 2012). Solo el Si ha exhibido mayor variabilidad, con valores fluctuando entre 5 y 40 uM (Anabalón et al., 2007; Montero et al., 2007). Tomando en consideración que los nutrientes (nitrato y fosfato) no han mostrado diferencias

estacionales significativas en esta zona, las elevadas tasas de producción primaria (> 2 g C m^{-2} d^{-1}) coinciden principalmente con el mejoramiento en las condiciones de luz durante la época estival, por lo tanto la productividad en el ecosistema de surgencia de Concepción está mayormente asociada a la estacionalidad de los niveles de radiación solar (Montero et al., 2007).

El aporte de nutrientes a la zona eufótica (Diehl et al., 2002) junto a las adecuadas condiciones de luz (Peterson et al., 1987) y temperatura (Nicklischt et al., 2008; Thomas et al., 2012), generan las condiciones necesarias para la formación de afloramientos fitoplanctónicos en la zona costera. Se ha reportado para la zona centro-sur de Chile, que durante primavera-verano predominan los afloramientos fitoplanctónicos constituidos principalmente por el microfitoplancton, con las diatomeas formadoras de cadenas como las más abundantes (*Chaetoceros* spp., *Thalassiosira* spp., y Skeletonema) (Morales et al., 2007; Vargas et al., 2007). Las diatomeas se adaptan bien a los ambientes altamente turbulentos y repletos de nutrientes (González et al., 2007), contribuyendo mayoritariamente a las altas concentraciones de clorofila en la época de surgencia (>5 mg/m^3) (Morales et al., 2007). En invierno predominan las fracciones menores, con pico y nanofitoplancton como las más abundantes, alcanzando concentraciones de clorofila <2 mg/m^3 durante esta época (Anabalón et al., 2007; Iriarte et al., 2012).

Las altas concentraciones de clorofila generadas en la costa, contribuyen a incrementar la productividad biológica en otras áreas. En el SCH de Chile centro-sur, varios autores han encontrado que el aumento en la concentración de clorofila en la zona de transición costera (CTZ, después del quiebre de la plataforma) es producto de la formación de filamentos (Grob et al., 2003) y de remolinos de mesoescala ciclónicos y anticiclónicos generados en la costa (Morales et al., 2012), los cuales inyectan nutrientes a zonas más oligotróficas. Algunos de los remolinos se generan en la época de primavera-verano y contienen altas concentraciones de clorofila, estos viajan durante meses fuera de la costa, lo cual permite fertilizar las zonas oceánicas durante invierno (Correa-Ramírez et al., 2007). Estas altas concentraciones de clorofila en la época invernal han sido encontradas también en las Islas del Archipiélago Juan Fernández, lo cual sería producto de los remolinos formados en la costa (Andrade et al., 2012, 2014).

Además de la capacidad adaptativa de las células a diferentes niveles de irradiancia y temperatura, la disponibilidad y co-limitación de nutrientes contribuyen entre otros factores a determinar la concentración y distribución espacial de clorofila en el océano (Geider et al., 1997). La co-limitación de nutrientes ocurre cuando dos (o más) nutrientes

han sido extraídos simultáneamente a niveles en los cuales, la adición de uno o de todos es requerida para estimular el crecimiento del fitoplancton (Moore et al., 2013). Concentraciones absolutas de nutrientes en la superficie del océano, o sus relaciones estequiométricas, pueden indicar el potencial de limitación existente en el área a estudiar (Saito et al., 2008).

En el SCH de Perú, se ha encontrado que el hierro limita el crecimiento del fitoplancton durante invierno (Hutchins et al., 2002; Bruland et al., 2004), mientras que el nitrato y el silicato limitan el crecimiento durante verano (Echevin et al., 2008). En el SSBO de California, el hierro también limita el crecimiento del fitoplancton, ejerciendo un control fundamental sobre la biogeoquímica de los principales nutrientes, sobre la producción de carbono orgánico particulado y sobre el crecimiento del plancton (Hutchins et al., 1998). Se ha encontrado en el SSBO de California que la adición de hierro permite, además, la generación de afloramientos de diatomeas formadoras de cadena altamente silicificadas (Hutchins et al., 1998; Bruland et al., 2001). En el SSBO de Benguela, Kyuper et al. (2005) identificaron una relación directa entre el anammox y la remoción de nitrógeno inorgánico en la Zona de Mínimo Oxígeno (ZMO), concluyendo que este proceso bacteriano es el principal responsable de la limitación de nitrógeno en este sistema. En el SCH de Chile, Quiñones et al. (2010) mediante la construcción de modelos biogeoquímicos de caja tipo LOICZ (Land-Ocean Interactions in the Coastal Zone; Gordon et al., 1996), sugieren que el nitrógeno podría ser limitante de la producción primaria en tres regiones localizadas en: 18–27°S, 27–33°S y 33–42°S. Los autores destacan que el déficit relativo de este elemento en comparación a la disponibilidad de fósforo en este ecosistema, es consistente con las altas tasas de desnitrificación asociadas a la Zona de Mínimo Oxígeno (Castro-González y Farías, 2004; Pantoja et al., 2004; Castro-González et al., 2005).

El crecimiento del fitoplancton, integra varias condiciones y procesos oceanográficos, entre los que destacan la profundidad de la capa de mezcla, la surgencia, la irradiación de la luz, y la concentración de nutrientes. La advección (o transporte) y mezcla de nutrientes, son procesos físicos que explican en parte la variabilidad de la clorofila en la zona costera (Williams y Follow, 2006; Dave y Lozier, 2015). Los movimientos verticales (advección vertical) juegan un rol clave en el intercambio de calor y propiedades biogeoquímicas entre la superficie y el océano profundo. En sistemas de surgencia, en áreas de frentes costeros y en remolinos de mesoescala, la velocidad vertical es fundamental y puede contribuir significativamente al suministro de nutrientes en la

zona eufótica (Mahadevan, 2014). En remolinos de mesoescala, tanto la advección horizontal como la vertical inducida por bombeo de Ekman y bombeo de remolinos (Klein y Lapeyre, 2009; Chelton et al., 2011; Siegel et al., 2011) influencian, entre otros factores, la distribución de la clorofila en el océano. Por otro lado, en otras áreas como el giro subtropical del Atlántico Norte, se ha establecido que la advección horizontal es la principal responsable de la variabilidad espacial y temporal del reservorio de nutrientes subsuperficial (Palter et al., 2005).

Determinar cuales son los nutrientes potencialmente limitantes del crecimiento del fitoplancton y comprender como la dinámica de advección y mezcla se correlacionan con la distribución de clorofila en la zona centro-sur de Chile, son tópicos fundamentales de la interacción biofísica en el SCH.

1.5. Justificación de este estudio

Esta Tesis Doctoral busca dilucidar la variabilidad espacial, estacional e interanual de los principales factores físicos en la zona sur del Sistema de Corrientes de Humboldt específicamente en la zona centro-sur de Chile (30°-40°S; 70°-80°W), tales como la surgencia/hundimiento, la Corriente Subsuperficial Chile-Perú (PCUC) y la dinámica de advección y mezcla de nutrientes potencialmente limitantes para el crecimiento del fitoplancton

La importancia de profundizar en la investigación de los factores mencionados anteriormente es la siguiente:

-Surgencia en la época invernal versus surgencia en primavera-verano austral: La surgencia es uno de los factores más importantes en promover las altas tasas de productividad en el Sistema de Corrientes de Humboldt Sur (Daneri et al., 2000) y es responsable en parte de altos desembarques de recursos bentónicos y pelágicos en la zona centro-sur de Chile (Neira y Arancibia, 2004; Cubillos et al., 2007; Yannicelli et al., 2008). Establecer la variabilidad de la surgencia a través del tiempo es fundamental para evaluar como inciden los cambios que experimenta sobre el Sistema de Corrientes de Humboldt Sur.

Se ha determinado que la surgencia en la zona centro-sur de Chile, puede ser dividida en tres épocas: primavera-verano donde la surgencia se intensifica (Shaffer et al., 1999), la época de "no" surgencia que se presenta en otoño-invierno, donde prevalecen los vientos favorables a hundimiento (Shaffer et al., 1999) y la época de transición que se observa a fines de invierno-principios de primavera (Fernández y Farías, 2012). Es relevante

destacar la relajación de la surgencia, la cual tiene una duración relativa que varía entre 2-8 días, generando la estabilidad necesaria para desencadenar afloramientos fitoplanctónicos (Daneri et al., 2012). En este contexto, la sincronización y la frecuencia de los eventos de surgencia/relajación constituyen un modulador clave de la alta productividad primaria descrita para el ecosistema de surgencia de la zona centro-sur de Chile, que se ha estimado en aprox. 1-1,4 kg Cm^{-2} $year^{-1}$ (Daneri et al., 2000; Montero et al., 2007). Sin embargo, ya que la surgencia se desarrolla en la escala sinóptica (Sobarzo et al., 2007), establecer épocas tan marcadas para este fenómeno en la zona centro sur de Chile requeriría una re-evaluación. Algunas investigaciones en otros SSBO por ejemplo, han determinado la importancia de la surgencia durante invierno y su influencia en el ecosistema (e. j. Álvarez et al., 2009; Schroeder et al., 2009; Varela et al., 2010; Black et al., 2011). Estos estudios "rompen" el paradigma que establece que la surgencia tiene un efecto positivo en la columna de agua solo durante primavera-verano.

En consecuencia, es importante determinar también para el Sistema de Humboldt de Chile, si estos "eventos anómalos" están relacionados con el aumento de la surgencia a través del tiempo (Álvarez et al., 2003; de Castro et al., 2008), asociada al cambio en el régimen de vientos (Sydeman et al., 2003; García-Reyes y Largier, 2010; Sydeman et al., 2014) o a una intensificación y desplazamiento del núcleo del Anticiclón del Pacífico Sur (Ancapichún et al., 2016; Schneider et al., 2017). Investigaciones que comenzaron en la década del 90, sugieren que los eventos de surgencia se modificarían en intensidad y duración producto del cambio climático (e.j. Bakun, 1990; Diffenbaugh et al., 2004; Bakun et al., 2010; Bakun et al., 2015), volviéndose cada vez menos frecuentes, más fuertes y de mayor duración (Iles et al., 2011).

El estudio de la dinámica de la surgencia en el centro-sur de Chile en distintas escalas temporales y espaciales, permitirá avanzar en la predicción de los efectos del cambio climático en esta región. Sumado a lo anterior, incrementar el conocimiento respecto de la dinámica de los eventos de surgencia durante invierno, es un tópico relevante para la comprensión del ecosistema en esta zona.

-Hundimiento en primavera-verano versus hundimiento en la época invernal: El hundimiento en los sistemas de surgencia de borde oriental, es un tópico que ha sido poco examinado. La mayoría de las investigaciones que estudian la variabilidad del viento y el futuro escenario climático, mencionan los eventos favorables a hundimiento de forma tangencial, enfocándose mayoritariamente en la surgencia (García-Reyes et al., 2015;

Rykaczewski et al., 2015; Wang et al., 2015). Sin embargo, los eventos favorables a hundimiento, tienen gran relevancia para los sistemas costeros, por ejemplo, asociados a larvas de recursos de importancia económica (Churchill et al., 2011; Rodríguez et al., 2015; Pfaff et al., 2015), asociados a afloraciones algales nocivas (Figueiras et al., 1994; Sordo et al., 2001; Barton et al., 2016) y asociados al transporte de plumas de ríos (Moffat y Lentz, 2012; Saldías et al., 2012). En algunos sistemas de borde oriental, se ha observado que el hundimiento presentó una alta correlación con el ciclo ENOS, destacándose que en épocas Niño los vientos favorables a hundimiento son más intensos y extensos en el tiempo, retrasando la transición primaveral a surgencia (Bograd et al., 2009; Bylhouwer et al., 2013). El hundimiento también se ha asociado a ciclos de baja frecuencia (33, 19 y 11 años) tales como circulación atmosférica, mareas nodales lunares y actividad solar (Saldívar-Lucio et al., 2016).

La mayoría de los estudios realizados en los SSBO han planteado que el hundimiento se presenta principalmente en épocas de otoño-invierno (ej. En el SBO de la Península Ibérica; Álvarez-Salgado et al., 2010), sin embargo eventos favorables a hundimiento también se desarrollan en primavera-verano generando importantes consecuencias en el ecosistema (Narváez et al., 2006). En las costas de Chile central (33°S), "eventos anómalos de calentamiento" asociados a hundimiento, se sincronizan con el reclutamiento de algunas larvas de invertebrados, las cuales podrían ser trasladadas en los frentes advectivos y ser liberadas en la costas (Narváez et al., 2016).

Por lo tanto, estudiar la sincronización de los eventos favorables a hundimiento (inicio, duración y término) en la zona centro-sur de Chile y los cambios que ha experimentado los últimos 25 años, permitirá caracterizar y comprender los efectos que ejercen en la columna de agua.

-Corriente subsuperficial Chile-Perú: El SCH, el cual es parte de la circulación general del giro Subtropical del Pacífico Sur, se compone de varias corrientes, entre las que destaca la Corriente subsuperficial Chile-Perú (PCUC) que fluye desde 5°S hasta 48°S, transportando la masa de agua subsuperficial ecuatorial (AESS) sobre la plataforma continental de Chile y Perú (Strub et al., 1995; 1998). Esta masa de agua tiene altas concentraciones de nutrientes (20-40 uM nitrato, 2.6-3 uM fosfato; 25-40 uM silicato; Silva et al., 2009) y bajo contenido de oxígeno (Fuenzalida et al., 2009; Ulloa y Pantoja, 2009; Hernández- Miranda et al., 2010) que en combinación con la surgencia estacional y sinóptica, conduce alta productividad biológica a lo largo de la costa chilena (Daneri et

al., 2000; Montero et al., 2007). Aunque se han realizado mediciones de la PCUC en Perú (Chaigneau et al., 2013) y en Chile (Shaffer et al., 1999), no se ha determinado aún su variabilidad estacional, zonal y meridional, ni el potencial de la PCUC para transportar partículas hacia el polo.

Establecer la dinámica latitudinal de la PCUC, permitirá determinar el origen y destino del agua transportada por esta corriente y el tiempo requerido para alcanzar la superficie. Esto es fundamental para comprender el proceso de exportación de oxígeno, nutrientes, clorofila y materia orgánica, entre otros, por la AESS.

-Advección de nutrientes potencialmente limitantes para el crecimiento del fitoplancton: Muchos son los factores que influyen en el crecimiento, distribución y biomasa del fitoplancton en las costas de los SSBO. Uno de los principales elementos, es la radiación solar (PAR, UV-A, UV-B), la cual en la zona centro–sur de Chile, presenta un carácter estacional (Hernández et al., 2012; Rain et al., 2014). Si bien la luz es un factor determinante en el crecimiento del fitoplancton, otros agentes hidrodinámicos pueden contribuir para que sistemas como SCH, presenten altas biomasas fitoplanctónicas (González et al., 2007; Montero et al., 2007) y como consecuencia, alta productividad primaria (Montero et al., 2007; Daneri et al., 2012). Entre algunos de estos destacan la surgencia la cual traslada a superficie AESS rica en nutrientes (Silva et al., 2009), la descarga de ríos, la cual inyecta a la zona costera materia orgánica terrestre (Vargas et al., 2011), metales traza y nutrientes (antrópicos y naturales) (Salamanca y Pantoja, 2009) y la profundidad de la capa de mezcla (Echevin et al., 2008). Los nutrientes limitan el crecimiento del fitoplancton de forma individual y en conjunto (co-limitación), viéndose influenciados por procesos físicos como la mezcla, la advección vertical y la advección horizontal (meridional y zonal) asociada a dinámicas de mesoescala. Algunos autores han enfatizado la importancia de la dinámica de mesoescala en el transporte de nutrientes limitantes y clorofila hacia zonas oligotróficas fuera de la costa. Gruber et al. (2011), por ejemplo, sugieren que altos niveles de actividad de remolinos, se asocian a bajos niveles de productividad en el SSBO de California, destacando que la reducción en la producción en algunas épocas en la zona costera, es resultado del transporte de nutrientes inducidos por la advección lateral de remolinos, desde el ambiente costero al océano abierto.

Los nutrientes potencialmente limitantes del crecimiento del fitoplancton en el SCH, varían. Así, por ejemplo, en el SCH de Perú, se ha determinado que el Fe limita al fitoplancton en invierno (Hutchins et al., 2002; Bruland et al., 2005), mientras que el

nitrato y silicato, limitan en verano (Echevin et al., 2008; Messié y Chávez, 2015). Quiñones et al. (2010) han reportado la existencia de un déficit de nitrógeno comparado a fósforo en varias áreas del SCH de Chile, sugiriendo que la producción primaria puede ser limitada por este elemento.

La comprensión del crecimiento y desarrollo del fitoplancton en SSBO, debe integrar una serie de elementos, incluyendo los procesos físicos, la irradiación de la luz y la disponibilidad de nutrientes. Por lo tanto, establecer la interacción de la co-limitación de nutrientes y luz, sumado a procesos de advección y mezcla, permitirá identificar los principales mecanismos que regulan el transporte de nutrientes en la zona centro-sur de Chile.

-Estado actual de Modelación Oceanográfica en Sistema de Corrientes de Humboldt:

La metodología escogida en esta Tesis de Grado, incluye análisis de series de tiempo y modelación biogeoquímica-física. Esta última herramienta ha sido ampliamente utilizada para resolver la complejidad de la integración de diferentes procesos en el ambiente marino.

Varios estudios de modelación han sido desarrollados en Chile. Entre estos destacan Batten et al. (1995), los cuales utilizando un modelo de alta resolución estudiaron la respuesta de la región costera (entre 22.5° y 35°S) al forzamiento del viento climatológico. Otros trabajos han utilizado el modelo físico POM (Princeton Ocean Model; Blumberg y Mellor, 1987), para caracterizar la circulación en el Golfo de Arauco (37°S) durante verano en una fase de surgencia activa (Mesias et al., 2001), para estudiar la variabilidad estacional de la circulación entre 30° y 45°S (Leth y Shaffer, 2001), para determinar los mecanismos que contribuyen a "realzar" la surgencia en la zona centro-sur de Chile (30°-43°S), destacando la importancia del viento y de los remolinos ciclónicos desarrollados en Punta Lavapie (Golfo de Arauco) (Leth y Middleton, 2004) y para investigar los efectos del forzamiento oceánico remoto sobre la circulación de la zona costera en Chile central (Leth y Middleton, 2006). Por otro lado, Baird et al. (2007), a través del acoplamiento de un modelo ecosistémico NPZ (Nitrogen-Phytoplankton-Zooplankton; Baird et al., 2004) con el modelo POM, estiman la respuesta del nitrógeno, zooplancton y fitoplancton a la circulación conducida por vientos estivales en Chile centro-sur.

En la actualidad, el Sistema de Modelación Oceánico Regional (ROMS; Shchepetkin y McWilliams, 2005) ha sido aplicado para analizar la circulación y variabilidad estacional

(Penven et al., 2005; Aguirre et al., 2012), interanual (e.g. the 1997–1998, El Niño event; Colas et al., 2008) e intraestacional (Belmadani et al., 2012; Echevin et al., 2014) en el SCH. Los procesos estudiados también han abordado el impacto de remolinos de mesoescala sobre el balance de calor (Colas et al., 2012), la dinámica oceánica superficial (Aguirre et al., 2012, 2014) y la presencia de remolinos anticiclónicos intratermoclina (Hormazábal et al., 2013). ROMS ha sido acoplado a modelos basados en el individuo (IBM; Lett et al., 2008) para explicar los patrones de transporte, retención, reclutamiento, sobrevivencia, mortalidad y conectividad de los estadios tempranos de *Engraulis Ringens* (Parada et al., 2012; Soto et al., 2012) y *Pleurocontes monodon* (Yannicelli et al., 2012) en la zona Centro-Sur de Chile (35º-37ºS), destacando la importancia de la circulación, temperatura y estacionalidad como factores determinantes en modular la distribución de estas especies. También ha sido implementado, junto a modelos biogeoquímicos como PISCES (Pelagic Interactive Scheme for Carbon and Ecosystem Studies; Aumont et al., 2003), para evaluar procesos principalmente en el SCH norte (Perú), entre los que destacan, el impacto de El Niño sobre la productividad fitoplanctónica (Espinoza-Morriberón et al., 2017), la influencia del rotor del viento sobre la circulación costera y la productividad primaria (Albert et al., 2010), el impacto del cambio climático sobre la sobrevivencia de los estadios de vida temprana de peces pelágicos (Brochier et al., 2013), el impacto de ondas intraestacionales atrapadas a la costa sobre la variabilidad estacional de la productividad costera (Echevin et al., 2014) y los procesos que controlan el ciclo estacional de la clorofila (Echevin et al., 2008). Recientemente, Gómez et al. (2017) han acoplado ROMS a un modelo biogeoquímico para determinar los patrones intraestacionales de la biomasa planctónica de Chile central.

Para más detalle del estado del arte de la Modelación en Chile ver Tabla II.

A pesar que estos trabajos representan grandes avances para el Sistema de Corrientes de Humboldt, aún en Chile se necesita avanzar en el conocimiento y la aplicación de este tipo de herramientas las cuales son capaces de integrar información proveniente de diferentes fuentes, permitiendo simular y analizar la dinámica a largo plazo y las propiedades de estabilidad de sistemas ecológicos complejos. Esto es particularmente importante en el contexto del dominio de uno de los grandes retos del futuro: la preservación de la biodiversidad y las funciones de los sistemas frente al cambio global (especialmente el clima).

Las simulaciones realizadas en esta tesis, mejoran nuestra comprensión de la variabilidad estacional de la circulación a lo largo y cerca de la costa en el SCH. Estudiar la dinámica

de la PCUC y las características (origen, trayectoria) de la masa de agua transportada por esta corriente (AESS), es un primer paso hacia un estudio más completo de los procesos físicos-biogeoquímicos acoplados que impulsan la próspera productividad del SCH de Chile centro-sur.

Junto a lo anterior, esta investigación constituye un avance en modelación de alta resolución (7,5 km) del ciclo estacional de procesos físico-biogeoquímicos acoplados en tres dimensiones en el SCH sur, examinando la co-limitación de los nutrientes potencialmente y la luz sobre el crecimiento del fitoplancton, así como la dinámica de transporte del silicato en la zona centro-sur de Chile (30°-40°S).

Tabla II: Estado actual de la modelación biofísica y trófica en el Sistema de Corrientes de Humboldt sur

Modelo	Tópico principal	Autor
ROMS	Dinámica estacional de la circulación superficial de Chile central	Aguirre et al. (2012)
	Propagaciones intraestacionales forzadas ecuatorialmente a lo largo de la costa de Perú-Chile y su relación con la actividad de remolinos entre 1992-2000	Belmadani et al. (2012)
	Remolinos intratermoclina remolinos en la zona de transición costera de Chile central (31-41º S)	Hormazábal et al. (2013)
	Remolinos intratermoclina en el Archipiélago Juan Fernández, sureste del Océano Pacífico	Andrade et al. (2014)
	El efecto de la variabilidad de alta frecuencia (sinóptica) de los vientos y flujos de calor en el océano superficial de la zona centro-sur de Chile	Aguirre et al. (2014)
	Las consecuencias del calentamiento global en la circulación oceánica del Sistema de Corrientes Perú-Chile Sistema (PCCS)	Oerder et al. (2015)
	Dinámica estacional de la Corriente Subsuperficial en la zona centro-sur de Chile (30º-40ºS)	Vergara et al. (2016)
	Reanálisis de la circulación del océano chileno para la región entre 20ºS y 40ºS	Aiken et al. (2017)
ROMS + Biogeochemical model (tipo NEMURO)	Patrones intraestacionales en la biomasa del plancton costero de Chile central	Gómez et al. (2017)
ROMS + IBM	Efectos de la variabilidad estacional en el transporte de larvas de anchoveta a lo largo y a través de la costa de Chile central	Parada et al. (2012)
	Transporte y supervivencia de huevos y larvas de anchoveta en la zona costera centro-sur de Chile	Soto-Mendoza et al. (2012)
	Distribución de larvas de langostino sobre la plataforma continental de la zona centro-sur de Chile: retención y transporte	Yanicelli et al. (2012)
	Conectividad y transporte de los estadios tempranos de anchoveta en el mar interior de Chiloé, Patagonia Norte	Soto-Mendoza et al. (2017), en revisión
Ecopath+Ecosim (EwE)	Análisis de los cambios en el ecosistema de Humboldt meridional para el período entre 1970 y 2004	Neira et al. (2014)
	Evaluación de los cambios en Humboldt sur durante el siglo XX utilizando modelo tróficos	Neira et al. (2014)
	Estructura comunitaria e interacciones tróficas en un área de manejo costera y de explotación de recursos bentónicos en Chile central	Giacaman-Smith et al. (2016)
POM	Variabilidad estacional de la circulación de Chile central	Leth y Shaffer (2001)
	Circulación en Chile central en respuesta a vientos locales y forzamiento remoto	Leth y Middleton (2006)
POM+NPZ	Respuesta biológica a la circulación conducida por vientos estivales	Baird et al. (2007)

2. HIPÓTESIS Y OBJETIVOS

2.1. Objetivo General

Evaluar la variabilidad sinóptica, estacional e interanual de algunos de los principales procesos físicos presentes en la zona sur del Sistema de Corrientes de Humboldt, tales como, la surgencia/hundimiento, la dinámica espacial/temporal de la Corriente Subsuperficial Chile-Perú (PCUC) y la dinámica de advección y mezcla de nutrientes potencialmente limitantes para el crecimiento del fitoplancton.

2.2. Hipótesis de Trabajo y Objetivos Específicos

2.2.1. Objetivo específico 1: Determinar la evolución temporal de los eventos de viento favorables a surgencia en la zona centro-sur de Chile durante los últimos 25 años, junto con evaluar si los vientos Sur-oeste durante la estación de invierno, presentan una intensidad, frecuencia y duración similares a los presentes en primavera-verano.

Fundamento de la hipótesis: La surgencia presenta un ciclo gobernado por la frecuencia sinóptica (Jury et al., 1985; Sobarzo et al., 2010; García-Reyes et al., 2014), escala de tiempo que se ajusta a la dinámica biogeoquímica en los sistemas de surgencia de borde oriental (Montecino et al., 2004; Botsford et al., 2006; Jacob et al., 2011; García-Reyes et al., 2014). El período de tiempo sinóptico y la posibilidad que los vientos del suroeste estén presentes durante todo el año, pueden promover los eventos surgencia no tan solo en primavera-verano, sino también durante otoño e invierno, tópico que ha sido poco estudiado en Chile. De hecho, el supuesto actual establece que este sistema es solamente influenciado por la surgencia durante la época de primavera-verano (e.j. Cuevas et al., 2004; Böttjer y Morales, 2005; Cornejo et al., 2007). Basado en esto, se plantean las siguientes hipótesis.

Hipótesis 1: La frecuencia e intensidad de vientos favorables a surgencia en la zona costera frente a Concepción (36°S) durante otoño-invierno, pueden generar eventos favorables a surgencia de gran magnitud, comparables a los que se presentan en la época estival.

Hipótesis 2: Los eventos favorables a surgencia que se presentan en la zona centro-sur de Chile han aumentado su intensidad durante el periodo 1988-2013.

2.2.2. Objetivo específico 2: Determinar la evolución temporal de los eventos de viento favorables a hundimiento en la zona centro-sur de Chile durante los últimos 25 años, junto con evaluar si estos vientos durante la estación de primavera-verano, presentan una intensidad, frecuencia y duración similares a los presentes en otoño-invierno.

Fundamento de la hipótesis: La estacionalidad en la fuerza del Anticiclón Pacífico Sur (APS), el cual migra hacia el norte durante fines de otoño y principios de invierno austral y se encuentra en su posición más costera (85º-95ºW) (Ancapichún et al., 2015), permite la llegada hacia la costa de bajas atmosféricas con circulación ciclónica del viento, es decir, vientos favorables de hundimiento (Sobarzo et al., 2007). En esta época, los vientos Sur-Sur-oeste favorables a surgencia en la plataforma centro-sur de Chile (30º-43ºS) son más débiles pues la influencia del APS, disminuye. A pesar que la estacionalidad en la migración del APS y su influencia sobre el régimen de vientos está bien documentada, la afirmación que existan épocas estacionales tan marcadas de surgencia y hundimiento, tal como ha sido afirmado por algunos trabajos en la zona, no es tan así pues los vientos favorables a hundimiento a lo largo de la costa, prevalecen en la escala de tiempo sinóptica (Garreaud et al., 2002; Garreaud y Muñoz, 2005), pudiendo presentarse durante todo el año. En base a lo anterior, se propone la siguiente hipótesis:

Hipótesis 3: Durante primavera-verano, en la zona costera frente a Concepción (36°S), la frecuencia de eventos favorables a hundimiento puede ser tan importante como en la época invernal.

2.2.3. Objetivo específico 3: Caracterizar la dinámica física de la zona sur del Sistema de Corrientes de Humboldt (30-40ºS, 70º-80ºW) utilizando un modelo físico de alta resolución y describir la variabilidad estacional e interanual de la Corriente Subsuperficial Chile-Perú (PCUC), en términos de transporte y velocidad a lo largo de la plataforma continental de Chile.

Fundamento de la hipótesis: La corriente subsuperficial Chile-Perú (PCUC), la cual presenta una variabilidad gobernada principalmente por el forzamiento ecuatorial, por el

estrés del viento y por el rotor del viento (Pizarro et al., 2002; Albert et al., 2010), transporta el Agua Ecuatorial Subsuperficial (AESS) a lo largo de la plataforma de Chile centro-sur (Silva y Neshyba, 1979; Silva et al., 2009), la cual es la responsable de la gran productividad en el SCH (Daneri et al., 2000). Esta masa de agua en épocas de surgencia activa, es advectada a la superficie aportando los nutrientes necesarios para sustentar los afloramientos fitoplanctónicos (Montero et al., 2007). En base a esto, se plantea la siguiente hipótesis:

Hipótesis 4: La Corriente Subsuperficial Chile-Perú (PCUC) disminuye su velocidad y transporte latitudinal (Sv) hacia el polo, presentando diferencias estacionales significativas.

Hipótesis 5: Un porcentaje significativo de partículas que transporta la PCUC a lo largo de la plataforma centro-sur de Chile, es trasladada a superficie a través de la surgencia.

2.2.4. Objetivo específico 4: Caracterizar la variabilidad espacial y temporal de los nutrientes potencialmente limitantes del crecimiento del fitoplancton en la zona sur del Sistema de Corrientes de Humboldt (30º-40ºS; 70º-80ºW) mediante de modelación biogeoquímica/física acoplada.

Fundamento de la hipótesis: En los SSBO se ha encontrado que el Fe (Hutchins et al., 2002; Bruland et al., 2004; Blain et al., 2008; Bonnet et al., 2008), nitrato y silicato (Echevin et al., 2008; Quiñones et al., 2010) pueden ser nutrientes limitantes para el crecimiento del fitoplancton en distintas épocas del año. El nitrógeno se asocia a las zonas de mínimo oxígeno y a procesos de desnitrificación (Pantoja et al., 2004; Kyupers et al., 2005). La distribución de estos nutrientes limitantes es gobernada principalmente por la dinámica de advección y mezcla física (Koné et al., 2009). Establecer la co-limitación de nutrientes potencialmente limitantes y luz en la zona centro-sur de Chile y como la mezcla y transporte de estos influye sobre la variabilidad espacial y temporal de la clorofila, son tópicos fundamentales para caracterizar la interacción físico-biológica en el SCH. Según este fundamento, se plantea la siguiente hipótesis:

Hipótesis 6: La advección vertical producto de la surgencia y la mezcla vertical generada principalmente por el viento se correlacionan positivamente con el ciclo anual de la clorofila en la zona centro-sur de Chile (30°-40°S; 70°-80°W).

3. MATERIALES Y MÉTODOS

Para desarrollar los objetivos específicos 1 y 2 de la presente Tesis, se utilizaron datos de la estación meteorológica del aeropuerto Carriel Sur, Talcahuano, localizada en 36º47'S; 73º04'W (Figura 3.1). Para llevar a cabo los objetivos específicos 2 y 3, se efectuaron simulaciones a través de modelación hidrodinámica y biogeoquímica acoplada en 29°-41°S; 69°-83°W (Figura 3.1). Para desarrollar estos dos últimos objetivos, se realizaron 10 años de simulación considerando un año de spin-up, que es el tiempo que toma un modelo oceánico para alcanzar un estado de equilibrio estadístico bajo el forzamiento aplicado. Por lo tanto, se utilizaron 9 años para comprender la dinámica biofísica del sistema en estudio.

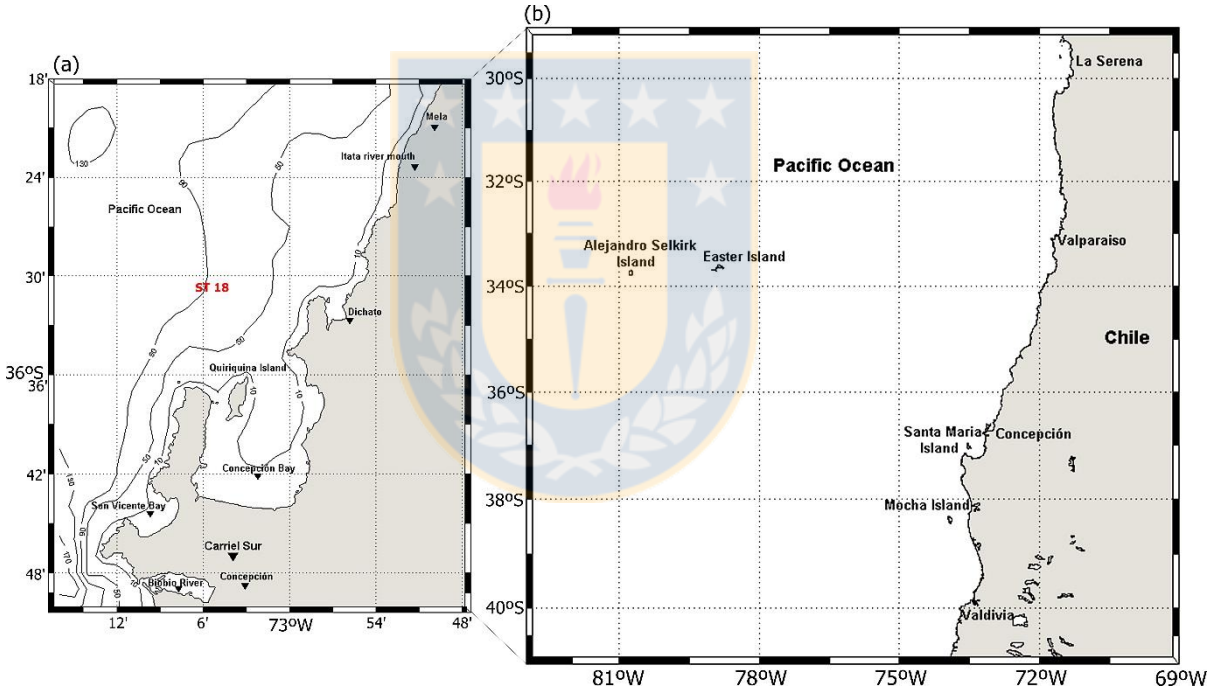

Figura 3.1: Mapa de la zona de estudio señalando la estación meteorológica Carriel Sur (a) y el dominio donde se desarrollaron las simulaciones (b). También se observa la Estación 18 (ST 18) localizada frente a Dichato (a).

Metodología del capítulo 1: Variabilidad diaria, sinóptica, estacional e interanual de los eventos favorables a surgencia/hundimiento en la zona sur del Sistema de Corrientes de Humboldt

Datos utilizados:

Los datos utilizados provienen de una estación meteorológica localizada en el Aeropuerto carriel Sur, Talcahuano (Lat. 36º47'S; Long.73º04'W, Figura 3.1). Se analizó una serie de 25 años, cuyo inicio fue el 21 de marzo de 1988 y su finalización el 30 de abril de 2013. Los datos de magnitud y dirección del viento fueron registrados cada 10 minutos. Para efectos de esta investigación, se trabajó con datos promedio horario. Los días 29 de febrero, correspondientes a años bisiestos (1988, 1992, 1996, 2000, 2004, 2008 y 2012) fueron eliminados de la serie total de tiempo.

La dirección del viento fue corregida considerando la declinación magnética de la zona durante el año 2016. Posteriormente, la dirección del viento fue alineada en relación a la línea de costa (18° respecto al Norte geográfico). Finalmente, el viento fue rotado en 180° invirtiendo la dirección del viento desde donde viene hacia donde va.

Cálculos:

Se calcularon las componentes V y U (meridional y zonal, m/s) del viento a partir de la Magnitud y Dirección, mediante las siguientes fórmulas:

Componente U (zonal) = Magnitud viento* seno (Dirección del viento) (1)

Componente V (meridional) = Magnitud del viento *coseno (Dirección del viento) (2)

A partir de las componentes anteriormente calculadas, se determinó el estrés del viento (Nm^{-2}) zonal ($\boldsymbol{\tau}_x$) y meridional ($\boldsymbol{\tau}_y$) a través de las siguientes fórmulas:

$$\tau_x = C_d * \rho_{a} * \text{comp.}U * U_{10} \quad (3)$$

$$\tau_y = C_d * \rho_{a} * \text{comp.}\ V * U_{10} \quad (4)$$

Donde C_d es el coeficiente adimensional de arrastre, aquí considerado como constante (típicamente, 0.002), ρ_a es la densidad del aire (1.24 kg/m^3), U_{10} es la velocidad del viento medida a 10 metros sobre el nivel del mar (Wo, 1982) y comp. U y comp. V corresponden a las componentes zonal y meridional, respectivamente.

Para efectos de esta tesis, se trabajó con el estrés del viento meridional ($\boldsymbol{\tau}_y$).

Una vez calculado $\boldsymbol{\tau}_y$, se separaron los valores positivos de los valores negativos para diferenciar eventos favorables a surgencia de los eventos favorables a hundimiento. Para determinar los eventos tanto favorables a surgencia como favorables a hundimiento, se realizó la suma acumulada de los valores del estrés del viento ($\boldsymbol{\tau}_y$) solo considerando horas seguidas ≥ 24 horas o equivalente a ≥ 1 día. Se obtiene de esta manera, el largo del evento y el esfuerzo acumulado máximo alcanzado en ese período de tiempo, lo cual es definido como intensidad. Por lo tanto la intensidad del evento fue determinada como el esfuerzo acumulado del estrés del viento ($\boldsymbol{\tau}_y$) durante el evento, con unidades de Nm^{-2} day (García-Reyes et al., 2014) y es calculada a través de la siguiente fórmula:

$$Intensidad = \sum_{t=1}^{t\geq 24} \tau_y \qquad (5)$$

A partir de esta fórmula se obtiene la intensidad (Nm^{-2} día) y duración (días) de cada evento. Finalmente, se obtuvo la frecuencia de los eventos, es decir, el número de eventos presentes en un mes con una intensidad (Nm^{-2} día) y duración (días) determinada cada uno de ellos.

Por otro lado, se ha comparado la intensidad ≥ 1 día con la intensidad ≥ 3 días, este último criterio, siguiendo lo sugerido por varios autores (Dugdale et al., 1990; Botsford et al., 2006; García-Reyes y Largier, 2010), los cuales plantean que vientos favorables a surgencia deben persistir por al menos tres días para obtener una respuesta ecológicamente significativa. Adicionalmente, se han separado y clasificado, los eventos en 3 categorías: eventos cortos (1-3 días), eventos medianos (3-10 días) y eventos largos (> 10 días) siguiendo la metodología propuesta por García-Reyes et al. (2014).

Finalmente, con el objetivo de determinar la variabilidad interanual, mensual y estacional del ciclo diario del estrés meridional del viento durante el periodo de estudio, calculamos el estrés del viento acumulado entre 0-11 AM y 12-23 PM. Se escogieron estos dos periodos de tiempo, ya que se han reportado previamente para esta zona diferencias notables entre el viento de la tarde y de la noche (12-23 PM) versus el viento de la mañana (0-11 AM) (Sobarzo et al., 2007).

Análisis estadístico:

Para observar la relación entre la intensidad y el largo del evento, tanto favorables a surgencia como favorables a hundimiento, se determinó la correlación entre estas dos

variables para los periodos de otoño-invierno y primavera-verano y para cada estación del año por separado. También se evalúa la relación entre la intensidad promedio anual y el periodo total de estudio.

Para esto se aplicó el coeficiente de correlación lineal de Spearman (rho), el cual es un coeficiente no paramétrico que mide el grado de covariación entre distintas variables relacionadas linealmente y cuyos valores absolutos oscilan entre 0 y 1 (Zar, 1999). Se calculó también el nivel de significancia de esta correlación (valor p). Junto con esto se aplican regresiones lineales simples, obteniendo el coeficiente de determinación (R^2). Finalmente, se realizaron test de pendientes e interceptos (Zar, 1999) para evaluar si las pendientes de las diferentes regresiones lineales analizadas presentaron diferencias significativas.

Metodología del Capítulo 2: Modelación de la dinámica de variables físicas y de la Corriente Subsuperficial Chile-Perú (PCUC) en la zona centro-sur de Chile (30°-40°S)

Modelo Hidrodinámico y Configuración de la grilla:

El modelo hidrodinámico utilizado en este estudio es el ROMS-AGRIF (Sistema Regional de Modelado Oceánico - Refinamiento de Redes Adaptativas en FORTRAN; Shchepetkin y McWilliams, 2005; Penven et al., 2006; http://www.romsagrif.org), el cual es un modelo de circulación que ha sido especialmente diseñado para realizar simulaciones precisas de los sistemas oceánicos regionales. ROMS ha sido aplicado para la simulación de diferentes regiones de los océanos del mundo entre estas, el Sistema de Surgencia de Benguela (Blanke et al., 2002), el Sistema de Corrientes de Humboldt norte (Penven et al., 2005), el Sistema de Surgencia de la Corriente de California (Renault et al., 2016) y el Sistema de Surgencia de la Península Ibérica (Cordeiro et al., 2016).

Este modelo utiliza coordenadas sigma en el plano vertical y coordenadas ortogonales-curvilíneas en el plano horizontal. El modelo resuelve las ecuaciones hidrostáticas primitivas con un esquema explícito de superficie libre.

Las ecuaciones primitivas que utiliza ROMS son las siguientes:

Conservación de Momentum:

$$\frac{\partial u}{\partial t} + \overrightarrow{u}.\nabla u - fv = -\frac{1}{\rho 0}\frac{\partial P}{\partial x} + \nabla_h(K_{Mh.}\nabla_h u) + \frac{\partial}{\partial z}(K_{Mv}\frac{\partial u}{\partial z}) \quad (6)$$

$$\frac{\partial v}{\partial t} + \overrightarrow{u}.\nabla v - fu = -\frac{1}{\rho 0}\frac{\partial P}{\partial y} + \nabla_h(K_{Mh.}\nabla_h v) + \frac{\partial}{\partial z}(K_{Mv}\frac{\partial v}{\partial z}) \quad (7)$$

Hidrostática:

$$0 = -\frac{\partial P}{\partial z} - \rho g \quad (8)$$

Continuidad:

$$0 = \frac{\partial u}{\partial x} + \frac{\partial v}{\partial y} + \frac{\partial w}{\partial z} \quad (9)$$

Conservación traza:

$$\frac{\partial T}{\partial t} + \overrightarrow{u}.\nabla T = \nabla_h(K_{Th.}\nabla_h T) + \frac{\partial}{\partial z}(K_{Tv}\frac{\partial T}{\partial z}) \quad (10)$$

$$\frac{\partial S}{\partial t} + \overrightarrow{u}.\nabla S = \nabla_h(K_{Sh.}\nabla_h S) + \frac{\partial}{\partial z}(K_{Sv}\frac{\partial S}{\partial z}) \quad (11)$$

Ecuación de estado :

$$\rho = \rho(S, T, p) \quad (12)$$

En la Tabla III se describen las variables utilizadas en las ecuaciones primitivas presentadas anteriormente.

Tabla III: Variables utilizadas en las ecuaciones primitivas del modelo ROMS

Variable	**Definición**
f (x,y)	Parámetro de Coriolis
g	Aceleración de gravedad
h (x,y)	Profundidad de fondo
K_{Mv} K_{Tv}, K_{Sv}	Difusión horizontal de momentum, temperatura y salinidad, respectivamente
K_{Mh}, K_{Th}, K_{Sh}	Difusión vertical de momentum, temperatura y salinidad, respectivamente
P	Presión total $\approx -\rho_0 gz$
t	Tiempo
S (x, y, z, t)	Salinidad
T (x, y, z, t)	Temperatura potencial
u, v, w	Las (x,y,z) componentes del vector velocidad ***u***
x, y	Coordenadas horizontales
z	Coordenada vertical
ρ *(x, y, z, t)*	Densidad

Para más detalle de las ecuaciones involucradas en ROMS, ver Shchepetkin y Williams (2005) y visitar: http://www.croco-ocean.org/.

La mezcla vertical está parametrizada usando el esquema de la capa límite de KPP (K-Profile Parameterization) (Large et al., 1994). La topografía de fondo procede de la base de datos SRTM30 (Becker et al., 2009) y fue interpolada sobre la grilla del modelo y

suavizada siguiendo a Penven et al. (2005) para reducir los errores del gradiente de presión.

Las simulación ejecutada en esta tesis, se realizó en una grilla localizada entre 29°S y 41°S y desde 69°Wa 83°W (Figura 3.1), con una resolución de 7,5 km y 32 niveles sigma. Los forzamientos atmosféricos utilizados fueron el estrés del viento de 0.25° x 0.25° SCOW (Scatterometer Climatology of Ocean Winds; Risien y Chelton, 2008) derivado de Quickscat y los flujos de calor y agua dulce fueron obtenidos de la climatología COADS (Comprehensive Ocean-Atmosphere Data Set; da Silva et al., 1994).

Se simularon 10 años, considerando 1 año de spin-up o tiempo para que la simulación alcanzara el equilibrio. 9 se utilizaron, por lo tanto, para obtener un año climatológico promedio de variables físicas como temperatura, salinidad, corrientes y nivel del mar y para realizar el análisis lagrangiano.

Corriente Subsuperficial Chile-Perú (PCUC):

Con los resultados obtenidos de la simulación, se calculó el transporte promedio mensual y estacional en diferentes latitudes: 30°S, 33°S, 36°S y 39°S, con el objetivo de determinar la variabilidad espacial y temporal del transporte de la PCUC a lo largo de la plataforma continental de la zona costera centro-sur de Chile. Para cada mes, los campos de velocidad fueron interpolados desde los niveles sigma a niveles z cada 5 metros. Posteriormente, las velocidades negativas (hacia el polo) entre la superficie y una profundidad máxima de 650 metros y entre la costa y 100 km fuera de la costa, fueron integradas para calcular el transporte.

El ancho promedio zonal de la PCUC en kilómetros y la velocidad máxima (núcleo de la PCUC) fueron determinados estacionalmente en 30°, 33°, 36° y 39°S. Se utilizó el módulo de seguimiento ROMS-off-line para calcular las trayectorias lagrangianas de las masas de agua a partir de campos de velocidad ROMS tridimensionales (Capet et al., 2004; Carr et al., 2008). Se lanzaron flotadores lagrangianos virtuales en el núcleo de la PCUC a lo largo de dos secciones transversales (33° y 37°S), con un espaciamiento vertical de 15 m en la vertical y de 2 km en la horizontal. Para cada mes de la simulación, aproximadamente 800 flotadores fueron lanzados inicialmente en la PCUC a profundidades entre 50m y 700m, y a 200 km de la costa. Sus trayectorias se integraron por seis meses, con un paso de tiempo de 14,4 min y usando salidas del modelo cada 3 días.

Se consideró que los flotadores se elevaban cuando alcanzaban la capa superficial delimitada por una profundidad de 50 metros. A continuación, se calculó la profundidad inicial de los flotadores que arribaron a 50 m dentro de las secciones de la PCUC y el tiempo de tránsito de los flotadores entre su posición inicial y final (es decir, cuando entraron en la capa superficial). Se calculó también, el promedio y la desviación estándar de las posiciones (latitud, prodifunidad y distancia de la costa) para los flotadores que no llegaron a la capa superficial (50 metros) después de 6 meses de tránsito.

Validación de la simulación:

Para evaluar la variabilidad de la altura del nivel del mar, se utilizaron datos de altimetría satelital AVISO entre los años 1992-2005 (Archiving, Validation and Interpretation of Satellite Oceanographic data; http://www.aviso.oceanobs.com/). Con estos datos se calcularon las anomalías del nivel del mar para otoño y primavera en el área de estudio. Se calculó adicionalmente, el promedio de la energía cinética de remolinos (EKE), a partir de las anomalías superficiales de las corrientes geostróficas derivadas de las anomalías del nivel del mar. El mismo cálculo se realizó con las salidas del modelo ROMS.

Se utilizaron datos satelitales de Temperatura Superficial del Mar (TSM) del producto AVHRR (Advanced Very High Resolution Radiometer) Pathfinder version 5.0 (Casey et al., 2010) para compararlos con la TSM de la simulación. Adicionalmente, secciones a través de la costa de temperatura y salinidad promedio ROMS en 32º y 36ºS, fueron comparadas con observaciones provenientes de la base de datos climatológica CSIRO (Atlas of Regional Seas-2006; CARS2006; Dunn y Ridgway, 2002; Ridway et al., 2002). Finalmente, se utilizaron datos de tres cruceros oceanográficos realizados en verano entre 35.5–40°S y entre 72.75–77.8°W, llevados a cabo por el Fondo de Investigación Pesquera y Acuicultura, Ministerio de Economía, Chile: FIP (http://www.subpesca.cl/fipa/613/w3-propertyname-678.html), para observar la presencia de las masas de agua presentes en el área y determinar el porcentaje de cada masa entre 0 y 700 metros. Los cruceros FIP fueron llevados a cabo en Diciembre de 2005 (FIP 2005-01), enero de 2009 (FIP 2008-20) y enero de 2011 (FIP 2009-39). Los diagramas TS y el porcentaje de masas de agua, fueron comparados con los resultados provenientes de la simulación ROMS.

Metodología Capítulo 3: Modelación de la variabilidad espacial y temporal del transporte de nutrientes potencialmente limitantes del crecimiento del fitoplancton en la zona sur del Sistema de Corrientes de Humboldt (30°-40°S)

Modelación Física: Detallada en el capítulo 2.

Modelación biogeoquímica: El modelo biogeoquímico PISCES (Pelagic Interactive Scheme for Carbon and Ecosystem Studies; Aumont et al., 2003; Aumont y Bopp, 2006; Aumont et al., 2015) fue elegido para representar la variabilidad del fitoplancton y la co-limitación de nutrientes a lo largo de la plataforma continental de la zona sur del Sistema de Corrientes de Humboldt.

PISCES simula los ciclos de carbono, oxígeno y los principales nutrientes que controlan el crecimiento del fitoplancton (PO_4^{3-}, NO_3^-, NH_4^+, Si, Fe). En este modelo el crecimiento del fitoplancton depende de las concentraciones externas de nutrientes. PISCES incluye dos clases de fitoplancton (diatomeas y nanofitoplancton) y dos clases de zooplancton (micro y mesozooplancton). Este modelo incorpora tres compartimentos "no vivos", estos son, materia orgánica disuelta semilábil, pequeñas partículas que se hunden y grandes partículas que se hunden. A continuación se presenta un esquema general que representa la arquitectura del modelo PISCES (Figura 3.2)

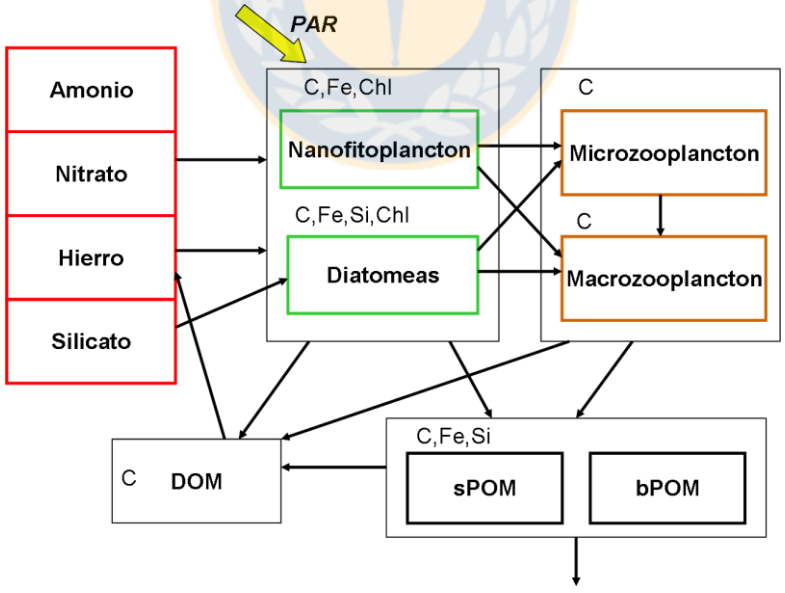

Figura 3.2: Arquitectura del modelo PISCES extraído de Aumont y Bopp (2006). Este esquema muestra el modelo ecosistémico omitiendo el oxígeno y el sistema de carbonato. Los elementos que están explícitamente modelados se indican en la esquina izquierda de cada cuadro.

Una descripción detallada de la estructura del modelo y las ecuaciones se pueden encontrar en Aumont et al. (2015).

Los campos biogeoquímicos de PISCES (nitrato, fosfato, silicato, oxígeno, carbono inorgánico disuelto, carbono orgánico particulado, alcalinidad) fueron iniciados en el dominio e impuestos en los límites abiertos del modelo utilizando la climatología CARS 2009 (CSIRO Atlas of Regional Seas, http://www.marine.csiro.au/~dunn/cars2009; Ridgway et al., 2002/). Las concentraciones de Fe se obtuvieron a partir de un modelo de climatología global (ORCA2-PISCES; Aumont et al., 2015), de Tegen y Fung (1995) y de Moore et al. (2004).

Colimitación de luz y nutrientes: La potencial limitación por luz y nutrientes fue estimada calculando los términos de limitación en la parametrización del modelo de producción primaria (Aumont et al., 2015). El modelo de producción primaria es proporcional a los términos de limitación de luz y nutrientes.

La limitación por luz fue calculada como:

$$L_{light} = 1 - e^{(-\alpha\left(\frac{Chl}{C}\right)*\frac{PAR}{\mu Lnut})} \quad (13)$$

Donde α es la pendiente inicial de la curva PI, Chl/C es el radio clorofila/carbono, PAR es la radiación fotosintéticamente activa y μ es la tasa de desarrollo dependiente de la temperatura. Cuando hay suficiente luz disponible, este término alcanza el valor 1, si la luz limita el desarrollo, este término tendrá valores <1.

La limitación por nutrientes se calculó con la siguiente fórmula:

$$L_{nut} = \min_{i=1\ldots n}\left[\left(\frac{C_i}{K_{i+C_i}}\right)\right] \quad (14)$$

Donde i, indica el nutriente específico (PO_4^{3-}, NO_3^-, NH_4^+, Si, Fe), C_i es la concentración del nutriente y K_i, es la constante de saturación media.

Dado que las diatomeas son las que contribuyen en mayor porcentaje a la clorofila total en la simulación (70%), la co-limitación de nutrientes sólo se calculó para este grupo de fitoplancton.

El denominado "nutriente limitante" en nuestro estudio es el (i0) con la proporción más baja:

$$\frac{C_i}{K_{i+C_i}} \leq \frac{C_i}{K_{i+C_i}} \quad (15)$$

Para determinar los mecanismos físicos que transportan nutrientes en la capa eufótica, la advección zonal (-U∂xC), meridional (-V∂yC) y vertical (-W∂zC), junto con la mezcla vertical (∂z(K∂zC) fueron calculados, donde U, V, W corresponden a los términos de velocidad zonal, meridional y vertical, respectivamente. K es la difusividad vertical, C la concentración de nutrientes y x, y, z las coordenadas zonal, meridional y vertical, respectivamente.

Se han simulado 15 años de ROMS/PISCES acoplado, considerando un periodo de spin-up de 5 años. Por lo tanto, 10 años fueron promediados para obtener la climatología de las variables biológicas a estudiar. Los parámetros biológicos utilizados en esta tesis, fueron similares a los de Echevin et al. (2014) y están descritos en la Tabla IV.

Tabla IV: Parámetros utilizados en la simulación PISCES (Echevin et al., 2014).

PISCES parameters	Standard value (Kane et al., 2011)	Value in Albert et al. (2010)	Parameter definition
Conc0	2.e-6	-	phosphate half saturation (umolP l−1)
Conc1	10E-6	-	phosphate half saturation for diatoms (umo P l−1)
Conc3	0.1E-9	-	iron half saturation for diatoms (nmo Fe l−1)
Grosip	0.151	0.08	mean Si/C ratio
Pislope	4	3	P-I slope for nano ((Wm−2)−1 d−1)
Pislope2	4	3	P-I slope for diatoms ((Wm−2)−1 d−1)
Excret	0.05	0.1	excretion ratio of nano
Excret2	0.05	0.1	excretion ratio of diatoms
Wsbio	3	**6**	POC sinking speed (m d−1)
Wsbio2	50	**20**	big particles sinking speed (m d−1)
Wchl	0.001	-	maximum aggregation rate for nano (d−1 molC−1)
Wchld	0.02	-	Maximum aggregation rate for diatoms (d−1 molC−1)
Resrat	0.03	-	exudation rate of zooplankton
Resrat2	0.008	0.005	excretion rate of mesozooplankton
Mprat	0.01	-	phytoplankton mortality rate (d−1)
Mprat2	0.01	-	diatoms mortality rate (d−1)
Grazrat	4	-	maximal microzoo grazing rate (d−1)
Grazrat2	0.7	-	maximal mesozoo grazing rate (d−1)
Mzrat2	0.03	0.05	mesozooplankton mortality rate ((umolC l−1) d−1)
Xprefc	1	-	zoo preference for phyto
Xprefp	0.	-	zoo preference for POC
Xprefz	1	-	zoo preference for zoo
Unass	0.3	-	nonassimilated fraction of phyto by zoo
Unass2	0.3	-	nonassimilated fraction of P by mesozoo
Xkgraz	20.E-6	-	half saturation constant for grazing (umolC l−1)
Xkgraz2	20.E-6	-	half saturation constant for grazing 2 (umolC l−1)
Xkmort	1.E-7	-	half saturation constant for mortality (umolC l−1)
Xksi1	2.E-6	1.5E-6	half saturation constant for Si uptake (umolSi l−1)
Xksi2	3.33E-6	4E-6	half saturation constant for Si/C (umolSi l−1)
Xremip	0.025	-	Degradation rate of POC (d−1)
Xremik	0.3	**2**	remineralization rate of DOC (d−1)
Xsirem	0.015	0.015	remineralization rate of Si (d−1)
Xkdoc2	417.E-6	-	second half-sat. of DOC remineralization (umolC l−1)
Xprefpoc	0.2	-	zoo preference for POC
Concnnh4	1.E-7	-	NH4 half saturation for phyto (umol P l−1)
Concdnh4	5.E-7	-	NH4 half saturation for diatoms (umol P l−1)
Nitrif	0.05	**0.05**	NH4 nitrification rate (d−1)
Epsher2	0.33	-	efficiency of mesozoo growth
Epsher	0.33	-	efficiency of microzoo growth
Sigma1	0.6	-	fecal pellets production
Sigma2	0.6	-	fecal pellets production
Zprefp	0.6	0.5	microzoo preference for nanophyto
Zprefd	0.5	-	microzoo preference for diatoms
Chlcnm	0.033	-	minimum Chl/C in nanophytoplankton (mgChl/mgC)
Chlcdm	0.05	-	minimum Chl/C in diatoms (mgChl/mgC)
cmask	0.1	0.1	nearshore source input of iron

Validación de la simulación ROMS/PISCES:

Se utilizó la capa de mezcla (MLD) climatológica de de Boyer Montégut et al. (2004), la cual tiene una grilla regular de 2º x 2º y una resolución mensual, para validar la MLD de la simulación ROMS.

La concentración de clorofila superficial estimada por el modelo ROMS/PISCES fue comparada con datos satelitales SeaWiFS durante el período 2000-2006 (http://oceancolor.gsfc.nasa.gov/SeaWiFS/).

Se utilizaron datos de la estación 18 ubicada en la plataforma centro-sur de Chile (36.5 ° S, 73.1°W; ver Figura 3.1) para construir una climatología mensual durante el período 2004-2014 de variables in situ como nitrato, fosfato, silicato y clorofila. Estas climatologías fueron comparadas con lo obtenido en la simulación ROMS/PISCES.

Cabe destacar que la estación 18 es una serie temporal iniciada por el Centro Oceanográfico COPAS en 2002, ubicada en la plataforma continental a 94 m de profundidad (Escribano y Schneider, 2007).

4.- CAPÍTULO DE RESULTADOS

4.1. Capítulo 1. Variabilidad interanual de los eventos favorables a surgencia y a hundimiento en la zona centro-sur de Chile (36ºS).

La literatura oceanográfica actual en la zona sur de la Corriente de Humboldt (centro-sur de Chile) asume en gran medida la marcada estacionalidad en los vientos favorables a surgencia (primavera-verano) y en los vientos favorables a hundimiento (otoño-invierno). Sin embargo, la presencia durante todo el año de vientos suroeste/noroeste que son potencialmente capaces de inducir la surgencia/hundimiento no sólo durante la primavera-verano/otoño-invierno, sino también en otoño-invierno/primavera-verano, no ha sido determinada. Junto a lo anterior, la evolución temporal de los eventos favorables a surgencia y de los eventos favorables a hundimiento en un sistema de clima cambiante, debe ser evaluada. Profundizar en el estudio del hundimiento, es particularmente importante ya que la literatura, tanto en el Sistema de Corrientes de Humboldt (norte y sur), como en la mayoría de los Sistemas de Surgencia de Borde Oriental, es escasa.

Los resultados mostraron una notable disminución ($p<0.05$) de la intensidad de la surgencia y su duración los últimos 25 años. A pesar de esto, la frecuencia en el número de eventos aumentó, es decir, los eventos son cada vez menos intensos, más cortos, pero más frecuentes. Por otro lado el hundimiento exhibió cambios considerables pero solamente en su intensidad, la cual al igual que la surgencia, disminuyó los últimos 25 años. La frecuencia y duración de los eventos de hundimiento, no han experimentado cambios significativos ($p>0.05$). Por otra parte, hemos encontrado que el número de eventos favorables a surgencia en la época otoño-invierno, es similar al número de eventos de primavera-verano, a pesar de esto, los eventos de la época otoño-invierno, no presentan la duración ni la intensidad de los típicos eventos de la época estival. También se observó un alto número de eventos favorables a hundimiento en primavera-verano, aunque considerablemente menor a los eventos de otoño invierno. Nuestros resultados demuestran que la dinámica intra e interanual de eventos favorables a surgencia/hundimiento en la zona centro-sur de Chile es más compleja de lo que se asumía previamente. Es necesario replicar y comparar nuestros análisis con otras fuentes de datos, tales como datos satelitales y datos de otras estaciones meteorológicas.

Interannual variability in upwelling and downwelling favorable wind events off central-southern Chile (36ºS)

Odette Vergara[1,2], Renato A. Quiñones[1,2,3,5], Rodrigo Montes[1,4], Eduardo Hernández-Miranda[1,5] & Marcus Sobarzo[1,2]

[1]Interdisciplinary Center for Aquaculture Research, Universidad de Concepción, Concepción, Chile

[2]Doctoral Program in Oceanography, Department of Oceanography, Universidad de Concepción, Concepción, Chile

[3]Department of Oceanography, Universidad de Concepción, Concepción, Chile

[4]COPAS Sur-Austral Program, Universidad de Concepcion, Casilla 160-C, Concepción, Chile

[5]Programa de Investigación Marina de Excelencia (PIMEX), Facultad de Ciencias Naturales and Oceanográficas, Universidad de Concepción, Concepción, Chile

*Artículo en preparación

Abstract

Current oceanographic literature about the southern part of the Humboldt Current (central southern Chile) has largely assumed that there is marked seasonality with regard to upwelling-favorable winds (spring-summer) and downwelling-favorable winds (autumn-winter). However, to date no quantitative study has been carried out to assess the presence of southeastern and northeastern winds capable of inducing upwelling and downwelling throughout the year. In fact, the knowledge on downwelling in eastern boundary systems is very scarce. Furthermore, the temporal evolution of upwelling- and downwelling-favorable events in this zone needs to be assessed in the context of climate change.

Our results show a notable decrease ($p<0.05$) in the intensity and duration of upwelling events in the last 25 years. Despite this, the frequency of events is increasing, that is the events are progressively less intense, shorter, but more frequent. A significant decrease in the intensity of downwelling-favorable events was found in the last 25 years. No significant changes were found in either the frequency or duration of downwelling events ($p>0.05$). The number of upwelling-favorable events in autumn-winter was similar to the number in spring-summer. However, the events in autumn-winter did not have the duration or the intensity of typical events in spring-summer. A high number of downwelling-favorable events were observed in spring-summer, although they were considerably less intense than events occurring in autumn-winter. Our results show that intra- and interannual dynamics of upwelling- and downwelling-favorable events in central southern Chile are more complex than previously assumed.

1. Introduction

The marine climate along the west coast of South America is the product of the interaction between basin-scale atmospheric systems and local and regional effects along the continent-ocean boundary. The South Pacific Anticyclone is the dominant atmospheric system, driving winds toward the equator along the coast of Chile and Peru. Associated with this anticyclone there is subsidence inversion at the top of the marine boundary layer that generates coast-ocean temperature gradients that in turn affect wind stress regionally along the coast (Strub et al. 1998).

There are different wind patterns along the Chilean coast. Prevailing winds between 20ºS and 35ºS favor coastal upwelling throughout the year owing to the South Pacific Anticyclone, which grows stronger and shifts southward in the austral summer (Strub et al., 1998). However, pronounced disturbances arise south of 27ºS, caused by the polar front on a synoptic scale (2-10 days) (Rutllant and Montecino, 2002). These disturbances generate coastal atmospheric lows that propagate as trapped atmospheric coastal waves (Strub et al. 1998), producing enhanced cycles of relaxation and upwelling over periods of 3 to 10 days (Rutllant 1993).

Winds in central-southern Chile (35ºS-45ºS) alternate between northern (downwelling-favorable), which are due to the polar front in winter, and southern (upwelling favorable), which are produced produced by the strengthening of the anticyclone in summer (Sobarzo et al. 2007). In addition to displaying marked synoptic frequencies, the wind in this zone is highly variable over a diurnal period (e.g. sea breeze) as a result of thermal ocean-land gradients that are stronger in spring-summer (Sobarzo et al. 2010). As a consequence of intense and persistent periods of upwelling activity between 36ºS and 38ºS, the subsurface poleward current near the coast extends along the sea floor and upwells with Equatorial Subsurface Water, resulting in low oxygen conditions (e.g. Ulloa and Pantoja 2009; Fuenzalida et al. 2009; Hernández-Miranda et al. 2010) and high nutrient concentrations that favor primary production (10-20 g C/m^2 day annual average; Daneri et al. 2000; Montero et al. 2007). Associated with upwelling events, low temperature plumes originate near the coast and propagate 50 to 150 km offshore, affected by the topography of the area (points, bays, river canyons, etc.), generating cyclonic or anticyclonic gyres (Leth and Middleton 2004) that transport chlorophyll (Chl-a) to offshore systems (Morales et al. 2012; Correa-Ramirez et al. 2012).

The variability of the Chilean coastal ocean has been widely studied, given that upwelling and other phenomena triggered by wind influence the distribution and abundance of fishery resources (Cubillos et al. 2007; Quiñones et al. 2009; Hernández et al. 2011), plankton (Daneri et al. 2012; Escribano et al. 2012), epibenthic macro- and megafauna (Veas et al. 2012; Hernández-Miranda et al. 2012), and water column biogeochemistry (Quiñones et al. 2010; Fernández and Farías 2012). The oceanographic literature on central-southern Chile largely assumes that there is marked seasonality in upwelling-favorable winds and thus a seasonal ecosystem response to this process (e.g. Cuevas et al. 2004; Montero et al. 2007). However, to date no quantitative study has been carried out to assess the presence of southeastern and northeastern winds capable of inducing upwelling and downwelling throughout the year.

Important biophysical consequences of upwelling have been observed at different time scales in the coastal ocean in other parts of the world. For example, Santos et al. (2001, 2004) concluded that an increase in upwelling events along the Portuguese coast has an important negative impact on mackerel and sardine recruitment during their spawning seasons. Varela et al. (2010) studied biogeochemical responses and bentho-pelagic coupling during winter upwelling, highlighting that events such as these have become recurrent along the western Iberian platform (Álvarez et al. 2003). Varela et al. (2010) reported the presence of a phytoplankton bloom during the study period as a consequence of solar radiation associated with NE upwelling-favorable winds, leading to a well-mixed water column. Schroeder et al. (2009) hypothesized that "anomalous" winter upwelling in the California current fertilizes the region with nutrients that ensure sufficient prey productivity and availability to maintain adult seabird populations in a healthy state and even result in an early reproductive period. Black et al. (2011) determined the existence of winter and summer upwelling conditions in the California Current. The former was characterized by high frequency variability associated with the North Pacific High and El Niño events, while the latter was associated with low frequency processes (multidecadal). The differentiation between these two sets of conditions could be important, not only on inter-annual time scales, but also in relation to long-term trends associated with climate change.

In addition to deepening our knowledge about the differences between autumn-winter and spring-summer upwelling-favorable winds along the coast of central-southern Chile in the last 25 years (1988-2012), we are interested in knowing whether there are significant differences between spring-summer and autumn-winter downwelling-favorable winds,

and whether there have been changes in the last 25 years in the intensity, duration and number of downwelling events.

As in other eastern boundary upwelling systems, winds in the Humboldt Current in central-southern Chile alternate between favoring upwelling and downwelling (Strub et al., 2013). The wind regime in the HCS is mainly controlled by the migration of the South Pacific Anticyclone (SPA), which gets stronger and shifts south in the summer and weakens and shifts north in the winter (Rutllant and Fuenzalida, 1991). The movement of the SPA in the winter results in the dominance of polewards northeastern winds favorable to downwelling (Garreaud and Muñoz, 2005).

There are few studies on downwelling-favorable winds in the Humboldt Current System. Castro et al. (2000) found that, under winter downwelling conditions, the highest levels of microplankton abundance off the coast at Concepción and Talcahuano (36.5°S) were located along multiple hyaline and thermal front structures, concurrent with the maximum densities of anchovy eggs and larvae. Narváez et al. (2006) found that large-scale warming events off the coast of central Chile (33°30'S) are associated with downwelling-favorable winds that are sometimes present in spring and summer. They reported that during these events there is significant synchronicity in the reccruitment of several invertebrate groups (decapods, gastropods, polychaetes, mussels and sea urchins), suggesting that the larvae are dragged by these advective fronts and released on the coast. It has been shown that microzooplankton grazing can remove an important fraction (>100%) of primary production in periods of downwelling-favorable winds in the HCS near Concepción (36°S) (Böttjer and Morales, 2004), indicating that there can be significant grazing pressure on phytoplankton beyond spring and summer.

In addition to the increase of downwelling-favourable winds during autumn and winter, estuarine circulation has been observed in autumn and winter due to the increase in fresh water inflow from the land, which creates opposing offshore and onshore flows in the surface and lower water column, respectively (Montecino et al., 2004). Residence times in the bays increase during the downwelling period. For example, residence time in the Bay of Concepción is typically 22 days during the estuarine season and 2 to 3 days during the upwelling season (Montecino et al., 2004).

In other SSBSs like the California Current system (CCS), poleward winds that prevail in the winter, together with downwelling, produce a depression or deepening of the pycnocline in the coast and forces surface waters toward the platform (Smith et al., 1994). The downward movement of the pynocline pushes subsurface waters rich in carbon and

nutrients crucial for phytoplankton growth from the continental shelf toward other adjacent ocean basins (Hales et al., 2005). The net annual carbon budget is directly affected by upwelling and downwelling, as well as by the bathymetric characteristics of the continental shelf (Ianson et al., 2009).

The intensity of winter downwelling has increased in the last 50 years in the northern part of the CCS (Foreman et al., 2011). Several models predict an increase in downwelling-favorable winds by 2100, although this prediction has not been confirmed by statistically significant trends (Merryfield et al., 2009). Various indicators have been used to estimate the beginning and development of an upwelling, including surface chlorophyll (Henson and Thomas, 2007), temperature (Tapia et al., 2009; Benazzous et al., 2014) and nutrients concentration (García-Reyes et al., 2014). However, only a few authors (Bograd et al., 2009; Foreman et al., 2011, Bylhouwer et al., 2013) have studied the timing (beginning, duration and end) of the downwelling period.

Better understanding is needed of downwelling dynamics at different temporal and spatial scales in central-southern Chile. As well, more in-depth comparison needs to be made of downwelling events in autumn and winter with those less frequent events in spring and summer, on the Chilean coast.

The objective of this work is to characterize and evaluate downwelling- and upwelling-favorable winds in terms of their duration, intensity and number of events monthly and annually, as well as seasonal differences. We seek to determine whether downwelling- and upwelling-favorable winds have increased or decreased in the last 25 years (1988-2012) and to evaluate if there are patterns associated with events like El Niño or La Niña.

2. Materials and methods

Wind data were taken at a meteorological station at Carriel Sur Airport, Talcahuano (36º47'S, 73º04'W, measured at 12 m high) (Figure 1). A 25-year time series was analyzed (21/03/1988-30/04/2013), in which wind magnitude and direction were recorded every 10 min. For the effects of this research, we worked with average hourly data. We eliminated February 29 for leap years (1988, 1992, 1996, 2000, 2004, 2008 and 2012) from the time series.

Wind direction was corrected based on the magnetic declination of the area in 2016. The wind direction was then aligned to the coast (18° with respect to the geographic north). Finally, the wind was rotated 180°, inverting the direction from where it's coming to where it's going.

The wind magnitude vector was broken down into east-west (perpendicular to the coast) and north-south (alongshore) components to determine wind stress ($\boldsymbol{\tau}_x$ and $\boldsymbol{\tau}_y$) (N m^{-2}). Once wind stress along the coast was calculated, we separated negative and positive values to differentiate between upwelling- and downwelling-favorable events. To determine both upwelling- and downwelling-favorable events, meridional wind stress values were added together, only considering consecutive hours. Accumulated positive and negative wind stress were calculated for spring-summer and autumn-winter. The accumulated positive along-shore wind stress can be used as a proxy of upwelling intensity in a given year (Barth et al. 2007; García-Reyes et al. 2014).

To determine inter-annual, monthly and seasonal variability of daily wind cycles, we calculated wind stress accumulated from noon to 23:00 pm and from midnight to 11:00 am. These two periods were chosen because notable differences had been reported between daytime and nighttime winds in the area (Sobarzo et al., 2007). We subsequently considered the periods ≥ 1 and ≥ 3 days, the latter having been recommended by several authors (Dugdale et al., 1990; Botsford et al., 2006; García-Reyes and Largier, 2010) who noted that upwelling-favorable winds have to blow for at least three days to obtain an ecologically significant response. We also separated events into three categories, short (1-3 days), medium-length (3-10 days) and long (> 10 days), following the methodology proposed by García-Reyes et al. (2014). We obtained the lengths of events and the accumulated force reached in this time period, which together are defined as intensity. In effect, the intensity of an event is determined as the accumulated effort of wind stress during the event, with units of Nm^{-2} day (García-Reyes and Largier, 2014).

Spearman correlation analysis (Zar, 1999) was done between length and intensity for both upwelling and downwelling favorable events. An F test for multiple comparisons among slopes and elevations, as described by Zar (1999), was used in comparing linear regression equations

Results

3.1. Intensity and length of the upwelling and downwelling events (dd>= 1 day)

The correlation between event intensity and length was determined for the autumn-winter and spring-summer periods throughout the series (Figure 2). The correlations for both periods were similar during upwelling-favorable events (rho=0.81, $p<0.05$, autumn-winter; rho=0.89, $p<0.05$, spring-summer). There were 754 upwelling-favorable events in autumn-winter (Figure 2a) and 767 in spring-summer (Figure 2b). In autumn-winter the maximum intensity was reached (~10 Nm^{-2} day) at ~11 days in April (Figure 2a), while in spring-summer it was reached (~25 Nm^{-2} day) at ~15 days in November and January (Figure 2b). The slopes of the two regressions (0.6, autumn-winter and 1.3, spring-summer) were different (α=0.05, error=0.0014).

With downwelling-favorable events, there were high correlations between event intensity and length in both periods (rho=0.71, $p<0.05$, autumn-winter; rho=0.64, $p<0.05$, spring-summer). There were 523 downwelling-favorable events in autumn-winter (Figure 2c) and 352 in spring-summer (Figure 2d). The maximum intensity (>25 Nm^{-2} day) in autumn-winter was reached at ~8 days in July (Figure 2c), and the maximum intensity (~10 Nm^{-2} day) in spring-summer was at ~6 days in September (Figure 2d). The slopes of the two regressions (3 for autumn-winter, and 1.5 for spring-summer) were different (α=0.05, error=0.0086).

There where 427 upwelling-favorable events in autumn and 327 in winter, with similar correlations between event intensity and length (days) in the two periods (rho= 0.82, $p<0.05$, autumn; rho=0.81, $p<0.05$, winter) (Figures 3a and 3b). There were 432 upwelling-favorable events in spring and 335 in summer, with similar correlations between event intensity and length (days) in the two seasons (rho=0.91, $p<0.05$ and rho=0.88, $p<0.05$, respectively) (Figure 3c and 3d). The slopes and intercepts for the last two periods did not present significant differences. Although there was a large number of upwelling-favorable events in the four analyzed periods, there were differences in the

maximum intensity, which was 10 Nm^{-2} day in autumn (12 days), 8 Nm^{-2} day in winter (9 days) and 25 Nm^{-2} day in spring and summer (15 days) (Figure 3a, b, c, d).
There were 279 downwelling-favorable events in autumn and 244 in winter, with similar correlations between event intensity and length (days) in the two seasons (rho= 0.71, $p<0.05$, autumn; rho=0.74, $p<0.05$, winter) (Figure 3e and 3f). There were 194 events in spring and 158 in summer, with similar correlations between the two periods (rho=0.64, $p<0.05$ and rho=0.68, $p<0.05$, respectively) (Figure 3g and 3h). The slopes and intercepts of the regressions for these two seasons did not present significant differences. Although there was a high number of downwelling-favorable events in the four seasons, there were differences in the maximum intensity: 25 Nm^{-2} day in autumn and winter (8 days), 10 Nm^{-2} day in spring (6 days) and ~11 Nm^{-2} day in summer (5 days) (Figures 3e, f, g, h).

3.2. Interannual and seasonal variability of upwelling and downwelling-favorable events
To determine interannual differences in the number of upwelling-favorable events in autumn-winter and spring-summer, the months of the two periods were considered separately (Figures 4 and 5). The spring-summer months in which the highest number of upwelling-favorable events were registered were: January (133) (Figure 4e), October (132) (Figure 4b), December (129) (Figure 4d) and November (122) (Figure 4c), while the lowest number of events were registered in: September (50) (Figure 4a), March (99) (Figure 4g) and February (107) (Figure 4f). The upwelling–favorable event with the greatest intensity during September occur in 1993 (~8 Nm^{-2} day) and the events with the lowests intensities in this month were in 1999, 1997 and 2012 (>5 Nm^{-2} day) (Fig. 4a). The average intensity of upwelling –favorable events in September was ~5 Nm^{-2} day (Fig. 4a). The most intense upwelling-favorable event in October was in 1998 (~18 Nm^{-2} day) and the lowest intensities in October were in 1991, 1994, 1995, 2000, 2004 and 2012 (Figure 4b). The highest intensities of upwelling-favorable event in this month were in the first ten years of the series (1988-1998), after which the level began to decrease (Figure 4b). The most intense upwelling-favorable event occurring in November was in 1995 (~24 Nm^{-2} day), followed by 1989 (~20 Nm^{-2} day) (Figure 4c). The most intense upwelling-favorable event (~25 Nm^{-2} day; Figure 4d) were registered in December in the year 1994. As October, the highest intensities registered in December occurred in the first ten years of the series (1988-1998), with an average intensity range between ~5 and 10 Nm^{-2} day (Figure 4d). January exhibited the largest number of years with high intensity upwelling-favorable events, the highest were observed in 1990 (~23 Nm^{-2} day), followed

by 1999 (~22 Nm^{-2} day), 2009 (~20 Nm^{-2} day) and 1995 (~18 Nm^{-2} day) (Figure 4e). The average ranged of intensity was between ~2 and 12 Nm^{-2} day (Figure 4e). The highest intensities of upwelling-favorable events during February were in the years 1993 and 1997 (~16 Nm^{-2} day) (Figure 4f). The most intense upwelling-favorable event in March was in 1995 (~23 Nm^{-2} day) (Figure 4g).

The autumn-winter months in which more upwelling-favorable events were registered were April (139) (Figure 4i), May (134) (Figure 4j), July (125) (Figure 4l) and August (122) (Figure 4m). The autumn-winter months in which less upwelling-favorable events were registered were March (51) (Figure 4h), June (105) (Figure 4k) and September (82) (Figure 4n). The most intense upwelling-favorable event registered in March (autumn-winter) was in 1988 with ~10 Nm^{-2} day. The average trend in this month was between ~1 and Nm^{-2} day (Figure 4h). The most intense event occurred in April was in 2011 (~9 Nm^{-2} day), followed by 1993 (~7 Nm^{-2} day) and 1989 (~6 Nm^{-2} day), the average was ~3 Nm^{-2} day (Figure 4i). The highest intensity in May was in 2011 (~6 Nm^{-2} day), the average intensity in this month was ~2.5 Nm^{-2} day (Figure 4j). As May, the average intensity in June was ~2.5 Nm^{-2} day, with the highest intensities registered during 2011 and 2012 (~4 Nm^{-2} day) (Figure 4k). The lowest average intensities for the autumn-winter period were registered in July (<2 Nm^{-2} day) and the highest intensities were observed in 2010 and 2012 (~4 Nm^{-2} day) (Figure 4l). The highest intensity in August was in 1990 (~7 Nm^{-2} day), with an interannual average trend of ~2 Nm^{-2} day (Figure 4m). The highest intensity in September was in 1996, with ~8 Nm^{-2} day. The average intensity for this month ranged from ~1 to 5 Nm^{-2} day (Figure 4n).

To determine interannual differences in the number of downwelling-favorable events in autumn-winter and spring-summer, the months of the two periods were considered separately (Figure 5). The autumn-winter months in which more downwelling-favorable events were registered were June (107) (Figure 5d), July (98) (Figure 5e), August (91) (Figure 5f) and May (84) (Figure 5c). The months with the fewer events were March (20) (Figure 5a), September (55) (Figure 5g) and April (68) (Figure 5b). The most intense downwelling-favorable event occurred in March was in 1990 with ~7 Nm^{-2} day (Fig. 5a). There were several years in which no downwelling-favorable events were observed during this month (1991, 1997, 1998, 1999, 2005, 2006, 2009 and 2012; Figure 5a). The most intense downwelling-favorable event occurred in April were in 1995, 1997 and 2004 (~14 Nm^{-2} day), and the average ranged between ~1 and 8 Nm^{-2} day (Figure 5b). The highest intensity of downwelling-favorable event occurred in May was in 1991 with >25

Nm^{-2} day, followed by 2012 (~20 Nm^{-2} day) (Figure 5c). High intensities were registered several years in June, the highest was in 1989 (~24 Nm^{-2} day), followed by 2000 (~22 Nm^{-2} day) and then by 1993, 1996, 2003, 2006 and 2010(Figure 5d). The highest intensities in July were in 2008 (>25 Nm^{-2} day), 1988 (24 Nm^{-2} day), 1994 and 1995 (20 Nm^{-2} day), with high interannual variability ranging from ~2 to 12 Nm^{-2} day (Figure 5e). The highest intensity of downwelling-favorable event in August was in 1995 (>25 Nm^{-2} day), followed by 2002 and 2010 (~15 Nm^{-2} day). As July, the average intensity in August was between ~2 and 12 Nm^{-2} day (Figure 5f). The highest intensities in September were in 1993, 1997 and 2000 (~10-15 Nm^{-2} day)(Figure 5g).

The spring-summer months in which there were more downwelling-favorable events were February (65) (Figure 5m), October (62) (Figure 5i), December (59) (Figure 5k), November (55) (Figure 5j) and January (51) (Figure 5l), while the months with the fewest events were September (18) (Figure 5h) and March (42) (Figure 5n). The highest intensities registered in September were in 1994 and 1997 (~8 Nm^{-2} day) (Figure 5h). There were no downwelling-favorable events in September in several years these being 1990, 1993, 1998, 1999, 2003, 2004, 2006, 2007, 2009, 2010, 2011 and 2012, in effect, half the time series (Figure 5h). The highest intensities occurred in October were in 1991 and 2002 (~9 Nm^{-2} day), while the average was between ~1 and 9 Nm^{-2} day (Figure 5i). The highest intensity of downwelling-favorable event during November was in 1997 (~6 Nm^{-2} day) (Figure 5j). The most intense downwelling-favorable events in December were in 1993 (~9 Nm^{-2} day), 1988 and 2006 (~6 Nm^{-2} day) (Figure 5k). The highest intensity in January was in 2011 (~6 Nm^{-2} day), while there were no downwelling-favorable events in the years 1990, 1995, 2004 and 2009 (Figure 5l). The highest intensities observed in February were in 1989, 1993, 2001 and 2009 (~5 Nm^{-2} day), while the average intensity for this month was ~2.5 Nm^{-2} day (Figure 5m). Finally, the highest intensity of downwelling-favorable event in March was in 2001 (~10 Nm^{-2} day), while the average for this month was ranged from ~1 to 10 Nm^{-2} day (Figure 5n).

The highest average interannual and seasonal intensities of upwelling-favorable events were in spring and summer, that is, in the months of January, February, October, November and December (Figure 6a). The years in which the highest average intensity (>10 Nm^{-2} day) was observed were in the first part of the analyzed period, from 1988 to 1998. Beginning in 2000 the intensity (5-10 Nm^{-2} day) in spring-summer decreased. Intensity in autumn-winter presented a range of 0 to 5 Nm^{-2} day. The average duration of downwelling-favorable events was 1 to 9 days, with the longest events (> 5 days) in the

spring-summer months from 1988 to 1998, although exceptionally there were long events (9 days) in November of 1993 and 2010 (Figure 6b). Upwelling-favorable events in autumn and winter had an average duration of 1 to 4 days throughout the studied period (Figure 6b). The largest number of upwelling-favorable events was in the autumn-winter between March and September (>5 events per month) (Figure 6c). There was a slight increase in the number of events beginning in 1998, with many of them concentrated between 2005 and 2010 (>7 events per month) (Figure 6c).

The highest intensity was observed in autumn-winter, that is, in the months of April, May, June, July and August, and exceptionally in March, September and October in some years (Figure 6d). Unlike the intensity of upwelling-favorable events, the interannual and intensity of downwelling-favorable events did not decrease during the studied period. There were some years with higher intensities (>10 Nm^{-2} day), these being 1991 (May and October), 1994 (July), 1996 (June), 2000 (June), 2001 (July), 2002 (August), 2005 (July), 2008 (July), 2010 (August) and 2012 (May) (Figure 6d). The intensity of downwelling-favorable events appears to be greater than that of upwelling-favorable events (Figure 6a and 6d).

The average length of events in autumn-winter was between 1 and 6 days, with the longest events > 5 days (Figure 6e). There were >5 events per month in the autumn-winter (Figure 6e), with a slight increase in the number of events beginning in 1998. The largest number of events per month (> 7 per month) occurred in July 1989, June 1993 and 1994, and May 1997 and 2005 (Figure 6e). It can be noted that downwelling-favorable events occur less frequently than upwelling-favorable events (Figures 6c and 6e).

To better observe the differences in intensity, duration and number of events, we have separated the series into two periods, autumn-winter and spring-summer (Figure 7). The autumn-winter months that registered the highest intensities (Figure 7a) were March, April and September, in effect, at the beginning and end of the period. The years in which the highest intensities were observed were 1990 (>5 Nm^{-2} day, March and September), 1996 and 2002 (>5 Nm^{-2} day, September) and 2010 and 2011 in March and April (>5 Nm^{-2} day) (Figure 7a).

With respect to the average duration of events (Figure 7b), the longest events (>5 days) were between 1988 and 1998, 2003 and 2006 and 2008 and 2012, and the months in which the longest events occurred were March, April, May, June and September (Figure 7b). The largest number of events per month (> 5 events per month) in the entire studied period were in 1990, 1992 and from 1998 to 2008. There were an exceptionally high

number of events (9 per month) in 2000, 2004 and 2007, with the highest number of events in the months of April, May, July and August (Figure 7c).

The autumn-winter months with the highest average intensities (>10 Nm^{-2} day) of downwelling-favorable events were May, June, July and August, with the most intense event in the studied period in June 1996 (~15 Nm^{-2} day), followed by May 1991, July 1994, June 2000, August 2010, and May 2012 (Figure 7d). There were high values for the average duration of events (> 5 days) in May, June, July and August (Figure 7e). The highest number of downwelling-favorable events was in May, June, July and August, with certain years in which the number was much higher (1989, 1993, 1994, 1997, 2004 and 2005) (Figure 7f).

The average intensity of upwelling-favorable events in spring-summer (Figure 7g) began to decrease as of 2000, with the highest intensities from 1988 to 1998 (> 10 Nm^{-2} day). An exception was observed between 2008 and 2010. The months with highest intensities were November, December, January and February (Figure 7g). The average duration of events in spring-summer followed a similar trend to that of intensity, with a decrease beginning in 2000 and the longest events occurring between 1988 and 1998, with the exception of long events between 2008 and 2010. The months with the longest events were November, January and February (Figure 7h). The periods 1991-1993, 1993-2000, 2003-2005 and 2007-2010 had the highest number of upwelling-favorable events per month (>7) in the spring and summer (Figure 7i). The months with the highest number of events were October, November, December and January (Figure 7i).

The highest average intensities of downwelling-favorable events in spring-summer (>5 Nm^{-2} day) occurred in October 1991 and March 2001. A high average intensity was also registered for the months of September and November in 1997 (Figure 7j). The longest average durations (> 4 days) were in 1991 (October), 1997 (September and November) and 2001 (March) (Figure 7k). The highest number of downwelling-favorable events in spring-summer (>5 events per month) occurred in 1989 (December and February), 1994 (October), 2004 (February), 2010 (February) and 2012 (November) (Figure 7l).

The intensity of upwelling-favorable events >= 1 day decreased over the course of the studied period, with the highest values in 1990, 1993, 1994, and 1995 (Figure 8a). The lowest accumulated intensities were registered in 1992, 1997, 1999, 2000, 2002, 2004, 2005, 2006, 2007, 2008, 2011, and 2012. The highest intensities occurred in January, February, October, November and December (Figure 8a). The highest values for accumulated intensity of upwelling-favorable events >= 3 days were in 1990, 1993 and

1995, while the lowest values were in 1992, 1997, 1999, 2000, 2006 and 2007 (Figure 8b). There were only three months in 1999 and 2006 with events ≥ 3 days and only four months in 2000 and 2007. In addition to decreased intensity as of 1999, the number of months with upwelling-favorable events ≥ 3 days began to decrease (Figure 8b).

Figure 8c shows the interannual variability in the accumulated intensity of downwelling-favorable events >= 1 day. The highest accumulated intensities were 1991, 1993, 1994 and 2002, while the lowest accumulated intensities were in 1998, 1999, 2009 and 2011. Beginning in 2003, the levels of accumulated intensity remained similar over the years, ranging between 30 and 40 Nm^{-2} day. Greater variability was registered in the period 1988 to 2002, with values between 25 and 55 Nm^{-2} day. The highest intensities were in April, May, June, July and August (Figure 8c). With respect to interannual variability in accumulated intensity of downwelling-favorable events of ≥ 3 days, the years with the highest values were 1991, 1996, 1997 and 2002, while the ones with the lowest values were 1990, 1992, 1995, 1999, 2004 and 2006 (Figure 8d). In 1991, 1996 and 1992 there were only three months with events ≥ 3 days and only four months in 1997. A decrease in intensity can also be noted beginning 2001, as well as a decrease in the number of months in which there were downwelling-favorable events ≥ 3 days. The highest frequency of events were in May, June, July and August (Figure 8d).

To determine the relationship among intensity, average duration and the number of events (>= 1 day), we determined the correlations among these variables and the total period for upwelling- and downwelling-favorable events (Figure 9). The average number of upwelling-favorable events increased (Figure 9a), although the correlation among these variables is not significant (rho=0.4, p=0.05). The average duration of these events tended to decrease over the studied period (Figure 9b), but the correlation among these variables is not significant (rho=-0.29, p>0.05). Average interannual intensity (Figure 9c) decreased notably, with a highly significant correlation with the studied years (rho=-0.72, p<0.05). The average intensity of the upwelling-favorable events had fallen to ~2 Nm^{-2} day by the end of the period (Figure 9c).

The number downwelling-favorable events (Figure 9d) did not present significant changes throughout the study period (average of 2 to 3 annually), with a non-significant correlation between number of events and the studied years (rho=-0.07, p>0.05). The average duration was similar throughout the entire studied period (~2 days), with a non-significant correlation (p>0.05) between the average duration and the studied years (Figure 9e). The average intensity of downwelling-favorable events decreased over the

studied period, but as with the other variables, there were no significant correlations among the years (rho=-0.28, p>0.05) (Figure 9f).

3.3. Seasonal and inter-annual variability in short (1-3 days), medium (3-10 days) and long (≥ 10 days) upwelling and downwelling events

There were upwelling-favorable events of 1 to 3 days throughout the year, with intensities between 1 and 2 Nm^{-2} day, with the lowest intensities in autumn-winter (Figure 10a). There were also events of 3 to 10 days throughout the year, with intensities between 2 and 6 Nm^{-2} day. As with short events, the lowest intensities with medium events were in autumn-winter (Figure 10a). In contrast, long events were only registered in some months, namely January, February, March, April, October, November and December, with intensities between 10 and 20 Nm^{-2} day (Figure 10a). The highest intensities in this category were registered in January, March, November and December (Figure 10a). There were upwelling-favorable events of 1 to 3 days throughout the year, with the highest intensities from March to October, with an average of three events per month (Figure 10b). There were also events of 3 to 10 days throughout the year, with the largest number of events in January, February, March, April, November and December (Figure 10b). There were only long events (≥ 10 days) in January, February, March April, October, November and December (Figure 10b).

There were events of 1 to 3 days throughout the year, with intensities between 1 and 3 Nm^{-2} day. The highest intensities were in autumn-winter months (April-September) (Figure 10c). There were also events of 3 to 10 days throughout the year, with the exception of February, with intensities between ~4 and 15 Nm^{-2} day. The highest intensities were in May, June, July and August (Figure 10c). In contrast to the upwelling period, no long events were registered. There were 1-to-3-day long events throughout the year, with an average of 2 to 3 events per month (Figure 10e). There were events 3 to 10 days long throughout the year, with the exception of February. The highest number of events were observed between May and August (Figure 10d).

Upwelling-favorable events between 1 and 3 days long presented similar levels of intensity throughout the year (2 Nm^{-2} day) (Figure 11a). Medium-length events (3-10 days) were more intense from the beginning of the series until 1996, with an intensity between ~3 and 8 Nm^{-2} day (Figure 11a). There were no long events (≥ 10 days) in 1992, 1993, 1994, 1996, 2002, 2004 and 2007. The highest accumulated intensity was in 1995, in which the longest events ~20 Nm^{-2} day were registered (Figure 11a). The intensity of

events in the three analyzed categories began to decrease in 2001 (Figure 11a). There were upwelling-favorable events of 1 to 3 days and 3 to 10 days in all the years of the studied period, but no long events were registered in 1992, 1993, 1994, 2002, 2004 and 2006 (≥ 10 days) (Figure 11b). The largest number of events occurred in 1999 (Figure 11b).

The highest accumulated intensity of downwelling-favorable events (>20 Nm^{-2} day) was registered in 2008, followed by 1995, 1996 and 2012 (~15 Nm^{-2} day) (Figure 11c). The lowest intensities were registered in 1999, 2002, 2009 and 2011 (~10 Nm^{-2} day). Events with durations of 3 to 10 days had the highest registered intensities, ranging between 8 and 15 10 Nm^{-2} day (Figure 11c). The levels of intensity of events between 1 and 3 days were similar throughout the year (2-4 Nm^{-2} day) (Figure 11c).

There were downwelling-favorable events of 1 to 3 days and 3 to 10 days in all the years, but the largest number of events (average of 5 to 6 per year) were reported in 1992, 1997 and 1999 (Figure 11d). The fewest events in both categories were in 1991, 1996, 1998 and 2009 (Figure 11d).

3.4. Accumulated intensity for upwelling- and downwelling-favorable events between midnight and 11:00 am, and between noon and 23:00 pm.

The lowest levels of intensity of upwelling-favorable events were registered from midnight to 11:00 am, with values that did not exceed 2 Nm^{-2} hour (Figure 12a), the intensity of events from noon to 23:00 pm reached higher levels of intensity (3 Nm^{-2} hour) (Figure 12b). The intensity of downwelling-favorable events was higher between noon and 11:00 pm than between midnight and 11:00 am (Figure 12c and 12d). Both series reached maximums of 7 Nm^{-2} hour in some periods (Figures 12c and 12d).

No major differences in intensities were registered for the entire period between midnight and 11:00 am (Figure 13). The mean for upwelling-favorable events was < 0.5 Nm^{-2} hour and the upper limit was < 1 Nm^{-2} hour (Figure 13a). There was a high degree of variability in atypical values of the intensity of downwelling favorable events toward the end of the period (Figure 13b). A decrease in the intensity of upwelling-favorable events from noon to 23:00 pm was observed (Figure 13c), the mean in this time period being ~0.5 Nm^{-2} hour (Figure 13c). The intensity of downwelling-favorable events between noon and 23:00 pm were also highly variable in atypical values, with no clear decrease observed near the end of the study period (Figure 13d).

A decrease in the intensity of upwelling-favorable events was clearly observed between noon and 23:00 pm, as well as a slight decrease from midnight to 11:00 am (Figure 14a). There was a slight decrease in downwelling-favorable events from noon to 23:00 pm, which was not as evident between midnight to 11:00 am (Figure 14b).

The highest intensities for upwelling-favorable events from midnight to 11:00 am over the entire study period occurred in January, February, November and December (Figure 15a). The event with the highest intensity was from noon to 11:00 pm, with a mean and median close to 0.5 Nm^{-2} hour (Figure 15b). The annual cycle of intensity of downwelling-favorable events had values than that of upwelling-favorable events, above all between noon and 23:00 pm, with extreme values of ~1.5 Nm^{-2} hour (Figure 15d). There were many atypical values in both time periods (Figure 15c and 15d).

Finally, there was a general trend in both periods for the intensity of upwelling- and downwelling-favorable events to remain relatively stable (Figure 16). The average intensity of upwelling-favorable events between noon and 23:00 pm was greater than between midnight and 11:00 am (0.5 and 0.2 Nm^{-2} hour, respectively) (Figure 16a and 16c). Changes in variability can be observed, above all from noon-to-23:00 pm (std dev), which decreased during the studied period (Figure 16c).

The average intensity of downwelling-favorable events for periods noon-to-23:00 pm and midnight-to-11:00 am were similar (0.5 Nm^{-2} hour) throughout the studied period (Figure 16b and 16d), and there was a high degree of variability (std) in both periods (Figure 16b and 16d).

4. Discussion

Our analysis of 25 years of winds off central-southern Chile showed that upwelling/downwelling events occur year-round, but exhibit different seasonal and interannual characteristics.

4.1. Event-scale characterization in the southern part of the Humboldt Current System (central-southern Chile)

Although our results show that upwelling-favorable events occur throughout the year, the majority of bio-oceanographic research on central-southern Chile has only identified upwelling in spring-summer as one of the causes of the degree of high variability in bacterial production (Cuevas et al. 2004), nanophytoplankton abundance, biomass and grazing (Bottjer and Morales 2007), microplankton abundance (Anabalón et al. 2007), N2O flow and annual cycle (Cornejo et al. 2007), the assimilation and primary production of inorganic nitrogen (NO3- and NH4+) (Fernández and Farías 2012), primary production (>1 g C m^{-2} d^{-1}; October-April, Daneri et al. 2000; Montero et al. 2007) and chemical-lithoautotrophic production and the CH4 cycle (Farías et al. 2009), among others. This perspective is likely to be based on the observed seasonal variation of primary productivity in this zone, which, although high throughout the year (Fossing et al. 1998; Daneri et al. 2000), is greatest in spring-summer (Montero et al. 2007). This temporal trend in primary productivity is a consequence, between others factors, of physical processes, such as the heat balance dominated by solar radiation (maximum in January, 200 Wm^{-2}) and the balance of fresh water dominated by the discharge of the Biobío and Itata Rivers, and precipitation (maximum monthly average in June and July, 0.4 mm) (Sobarzo et al. 2007).

Although upwelling-favorable events prevail most of the year in the study area, our results show that there were also a substantial number of downwelling-favorable events. In fact, there were 1521 upwelling-favorable events (considering autumn-winter and spring-summer) and 875 downwelling-favorable events (considering autumn-winter and spring-summer) (see Figure 2). Of a total of 2396 events, 63% are favorable to upwelling and 37% are favorable to downwelling. Although the percentage of downwelling-favorable events is not small, upwelling continues to predominate in the area.

At the seasonal level (Figure 3), the highest number of upwelling-favorable events (432) and the events with highest intensity (25 Nm^{-2} day) occurred in spring. The largest number of downwelling-favorable events (279), and again with the highest intensity >25 Nm^{-2}

day, occurred in autumn (Figure 3). Our analysis has allowed to determine the relationship between the intensity of an event and its duration, a relationship that is clearly significant ($p<0.05$). We also observed that upwelling-favorable events are intense and long (e.g. spring: 25 Nm^{-2} day, 16 days), while downwelling-favorable events are intense and short (e.g. winter: >25 Nm^{-2} day, 8 days) (Figure 3). The duration of an event, and consequently its intensity, have significant effects on the coastal zone and associated physical variables, among them density (Kämpf and Chapman, 2016).

Cushman-Roisin (1994) developed an index based on the magnitude and duration of upwelling-favorable wind stress, termed "wind impulse", which causes the density interface to rise towards the coast and it may or may not eventually reach the sea surface, leading to either partial or full upwelling (Csanady, 1977). Full upwelling implies the formation of a surface density front, which is a narrow frontal zone across rapid changes in density, also called an upwelling front. Cushman-Roisin (1994) determined the duration and final offshore distance of an upwelling front using the internal deformation radius (R) and other parameters. For example, upwelling events with a duration of 10-12 days could mobilize the density front at distance of 5 km offshore. Consequently, based on our results, we can affirm that upwelling-favorable events with a duration of 16 days and reaching a maximum intensity of 25 Nm^{-2} day can move the density front at a distance of ~8 km offshore. This criterion probably is not useful to determine the duration and final distance that downwelling fronts reach at the coast because the water column during a downwelling-favorable event follows another dynamic. This has been described for other systems, like the Oregon continental shelf, where the time-dependent response of the coastal ocean at rest to constant downwelling-favorable wind stress (Allen and Newberger, 1996). Under downwelling conditions, wind stress forces onshore flow in a turbulent surface boundary layer. The compensating flow below the surface layer advects the density field downward and offshore and accelerates an alongshore current in the form of a vertically and horizontally sheared coastal jet. The dominant feature of the response flow field is a downwelling front that moves slowly offshore, leaving behind an inshore region where the density is well mixed. The downwelling front in the density field is concentrated near the bottom, while the front in alongshore velocity extends over the full depth and is nearly vertical, separating weak alongshore velocities inshore from the coastal jet offshore (Allen and Newberger, 1996, Lentz and Fewings, 2012)

As our results indicate, the intensity and duration of upwelling-favorable events have decreased in the period between 1988 and 2012 (Figures 6a, 6b, 7b, and 7c), which can

have consequences in terms of the maximum distance that an upwelling front can reach. As we have reported, if an event decreases to 7 days, the distance it can be moved offshore is on average ~3.5 km. Although these indicate that the front will reach a shorter distance, the increased frequency of upwelling-favorable events observerved in the time series analyzed, especially in autumn-winter (Figure 6c and Figure 7c), could compensate for the shorter duration and distance reached.

4.2. Seasonal and inter-annual variability in upwelling- and downwelling-favorable events in the southern part of the Humboldt Current System

Our results show marked seasonality in the intensity and number of upwelling- and downwelling-favorable events (Figure 10). The seasonal cycle in the number and intensity of upwelling-favorable events (Figures 10a and 10b) suggests that events >=10 days prevail in spring-summer months, with an intensity that ranged between 10-20 Nm^{-2} day. Short (>=3 days) and medium-length events (3 to 10 days) occur year-round (Figure 10b).

Similar results were obtained for the central-northern California coast, with the highest values from March to August (spring-summer in the northern hemisphere), and a maximum in June (García-Reyes et al., 2014). The intensity of the system increases rapidly in March, when long (>10 days) events begin, and declines sharply in July (García-Reyes et al., 2014).

The inter-annual variability showed that although there were long events in the last five years of the series (2008-2012) (Figure 11b) they had average intensities of less than 15 Nm^{-2} day (Figure 11a). The highest accumulated intensities (>25 Nm^{-2} day) were registered in the first ten years of our series (1988-1999), while the lowest were in the last decade (2002-2010) (Figure 11a), which is in contrast to García-Reyes et al. (2014), who found that the least intense upwelling was in 1985 and 1992 (first seven years of their series) and that high intensity values were more frequent during the last decade (2002-2012), resulting in a positive although weak trend (1.2 Nm^{-2} day per decade, $p < 0.05$). Our data show that in 1992, 1993, 1994 and 1996 of the first period analyzed no events were registered that were = > 10 days (Figure 11a and 11b).

The seasonal cycle also predominates in downwelling-favorable events (Figure 10c), with the highest intensity (~10 Nm^{-2} day) reached in autumn-winter (April-September), with only short (1-3 days) and medium events (3-10 days) (Figures 10c and 10d). There were no significant inter-annual changes in the intensity and number of downwelling-favoring

events (Figures 11c and 11d). However, accumulated intensity was lower than normal in 1992, 1993, 1997, 1998, 1999, 2009 and 2011, while it was higher in other years like 2008 (>25 Nm^{-2} day) (Figure 11c). Although accumulated intensity was low in 1992, there were more events (six) than in any other year in the series, while the highest accumulated intensity was in 2008, but there were no more than four events on average that year. In other eastern boundary systems, like the California Current System, warm phases of the El Niño Southern Oscillation are reported to be associated with a later onset of summer upwelling and more intense downwelling (Bograd et al., 2009, Bylhouwer et al., 2013). Other authors have found that spatial covariation of upwelling/downwelling present three dominant low-frequency signals in the range of 33, 19 and 11 years, resembling periodicities of atmospheric circulation, nodal moon tides and solar activity (Saldívar-Lucio et al., 2016). In our work low-frequency scales were not analyzed but the evidence from other systems indicates that this should be considered in future investigations.

4.3 Increase in upwelling favorable winds in the southern area of the Humboldt Current System and possible consequences

There have been numerous studies that indicate changes in upwelling favorable winds in the recent decades (e.g. Sydeman et al. 2014; Varela et al., 2015). Some studies have proposed that in eastern boundary current systems global warming should intensify upwelling-favorable winds, in the warmer seasons (spring-winter), as a result of the increase in the land-ocean pressure gradient (Bakun, 1990). Other authors have proposed that as a result of the intensification of the South Pacific Anticyclone and a southward shift of its nucleus (Falvey & Garreaud, 2009, Goubanova et al., 2011; Belmadani et al., 2014), upwelling-favorable winds will intensify all along the Chilean coast (Garread & Falvey, 2008).

The increase in upwelling favorable winds has physical, as well as biogeochemical effects. Using numerical physical-biogeochemical experiments in the Humboldt Current System (ROMS, PISCES, IBM), Brochier et al. (2013) predicted that larval retention throughout the continental shelf will increase with greater stratification as a result of global warming, although retention will be compensated by a decrease in the nursery area and a decrease in the depth of the oxycline.

Aiken et al. (2011) used numerical simulation to investigate larval dispersion and connectivity along the coast of central Chile with an increase in upwelling favorable

winds. They found that the ocean surface temperature in this zone will decrease by 1ºC and that sub-surface poleward current and mesoscale gyres will become more energetic. These processes can have negative consequences for neutrally buoyant larvae, while larvae that possess the ability to sink below the surface Ekman layer were found to have higher rates of settlement under present conditions and under the IPCC-A2 scenario.

Our results indicate the opposite, that is, that the intensity and duration of upwelling-favorable winds have been decreasing, in particular since 1998, but that the number of event increases, above all in autumn-winter (Figuras 6, 7, 8 and 9).

Deeper knowledge is needed of upwelling dynamics in central-southern Chile at different temporal and spatial scales to better understand the possible effects of climate change in this highly productive system.

3. Conclusion

The results presented in this analysis show that upwelling-favorable events from 1988 to 2013 have decreased in intensity and duration, although not in terms of the number of events, which are increasingly more common. The intensity of downwelling-favorable events has decreased, but their duration and frequency has remained unchanged.

We have shown that the number of upwelling-favorable events in autumn-winter is similar to that in spring-summer, with 754 and 767 events, respectively. However, the events in autumn-winter were shorter and less intense than the typical summer events. A high number of downwelling-favorable events (352) were observed in spring-summer, although still considerably less that the number of events that occurred in autumn-winter (523).

Upwelling-favorable events represented 63% of all events, and downwelling events represented the remaining 37%. While the percentage of downwelling-favorable events is not negligible, upwelling continues to predominate in the area under study.

In relation to the temporal evolution from 1988 to 2013 as evidenced in the daily cycle, a decrease was observed in the intensity of upwelling-favorable events from noon to midnight (12-23 PM), as well as a slight decrease between 0-11 AM. Also, a decrease was observed in the intensity of downwelling-favorable events between 12-23 PM (0-11 AM). A slight decrease in downwelling-favorable events between noon and midnight was also registered, which was not as evident between 0-11 AM.

Acknowledgments

This study was funded by the Interdisciplinary Center for Aquaculture Research (INCAR; FONDAP Grant Nº15110027; CONICYT, Chile) and by the Programa de Investigación Marina de Excelencia (PIMEX) of the Faculty of Natural and Oceanographic Sciences of the University of Concepción. The latter is funded by Celulosa Arauco and Constitución S.A. This paper is part of O.V.'s doctoral thesis (Doctorate Program in Oceanography, University of Concepción). OV was supported by a Doctorate Scholarship from the Comisión Nacional de Investigación Científica y Tecnológica (CONICYT, Chile).

References

Aiken, C. M., Navarrete, S. A. and J. L. Pelegri. 2011. Potential changes in larval dispersal and alongshore connectivity on the central Chilean coast due to an altered wind climate. J. Geophys Res., 116: G04026. doi:10.1029/2011JG001731.

Álvarez, I., de Castro, M., Prego, R., and M. Gómez-Gesteira. 2003. Hydrographic characterization of a winter-upwelling event in the Ria of Pontevedra (NW Spain). Estuar. Coast and Shelf Sciencie, 56: 869-876.

Allen, J. S., Newberger, P.A., and J. Federiuk. 1995. Upwelling circulation on the Oregon continental shelf. Part 1: response to idealized forcing. J. Phys. Oceanogr., 25: 1843–1866.

Anabalón, V., Morales, C. E., Escribano, R. and M. A.Varas. 2007. The contribution of nano- and micro-planktonic assemblages in the surface layer (0-30 m) under different hydrographic conditions in the upwelling area off Concepción, central Chile. Progr. Oceanogr., 75: 396-414.

Bakun A 1990. Global climate change and intensification of coastal upwelling. Science, 247: 198-201.

Barth, J. A., B. A. Menge, J. Lubchenco, F. Chan, J. M. Bane, A. R. Kirincich, M. A. McManus, K. J. Nielsen, Pierce, S. D. and L. Washburn. 2007. Delayed upwelling alters nearshore coastal ocean ecosystems in the Northern California Current. Proceedings of the National Academy of Sciences of the United States of America, 104(10): 3719–3724.

Belmadani, A., Echevin, V., Codron, F., Takahashi, K., and C. Junquas. 2014. What dynamics drive future wind scenarios for coastal upwelling off Peru and Chile?, Clim. Dyn., 43(7–8): 1893–1914.

Black, B. A., Schroeder, I. D., Sydeman, W. J., Bograd, S. J., Wells, B. K. and F. B. Schwing. 2011. Winter and summer upwelling modes and their relevance to climate

impacts and ecological response in the California Current Ecosystem. Global Change Biology, 17: 2536–2545.

Bograd, S. J., Schroeder, I. D., Sarkar, N., Qiu, X. M., Sydeman, W. J. and F. B. Schwing. 2009. Phenology of coastal upwelling in the California Current. Geophysical Research Letters, 36, L01602.

Böttjer, D. and C. E. Morales. 2005. Microzooplankton grazing in a coastal embayment off Concepción, Chile, (~36°S) during non-upwelling conditions. Journal of Plankton Research (27) 4: 383, 391.

Böttjer, D. and C. E. Morales. 2007. Nanoplanktonic assemblages in the upwelling area off Concepción (36ºS), central Chile: Abundance, biomass, and grazing potential during the annual cycle. Progr. Oceanogr., 75: 415-434.

Botsford, L. W., Lawrence, C. A., Dever, E. P., Hastings, A. and J. Largier. 2006. Effect of variable winds on biological productivity on continental shelves in coastal upwelling systems. Deep-Sea Research II, 53: 3116–3140.

Brochier, T., Echevin, V., Tam, J., Chaigneau, A., Goubanova, K. and A. Bertrand. 2013. Climate change scenarios experiments predict a future reduction in small pelagic fish recruitment in the Humboldt Current system. Glob. Chan. Biol., 19: 1841-1853.

Bylhouwer, B., Ianson, D. and K. Kohfeld. 2013. Changes in the onset and intensity of wind-driven upwelling and downwelling along the North American Pacific coast, J. Geophys. Res. Oceans., 118: 2565–2580. doi:10.1002/jgrc.20194.

Correa-Ramírez, M. A., Hormazábal, S. and C. E. Morales. 2012. Spatial patterns of annual and interannual surface chlorophyll – a variability in the Peru-Chile Current System. Progress in Oceanography, 92-95C: 8–17.

Cubillos, L. A., Ruiz, P., Claramunt, G., Gacitúa, S., Núñez, S., Castro, L. R., Riquelme, K., Alarcón, C., Oyarzún, C. and A. Sepúlveda. 2007. Spawning, daily egg production,

and spawning stock biomass estimation for common sardine (*Strangomera bentincki*) and anchovy (*Engraulis ringens*) off central southern Chile in 2002. Fish. Res., 86: 228-240.

Cuevas, L. A., Daneri, G., Jacob, B. and P. Montero 2004. Microbial abundance and activity in the seasonal upwelling area off Concepción (~36ºS), central Chile: a comparison of upwelling and non-upwelling conditions. Deep-Sea Research II, 51: 2427–2440.

Cushman-Roisin, B., 1994. Introduction to Geophysical Fluid Dynamics. Prentice-Hall, Englewood Ciffs, NJ, 320pp.

Csanady, G. T. 1977. The coastal jet conceptual model in the dynamics of shallow seas, in The Sea, Vol. 6, Marine modelling, Goldberg, E. D., McCave, I. N., O'Brien, J. V., and Steele, J. H., Eds., Wiley, New York, 117.

Daneri, G., Dellarossa, V., Quiñones, R., Jacob, B., Montero. P. and O. Ulloa. 2000. Primary production and community respiration in the Humboldt Current System off Chile and associated oceanic areas. Mar. Ecol. Prog. Ser., 197: 41-49.

Daneri, G., Lizárraga, L., Montero, P., González, H. E. and F. J. Tapia. 2012. Wind forcing and short-term variability of phytoplankton and heterotrophic bacterioplankton in the coastal zone of the Concepción upwelling system (Central Chile). Progr. Oceanogr., 92-95: 92-96.

Dugdale, R. C., Wilkerson, F. P. and A. Morel. 1990. Realization of new production in coastal upwelling areas: a means to compare relative performance. Limnology and Oceanography, 35 (4): 822–829.

Escribano, R., Hidalgo, P., Fuentes, M. and K. Donoso. 2012. Zooplankton time series in the coastal zone off Chile: Variation in upwelling and responses of the copepod community. Progr. Oceanogr., 97-100: 174-186.

Falvey, M. and R. D., Garreaud. 2009. Regional cooling in a warming world: Recent temperature trends in the southeast Pacific and along the west coast of subtropical South America (1979–2006). J. Geophys. Res. 114. http://dx.doi.org/10.1029/2008jd010519.

Farías, L., Fernández, C., Faúndez, J., Cornejo, M. and M. E. Alcaman. 2009. Chemolithoautotrophic production mediating the cycling of the greenhouse gases N2O and CH4 in an upwelling ecosystem. Biogeosciences, 6: 3053-3069.

Fernández, C., and L. Farías. 2012. Assimilation and regeneration of inorganic nitrogen in a coastal upwelling system: ammonium and nitrate utilization. Mar. Ecol. Progr. Ser., 451: 1-14.

Foreman, M. G., Pal, G., B. and W. J. Merryfield. 2011. Trends in upwell- ing and downwelling winds along the British Columbia shelf, J. Geo- phys. Res. Oceans, 116, C10023, doi:10.1029/2011JC006995.

Fossing, H., Gallardo, V. A., Joergensen, B. B., Huttel, M., Nielsen, L. P., Schulz, H., Canfield, D. E., Foster, S., Glud, R. N., Gundersen, J. K., Kuver, J., Ramsing, N. B., Teske, A., Thamdrup, B. and O. Ulloa. 1995. Concentration and transport of nitrate by the mat-forming sulphur bacterium Thioploca. Nature, 374: 713–715.

Fuenzalida, R., Schneider, W., Garcés-Vargas, J., Bravo, L. and C. Lange. 2009. Vertical and horizontal extension of the oxygen minimum zone in the eastern South Pacific Ocean. Deep Sea Res. II, 56 (16): 992–1003.

García-Reyes, M. and J. L. Largier. 2010. Observations of increased wind-driven coastal upwelling off central California. J. Geophys. Res., 115: C04011.doi:10.1029/2009JC005576.

García-Reyes, M., Largier, J. L. and W. J. Sydeman. 2014. Synoptic-scale upwelling indices and predictions of phyto- and zooplankton populations. Progr. Oceanogr., 120: 177-188.

Garreaud, R., and R. Muñoz. 2005. The low-level jet off the west coast of subtropical South America: Structure and variability. Mon. Wea. Rev., 133: 2246-2261.

Garreaud, R. and M. Falvey. 2008. The coastal winds off western sub- tropical South America in future climate scenarios, Int. J. Climatol., 29: 543–554. doi:10.1002/joc.1716.

Goubanova, K., Echevin, V., Dewitte, B., Codron, F., Takahashi, K., Terray, P. and M. Vrac. 2011. Statistical downscaling of sea-surface wind over the Peru–Chile upwelling region: diagnosing the impact of climate change from the IPSL-CM4 model. Clim. Dyn., 36(7–8):1365–1378. doi:10.1007/s00382-010-0824-0.

Hales, B., Takahashi, T. and L. Bandstra. 2005. Atmospheric CO2 uptake by a coastal upwelling system, Global Biogeochem. Cycles, 19, GB1009, doi:10.1029/2004GB002295.

Henson, S. A. and A. C. Thomas. 2007. Interannual variability in timing of bloom initiation in the California Current System, J. Geophys. Res., 112, C08007, doi:10.1029/2006JC003960.

Hernández-Miranda. E., Quiñones, R. A., Aedo, G., Valenzuela, A., Mermoud, N., Román, C. and F. Yañez. 2010. A major fish stranding caused by a natural hypoxic event in a shallow bay of the eastern South Pacific. J. Fish Biol., 76: 1543-1564.

Hernández-Miranda, E., Veas, R., Labra, F. A., Salamanca, M. and R. A. Quiñones. 2012a. Response of the epibenthic macrofaunal community to a strong upwelling-driven hypoxic event in a shallow bay of the southern Humboldt Current System. Marine Environmental Research, 79: 16-28.

Hernández, A., Cubillos, L. A. and R. A. Quiñones. 2011. Evaluación de la talla estructurada de los stocks de Ensis macha y Tagelus dombeii en el Golfo de Arauco, Chile. Revista de Biología Marina y Oceanografía, 46 (2): 157-176.

Ianson, D.,. Feely, R. A., Sabine, C. L. and L. W. Juranek. 2009. Features of coastal upwelling regions that determine net air-sea CO2 flux, J. Oceanogr., 65: 677–687.

Kämpf, J. and P. Chapman. 2016. Upwelling Systems of the World: A Scientific Journey to the Most Productive Marine Ecosystems. Chapter 2: The Functioning of Coastal Upwelling Systems. Springer, Cham. doi 10.1007/978-3-319-42524-5_2

Lentz, S. J. and M. R. Fewings. 2012. The wind- and wave-driven inner-shelf circulation. Ann. Rev. Mar. Sci., 4: 317–343. http://dx.doi.org/10.1146/ annurev-marine-120709-142745.

Leth, O. and J. F. Middleton. 2004. A mechanism for enhanced upwelling off central Chile: Eddy advection. J. Geophys. Res., 109: 1-17.

Merryfield, W. J., Pal, B. and M. G. G. Foreman. 2009. Projected future changes in surface marine winds off the west coast of Canada, J. Geo- phys. Res., 114, C06008, doi:10.1029/2008JC005123.

Montero, P., Daneri, G., Cuevas, L. A., González, H. E., Jacob, B., Lizárraga, L. and E. Menschel. 2007. Productivity cycles in the coastal upwelling area off Concepción: the importance of diatoms and bacterioplankton in the organic carbon flux. Prog. Oceanogr., 75: 518–530.

Morales, C. E., Hormazábal, S., Correa-Ramírez, M., Pizarro, O., Silva, N., Fernández, C., Anabalón, V. an M. L. Torreblanca. 2012. Mesoscale variability and nutrient–phytoplankton distributions off central-southern Chile during the upwelling season: The influence of mesoscale eddies. Progr. Oceanogr., 104: 17-29.

Narváez, D. A., Navarrete, S. A., Largier, J. and C. A. Vargas. 2006. Onshore advection of warm water, larval invertebrate settlement, and relaxation of upwelling off central Chile. Marine Ecology Progress Series, 309: 159–173.

Quiñones, R. A., Hernández, A., Carrasco, P., Araya, I. y H. Muñoz.2009. Las pesquerías del sistema costero de la cuenca del río Itata. In: Parra, O., Castilla, J.C., Camaño, A., Quiñones, R., Romero, H. (Eds.), La Cuenca Hidrográfica del río Itata. Aportes Científicos para su Gestión Sustentable. Universidad de Concepción, Chile, pp. 193-211.

Quiñones, R. A., Gutiérrez, M. H., Daneri, G., Gutiérrez, D. A., González, H. E. and F. Chávez. 2010. Pelagic carbon fluxes in the Humboldt Current System. In: Liu KK, Atkinson L, Quiñones RA, Talaue-McManus L (eds) Carbon and nutrient fluxes in global continental margins: a global synthe- sis. Springer-Verlag, New York, NY, p 44–64.

Rutllant, J. and H. Fuenzalida. 1991. Synoptic aspects of the central Chile rainfall variability associated with the Southern Oscillation. International Journal of Climatology, 11: 6376.

Rutllant, J. 1993. Coastal lows and associated southerly wind events in north-central Chile. In Preprints, Fourth Int. Conf. on Southern Hemisphere Meteorology and Oceanography. American Meteorological Society, Boston, pp. 235-253.

Saldívar-Lucio, R., Di Lorenzo, E., Nakamura, M., Villalobos, H., Lluch-Cota, D. and P. Del Monte-Luna. 2016. Macro-Scale Patterns in Upwelling/ Downwelling Activity at North American West Coast. PLoS ONE 11(11): e0166962. doi:10.1371/ journal.pone.0166962.

Santos, A. M., Borges, M. F. and S. Groom. 2001. Sardine and horse mackerel recruitment and upwelling off Portugal. ICES J. Mar. Sci., 58: 589-596.

Santos, A. M., Kazmin, A. S. and A. Peliz. 2005. Decadal changes in the Canary upwelling system as revealed by satellite observations: Their impact on productivity. J. Mar. Res., 63: 359-379.

Schroeder, I. D., Snydeman, W. J., Sarkar, N., Thompson, S. A., Bograd, S. J. and F. B. Schwing. 2009. Winter pre-conditioning of seabird phenology in the California current, Mar. Ecol. Prog. Ser., 393: 211–223.

Smith, R. L. 1994. The physical processes of coastal ocean upwelling sys- tems, in Upwelling in the Ocean, edited by C. P. Summerhayes et al., pp. 39–64, John Wiley, New York.

Sobarzo, M., Bravo, L., Donoso, D., Garcés-Vargas, J. and W. Schneider. 2007a. Coastal upwelling and seasonal cycles that influences the water column over the continental shelf of central Chile. Progr. Oceanogr., 75: 363-382.

Sobarzo, M., Bravo, L. and C. Moffat. 2010. Diurnal-period, wind-forced ocean variability on inner shelf of Concepción, Chile. Cont. Shelf Res., 30: 2043-2056.

Strub, P. T., Mesías, J., Montecino, V., Ruttlant, J. and S. Salinas. 1998. Coastal ocean circulation off western South America. Coastal Segment (6,E), in: Robinson, A., Brink, K. (Eds), The Sea, Vol. 11. John Wiley & Sons, Hoboken, pp. 273-313

Strub, P. T., Combres, V., Shillington, F. A. and O. Pizarro. 2013. Currents and Processes along the Eastern Boundaries. Ocean Circulation and Climate 2nd Edition. Edited by Dr. Gerold Siedler, Dr. John Church, Dr. W. John Gould and Dr. Stephen M. Griffies. Academic Press. ISBN: 978-0-12-391851-2.

Sydeman, W. J., García-Reyes, M., Schoeman, D. S., Rykaczewski, R. R., Thompson, S. A., Black, B. A. and S. J. Bograd. 2014. Climate change and wind intensification in coastal upwelling ecosystems. Science, 345 (6192): 77-80.

Tapia, F. J., Navarrete, S. A., Castillo, M., Menge, B. A., Castilla, J. A., Largier, J., Wieters, E. A., Broitman, B. L., Barth, J. A. 2009. Thermal indices of upwelling effects on inner- shelf habitats. Prog. Oceanogr., 83: 278−287.

Ulloa, O. and S. Pantoja. 2009. The oxygen minimum zone of the eastern South Pacific. Deep Sea Res., II 56(16): 987-991.

Varela, M., Álvarez-Ossorio, M. T., Bode, A., Prego, R., Bernárdez, P. and C. García-Soto. 2010. The effects of a winter upwelling on biogeochemical and planktonic components in an area close to the Galician Upwelling Core: The Sound of Corcubión (NW Spain). J. Sea Res., 64: 260-272.

Varela, R., Álvarez, I., Santos, F., deCastro, M. and M. Gómez-Gesteira. 2015. Has upwelling strengthened along worldwide coasts over 1982–2010? Sci Rep., 5: 1–15.

Zar, J. H. 1999. Biostatistical Analysis. Fourth Edition. Prentice Hall: New Jersey, 663 pp.

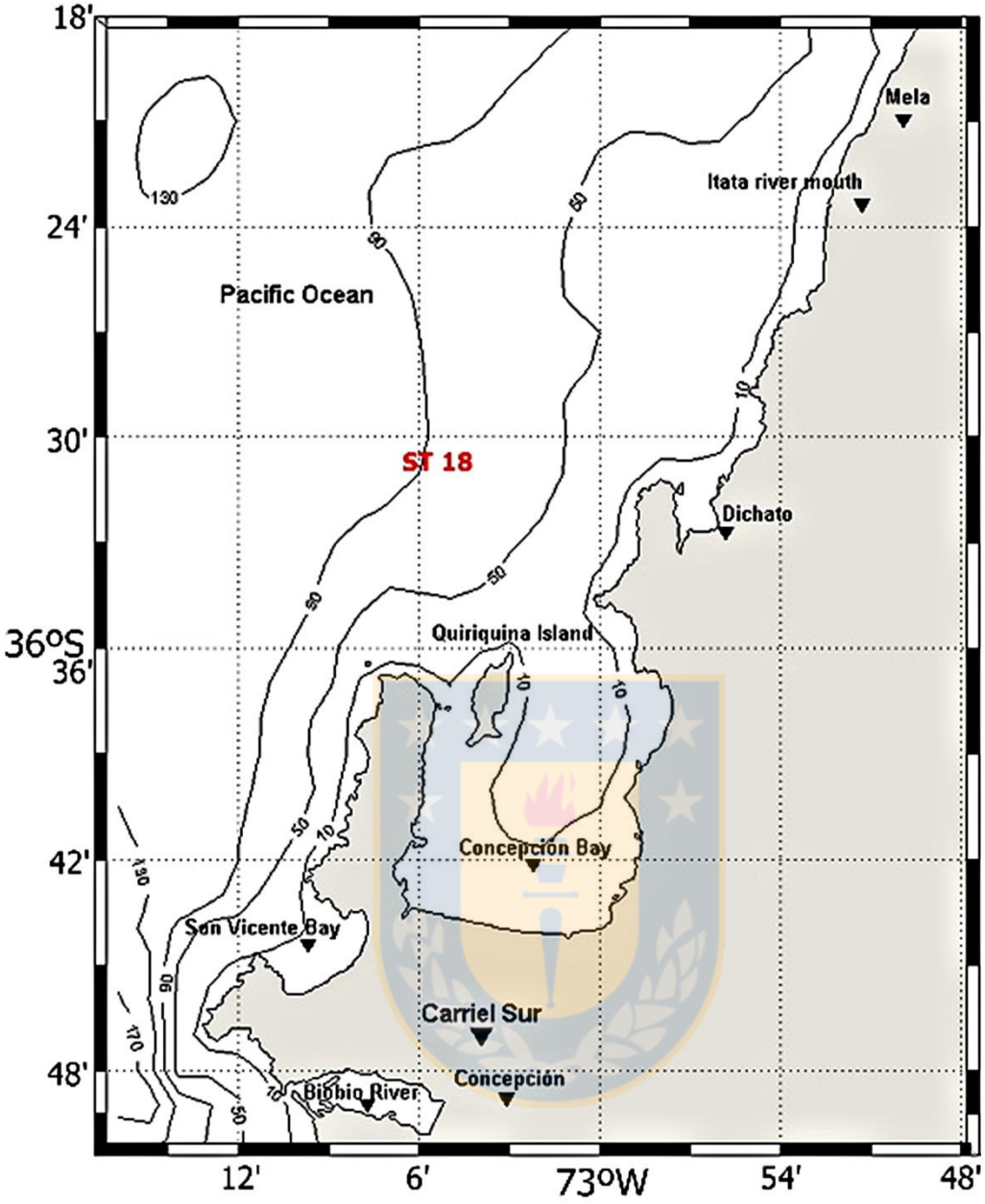

Figura 1: Localization of Carriel-sur meteorological station.

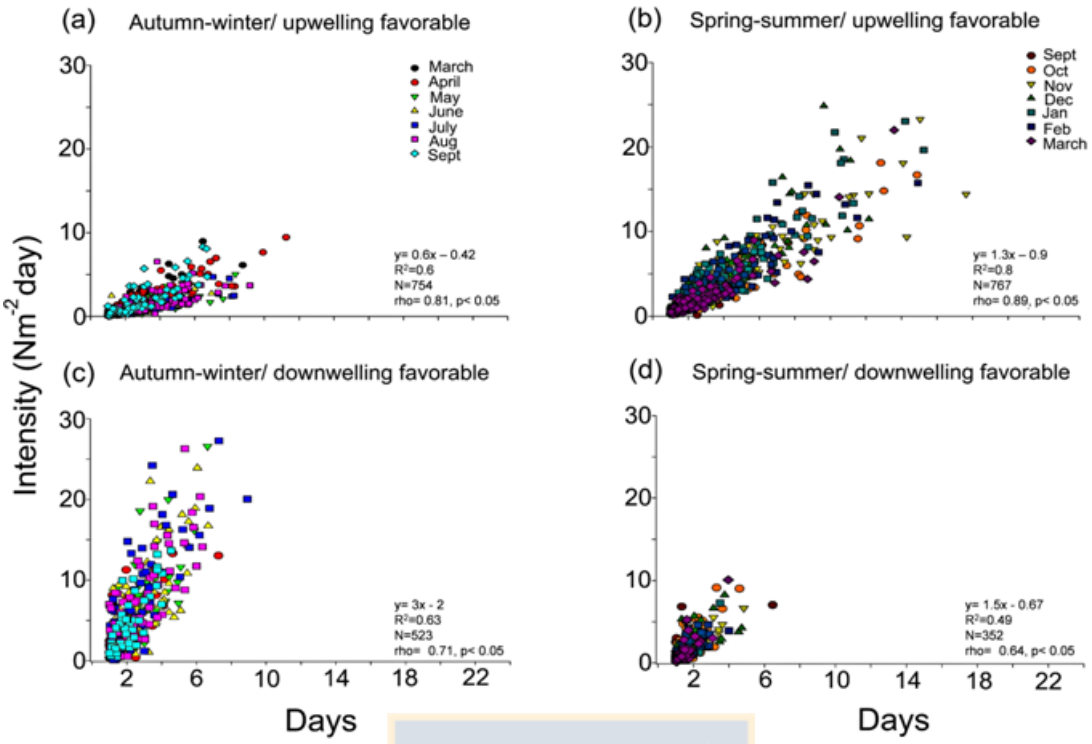

Figure 2. Intensity versus lenght (days) of upwelling-favorable events in autumn-winter (a) and spring-summer (b) and intensity versus lenght (days) downwelling-favorable events in autumn-winter (c) and spring-summer (d).

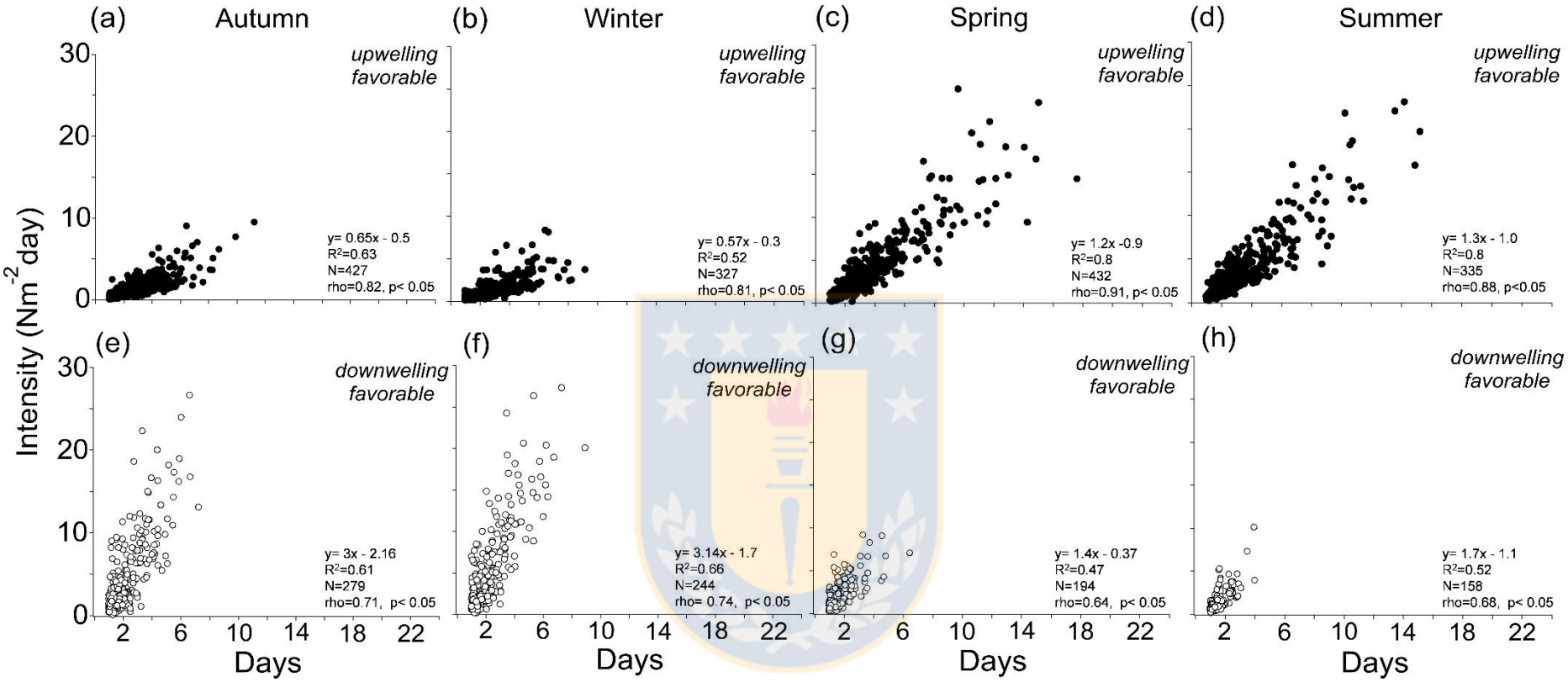

Figure 3: Intensity versus lentgth (days) of upwelling-favorable events in autumn (a), winter (b), spring (c) and summer (d) and downwelling-favorable events in autumn (e), winter (f), spring (g) and summer (h).

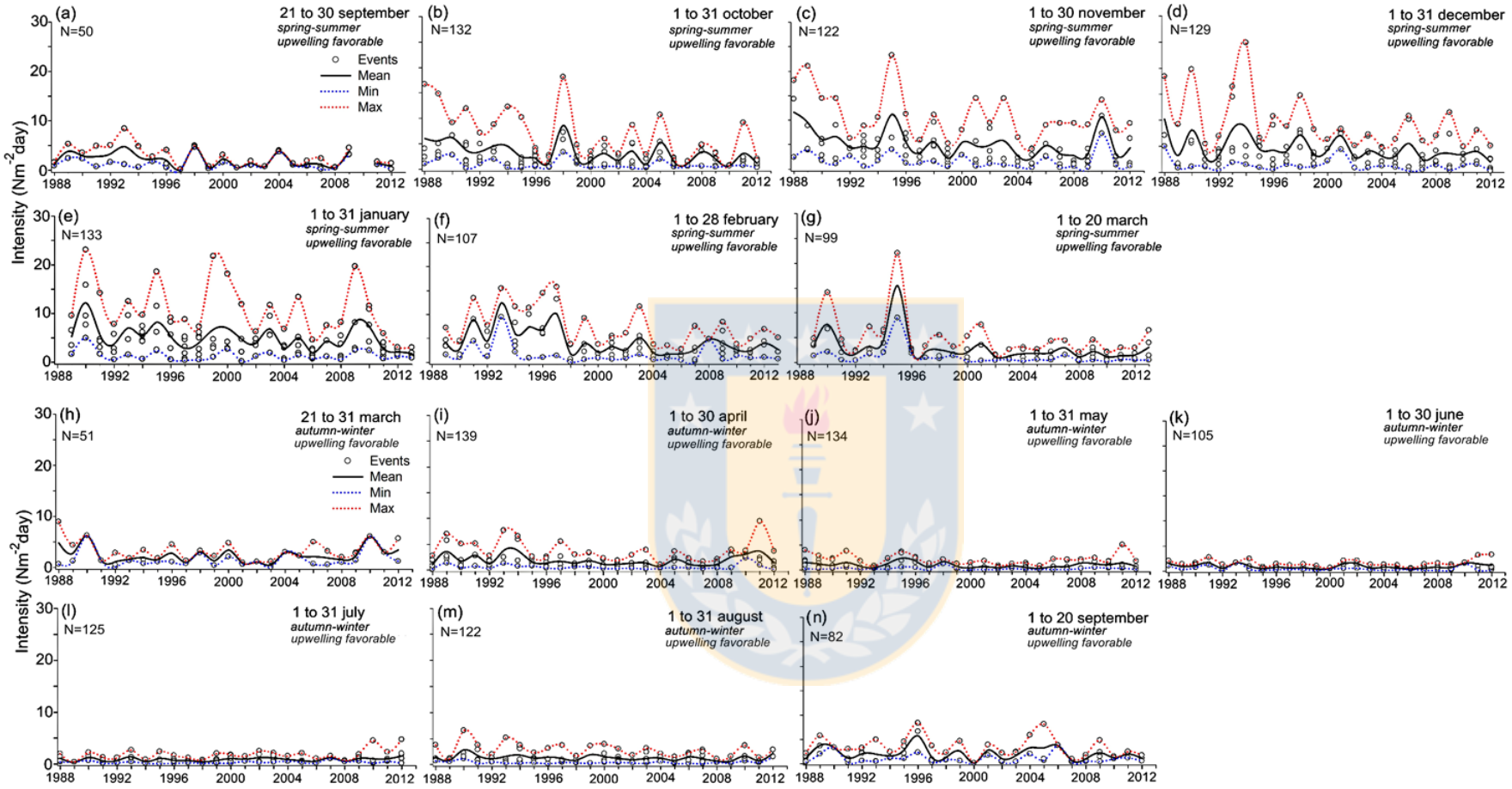

Figure 4. Intensity of upwelling-favorable events for spring-summer months (a-g) and autumn-winter months (h-n)

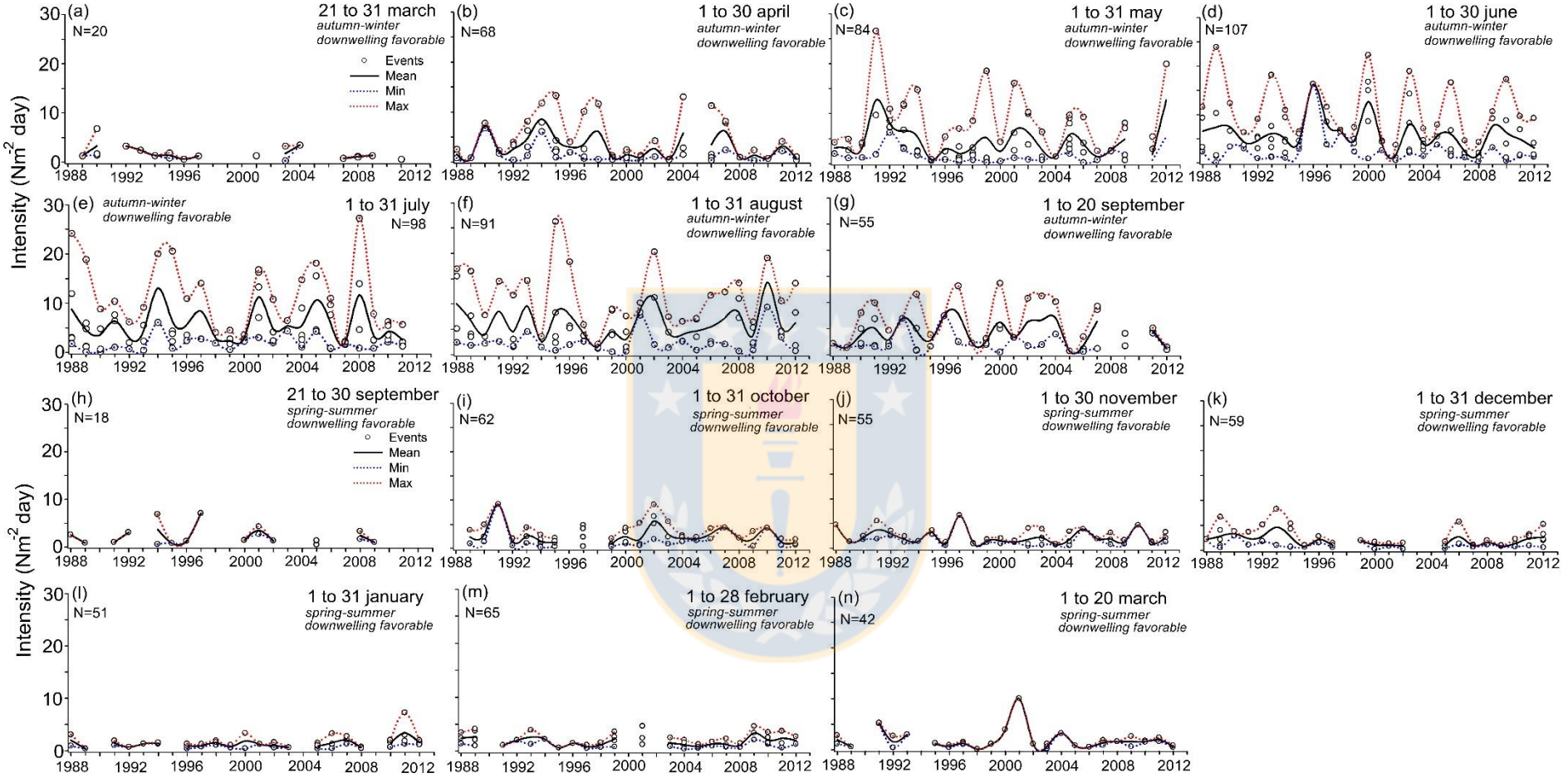

Figure 5: Intensity of downwelling-favorable events for autumn-winter months (a-g) and spring-summer months (h-n)

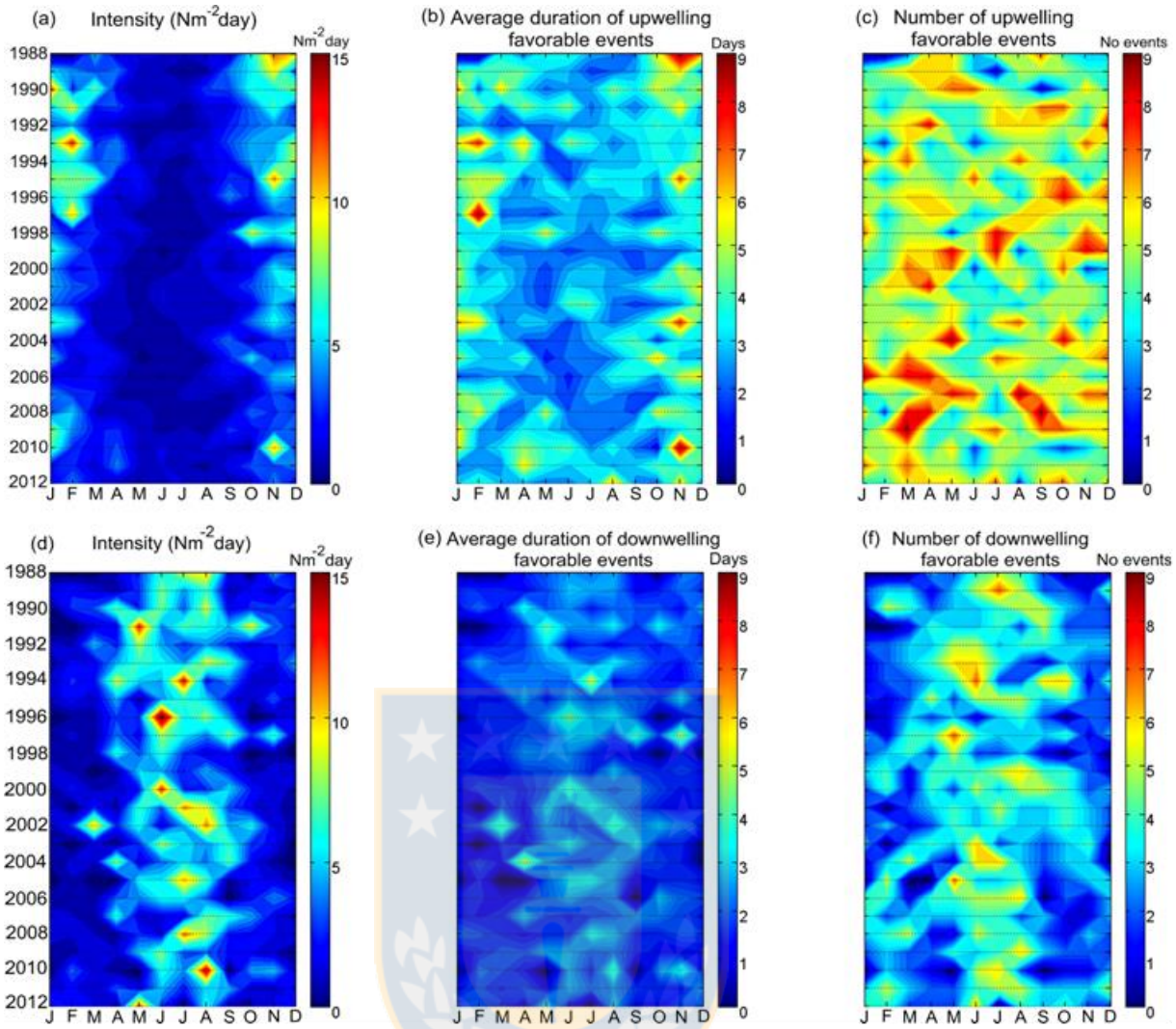

Figure 6. Interannual and monthly variability of intensity, average duration, and number of upwelling-favorable events (a, b, c) and downwelling-favorable events (d, e, f).

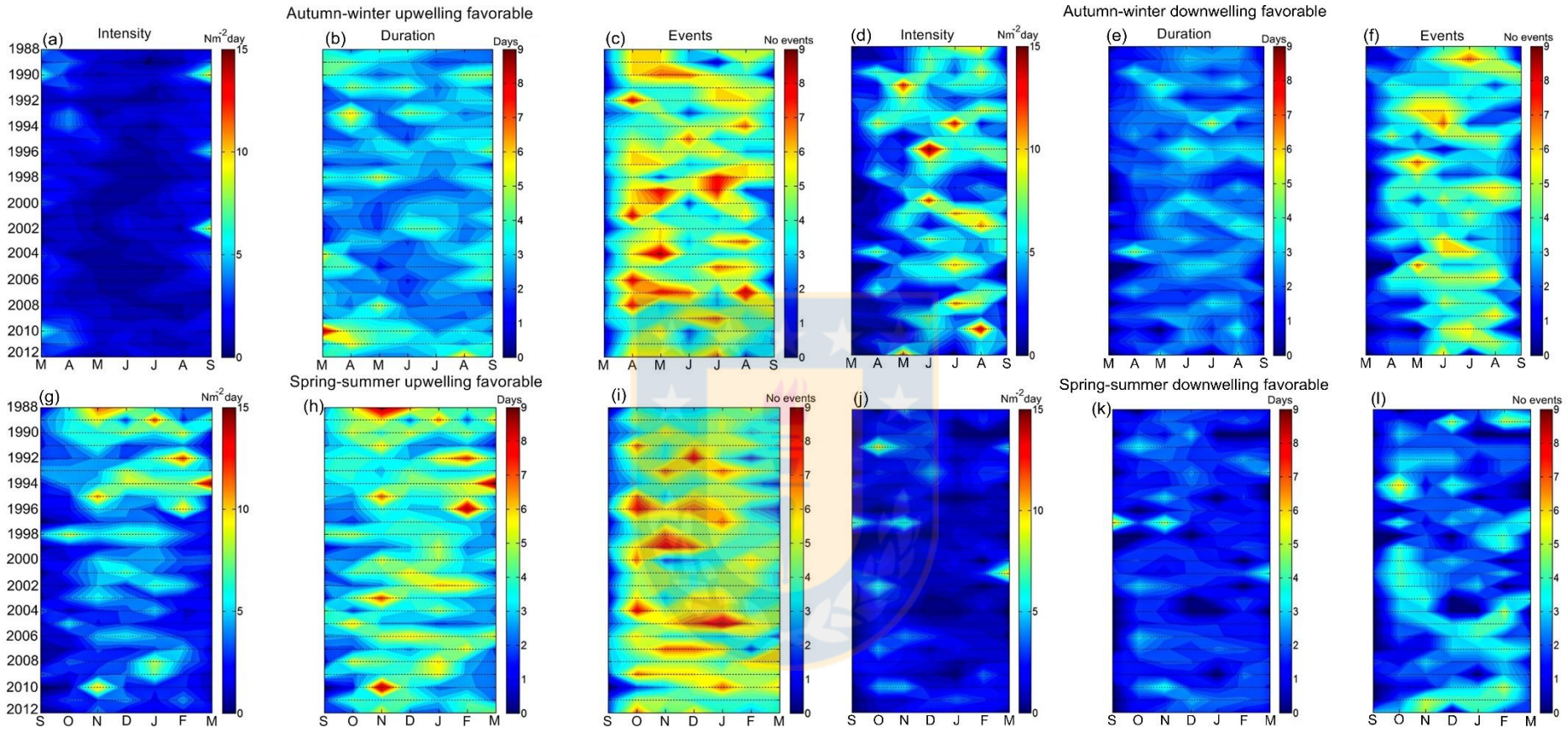

Figure 7. Interannual and monthly variability of intensity, average duration and number of upwelling-favorable (a, b, c, g, h, i) and downwelling-favorable events (d, e, f, j, k, l).

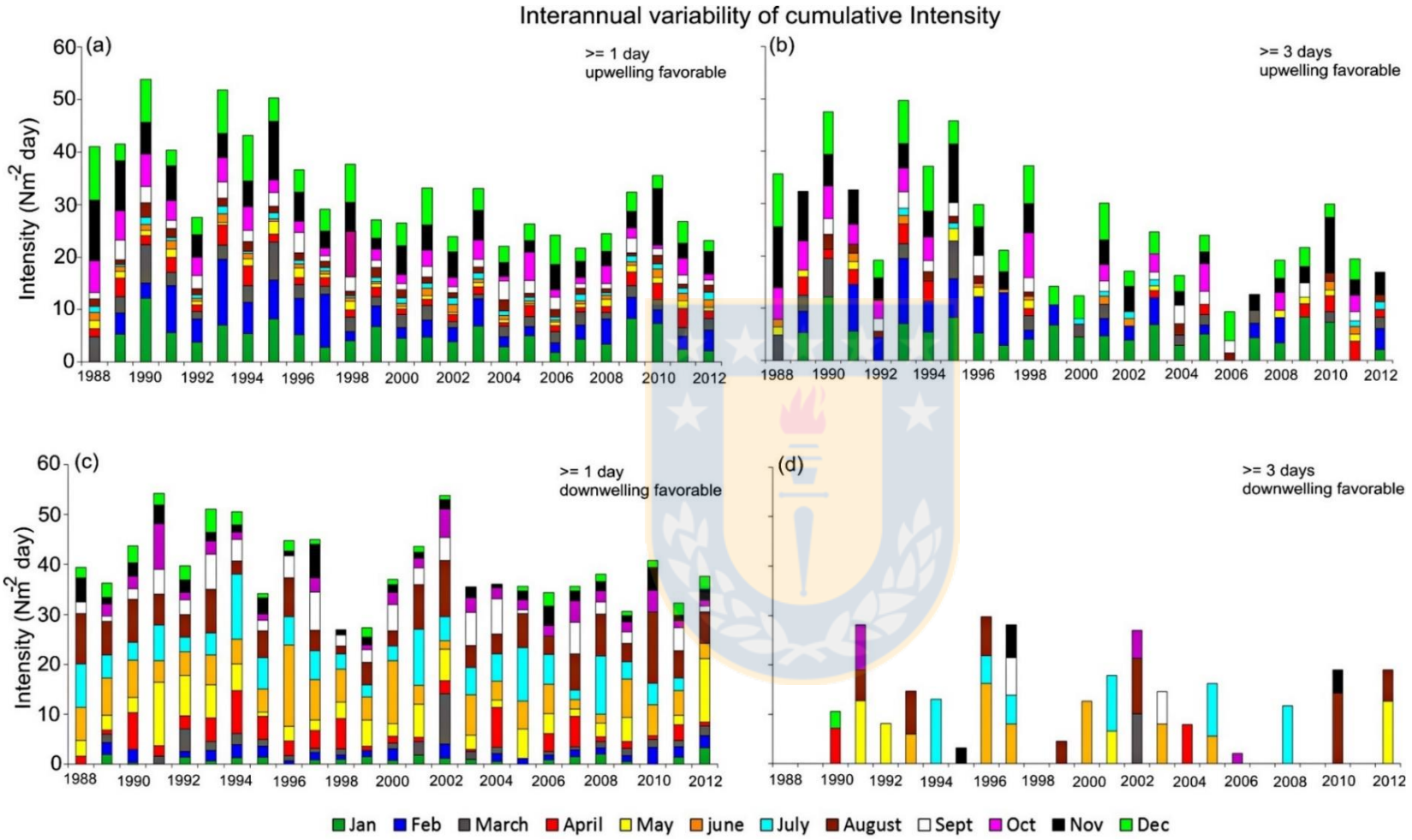

Figure 8.Interannual variability of cumulative intensity of upwelling-favorable events >= 1 day (a) and >= 3 days (b) and cumulative intensity of downwelling-favorable events >= 1 day (c) and >= 3 days (d).

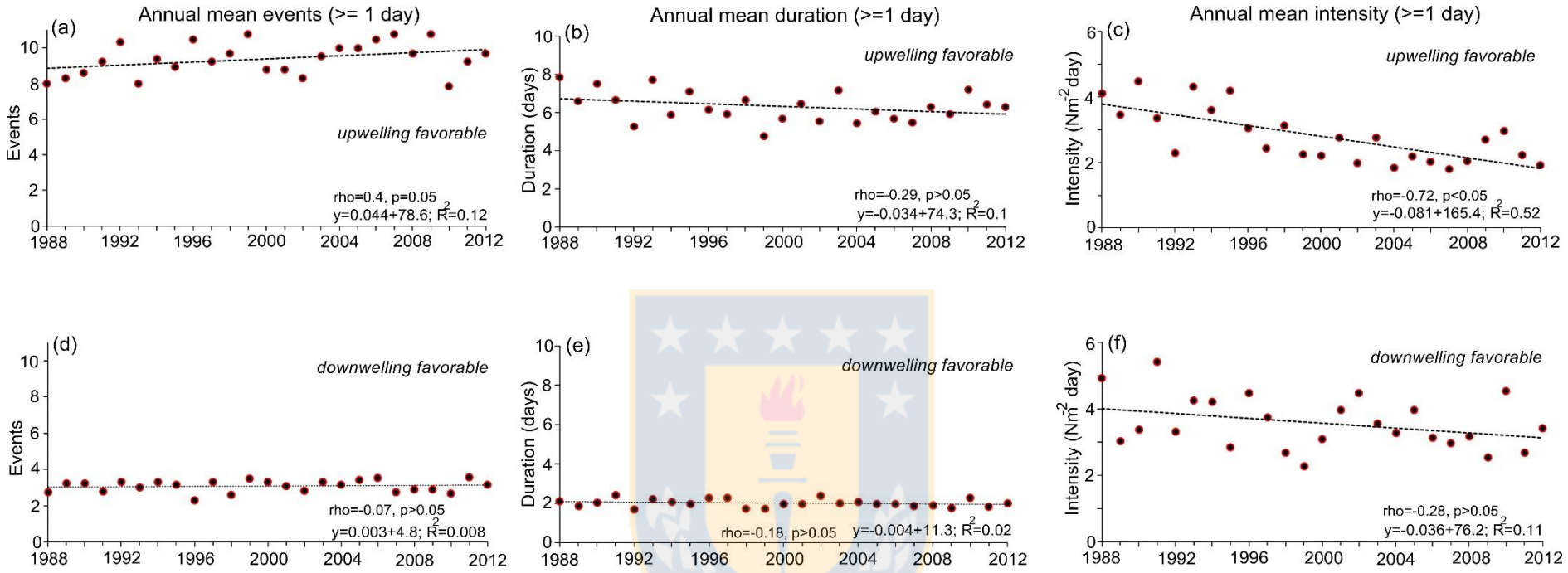

Figure 9. Annual mean of events number, duration and intensity of upwelling-favorable (a, b, c) and downwelling-favorable (d, e, h).

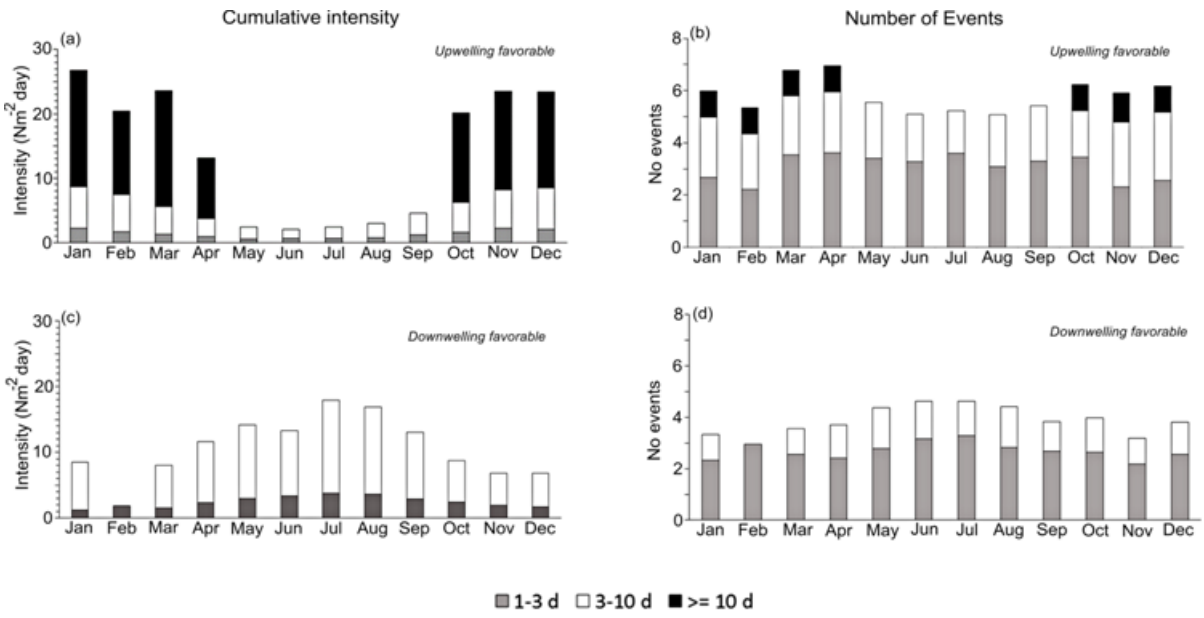

Figure 10: Annual cycle of cumulative intensity and number of upwelling-favorable (a, b) and downwelling-favorable events (d, c) of short events (1-3 days), medium-lenght events (3-10 days) and long events (>= 10 days).

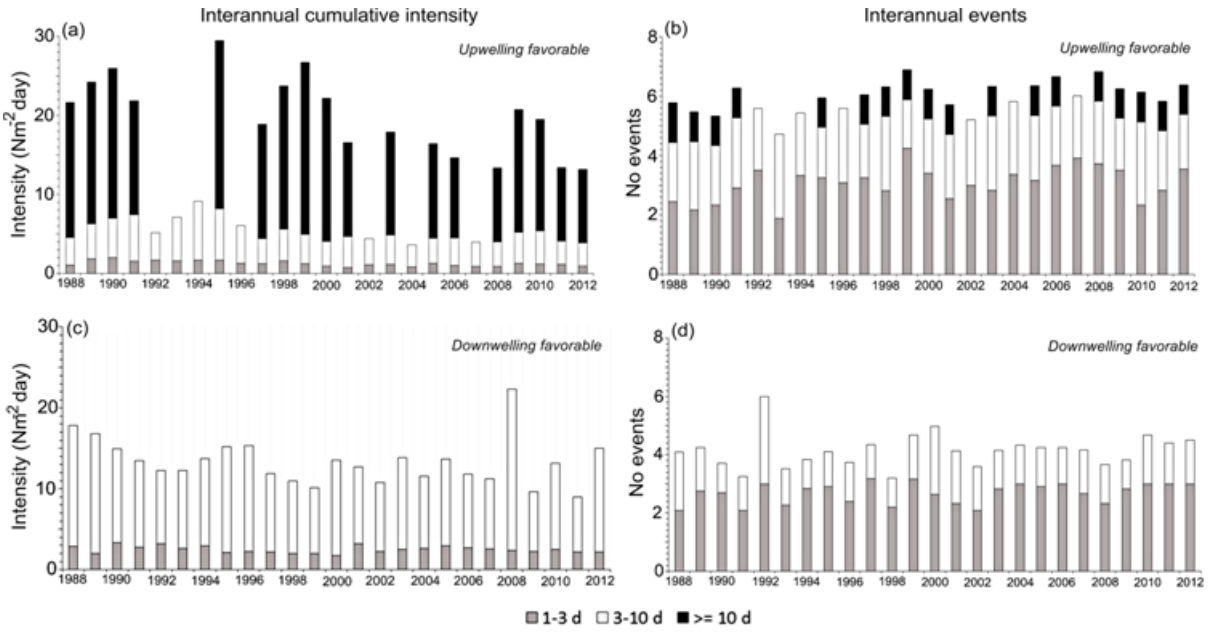

Figure 11: Interannual variability of cumulative intensity and number of upwelling favorable (a, b) and downwelling-favorable events (c, d) of short events (1-3 days), medium-length events (3-10 days) and long events (>= 10 days).

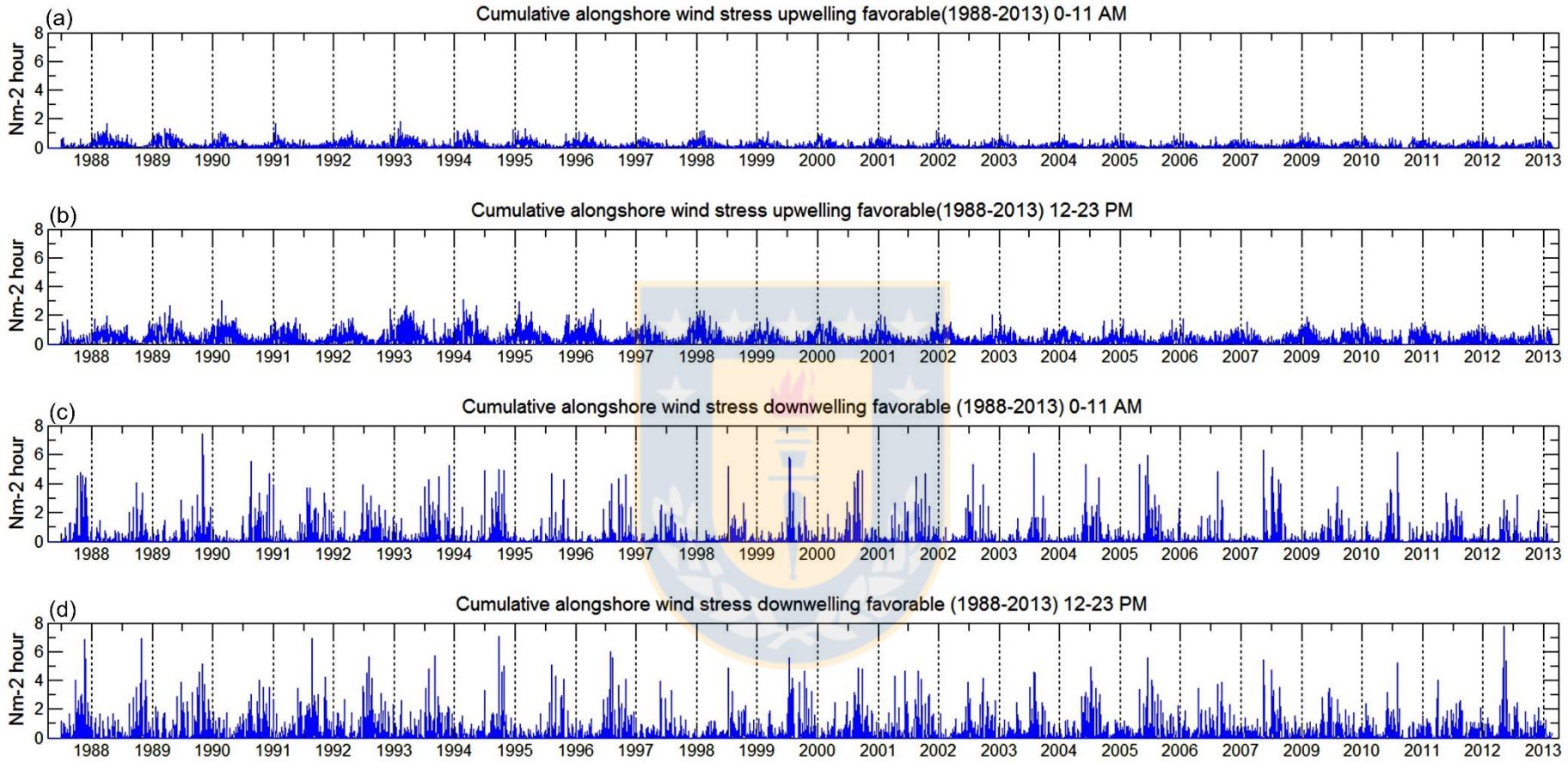

Figure 12: Cumulative wind stress of upwelling-favorable events between 0-11 am (a) and 12-23 pm (b) and downwelling-favorable events between 0-11 (c) am and 12-23 pm (d).

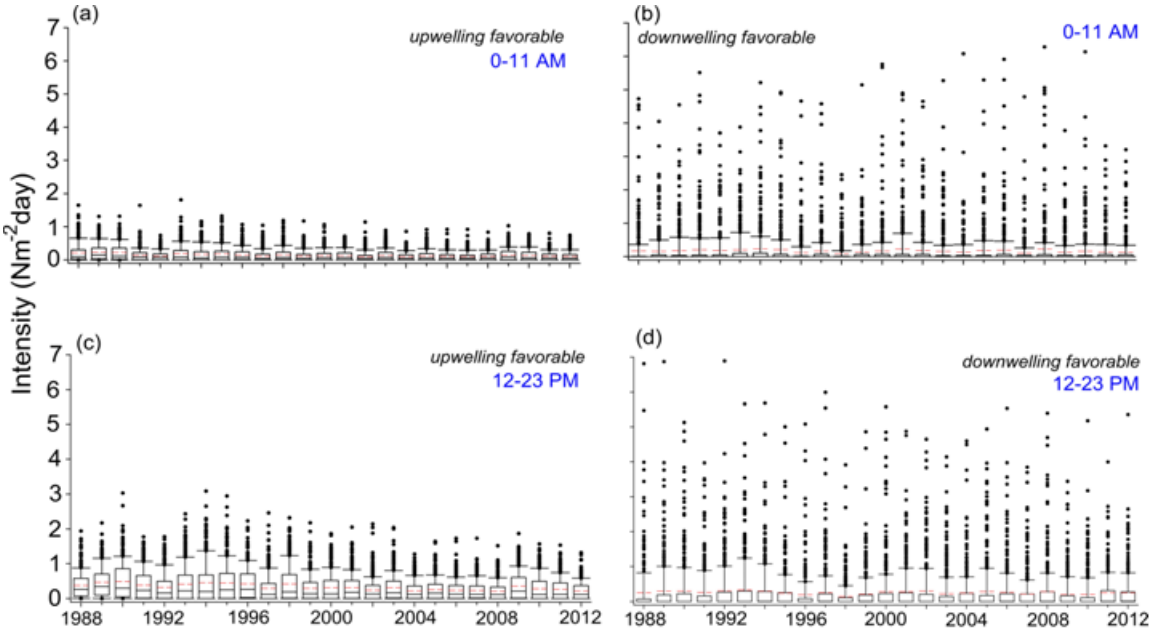

Figure 13: Interannual variability of upwelling-favorable intensity between 0-11 am (a) and between 12-23 pm (b) and downwelling-favorable intensity between 0-11 am (c) and between 12-23 pm (d).

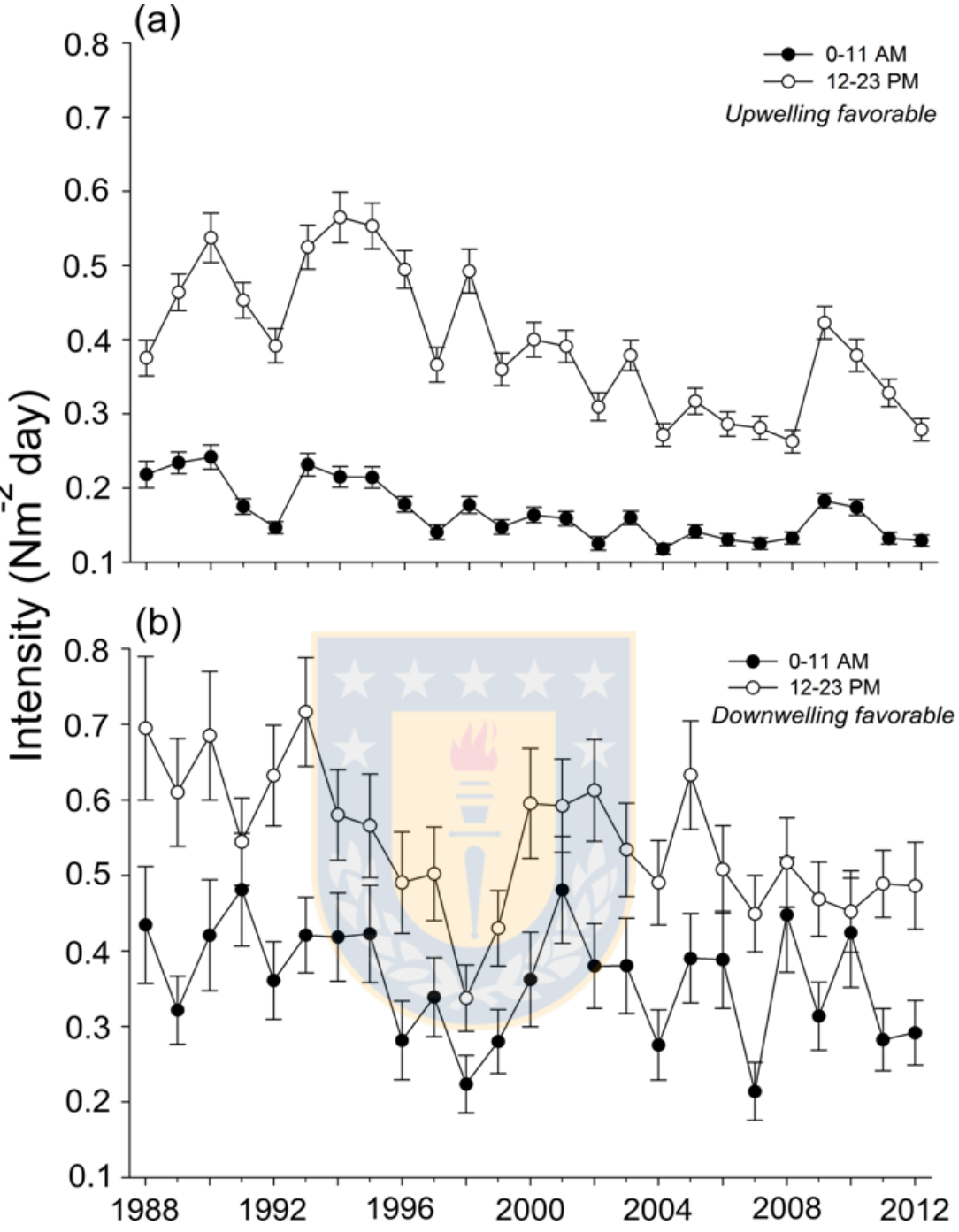

Figure 14: Average intensity of upwelling-favorable events (a) and downwelling-favorable events (b). Bars represent the standard error.

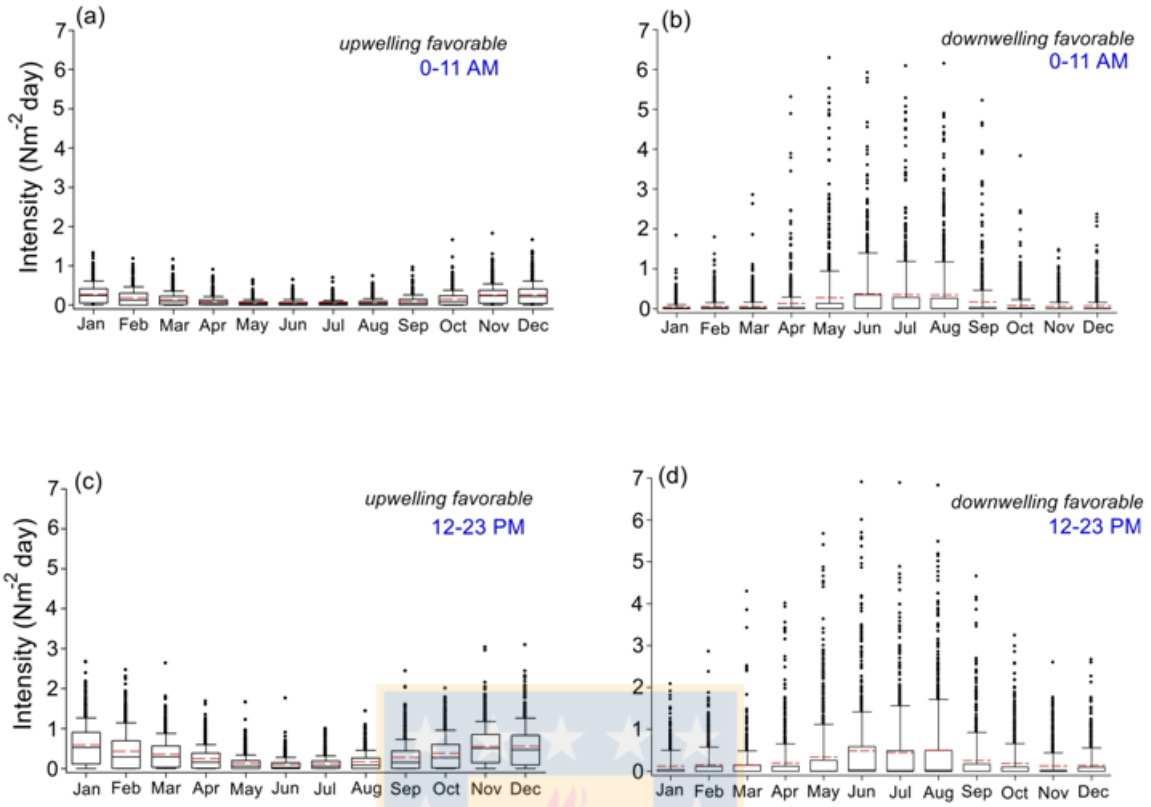

Figure 15: Seasonal variability of upwelling-favorable events between 0-11 am (a) and between 12-23 pm (b) and downwelling-favorable events between 0-11 am (c) and between 12-23 pm (d).

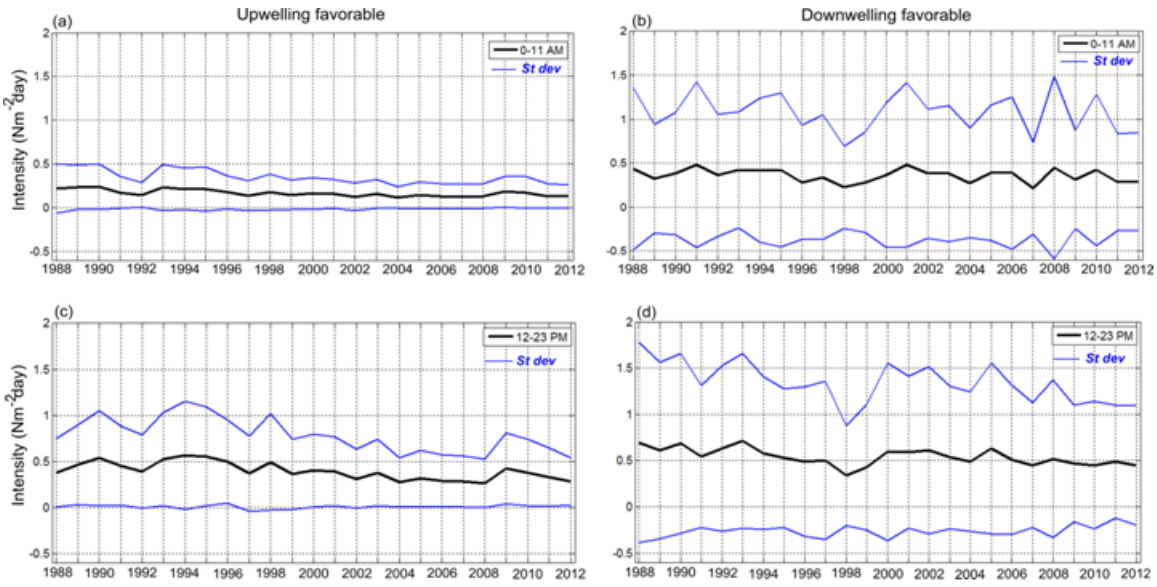

Figure 16: Interannual variability of mean intensity of upwelling-favorable events between 0-11 am (a) and between 12-23 pm (b) and mean intensity of downwelling-favorable events between 0-11 am (c) and between 12-23 pm (d).

4.2. Capítulo 2. Modelación de la dinámica estacional de la Corriente Subsuperficial Chile-Perú (30º-40ºS)

Manuscrito publicado en revista Continental Shelf Research (https://doi.org/10.1016/j.csr.2016.04.001): Vergara, O.A., Echevín, V., Sepúlveda, H.I.., Colas, F., Quiñones, R. A. Modelling the seasonal dynamics of physical variables and the Peru- Chile Undercurrent off Central Chile (30°-40°S).

Resumen: La variabilidad estacional de la hidrología y de la Corriente Subsuperficial Perú-Chile (PCUC) frente a la costa de Chile centro-sur (29°-41°S) fueron examinadas utilizando un modelo regional de alta resolución. El modelo reproduce de forma realista la variabilidad observada en el nivel del mar, tales como intensos remolinos anticiclónicos, la intensificación fuera de la costa del flujo hacia el polo, la reducción del flujo hacia el ecuador cerca de la costa durante otoño, así como la intensificación del flujo hacia el ecuador de meandros cerca de la costa durante la primavera. Los valores de la energía geostrófica cinética de remolinos, fueron altos a lo largo de la costa entre 30° y 37°S, y más bajos al sur de esta zona. La corriente subsuperficial hacia el polo exhibió variabilidad latitudinal en la velocidad y el transporte. El transporte promedio máximo reportado fue de 0.8 Sv en 30°S, consistente con previos estudios de modelación y estimaciones derivadas de las observaciones in situ. Se observó reducción de la fuerza de esta corriente hacia el sur generada en parte por la disminución del wind stress curl hacia el polo y por la formación de un jet cerca de 35°S asociado con la propagación de remolinos hacia el oeste. Un análisis lagrangiano de las parcelas de agua modeladas transportadas por la corriente muestra que sólo el 14-20% de los flotadores subsuperficiales transportados por la corriente son advectados a superficie dentro de los siguientes seis meses después de su liberación. Los flotadores que quedan dentro de la capa subsuperficial probablemente son transportados más al sur por la corriente, fuera de la costa por los remolinos que se propagan hacia el oeste o hacia el ecuador en la parte subsuperficial de la corriente costera superficial.

Continental Shelf Research 123 (2016) 61–79

Contents lists available at ScienceDirect

Continental Shelf Research

journal homepage: www.elsevier.com/locate/csr

Research papers

Modelling the seasonal dynamics of the Peru-Chile Undercurrent off Central Chile (30–40°S)

Odette A. Vergara [a,b], Vincent Echevín [c], Héctor H. Sepúlveda [d], Francois Colas [c], Renato A. Quiñones [a,b,*]

[a] Interdisciplinary Center for Aquaculture Research, Universidad de Concepción, O'Higgins 1695, Concepción, Chile
[b] Doctorate Program in Oceanography, Department of Oceanography, Universidad de Concepción, Casilla 160-C, Concepción, Chile
[c] Laboratoire d' Oceanographie et de Climatologie: Expérimentation et Analyse Numérique (LOCEAN), Institute Pierre-Simon Laplace (IPSL), UPMC/CNRS/IRD/MNHN, 4 Place Jussieu, Case 100, 75252 Paris Cedex 05, France
[d] Department of Geophysics, University of Concepción, Concepción, Chile

ARTICLE INFO

Article history:
Received 17 July 2015
Received in revised form
20 January 2016
Accepted 1 April 2016
Available online 2 April 2016

Keywords:
Ocean modelling
Poleward subsurface Peru-Chile Undercurrent
Eastern Boundary Upwelling System
Humboldt Current System

ABSTRACT

The seasonal variability of the hydrology and the poleward subsurface Peru-Chile Undercurrent (PCUC) off the central Chilean coast (29–41°S) were examined using a high-resolution regional model. The model realistically reproduced observed sea level variability, such as intense anticyclonic eddies, the offshore intensification of the poleward flow and the reduced nearshore equatorward flow during autumn, as well as the equatorward intensification of nearshore meandering flow during spring. Values for geostrophic eddy kinetic energy were high along the coast between 30° and 37°S, and lower south of this area. The modelled poleward undercurrent showed latitudinal variability in velocity and transport. The maximum average transport reported was 0.8 Sv near 30°S, consistent with previous modelling studies and estimations derived from in situ observations. The poleward reduction in undercurrent strength was shown to be partly generated by the poleward decrease in wind stress curl and by the formation of a westward jet near 35°S associated with westward-propagating eddies. A Lagrangian analysis of the modelled water parcels transported by the undercurrent shows that only 14–20% of the subsurface floats transported by the undercurrent upwelled into the surface layer within the subsequent six months after their release. The floats remaining within the subsurface layer were likely transported further south by the current, offshore by westward-propagating eddies or equatorward by the deeper part of the surface coastal current.

1. Introduction

The Eastern Boundary Upwelling (EBUS), California, Humboldt, Canarias and Benguela systems, are among the most productive marine systems in the world and support the greatest pelagic fisheries on earth (Chávez et al., 2003, 2008; Pauly and Christensen, 1995). In these regions the wind is generally parallel to the coastline and forces a nearshore upwelling, which brings cold, nutrient-replete deep water to the surface, generating high levels of biological productivity. Understanding the dynamics of the EBUS is highly relevant given the local manifestations of climate change, such as ocean acidification (Gruber et al., 2012) and wind regime change (Bakun, 1990; Bakun et al., 2010; Belmadani et al., 2014; Garreaud and Falvey, 2009; Sydeman et al., 2014). Changes in winds due to increased greenhouse gases could modify upwelling, which together with changes in the characteristics of water masses (e.g. subsurface nutrient concentration), could significantly affect coastal ecosystems (Aiken et al., 2011; Brochier et al., 2013; Gutiérrez et al., 2011; Oerder et al., 2015).

The Humboldt Current System (HCS) is part of the general

Abbreviations: AAIW, Antarctic Intermediate Water; AVHRR, Advanced Very High Resolution Radiometer; AVISO, Archiving, Validation and Interpretation of Satellite Oceanographic data; CARS, CSIRO Atlas of Regional Seas; CCC, Chile Coastal Current; COADS, Comprehensive Ocean-Atmosphere Data Set; CSIRO, Commonwealth Scientific and Industrial Research Organisation; CTW, coastal trapped waves; EBUS, Eastern Boundary Upwelling Systems; EKE, Eddy Kinetic Energy; ESSW, Equatorial Subsurface Water; ETOPO2, Earth Topography and Bathymetry; EUC, Equatorial Undercurrent; HCS, Humboldt Current System; FIP, Fondo de Investigación Pesquera y Acuicultura; IEKW, intraseasonal equatorial Kelvin waves; KPP, K-Profile Parameterization; PCCC, Peru-Chile Countercurrent; PCUC, Peru-Chile Undercurrent; PDW, Pacific Deep Water; POM, Princeton Ocean Model; ROMS-AGRIF, Regional Oceanic Modeling System - Adaptive Grid Refinement in FORTRAN; SAAW, Sub-Antarctic Water; SCDW, Scatterometer Climatology of Ocean Winds; SLA, Sea Level Anomaly; SSCC, Southern Subsurface Countercurrent; SST, Satellite Sea Surface Temperature; STW, Subtropical Water

* Corresponding author at: Interdisciplinary Center for Aquaculture Research, Universidad de Concepción, O'Higgins 1695, Concepción, Chile.

http://dx.doi.org/10.1016/j.csr.2016.04.001
0278-4343/

circulation of the Southeastern Pacific Subtropical Gyre and contains complex movements of surface waters towards the equator and the pole (Schneider et al., 2004). Off Central Chile (30–40°S), the flow of oceanic and coastal branches of the HCS driven by the meridional winds associated with the South Pacific anticyclone intensify during summer and diminish during winter (Fuenzalida et al., 2008). The HCS is composed of several currents: the surface Chile Coastal Current (CCC) above a depth of 100 m between the continental shelf and the slope flowing towards the equator during summer; the poleward surface Peru-Chile Countercurrent (PCCC), which flows between 100 and 300 km offshore above a depth of 100 m, reaching maximum velocities in spring and minimum velocities in autumn (Strub et al., 1995, 1998); and the poleward subsurface Peru-Chile Undercurrent (PCUC), which flows below the CCC between 100 and 400 m (Strub et al., 1998). The northern and central coast of Chile (18–38°S), where the PCUC dominates, is highly productive in terms of fisheries. Sardine and anchovy are among the most abundant resources in the first 100 nm from the coast (Cubillos et al., 2002, 2007; Cubillos and Arancibia, 1993). These important biological resources are generated by the combination of upwelling and the fuelling of nutrients by the PCUC (Fonseca, 1989; Quiñones et al., 2010).

Poleward subsurface currents such as the PCUC are present in every EBUS (Fonseca, 1989; Hill et al., 1998; Neshyba et al., 1989) at mid-latitudes, opposing the equatorward surface flow (Pierce et al., 2000). These subsurface currents generally reach average velocities along the coast of ~0.05 m/s to ~0.2 m/s, distributed between depths of 150 and 300 m, as reported for the California Undercurrent (e.g. Gay and Chereskin, 2009; Hickey, 1979; Thomson and Krassovski, 2010) and the Iberian Peninsula (0.2 m/s; Haynes and Barton, 1990; Torres and Barton, 2006). In the HCS, the PCUC originates off the coast of Peru near 5°S and flows as far south as the Gulf of Penas (48°S; Silva and Neshyba, 1979; Wooster and Gilmartin, 1961; Wooster and Reid, 1963). The origin of the PCUC is generally recognized as stemming from the EUC (Equatorial Undercurrent) and two branches of the SSCC (Southern Subsurface Countercurrent; Montes et al., 2010; Czeschel et al., 2011).

Direct measurements of the PCUC have been made off the coast of Peru (Chaigneau et al., 2013; Huyer et al., 1987) and Chile (Codispoti et al., 1989; Pizarro et al., 2002; Shaffer et al., 1997, 1999). Based on 6 years of data at 30°S, Shaffer et al. (1999) reported an average velocity of 12.8 cm/s at 220 m, with semiannual variation and an intensified poleward flow in spring. The average estimated transport of the PCUC at 30°S is 1–1.3 Sv (Huyer et al., 1987; Shaffer et al., 1999, 2004).

The semi-annual variations of the PCUC are responses to the combination of local wind stress curl and disturbances caused by remote tropical forcing (Pizarro et al., 2002; Ramos et al., 2006). This flow is also modulated interannually by Rossby waves forced by trapped waves propagating southward along the coast of South America (Belmadani et al., 2012; Pizarro et al., 2002), a physical mechanism that also partly explains the variability in the oxygen minimum zone off Chile (Hormazábal et al., 2006).

The PCUC is thought to be fuelled by Equatorial Subsurface Water (ESSW) as a consequence of periods of intense and persistent wind-driven upwelling in southern-central Chile, leading to low oxygen conditions (Fuenzalida et al., 2009; Hernández-Miranda et al., 2010; Ulloa and Pantoja, 2009) and high nutrient concentrations, which favour primary productivity (average annual of 10–20 g C m^{-2} day^{-1}, Daneri et al., 2000; Montero et al., 2007). The ESSW is located below the subtropical water mass (STW) off Peru (10–18°S) and above Subantarctic Water (SAAW) off Chile (25–48°S; Silva et al., 2009). Originally described by Gunther (1936), this water mass is characterized by a subsurface salinity maximum (~34.9) and by low dissolved oxygen concentrations (4.4–44.6 μM, 2–15% saturation) and high nutrient concentrations (20–40 μM nitrate, 2.6–3 μM phosphate; 25–40 μM silicate; Silva et al., 2009). The PCUC transports this water mass along the continental slope off Peru and Chile (Silva and Fonseca, 1983; Strub et al., 1998; Wooster and Gilmartin, 1961; Wyrtki, 1967), until it disappears near 48°S (Silva and Neshyba, 1979).

Given the influence of the PCUC on the poleward transport of the ESSW, studying its dynamics on the continental slope along the coast of Chile is relevant to understand north-south nutrient, oxygen and plankton fluxes, which play an important role in sustaining high biological productivity in the HCS. Numerical modelling is a very useful approach to understand the characteristics and dynamics of currents. Several modelling studies have been conducted in the Chile region. Using a high-resolution model, Batteen et al. (1995) studied the response of the Chile coastal region from 22.5°S to 35°S to climatological wind forcing. They showed that equatorward winds generate mesoscale features and a poleward flow of 5–15 cm/s. Other works have employed the Princeton Ocean Model (POM, Blumberg and Mellor, 1987). Mesias et al. (2001) characterized circulation in the Gulf of Arauco (37°S) during summer and the effect of seafloor topography and coastal geometry on the upwelling regime, highlighting the formation of an equatorward coastal jet during the active upwelling phase. Leth and Shaffer (2001) used POM to study circulation off central Chile, reproducing an equatorward coastal current, a poleward undercurrent and the formation of meanders and eddies in response to the baroclinic instability of the flow. Leth and Middleton (2004) found that the presence of a cyclonic gyre in conjunction with the upwelling-favourable wind enhanced upwelling in the Gulf of Arauco. More recently, the Regional Ocean Modeling System (ROMS, Shchepetkin and McWilliams, 2005, see Section 2.1) has been applied to upwelling regions in the southeast Pacific, analysing circulation and seasonal (Aguirre et al., 2012; Penven et al., 2005), interannual (e.g. the 1997–1998 El Niño event, Colas et al., 2008) and intraseasonal variability (Belmadani et al., 2012; Echevin et al., 2014). Process studies have also addressed the impact of mesoscale eddies on heat balance (Colas et al., 2012), ocean surface dynamics (Aguirre et al., 2012, 2014) and their impact on larval transport (Parada et al., 2012; Soto-Mendoza et al., 2012; Yanicelli et al., 2012). However, none of the previous studies have focused in detail on the seasonal dynamics of the PCUC along the Chilean coast and their influence on the poleward transport of water masses.

The objectives of the present study are to: (a) characterize the nearshore dynamics of the HCS in central Chile (30–40°S, 70–80°W) using a high-resolution regional model and to determine the seasonal variability of physical variables (temperature, salinity, density and sea surface height); (b) describe the seasonal variability of the PCUC in terms of transport and velocity along the Chilean coast; and (c) study the trajectory of water masses using Lagrangian float diagnostics. In this study, we focus on the nearshore zone, which corresponds a ~100–200 km-wide coastal band as opposed to the open ocean off the continental margin. The methodology is described in Section 2. The hydrodynamic model configuration is presented in Section 2.1, and the diagnostics for the PCUC characteristics and for the Lagrangian analysis of water masses transported by the PCUC are described in Section 2.2 and 2.3, respectively. The water masses are described in Section 2.4 and the data used to assess the realism of the model are presented in Section 2.5. The results on the mean and seasonal cycle of the main physical variables of the model are presented in Section 3.1, while Section 3.2 presents the results of the Lagrangian analysis. The discussion is presented in Section 4 and the conclusions are summarized in Section 5.

2. Methods

2.1. Hydrodynamic model and grid configuration

The hydrodynamic model used in this study is the ROMS-AGRIF (Regional Oceanic Modeling System – Adaptive Grid Refinement in FORTRAN, Shchepetkin and McWilliams, 2005; Penven et al., 2006; http://www.romsagrif.org). This model utilizes sigma (terrain-following) coordinates in the vertical plane and orthogonal-curvilinear coordinates in the horizontal plane. It solves the primitive hydrostatic equations with an explicit free-surface scheme. Subgrid-scale vertical mixing is parameterized using the KPP (K-Profile Parameterization) boundary layer scheme (Large et al., 1994). Bottom topography from the SRTM30 database (Becker et al., 2009) was interpolated onto the model grid and smoothed following Penven et al. (2005) to reduce pressure gradient errors. Simulations were carried out on a grid between 29°S and 41°S, and from 69°W to 83°W (Fig. 1), with a resolution of 7.5 km and 32 sigma levels. The initial and open boundary fields were obtained from a monthly climatology of a simulation analysed by Colas et al. (2012; Peru-Chile Model, with a spatial resolution of 7.5 km and 32 vertical sigma levels) using the "Roms2Roms" offline interpolation package (Mason et al., 2010). Open boundary conditions were treated using an Orlanski scheme for the tracers and baroclinic velocities, and a Flather scheme for the barotropic mode (Marchesiello et al., 2001).

The atmospheric forcings used were the 0.25° × 0.25° SCOW wind stress (Scatterometer Climatology of Ocean Winds, Risien and Chelton, 2008, Fig. 2) derived from Quikscat data and heat and fresh water fluxes from COADS climatology (Comprehensive Ocean-Atmosphere Data Set, da Silva et al., 1994). A relaxation of the modelled sea surface temperature to the Pathfinder monthly climatology (Casey et al., 2010) was imposed following the parameterization of Barnier et al. (1995) with a nudging coefficient with slight spatial and temporal variations, between ~−25 and ~33 W m^{-2} °C^{-1}. A relaxation to COADS surface salinity with a time scale of 30 days was also included, whereas the runoffs of Chilean rivers (e.g. The Biobio River near 36°S) were not explicitly incorporated into the simulation.

Ten years were simulated, of which 9 were used to obtain an average climatological year of physical variables (temperature, salinity, currents and sea level) and to do the Lagrangian analysis.

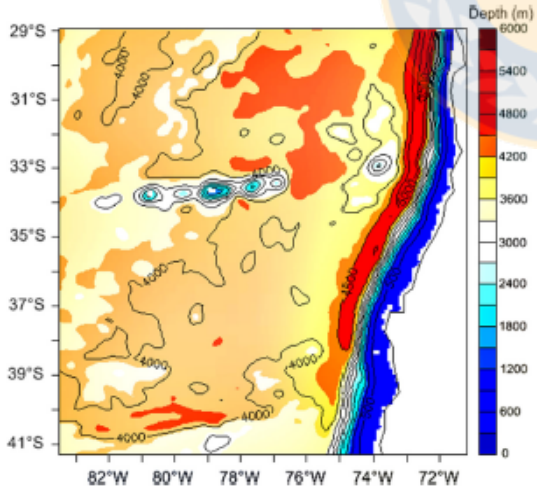

Fig. 1. Simulated bathymetry of the study area.

Seasonal means correspond to JFM (summer), AMJ (autumn), JAS (winter), and OND (spring).

2.2. Currents

2.2.1. Transport along the coast

Average monthly and seasonal transports were calculated at 30°S, 33°S, 36°S and 39°S to determine the spatial and temporal variability of the PCUC along the continental slope in the study area. For each month of model output, velocity fields were interpolated from sigma levels to z levels every 5 m. Then, negative (poleward) velocities between the surface and a maximum depth of 650 m and between the coast and 100 km offshore were integrated to compute poleward transport. The modelled transport was also compared to that obtained in other studies (Leth et al., 2004; Pizarro et al., 2002; Shaffer et al., 1997, 1999), and in previous model simulations (Aguirre et al., 2012; see Table 1).

2.2.2. Longitudinal width and nucleus of maximum PCUC velocity

The average east-west (zonal) width of the poleward current (defined as negative velocity) and the maximum velocity at a depth of 200 m (which corresponds to the average shelf break depth between 30°S and 40°S) were determined seasonally (autumn, winter, spring, summer) at 30°, 33°, 36° and 39°S.

2.3. Trajectory of the water masses transported by the PCUC

The ROMS-offline tracking module was used to calculate numerical Lagrangian trajectories of water parcels from three-dimensional ROMS velocity fields (Capet et al., 2004; Carr et al., 2008). This type of numerical method has proved to be appropriate for studying the origin and the trajectory of ocean water masses (Blanke et al., 2002; Mason et al., 2012; Montes et al., 2010). Virtual Lagrangian floats were launched in the PCUC core along two cross-shore sections (33° and 37°S) with a vertical spacing of 15 m in the vertical and 2 km in the horizontal. For each month of the 9-year-long simulation, approximately 800 floats were initially released along the sections in the PCUC at depths between 50 m and 700 m, and within 200 km from the coast. Their trajectories were then integrated for a period of six months, with a time step of 14.4 min and using model outputs every 3 days. Statistics on the trajectories of the floats originating from the PCUC were computed. Floats were considered to be upwelled when they reached the surface layer delimited by a depth of 50 m. We then computed the initial depth of the "upwelled" floats within the PCUC sections and the transit time of the floats between their initial and final position (i.e. where they entered the surface layer) (see Table 2). Statistics were compiled for the floats that were not upwelled in their 6-month transit: the distance to the coast, latitude and initial depth of the floats (see Table 3).

2.4. Water masses

Using the ROMS data, a temperature-salinity (TS) diagram was plotted for the region [35.5–40°S; 72.75–77.8°W] to determine the water masses present in the study area during the summer season. The water masses from this study area (Bernal et al., 1982; Silva et al., 2009; Silva and Konow, 1975) are characterized as follows: Subtropical Water (STW), > 18.5 °C > 34.9, Subantarctic Water (SAAW), 11.5–14.5 °C, 34.1–34.8, Equatorial Subsurface Water (ESSW), 8.5–10.5 °C, 34.4–34.9 Antarctic Intermediate Water (AAIW), 4–8 °C, 34.3–34.5 and Pacific Deep Water (PDW), 1.75 °C, 34.68.

Additionally, the composition of each water mass (percentage) at 37°S; 75.3°W (Gulf of Arauco) in the vertical profile of salinity and temperature during summer was calculated. The percentage

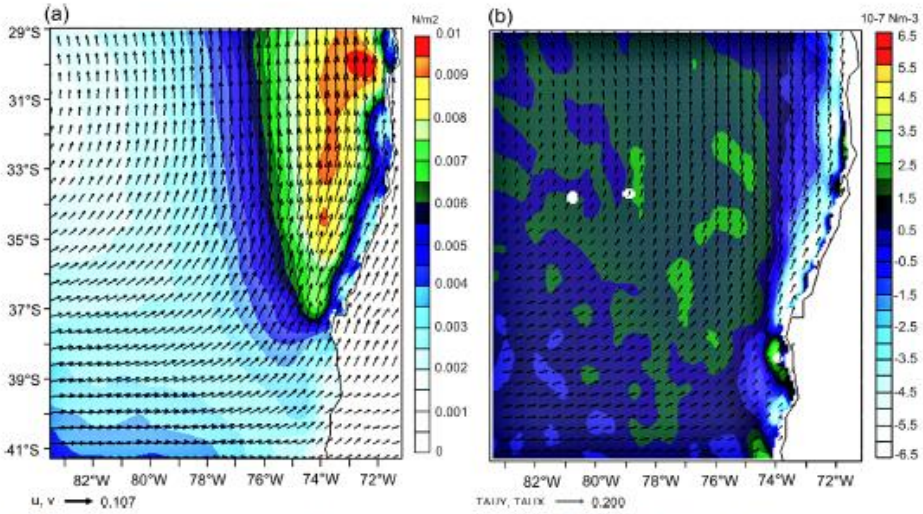

Fig. 2. Annual average of wind stress magnitude (N m^{-2}) (a) and wind stress curl 10^{-7} N m^{-3} (b) derived from SCOW in the study zone.

Table 1
Seasonal and annual mean poleward transport (in Sv, positive poleward) of the Peru-Chile Undercurrent at 30°S, 33°S, 36°S and 39°S. The transport was calculated from model output in our study and Aguirre et al. (2012), and from observations in Leth et al. (2004) and Shaffer et al. (1997, 1999). Variability corresponding to the standard deviation around the mean for the 9-year simulation is indicated.

Latitude/ Season	*This study*	Aguirre et al. (2012)	Leth et al. (2004)	Shaffer et al. (1997, 1999)
28°S			1.3	
30°S				
Fall	0.85 ± 0.36	1.06		
Winter	0.68 ± 0.37	0.86		
Spring	0.94 ± 0.41	0.87		
Summer	0.73 ± 0.54	0.81		
Average	0.80 ± 0.4	0.9		1
33°S				
Fall	0.82 ± 0.23	0.81		
Winter	0.46 ± 0.29	0.61		
Spring	0.81 ± 0.29	0.7		
Summer	0.90 ± 0.24	0.73		
Average	0.76 ± 0.17	0.71		
35°S				
Average	0.76 ± 0.36		1.3	
36°S				
Fall	0.50 ± 0.32	0.68		
Winter	0.22 ± 0.26	0.55		
Spring	0.45 ± 0.35	0.43		
Summer	0.71 ± 0.49	0.85		
Average	0.47 ± 0.17	0.62		
39°S				
Fall	0.48 ± 0.16	0.34		
Winter	0.15 ± 0.10	0.20		
Spring	0.08 ± 0.09	–		
Summer	0.34 ± 0.17	0.17		
Average	0.26 ± 0.09	0.27 ± 0.09		
43°S			1.1	

of water types was calculated by the mixing triangle method (Silva and Konow, 1975), using the values indicated by Silva and Konow (1975) and Silva et al. (2009). This latitude was chosen because of the enhanced upwelling in the Gulf of Arauco (Leth and Middleton, 2004).

Table 2
Percentage/initial depth of floats that upwell in the surface layer (50 m depth) with respect to the total number of floats launched in the PCUC at 33°S and 37°S, for each season. Standard deviations indicate interannual variability due to the impact of mesoscale turbulence, which differs from year to year.

Percentage/initial depth of upwelled floats		
Season	***33°S***	***37°S***
Autumn	19.6 ± 4.6/110 ± 28	13.9 ± 4.5/108 ± 16
Winter	20.2 ± 7.1/131 ± 42	16.5 ± 5.9/102 ± 20
Spring	19.2 ± 4.5/120 ± 38	12.8 ± 4.9/119 ± 56
Summer	19.3 ± 3.7/107 ± 30	16 ± 4.9/116 ± 22

Table 3
Statistics (mean and standard deviation) of the positions (latitude, depth and distance to the coast) of the floats that had not upwelled 6 months after being launched from the 33°S and 37°S sections.

Latitude of launch	*Season*	*Latitude* (°S)	*Distance to coast* (km)	*Depth* (m)
33°S	Winter	33.0 ± 1.5	294 ± 157	322 ± 167
37°S	Winter	36.2 ± 1.5	330 ± 202	340 ± 174
33°S	Summer	34.5 ± 2.0	284 ± 198	327 ± 169
37°S	Summer	37.3 ± 1.7	263 ± 153	361 ± 184

2.5. General assessment of the simulation

2.5.1. Sea level height and eddy kinetic energy

AVISO (Archiving, Validation and Interpretation of Satellite Oceanographic data) satellite altimetry data was used for 1992–2005 to assess the variability of the modelled sea level height (http://www.aviso.oceanobs.com/). With these data the sea level anomalies for autumn and spring in the study area were calculated. The average geostrophic eddy kinetic energy (EKE), a measure of surface mesoscale turbulence, was computed from the surface geostrophic current anomalies derived from the sea level anomalies. The same calculation was made using the model output.

2.5.2. Temperature and salinity

Satellite Sea Surface Temperature (SST) from the Advanced

Very High Resolution Radiometer (AVHRR) Pathfinder product version 5.0 (Casey et al., 2010) was compared to simulated SST. In addition, cross-sections of average ROMS temperature and salinity at 32° and 36°S were compared to observations from the CSIRO Atlas of Regional Semipunctoribates as (CARS2006; Dunn and Ridgway, 2002; Ridway et al., 2002) climatological database.

Hydrographic data from three summer cruises at 35.5–40°S; 72.75–77.8°W carried out by the Chilean Fund for Fisheries and Aquaculture Research (Fondo de Investigación Pesquera y Acuicultura, Ministry of Economy, Chile: FIP, www.fip.cl) were used to observe the presence of water masses using TS diagrams and to determine the percentage of each water mass between 0 and 700 m depth (REF). These cruises were carried out in December 2005 (FIP 2005-01), January 2009 (FIP 2008-20) and January 2011 (Fip 2009-39). The TS diagram and percentage of water masses from the FIP cruises were compared to the ROMS simulation.

3. Results

3.1. Average fields and seasonal variability

3.1.1. Sea level variability

The seasonal climatology of the modelled sea level anomaly (SLA) was compared to the climatology of AVISO for the period 1992–2005 (Fig. 3). The simulated and observed SLA anomalies were consistent in magnitude and their patterns were qualitatively similar. The spatial correlations and standard deviations are compared in a Taylor diagram (Fig. 3e). The correlations vary between 0.4 (spring), 0.5 (summer) and 0.6 (autumn and winter). Standard deviations are between 40% (spring) and 70% (winter) higher in the model than in the observations, suggesting that the modelled mesoscale activity is slightly overestimated.

The most significant seasonal changes occur in a 300-km-wide coastal band, from ~73° to 76°W. The gradients of SLA indicate the presence of anomalous surface geostrophic currents, tangential to the isolines, and not the total geostrophic current. Positive SLA dominated near the coast in autumn (Fig. 3a, b), with relatively higher values (1–3 cm) in the model. The presence of relatively intense anticyclonic mesoscale eddies in the model associated with positives anomalies, can be noted both offshore (near 33°S–80°W and 39°S–79°W in autumn, Fig. 3a) and nearshore (within 2° from the coast, Fig. 3a). The nearshore anticyclonic structure (32°S–73°W, see label A1 in Fig. 3a) was also found nearly at the same location in longer model simulations (e.g. 20 years, Figure not shown), which suggests that this eddy is triggered seasonally in autumn at this location. The negative SLA along the coast (≤2 cm) in spring (Fig. 3d) indicates an intensification of the

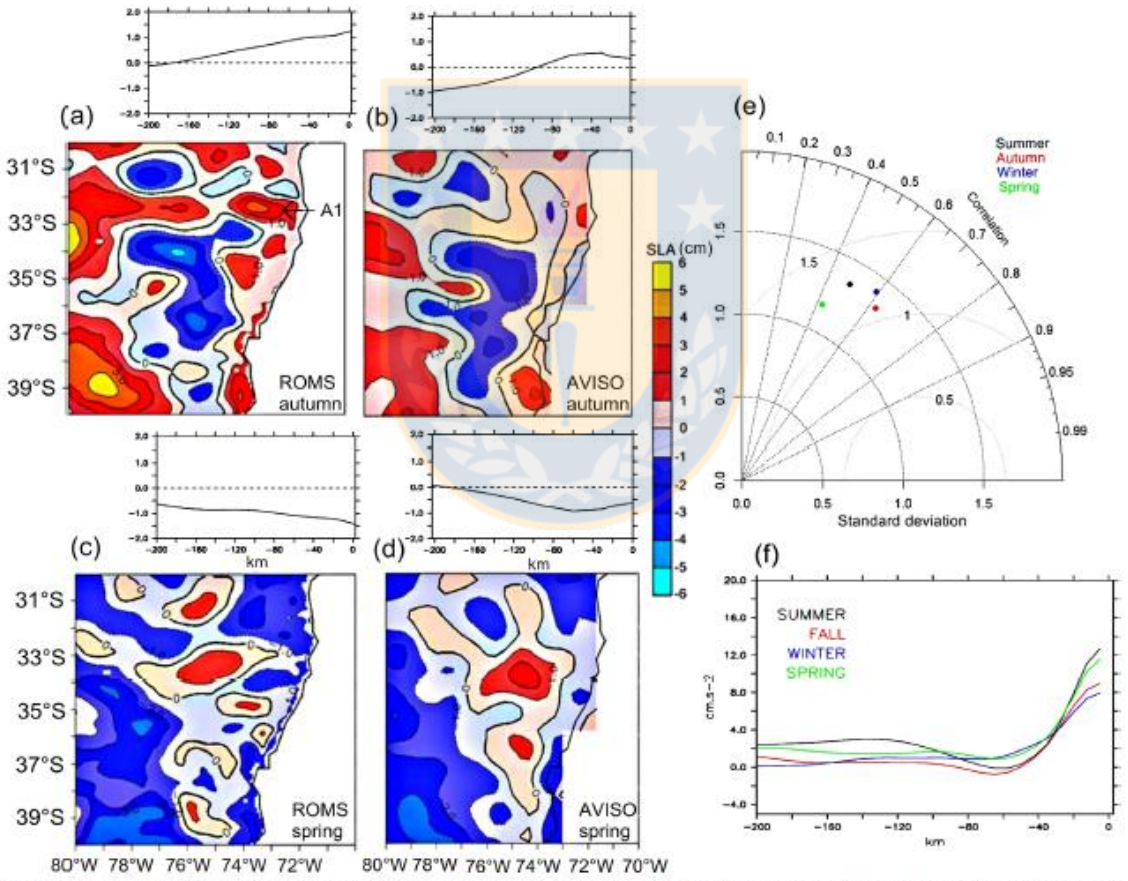

Fig. 3. Cross-shore profile of the alongshore average sea level anomaly in autumn (a, b) and spring (c, d). Taylor diagram of sea level anomaly for autumn, winter, spring and summer (e). Alongshore average of surface geostrophic velocity from the model (f).

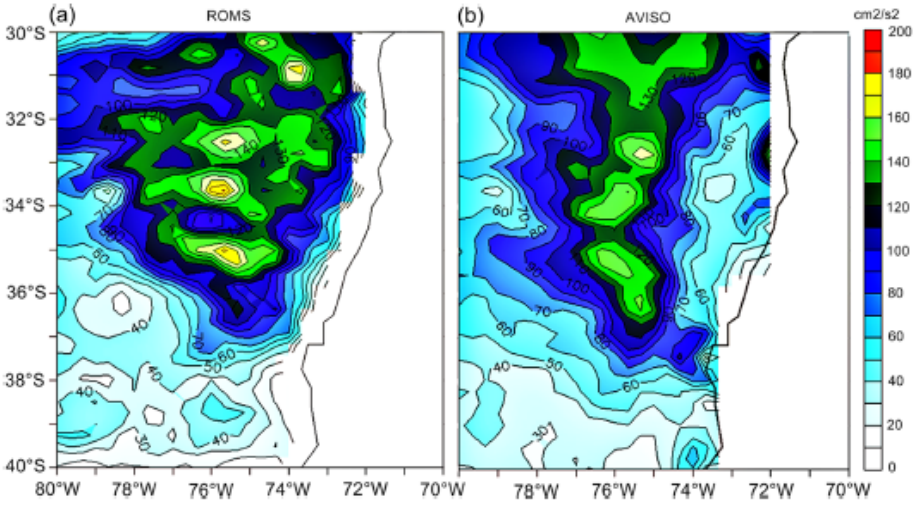

Fig. 4. Eddy Kinetic Energy (EKE): (a) ROMS and (b) AVISO.

equatorward geostrophic meandering flow (Fig. 3f), while positive offshore values (1–2 cm) suggest the presence of a strong poleward meandering flow between 78°W and 76°W. Overall, the meridional, alongshore-averaged, surface geostrophic current is equatorward nearshore and intensifies in spring and summer (Fig. 3f).

The modelled geostrophic EKE was compared to the geostrophic EKE derived from AVISO data, with relatively good agreement ($r=0.7768$, $p<0.05$) as both the modelled and observed patterns of EKE displayed high values ($>120\,cm^2\,s^{-2}$) in a offshore strip between 30° and 37°S, and lower values south of this area (Fig. 4). As in other upwelling systems, there was an EKE nearshore minimum in both the simulation and the observations, supporting the idea that the EKE originate from instabilities in the nearshore region that amplify while moving offshore (Marchesiello et al., 2003). Note that the modelled EKE was nevertheless higher than the observed between 30° and 38°S in a 200–300-km wide coastal band, which indicates that the modelled current system tends to be more unstable than the real one. These discrepancies may also be partly due to lower quality data for nearshore regions (Capet et al., 2014).

3.1.2. Temperature and salinity

The average SST model oscillated between 11° and 18 °C and displayed minimum values near the coast as expected from coastal upwelling. It compared well with Pathfinder data, with differences of less than ~1 °C (Fig. 5a).

The SST Hovmöller computed in a coastal band (Fig. 5b) revealed good agreement between the modelled SST and the data, especially from April to December (autumn, winter and spring season). An exception was observed during summer months (January to March) in the north of the study area (30–33°S) where Pathfinder data revealed a maximum of 20 °C, differing from the ROMS simulation with a maximum of 18 °C.

Yearly averages of simulated temperature cross-sections at 33° and 36°S compared well to observed values (Fig. 6). At 33°S between 0 and 200 m the model simulated a temperature between 10.5 and 17 °C (Fig. 6a), while CARS data revealed slightly lower temperatures of 10–15 °C (Fig. 6b). At 36°S between 0 and 200 m, temperatures were between 10.5° and 16 °C in the model (Fig. 6c) and between 10° and 15 °C in CARS data (Fig. 6d). The model and observed isotherm shoaling toward the shore both indicate coastal upwelling. The thermal stratification over the top 100 m is relatively similar in the model and observations, although the thermocline seems more pronounced in CARS. However, the model did not realistically represent the weakly stratified layer near the coast, located between the surface and a depth of ~200 m, at 36°S (Fig. 6d). The resolution of the CARS gridded product is limited to 50 km, which could explain some of the discrepancies between the observations and the model fields.

Maximum salinity was located near the coast, at slightly greater depths (~200–400 m, S~34.52, Fig. 6) in the model than in CARS (~150–300 m, S~34.64, Fig. 6f, h). Maximum salinity was found at a depth of approximately 250 m, which corresponds closely to the subsurface salinity maximum associated with the PCUC, with a lower value in the model than in the data. Colas et al. (2012) found the same bias in the value of the maximum salinity in their simulation of the HCS, which was used as boundary conditions for our model. The salinity maximum diminishes poleward, with a ~0.04 decrease between 33° and 36°S in the model and in the observations.

3.1.3. Density and water masses

Both the model and observed density values from FIP summer cruises (January, February, March) at 35.5–40°S; 72.75–77.8°W, are between 27.5 kg m^{-3} for deep waters and 24.5 kg m^{-3} for surface waters (Fig. 7a, b). However, the FIP data at the surface reached salinities close to 33 while simulated values were no lower than 34. The salinity range for densities between 24.5 and 26.5 is also much lower in the model (33.7–34.4) than in the FIP data (33.3–34.6). The modelled WM characteristics are consistent with those imposed at the northern and southern boundary of the model (Fig. 7c, d). They are particularly similar to the T/S characteristics from the northern boundary (Fig. 7c), which suggests that the nearshore WMs are mainly of northern origin, transported poleward by the PCUC and upwelled. The low salinity (33.3–33.7) surface waters encountered at the southern boundary (41°S, Fig. 7d) are likely mixed with more saline surrounding waters before they reach the FIP cruise sites.

The simulated and observed water masses in summer at 37°S;

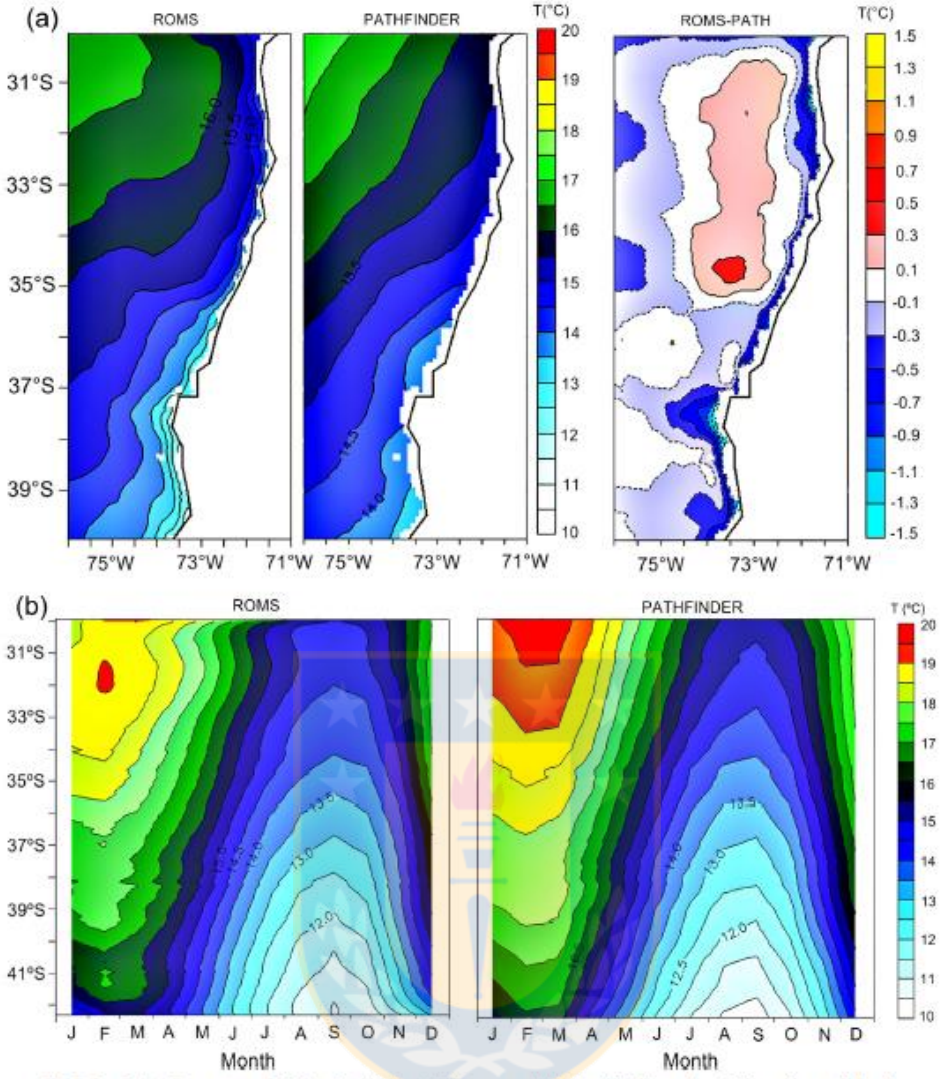

Fig. 5. Sea Surface Temperature: ROMS and Pathfinder, (a) Difference and (b) Hovmöller diagram in a 50-km wide coastal band.

75.3°W were: STW, SAAW, ESSW, AAIW and PDW (Fig. 7e). Several discrepancies were observed in the percentages of some of the water masses in the water column between 0 and 700 m. STW in the data and the simulation amounted to up to 10% at 100 m, while SAAW was apparent between 80 and 300 m, representing 80% in the simulation and almost 90% in the FIP data. Greater differences were observed for ESSW, which displayed a high percentage (55%) at 300 m in the simulation and a higher value (70%) at 250 m in the data. AAIW represented a high percentage at 350 m (45%) in the simulation and at 400 m (45%) in the data (Fig. 7e).

3.1.4. Currents

Meridional cross-sections were taken at 30°, 33°, 36° and 39°S to observe the location of the PCUC nucleus, width and depth and to determine latitudinal gradients in the simulated alongshore currents (Fig. 8). The mean current displayed significant changes between 30° and 39°S. At 30°S the mean flow displayed a well-marked PCUC at depths between ~100 and 600 m (Fig. 8a) trapped along the continental slope, with a shallow maximum trapped along the coast at depths between 50 and 200 m. Above the PCUC, the equatorward CCC was linked to a quasi-barotropic offshore equatorward flow, particularly marked in autumn and winter (Fig. 8a). Near 33°S the PCUC had a subsurface maximum trapped on the slope near ~200–300 m depth. It was linked to an offshore surfacing poleward flow, likely the PCCC (Strub et al., 1995), located between 50 and 100 km from the coast and particularly intense in spring and summer (Fig. 8b). Both the PCUC and PCCC weakened further south. Near 36°S there was no clear evidence of a coastally-trapped PCUC, and the offshore poleward flow associated with the PCCC had also weakened (Fig. 8c). At 39°S (Fig. 8d) both the cores of the PCUC and PCCC reappeared near the slope

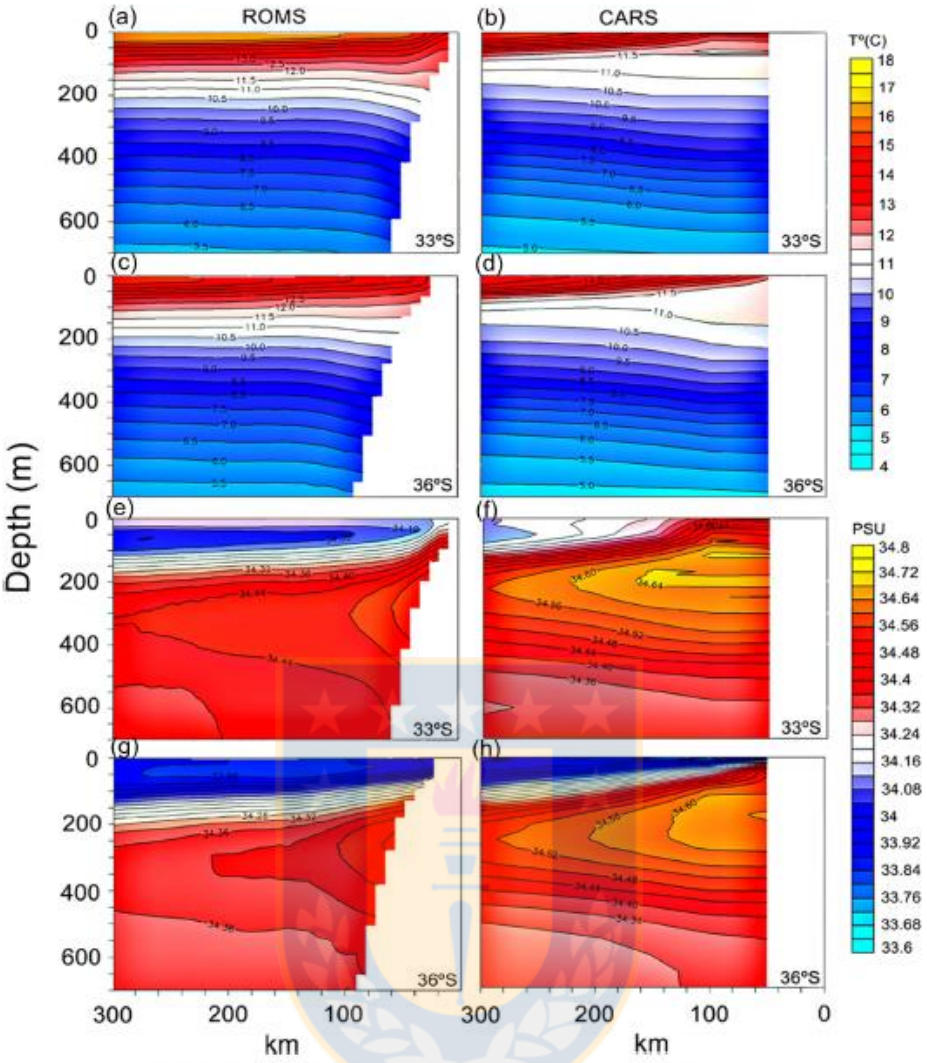

Fig. 6. Temperature and salinity cross-sections from ROMS simulation vs CARS data at 32°S and 36°S.

(mainly in summer) and ~100–120 km from the coast (mainly in winter), respectively. Their intensities were weaker than near 30° and 33°S. At the coast, the surface equatorward CCC strengthened and thickened at 39°S in comparison to further north. Differences in position, width, and strength of the HCS can partly be explained by the region's wind stress pattern (Fig. 9). There are seasonal differences in wind stress, mainly between winter and summer (Fig. 9c), which creates a distinct wind stress curl pattern for the two seasons (Fig. 9d). Nearshore negative wind stress curl was found along the four sections (Fig. 9b), except over a narrow band along the coast at 36° and 39°S. As negative nearshore wind stress curl drives a poleward transport according to the Sverdrup relation (Sverdrup, 1947), the poleward increase of wind stress curl (Fig. 9b) may partly drive the poleward decrease in PCUC intensity (see also Fig. 10). The surfacing poleward flow (PCCC) detected at 33°S (Fig. 8b) and 39°S (Fig. 8d) resembles the outcropping of the modelled PCUC off Peru (Penven et al., 2006), which may reach the surface in the case of cyclonic stress curl (McCreary and Chao, 1985). The reduction in PCUC intensity near 35°S (Figs. 8b–c and 10a) might also be related to the formation of a westward subsurface jet near 35°S, associated with westward-propagating eddies (Fig. 10b).

The east-west width and depth of the maximum velocity nucleus of the PCUC varied seasonally and latitudinally (Fig. 11). At 30°S the current was located near the shelf with no major seasonal changes in width and cross-shore position of maximum velocity. The PCUC at this latitude reached a width of ~50 km and the maximum velocity nucleus was located 20 km from the shelf. The depth of the nucleus was found at 100 m in autumn, spring and summer, and 150 m in winter (Fig. 11). This weak seasonality at 30°S could be related to the narrow continental shelf and the year-round upwelling-favourable winds. At 33°S, there was greater

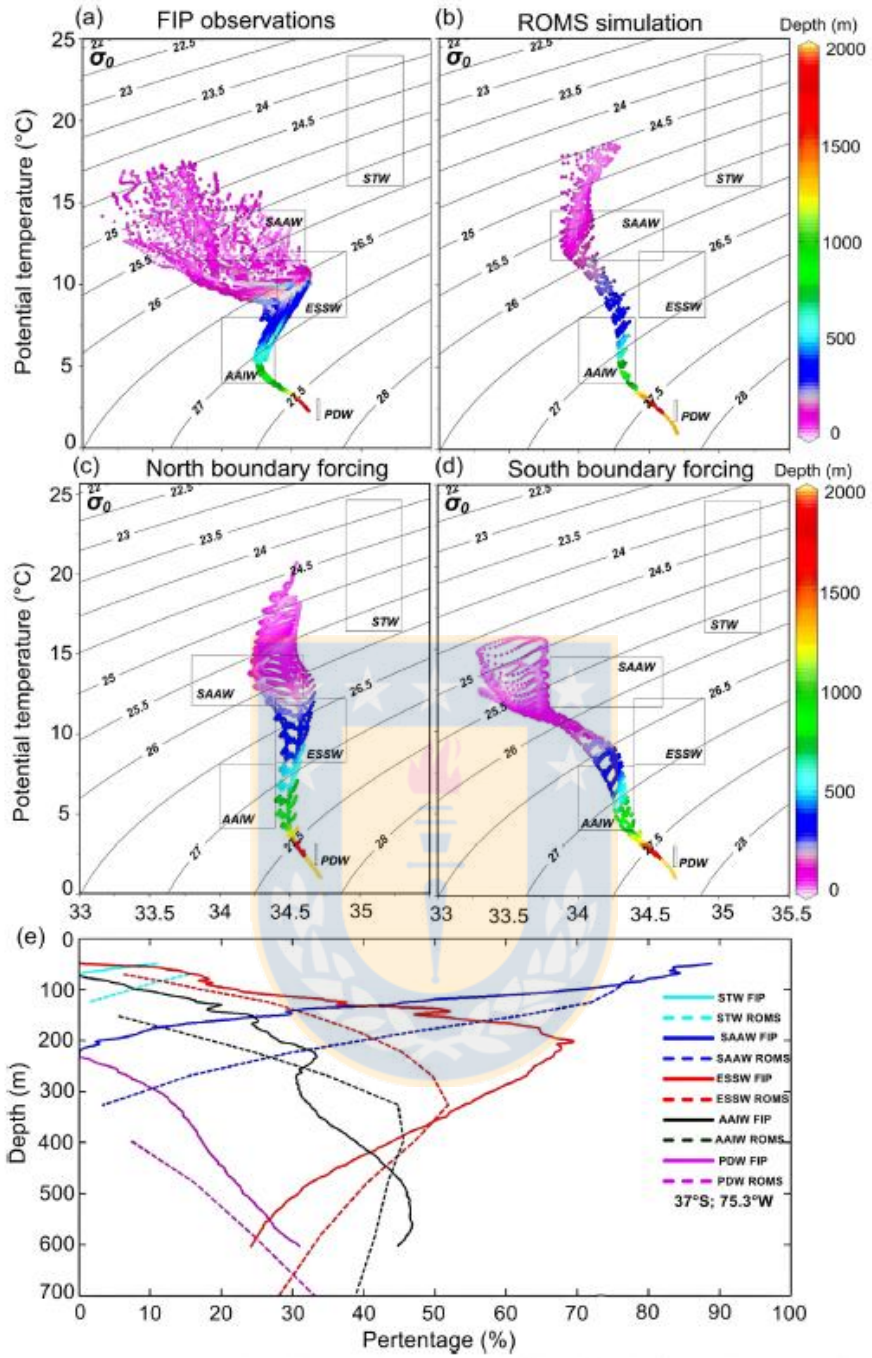

Fig. 7. TS diagram at 35.5–40°S; 72.75–77.8°W (a) FIP data and (b) ROMS, TS diagram (c) north and (d) south boundary forcing and (e) percentage of water masses at 37°S; 75.3°W. FIP data (solid line) vs ROMS model (dashed line).

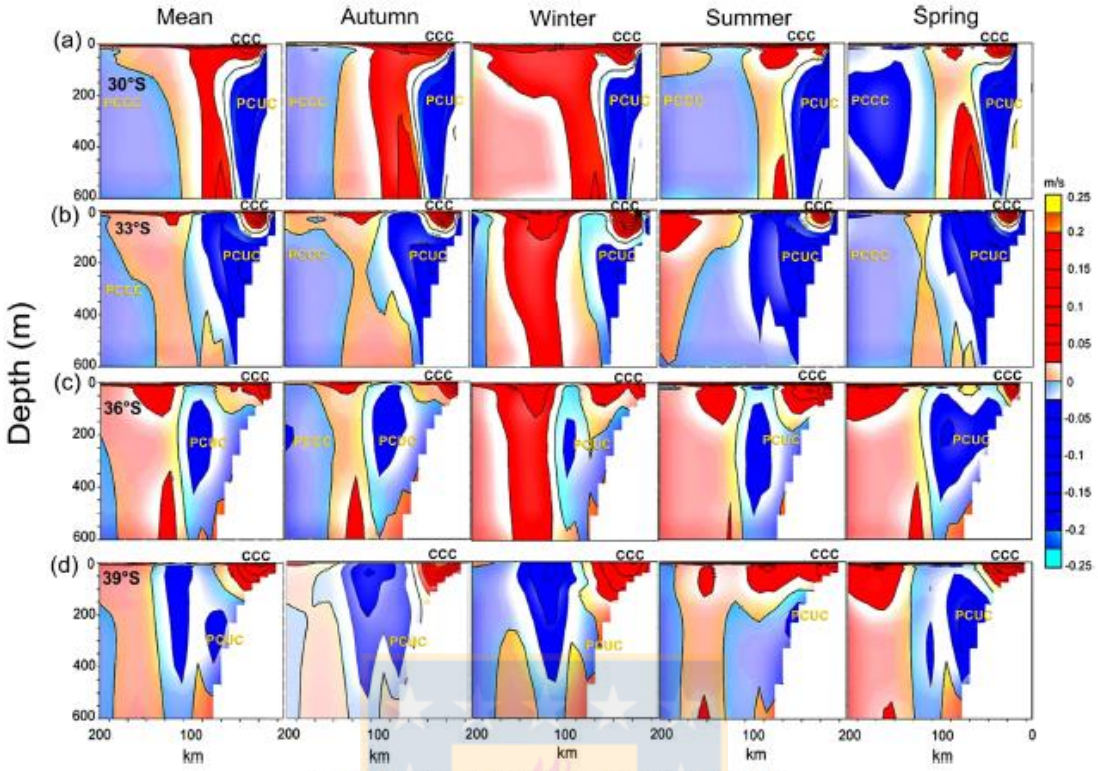

Fig. 8. Current cross-sections at (a) 30°S, (b) 33°S, (c) 36°S and (d) 39°S.

seasonal variability; during autumn and winter the average width was 50 km, centred on the nucleus of maximum velocity at approximately 30 km from the shelf (Fig. 11). In depth there were also marked seasonal differences; the maximum velocity nucleus was located at a depth of 200 m in autumn and summer, at 250 m in winter and at 230 m in spring (Fig. 11).

At 36°S the PCUC was often composed of two cores of poleward velocity (Fig. 8c). We computed the total width of the poleward flow, i.e. the sum of the widths of the two branches. During winter and spring the average width was approximately 110 km, and the nucleus of maximum velocity was located in the offshore current vein at 80 km from the shelf (Fig. 11). In autumn the average width of the current was 130 km, with a nucleus 60 km from the shelf (Fig. 11). During summer the PCUC was on average 120 km wide, with a maximum velocity nucleus at 60 km from the shelf (Fig. 11). In winter and summer the maximum velocity was registered at a depth of 250 m; at 200 m in autumn and at 225 m in spring (Fig. 11). At 39°S, the current was weaker (Fig. 8d) and narrower than at other latitudes. In autumn and winter the average east-west width was 30 km, with a maximum velocity at approximately 20 km from the shelf (Fig. 11). In spring the PCUC acquired an average width of 25 km, with a nucleus of maximum velocity at 25 km from the shelf, and in summer the current reached a width of 45 km, with a nucleus of maximum velocity at 15 km from the shelf (Fig. 11). The maximum depth of the nucleus at this latitude varied seasonally. In spring and summer it was restricted to 250 m, 260 m in autumn and 280 m in winter, approximately (Fig. 11). Overall, the depth of the maximum poleward current increased with latitude and reached a maximum in winter.

PCUC transport values (Table 1) were relatively similar to those computed in the modelling study of Aguirre et al. (2012) and to those reported at 30°S by Shaffer et al. (1997, 1999). There was relatively significant difference at 35°S from the findings of Leth et al. (2004), who reported a value of 1.3 Sv vs 0.76 Sv in our study. Overall, PCUC transport decreased poleward from a mean value of 0.80 Sv at 30°S to 0.26 Sv at 39°S (Table 1). The standard deviation of the modelled transport can be as great as 0.4 Sv depending on the latitude and season (see also Fig. 12), due to the model's internal mesoscale variability.

Maximum transport was recorded during spring and summer, with the highest values at 30° and 33°S with 0.94 Sv (spring) and 0.9 Sv (summer), respectively (Fig. 12). At 36°S the transport was lower further north, with the highest values in summer (0.71 Sv) and the lowest in winter (0.22 Sv) (Fig. 12). At 39°S, maximum transport occurred during autumn (0.48 Sv) and minimum transport in winter (0.15 Sv) (Fig. 12). At 39°S during winter/beginning of spring, lower PCUC transport coincided with the lowest values of coast-ocean wind stress (Fig. 9a) and wind stress (Fig. 9c). As well, wind stress curl between 37° and 40°S was highest between May and October (Fig. 9d), i.e. during the austral winter and spring. The decrease in the intensity of the PCUC towards the pole could be due to lower wind stress and higher wind stress curl towards the south.

3.2. Lagrangian analysis of water masses transported by the PCUC

We investigated the trajectory of the water masses transported by the PCUC, particularly that of water parcels seeded in the PCUC

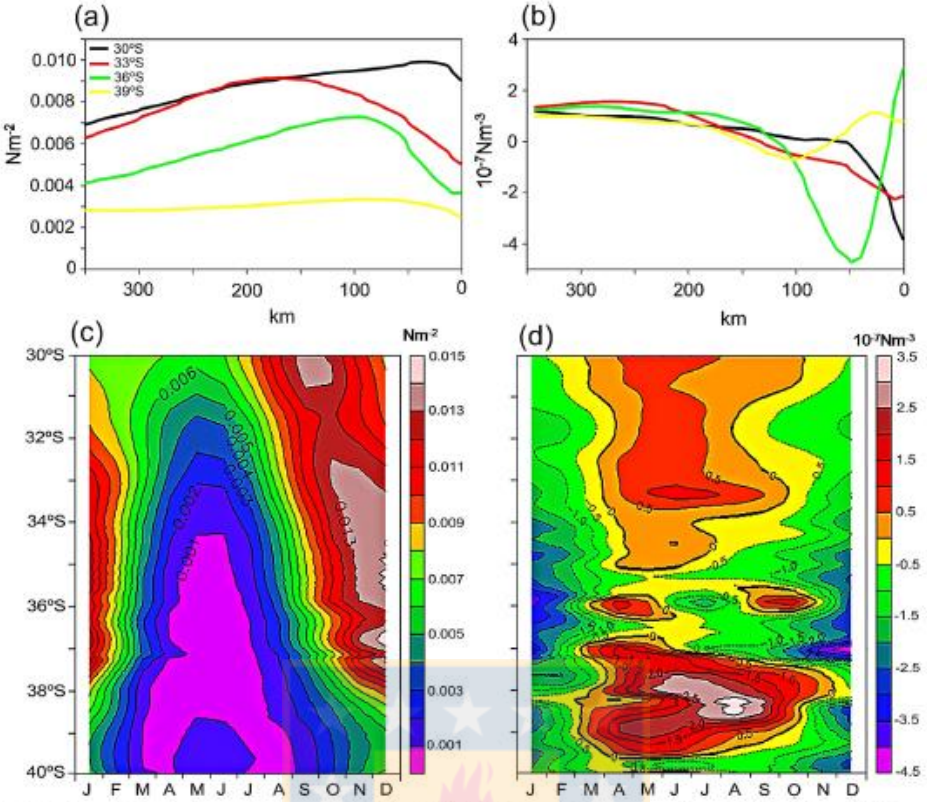

Fig. 9. Mean wind stress intensity, N m^{-2} and mean wind stress curl, 10^{-7} N m^{-3} at 30°, 33°, 36°, and 39°S in a cross section at 0–350 km offshore (a, b). Seasonal alongshore wind stress and seasonal wind stress curl, in a 300-km-wide coastal band (c, d).

at two zonal sections, at 33°S and at 37°S, to account for alongshore variability.

Approximately ~20% and ~14% of the floats released in the PCUC at 33° and 37°S, respectively, were transported and upwelled in the surface layer in the following six months after leaving the cross-shore sections (Table 2). The number of upwelled floats varied little (~1–2%) seasonally in spite of the seasonal variability of the upwelling-favourable winds off Chile. Moreover, the year-to-year variation due to the model's intrinsic mesoscale variability reached a maximum (~6–7%) in winter (Table 2). The majority of the upwelled floats were initially located in the PCUC at depths between 110 m and 130 m (Table 2).

Nearly half of the upwelled floats launched at 33°S (50.1% and 47.5% in winter and spring, respectively) were upwelled in a 1° band south of the section, between 33° and 34°S (Fig. 14), while the journey of the floats took ~58.5 and ~38 days, respectively (Fig. 14). High percentages of upwelled floats were found south of the section between 34° and 35°S during autumn (16.1%) and summer (13.8%), taking 132 and 95 days, respectively, to reach the surface (Fig. 14). The number of upwelled floats decreased poleward of 35°S (Fig. 14). High percentages of upwelled floats were also recorded north of 33°S, as some water parcels were first transported southward by the PCUC and then transported to the north of the section prior to being upwelled. The recorded values were 23.2% and 22.6% during winter and spring, taking on average 72 and 48 days, respectively, to upwell between 32° and 33°S (Fig. 14). As expected, the lowest percentages were observed several degrees north and south of the section, between 30° and 31°S, with 2.8% of floats emerging after 180 days in winter, and between 37° and 38°S, with 4% of floats emerging after 200 days in summer (Fig. 14).

The majority of the floats launched at 37°S upwelled south of the section. More than half of the floats upwelled between 37° and 38°S in autumn (61.1%) and summer (65.1%), taking 70 and 37 days, respectively (Fig. 15). In contrast to those launched at 33°S, a larger number of the floats (nearly one third in winter and spring) escaped from the PCUC flow, recirculated northward and upwelled between 36° and 37°S. Between 1.4% and 3% of the floats were upwelled further north (33–34°S).

These results showed that the great majority of the floats (~80% at 33°S and ~85% at 37°S, Table 2) initially transported by the PCUC did not upwell but remained submerged for more than half a year. The situation of subsurface floats differed in winter and summer. In summer they were located respectively +1.5° and +0.3° south of the sections at 33° and 37°S (Table 3), while in winter they were located 0° and −0.8° north of the sections at 33°S and 37°S, respectively. Thus, after the floats separated from the PCUC poleward flow, recirculation to the north of their initial positions was more efficient in winter than in summer, and in the south of the region (37°S) than in the north (33°S). The enhanced seasonality at 37°S is consistent with the greater distance from the coast (330 km) of the floats launched in winter than of those

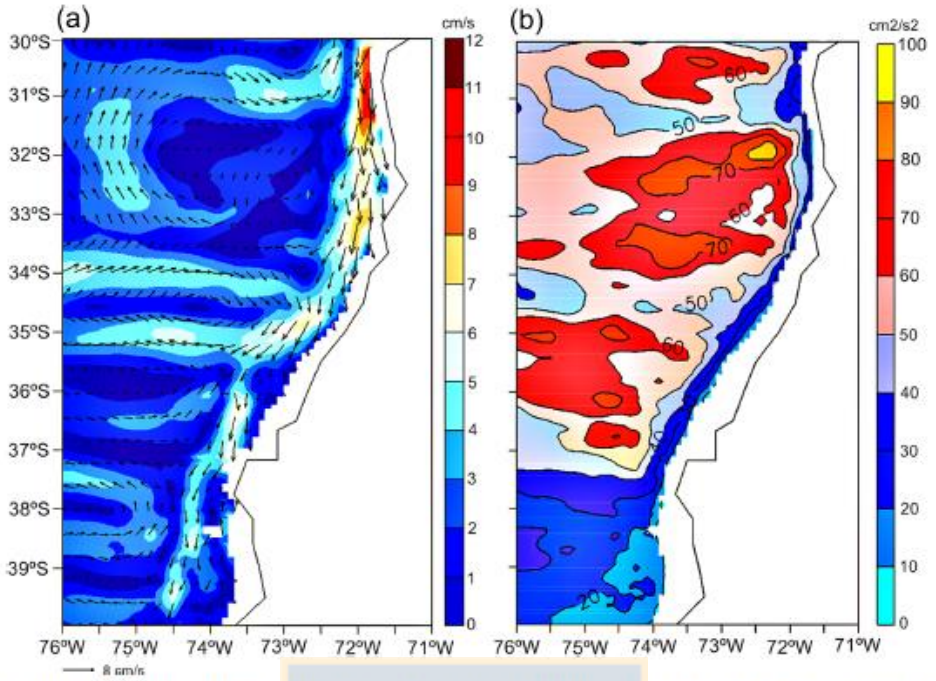

Fig. 10. (a) Mean current intensity (cm s^{-1}) and direction (arrows) between depths of 100–300 m and (b) Eddy kinetic energy (cm^2 s^{-2}) averaged between 200 and 300 m deep.

launched in summer (263 km). Furthermore, the mean depths of the floats were between 320 m (33°S) and 350 m (37°S), with very little seasonal changes. The moderate increase (~ 20–30 m) in the mean depth of the floats launched at 33°S and 37°S could be due to the poleward deepening of the PCUC, which allows water at greater depths to be captured by the PCUC flow at 37°S. Overall, these diagnostics suggest that the stirring of water masses transported by the PCUC is more efficient in winter than in summer, and in the south of the domain (37°S) than further north (33°S).

4. Discussion

4.1. Sea level anomaly and eddy kinetic energy (EKE)

Fig. 3 shows a comparison of the seasonal SLA averages from simulated and satellite data and reveals substantial discrepancies depending on the season. In autumn, the modelled cyclonic and anticyclonic eddies were more intense than in the AVISO dataset. Some of the modelled anticyclonic structures (e.g. near 33°S;74°W in Fig. 3a) present in both seasons were not observed with altimetry. However, anticyclonic intrathermocline eddies associated with a positive SLA have been observed at this location (Hormazabal et al., 2013).

In spring, during the peak of upwelling-favourable winds (Fig. 9c), the SLA is minimal along the coast for both the model and observations. The strong sea level gradients observed in the model indicated a poleward intensification of the nearshore geostrophic flow. Aguirre et al. (2012) also reported a well-defined jet-like structure during spring and autumn. A Taylor diagram comparing SLA patterns revealed that the model's surface mesoscale activity was 40–70% stronger than observed activity, depending on the season. However, the discrepancies may be partly due to data processing. Indeed, the observed SLA maps used in this study were obtained from optimal interpolation of satellite data, processed by AVISO, while the modelled SLA maps resulted from a simple interpolation of the modelled sea level at 1/12° onto the coarser AVISO grid. Further investigation of the impact of the SLA data is beyond the scope of the present study.

The EKEs (Fig. 4) from the simulation and from satellite data differed significantly, with the highest values concentrated in the central zone of the study area (32–37°S). The simulated EKE pattern was quite similar to that of other climatological simulations by Parada et al. (2012) and Aguirre et al. (2014) for the same region of study. However, the present simulation presented slightly higher maximum values offshore (180 cm^2/s^2) than those from AVISO (160 cm^2/s^2). Closer to the shore between 31° and 36°S the EKE levels were also higher in the model (~80–140 cm^2/s^2) than those calculated from AVISO data (~60–80 cm^2/s^2), which could be related to errors in nearshore wind forcing. The intraseasonal waves, which were not introduced in our climatological boundary forcing, may also modify the stability of nearshore flow. Some authors have reported that coastal-trapped waves (CTW), forced by intraseasonal equatorial Kelvin waves (IEKW), have an important impact on coastal hydrography and currents (Hormazábal et al., 2001, 2006). Seasonal CTW, for example, can modify vertical shears between the PCUC and the equatorward surface jet, modulating baroclinic instabilities (Echevin et al., 2011) and thereby the nearshore generation of westward propagating mesoscale eddies (Belmadani et al., 2012). Near the coast of Peru (12–14°S) and central Chile (26–30°S) 60-day intraseasonal CTW have a relatively moderate effect (~10%) on EKE (Belmadani et al., 2012), indicating that IEKW-induced CTW enhance EKE near the coast but have a weak impact on the ocean interior (Belmadani et al.,

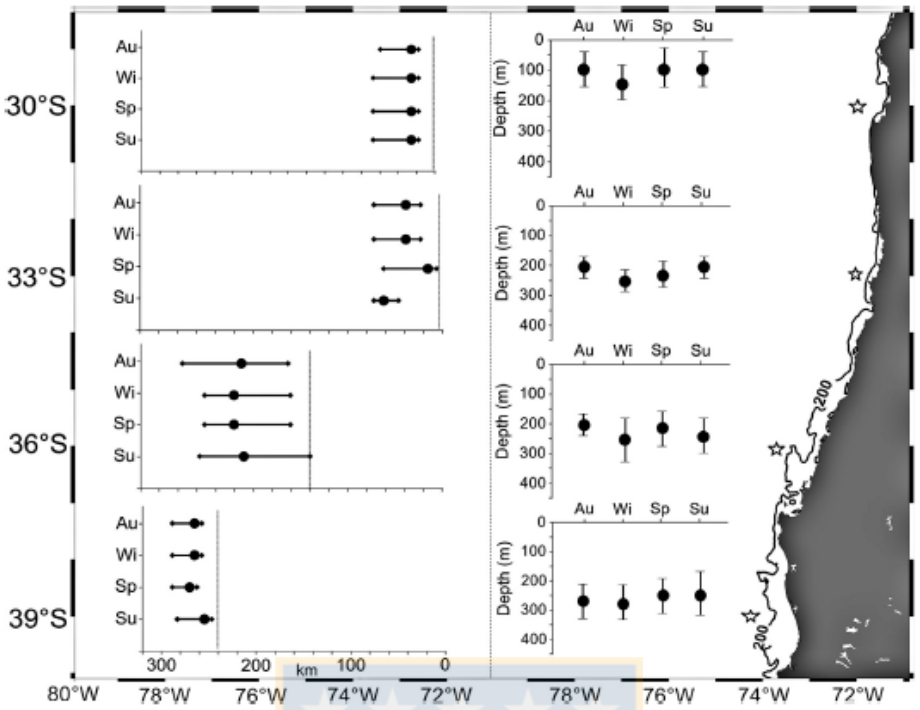

Fig. 11. Longitudinal width and nucleus (black circles) of the PCUC at depth during autumn (Au), winter (Wi), spring (Sp), summer (Su) at 30°, 33°, 36° and 39°S. The black line indicates the continental shelf (ROMS) at 200 m depth.

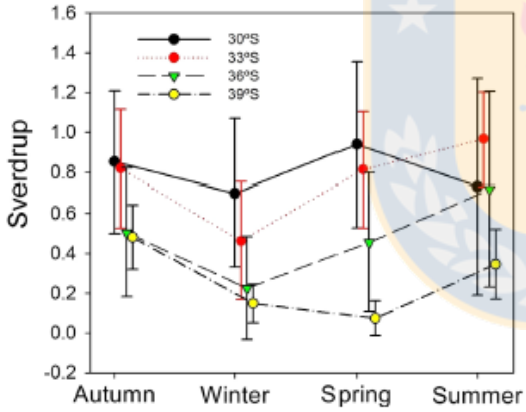

Fig. 12. Average monthly Sverdrup transport (Sv, poleward positive) of the PCUC at 30°, 33°, 36° and 39°S.

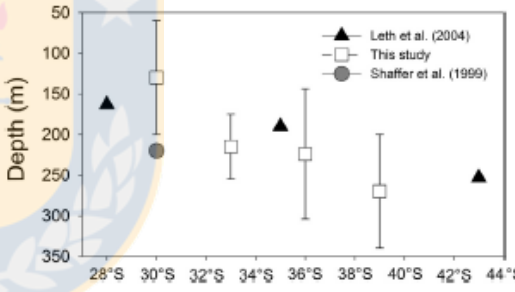

Fig. 13. Average deepening of maximum velocity nucleus of PCUC with Latitude (°S) by Leth et al. (2004), Shaffer et al. (1999) and this study.

2012). However, further investigation of this issue is beyond the scope of the present study.

4.2. Temperature and salinity

The simulated SST and the Pathfinder data differed, especially nearshore (Fig. 5), where modelled temperature was lower than that in satellite data. The largest biases were found at 35°S (0.9 °C) and close to the coast at 38°S (−1.3 °C). The cooler than observed near-shore SST is a bias common to ROMS simulations in other EBUS, which is partly explained by a warm bias of ~1–2 °C in the Pathfinder SST (Dufois et al., 2012). This bias can also be partly explained by the over-estimation of the very nearshore wind stress from SCOW data, which cannot resolve the coastal wind drop-off and may thus drive an overly strong coastal upwelling (Renault et al., 2012). Nevertheless, the simulated SST coincided with previous studies (Hormazábal et al., 2001; Letelier et al., 2004) where the annual averages were found to be 12 °C at 34–40°S, and 18 °C offshore at 30–34°S.

The temperature and salinity cross-sections from the simulation compared to CARS data at 32° and 36°S (Fig. 6) also presented some discrepancies. ROMS simulated slightly lower temperature

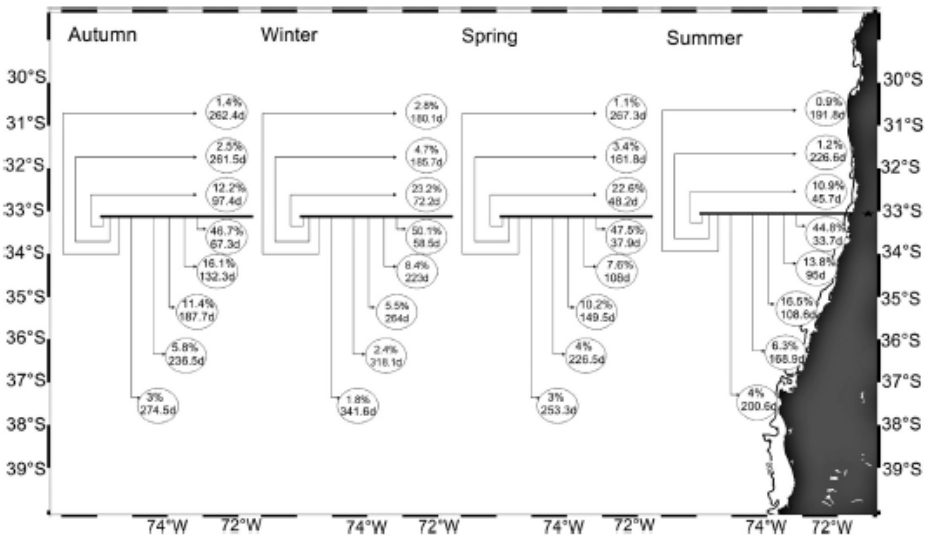

Fig. 14. Number of particles (in percent) that were launched seasonally in the PCUC at 33°S and upwelled (i.e. reached the 50 m-deep surface layer) 6 months later in different latitude ranges. The mean time (in days) taken for the particles to upwell is also indicated.

and salinity values than those from in situ observations.

The temperature/salinity diagram (TS) (Fig. 7a) and the water mass percentages in the water column (Fig. 7b) from the simulation compared to the FIP data revealed some differences. In the simulation the low densities observed in the FIP data were not detected, an expected consequence of the exclusion of major rivers in the simulation. As rivers modify the physical and biological properties of the water column via stratification and nutrient and organic matter supply (Iriarte et al., 2012; Sobarzo et al., 2007; Sobarzo and Bravo, 2009; Vargas et al., 2011,), a challenge for future research in the study area (i.e Bío-Bío, Itata, Maipo, Valdivia, etc.) is to incorporate the runoffs from the major rivers into ROMS simulations.

Furthermore, model parameterizations can also induce biases in temperature and salinity. High order diffusive advection schemes in sigma coordinate models such as ROMS may lead to spurious diapycnal mixing. The consequences are that the salinity minimum may erode rapidly along the slope, as for example near the reefs of the steepest islands in the western part of New Caledonia (Marchesiello et al., 2009). This can lead to the

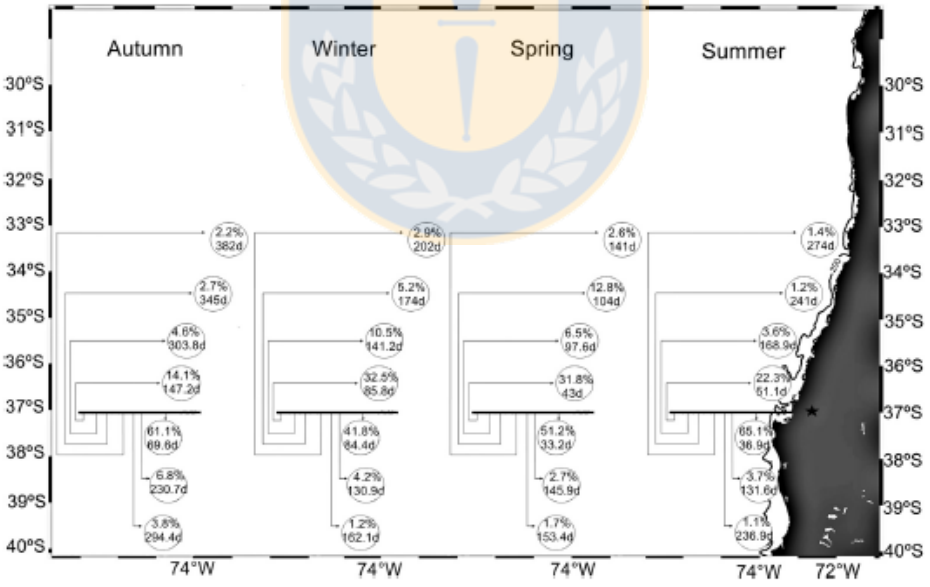

Fig. 15. Same as Fig. 14 but for particles released at 37°S.

misrepresentation of the low modelled salinity in comparison to in situ data from FIP cruises (Fig. 7a).

4.3. Peru-Chile Undercurrent (PCUC)

The velocity range of the main simulated currents was similar to those reported in other modelling studies (Aguirre et al., 2012), especially the PCUC, whose maximum reported transport in this study was 0.94 Sv (Table 1) in the northern part of the study area (30°S) during spring, which is close to estimates at the same latitude reported by other authors (1 Sv; Pizarro et al. 2002; Shaffer et al., 1997, 1999). Leth et al. (2004) estimated the geostrophic transport of the PCUC from Profiling CTD (Conductivity, Temperature and Depth) data collected at different latitudes taken in May–June 1995 along 28–35°S off the Chilean coast to 86–88°W. They estimated geostrophic transport of the PCUC of 1.3 Sv at 28°S and 35°S, and 1.1 Sv at 43°S. These values are higher than those in our simulation, which could be attributed to the fact that the in situ measurements in Leth et al. (2004) are "snapshots" of PCUC transport, while our measurements are climatological means. Furthermore, the model does not realistically represent the spreading of isotherms at 36°S (Fig. 6c), which could partly explain the discrepancy.

The modelled PCUC displayed latitudinal changes, with velocity (Figs. 8 and 10a) and transport decreasing poleward (Fig. 12). Such latitudinal variation was reported by Silva and Neshyba (1979), who estimated an average poleward velocity in the core of 5–10 cm/s from 20° to 30°S, decreasing to 0–5 cm/s from Valparaiso (33°S) southward. Fonseca (1989) reported that this undercurrent maintained a seasonal cycle, with the highest level of transport (off the shelf) occurring during summer. Its core is located around 150–200 m, with a characteristic maximum geostrophic velocity of about 20 cm/s.

In order to investigate the link between current and wind forcing, we compared PCUC transport to Sverdrup transport (Sverdrup, 1947), which relates vertically integrated meridional mass transport in the interior ocean to open ocean wind stress curl. Sverdrup transport was computed over two coastal bands 50 and 100 km wide using the SCOW wind stress curl (Figs. 2 and 9). Mean Sverdrup transport computed in the 50 km band (Table 4) was in reasonable agreement with the modelled transport at 30° and 36°S, but not at 33°S and 39°S. In the 100 km band (Table 4) there was a relative agreement at 30°S and a 50% discrepancy at 36°S. The standard deviation of the modelled transport associated with internal interannual variability is greater than the mean, except at 39°S. Aguirre et al. (2012) also compared the modelled transport between 90°W and the coast to Sverdrup transport computed from Quikscat data and found a reasonable agreement (within ~20–30% of error) away from the coast (between 90° and 80°W) and strong discrepancies nearshore. The Sverdrup transport they obtained in the 100–200 km coastal band was much lower (i.e.~0.3 Sv at 30°S) than in our case (~1.4–1.5 Sv, Table 4). Sverdrup transport may be underestimated nearshore when using low-resolution wind products that do not represent the strong drop-off close to the coast (e.g. Renault et al., 2016). Thus the weaker nearshore wind stress curl near the coast, associated with the coarser (0.5°) Quikscat wind product that they used may explain the discrepancies between our results and those of Aguirre et al. (2012). These results suggest that the PCUC mean flow is partly explained by simple wind-forced Sverdrup theory at some locations along the Chile coast, but not in all the studied area.

Table 4
Meridional transport (in Sv, positive poleward) between 0 and 650 m at different latitudes, and Sverdrup transport (in Sv, positive poleward) in a coastal band of 50–100 km from the coast.

Transport	*Distance*	*30°S*	*33°S*	*36°S*	*39°S*
Model	50 km band	1.03 ± 1.08	−0.54 ± 1.2	0.31 ± 0.69	0.79 ± 0.46
Model	100 km band	1.65 ± 1.60	−1.07 ± 1.3	0.49 ± 1.2	1.19 ± 0.7
Sverdrup	50 km band	1.39	0.20	0.40	0.29
Sverdrup	100 km band	1.48	0.64	1.1	0.32

Aguirre et al. (2012) further investigated the role of wind stress curl on the dynamics of the near-surface alongshore flow off central Chile with a no-curl wind forcing ROMS model. They found little impact of the curl on the vertical PCUC structure at 30° and 36°S, and a decrease in PCUC intensity at 36°S.

The dynamic impact of the curl on the undercurrent may also occur in other EBUS where strong coastal wind stress curl is observed. Pedlosky (1974) indicates that a poleward undercurrent along an eastern boundary benefits from negative (in the Southern Hemisphere) wind stress curl along the coast. Marchesiello et al. (2003) reported that the regional model (ROMS) and Sverdrup transports were consistent in the California current system. Albert et al. (2010) showed that strong upwelling-favourable nearshore wind stress curl in the Peru upwelling system induces shoaling of the coastal undercurrent and a wide productive coastal zone through upwelling of nutrient-replete waters.

The PCUC is of crucial importance because it carries equatorial subsurface water along the coasts of Peru (Montes et al., 2010) and Chile and disperses it offshore through coherent anticyclones with salty cores (Colas et al., 2012). Intrathermocline eddies, which break off from the PCUC near 37°S, move northeast at a speed of ~2 km day^{-1}, which represents an average westward flux of ~1 Sv (Hormazábal et al., 2013). This mass flux is on the same order of magnitude as the PCUC flux reported by Shaffer et al. (1997, 1999) and in this study (Table 1). Furthermore, the PCUC flux decreases significantly between 36° and 39°S, suggesting that a large portion of PCUC water is trapped in intrathermocline eddies and dispersed offshore (Fig. 10b).

Other aspects of the simulation are the changes in PCUC width and nucleus depth. The PCUC generally presented a mean latitudinal climatological width of 60 km, with lower values (15 km in spring) around 39°S (Fig. 11). The nucleus of maximum current velocity was located at a depth of approximately 120 m at 30°S, and deepened further south in the study area, reaching ~218 m at 33°S, ~230 m at 36°S, and ~260 m at 39°S (Fig. 13). The nucleus deepened in winter at all studied latitudes, and became shallower during spring-summer. In previously reported observations, the PCUC nucleus was found at depths of 180 m (2 years record, Shaffer et al., 1995) and 220 m (6-year record, Shaffer et al., 1999) at 30°S, with a maximum velocity of 12.8 cm/s. This result differs slightly from ours as we obtained an average velocity core of 10 cm/s at 120 m depth at 30 °S (Fig. 13). Leth et al. (2004) found alongshore differences in poleward velocity, revealing maxima of 7.6 cm/s at 163 m (28°S), 11.8 cm/s at 190 m (35°S) and 9.5 cm/s at 253 m (43°S) (Fig. 13). Silva and Neshyba (1979) also found evidence of a high velocity nucleus that deepens towards the poles in the PCUC.

The deepening also occurs in other EBUS. Mittelstaedt (1976) and Barton (1989) reported the nucleus of the poleward undercurrent off the northeast coast of Africa, which deepens as it extends polewards (Barton, 1989; Clarke, 1989; Mittelstaedt, 1991). Off the US west coast, Pierce et al. (2000) observed a deepening undercurrent, consistent with PV conservation.

Using ROMS in the Peru region, Penven et al. (2005) found a clear deepening of the PCUC's lower limit, which was trapped along the slope. In our case, while the upper part of the PCUC sometimes outcropped as a counter current (e.g. between 33° and 39°S, Fig. 8b-d), the depth of the bottom of this poleward undercurrent varied meridionally so that planetary vorticity f/H was conserved over a range of latitudes (where f is the Coriolis

parameter and H the thickness of the PCUC layer). Our present results do not seem to be consistent with those reported by Penven et al. (2005) since the thickness of the bottom-trapped PCUC is clearly thinner south of 33°S (Fig. 8). However, the bias in isopycnal spreading at 36°S (Fig.6c) also suggests there is a bias in PCUC thickness in this latitude range, so the f/H theory cannot be ruled out.

Other authors have tried to explain the deepening of the PCUC. For example, Pizarro (1999) used the approach of McCreary (1981), which showed that a linear model driven by alongshore wind could represent the deepening of the California undercurrent poleward of the wind patch, without invoking the role of wind-stress curl. Pizarro (1999) applied this model to the PCUC and found a clear poleward deepening of the PCUC core (marked by the 0.1 m s^{-1} isoline in his study) between 30° and 35°S from ~450 m to ~600 m. PCUC velocities in this case were roughly twice as high as those generated in our simulation. In our case, the depth of the simulated PCUC lower limit (e.g. marked by the 0.05 m s^{-1} isoline) only slightly decreased from 30° to 33°S (Fig. 8a-b). Their model also showed slight poleward intensification and widening of the PCUC core, which were not identified in our case. This simplified model did not take into account the effects of the seafloor topography, the curved coastline or nonlinear rectification of the current.

4.4. Upwelling and PCUC water mass pathways

To determine the paths of particles transported by the PCUC and the time necessary for them to upwell to the surface (up to 50 m), virtual floats were released into the current at 33° and 37°S. The average duration of the journeys of floats that upwelled was determined for each season. Most upwelled floats from both latitudes travelled southward along the PCUC and were upwelled south of the release sections. The highest percentages of upwelled floats were recorded at latitudes close to the area of release. For example, 40% of floats released at 33°S upwelled between 33° and 34°S and took on average 50 days to reach a depth of 50 m (Fig. 14). Similarly, over 50% of floats released at 37°S upwelled between 37° and 38°S and took approximately 56 days to do so (Fig. 15). However, a significant percentage of floats changed direction and ended up north of the sections. They were likely transported north via surface currents (at depths greater than 50 m) induced by wind forcing or trapped and transported by currents associated with subsurface eddies. Some authors have described the presence of intrathermocline eddies (Hormazábal et al., 2013; Leth and Middleton, 2004) generated by baroclinic instabilities around 37°S (Punta Lavapie). These eddies, which transport nutrients and low oxygen concentrations offshore, may also transport particles north (Figs. 14 and 15), making it quite complex to determine the origin of particles reaching the surface during upwelling.

Moreover, the percentage of particles that effectively reached the surface via upwelling did not exceed 20% at either 33°S or 37°S. Small seasonal differences were detected at 33°S, with 19.2% and 20.2% of particles emerging in spring and winter, respectively (Table 2). These small seasonal differences may be associated with wind stress values used to force the simulation, which were climatological and did not represent daily and synoptic frequencies, and which have been described as the main components of the wind stress along the coastal of central-southern Chile (Sobarzo et al., 2007; Sobarzo et al., 2010). Results in line with the present study were found in a numerical study of upwelling source waters in the California upwelling off Oregon (Rivas and Samelson, 2010). Using Lagrangian diagnostics to identify the origin and depth of upwelled waters, they found that the modelled poleward undercurrent, with a similar depth range as in our case, only made a small direct contribution to the source waters in a climatological simulation comparable to ours, and that this proportion decreased with high frequency wind forcing of nearshore dynamics. Thus, the impact of high frequency winds on the trajectory of PCUC water masses should be considered in future work.

5. Conclusions

The simulation results are consistent with observed spatial patterns in most of the analysed variables. For example, EKE showed high values in a narrow band along the coast (from 30° to 37°S), and a decline south of this zone, but simulated EKEs were higher, particularly between 30° and 38°S in a coastal strip of 200–300 km.

The simulated average field of SST exhibited low SST values near the coast due to the upwelling of cool waters, but these were slightly lower than those of the Pathfinder data, which is likely due to the overestimation of the nearshore wind stress from SCOW data used in this ROMS simulation. The monthly climatological wind used here does not represent the alternation of highly frequent upwelling and relaxing events, which may also affect the model SST. Annual averages of simulated temperature at 32° and 36°S compared well to real data. In these latitudes, the model and observed isotherm shoaling to the shore both indicated active upwelling. Nevertheless, the model failed to accurately represent thermal stratification in the first 100 m (of 50–300 km) observed in CARS data. The yearly averages of simulated salinity cross-sections at 32° and 36°S also compared well to CARS data. It was observed in the model that maximum subsurface salinity was located near the coast at a depth of approximately 250 m, associated with the PCUC.

The density values from the model and from cruises during summer months (at 35.5–40°S; 72.75–77.8°W) were very similar. However, low water densities were not appropriately represented in the simulation (Fig. 7). This could be an effect of the exclusion of major rivers in the simulation. Additionally diffusive advection schemes in sigma coordinate models may lead to spurious diapycnal mixing and errors in salinity.

The velocity and transport of the simulated PCUC decreased poleward, which agrees well with the results previously reported for this area (Leth and Shaffer, 2001; Pizarro et al., 2002; Shaffer et al., 2004). In some latitudes a link was observed between the PCUC and the surface poleward PCCC flow, which was intense in summer and spring. The average width of the PCUC also changed toward the south of the study area, with approximately 50 km at 30° and 33°S, ~100 km at 36°S and ~30 km at 39°S. The abrupt width changes at 36°S may be the result of changes in topography, the presence of an irregular coastline or intrathermocline eddies that alter the undercurrent at this latitude range. In addition, our results showed that the core of maximum velocity of PCUC deepened from ~120 m at 30°S to ~250 m at 39°S, which is in agreement with what has been reported for other poleward undercurrents (e.g. California; Thomson and Krassovski, 2010).

Twenty and 14% of the Lagrangian floats transported from 33° and 37°S respectively, were observed in the surface layer (50 m) 6 months after release. At these latitudes, most of the upwelled floats travelled southward along the PCUC and were upwelled south of the launch sections. The highest percentages of upwelled floats were found at latitudes adjacent to the release zones. A large portion of them altered their trajectory and ended up north of the sections, probably conducted north by surface currents driven by wind forcing or by subsurface eddies.

The large majority of the floats transported by the PCUC did not upwell but remained submerged for more than 6 months. In both latitude ranges (33° and 37°S), more floats recirculated to the

north of the sections in winter than in summer. This suggests that the mixing of PCUC water with offshore waters was more intense during winter and spring than during summer and fall.

The simulations in this study improve our understanding of alongshore circulation and seasonal variability of nearshore circulation in the HCS. Studying the dynamics of the PCUC and the characteristics (origin, trajectory) of the transported water mass is a first step towards a more comprehensive study of the coupled physical-biogeochemical processes that drive the thriving productivity of the HCS. This will be the purpose of future work.

Acknowledgements

This study was funded by the Interdisciplinary Center for Aquaculture Research (INCAR; FONDAP Project No 15110027; CONICYT). Odette Vergara was also supported by a Doctoral Scholarship from the Comisión Nacional de Investigación Científica y Tecnológica (CONICYT, Ministry of Education, Chile). We acknowledge the financial support for O. Vergara's internships at LOCEAN received from the French Embassy in Chile, the REDOC. CTA (Red Doctoral en Ciencia, Tecnología y Ambiente, University of Concepción, Chile) and LIA MORFUN (International Associated Laboratory) project (LIA 1035 CNRS).

References

Aguirre, C., Pizarro, O., Strub, P.T., Garreaud, R., Barth, J., 2012. Seasonal dynamics of the near-surface alongshore flow off central Chile. J. Geophys. Res. 117, 1–17.

Aguirre, C., Garreaud, R., Rutllant, J.A., 2014. Surface ocean response to synoptic-scale variability in wind stress and heat fluxes off south-central Chile. Dyn. Atmos. Oceans 65, 64–85.

Aiken, C.M., Navarrete, S.A., Pelegri, J.L., 2011. Potential changes in larval dispersal and alongshore connectivity on the central Chilean coast due to an altered wind climate. J. Geophys. Res. 116, 1–14.

Albert, A., Echevin, V., Lévy, M., Aumont, O., 2010. Impact of nearshore wind stress curl on coastal circulation and primary productivity in the Peru upwelling system. J. Geophys. Res. 115, 1–13.

Bakun, A., 1990. Global climate change and intensification of coastal upwelling. Science 247, 198–201.

Bakun, A., Field, D.B., Redondo-Rodríguez, A., Weeks, S.J., 2010. Greenhouse gas, upwelling favorable winds, and the future of coastal ocean upwelling ecosystems. Glob. Change Biol. 16, 1213–1228.

Barnier, B., Siefridt, L., Marchesiello, P., 1995. Thermal forcing for a global ocean circulation model using a three-year climatology of ECMWF analyses. J. Mar. Syst. 6, 363–380.

Barton, E.D., 1989. The poleward undercurrent on the eastern boundary of the subtropical North Atlantic. Coast. Estuar. Stud. 34, 82–95.

Batteen, M.L., Hu, C.-P., Bacon, J.L., Nelson, C.S., 1995. A numerical study of the effects of wind forcing on the chile current system. J. Oceanogr. 51, 585–614.

Becker, J.J., Sandwell, D.T., Smith, W., et al., 2009. Global Bathymetry and elevation data at 30 arc seconds resolution: SRTM30 PLUS. Mar. Geod. 32, 355–371.

Belmadani, A., Echevin, V., Dewitte, B., Colas, F., 2012. Equatorially forced intraseasonal propagations along the Peru-Chile coast and their relation with the nearshore eddy activity in 1992–2000: a modeling study. J. Geophys. Res. 117, 1–20.

Belmadani, A., Echevin, V., Codron, F., Takahashi, K., Junquas, C., 2014. What dynamics drive future winds scenarios for coastal upwelling off Peru and Chile? Clim. Dyn. 43 (7–8), 1893–1914.

Bernal, P., Robles, L., Rojas, O., 1982. Variabilidad física y biológica en la región meridional del sistema de corrientes Chile-Perú. Mon. Biol., Pontificia Universidad Católica de Chile. 2, pp. 75–102.

Blanke, B., Arhan, M., Lazar, A., Prévost, G., 2002. A Lagrangian numerical investigation of the origins and fates of the salinity maximum water in the Atlantic. J. Geophs. Res. 107 (C10), 1–15.

Blumberg, A.F., Mellor, G.L., 1987. A description of a three-dimensional coastal ocean circulation model. In: Heaps, N. (Ed.), Three-Dimensional Coastal Ocean Models, Coastal Estuarine Series 4. AGU, Washington, D.C., pp. 1–16.

Brochier, T., Echevin, V., Tam, J., Chaigneau, A., Goubanova, K., Bertrand, A., 2013. Climate change scenarios experiments predict a future reduction in small pelagic fish recruitment in the Humboldt Current system. Glob. Change Biol. 19, 1841–1853.

Capet, X.J., Marchesiello, P., McWilliamns, J.C., 2004. Upwelling response to coastal wind profiles. Geophys. Res. Lett. 31, 1–4.

Capet, A., Mason, E., Rossi, V., Troupin, C., Faugère, Y., Pujol, I., Pascual, A., 2014. Implications of refined altimetry on estimates of mesoscale activity and eddy-driven offshore transport in the Eastern Boundary Upwelling Systems. Geophys. Res. Lett. 41, 7602–7610. http://dx.doi.org/10.1002/2014GL061770.

Carr, S., Capet, X., McWilliams, J.C., Pennington, J.T., Chávez, F.P., 2008. The influence of diel vertical migration on zooplancton transport and recruitment in an upwelling region: estiamtes from a coupled behaviorial-physical model. Fish. Ocean. 17, 1–15.

Casey, K.S., Brandon, T.B., Cornillon, P., Evans, R., 2010. The past, present and future of the AVHRR Pathfinder SST program. In: Gower, J.F.R., Barale, V., Alberotanza, L. (Eds.), Oceanography from Space. Revisited. Springer, Netherlands.

Chaigneau, A., Dominguez, N., Eldin, G., Vasquez, L., Flores, R., Grados, C., Echevin, V., 2013. Near-coastal circulation in the Northern Humboldt Current System from shipboard ADCP data. J. Geophys. Res. Oceans 118, 1–16.

Chávez, F.P., Ryan, J., Lluch-Cota, S.E., Niquen, M., 2003. From anchovies to sardines and back: multidecadal change in the Pacific. Ocean Sci. 299, 217–221.

Chávez, F.P., Bertrand, A., Guevara-Carrasco, R., Soler, P., Csirke, J., 2008. The northern Humboldt Current System: brief history, present status and a view towards the future. Prog. Oceanogr. 79, 95–105.

Clarke, A.J., 1989. Theoretical understanding of eastern ocean boundary poleward currents. In: Neshyba, S.J., Mooers, CH.N.K., Smith, R.L., Barber, R.T. (Eds.), Poleward Flows Along Eastern Ocean Boundaries. Springer-Verlag, New York Inc., pp. 26–39.

Codispoti, L.A., Barber, R.T., Friederich, G.E., 1989. Do nitrogen transformations in the poleward undercurrent off Perú and Chile have a globally significant influence?. In: Neshyba, S.J., Mooers, CH.N.K., Smith, R.L., Barber, R.T. (Eds.), Poleward Flows Along Eastern Ocean Boundaries. Springer-Verlag, New York Inc., pp. 281–314.

Colas, F., Capet, X., McWilliams, J.C., Shchepetkin, A., 2008. 1997–98 El Niño off Peru: a numerical study. Prog. Oceanogr. 79, 138–155.

Colas, F., McWilliams, J.C., Capet, X., Kurian, J., 2012. Heat balance and eddies in the Peru-Chile current system. Clim. Dyn. 39 (1–2), 509–529.

Cubillos, L.A., Arancibia, H., 1993. On the seasonal growth of common sardine (Strangomera bentincki) and anchovy (*Engraulis ringens*) off Talcahuano, Chile. Rev. Biol. Mar. 28, 43–49.

Cubillos, L.A., Bucarey, D., Canales, M., 2002. Monthly abundant estimation for common sardine Strangomera bentincki and anchovy *Engraulis ringens* in the central-southern area off Chile (34–40°S). Fish. Res. 57, 117–130.

Cubillos, L.A., Ruiz, P., Claramunt, G., Gacitúa, S., Núñez, S., Castro, L.R., Riquelme, K., Alarcón, C., Oyarzún, C., Sepúlveda, A., 2007. Spawning, daily egg production, and spawning stock biomass estimation for common sardine (Strangomera bentincki) and anchovy (*Engraulis ringens*) off central southern Chile in 2002. Fish. Res. 86, 228–240.

Czeschel, R., Stramma, L., Schwarzkopf, F.U., Giese, B., Funk, S., Karstensen, J. A., 2011. Mid depth circulation of the eastern tropical South Pacific and its link to the oxygen minimum zone. J. Geophys. Res. 116 (C01015), 1–13.

Daneri, G., Dellarossa, V., Quiñones, R., Jacob, B., Montero, P., Ulloa, O., 2000. Primary production and community respiration in the Humboldt Current System off Chile and associated oceanic areas. Mar. Ecol. Prog. Ser. 197, 41–49.

da Silva, A.M., Young, C.C., Levitus, S. (Eds.), 1994. Atlas of Surface Marine Data 1994, vol. 1. Algorithms and Procedures. NOAA Atlas NESDIS, vol. 6. Technical Report. U. S., NOAA, Silver, Spring, MD. pp. 83.

Dufois, F., Penven, P., Whittle, C., Veitch, J., 2012. On the warm nearshore bias in Pathfinder monthly SST products over Eastern Boundary Upwelling Systems. Ocean Modell. 47, 113–118.

Dunn, J.R., Ridgway, K.R., 2002. Mapping ocean properties in regions of complex topography. Deep Sea Res. 49 (3), 591–604.

Echevin, V., Colas, F., Chaigneau, A., Penven, P., 2011. Sensitivity of the Northern Humboldt Current System nearshore modeled circulation to initial and boundary conditions. J. Geophys. Res. 116 (C07002), 1–16.

Echevin, V., Albert, A., Lévy, A., Graco, M., Aumont, O., Piétri, A., Garric, G., 2014. Intraseasonal variability of nearshore productivity in the Northern Humboldt Current System: the role of coastal trapped waves. Cont. Shelf Res. 73, 14–30.

Fonseca, T., 1989. An overview of the poleward undercurrent and upwelling along the Chilean coast. In: Neshyba, S.J., Mooers, CH.N.K., Smith, R.L., Barber, R.T. (Eds.), Poleward Flows Along Eastern Ocean Boundaries. Springer-Verlag, New York Inc., pp. 203–228.

Fuenzalida, R., Schneider, W., Garcés-Vargas, J., Bravo, L., 2008. Satellite altimetry data reveal jet-like dynamics of the Humboldt Current. J. Geophys. Res. 113, 1–11.

Fuenzalida, R., Schneider, W., Garcés-Vargas, J., Bravo, L., Lange, C., 2009. Vertical and horizontal extension of the oxygen minimum zone in the eastern South Pacific Ocean. Deep Sea Res. II 56 (16), 992–1003.

Garreaud, R., Falvey, M., 2009. The coastal winds off western subtropical South America in future climate scenarios. Int. J. Climatol. 29, 543–554.

Gay, P.S., Chereskin, T.K., 2009. Mean structure and seasonal variability of the poleward undercurrent off southern California. J. Geophs. Res. Oceans 114, 1–17.

Gruber, N., Hauri, C., Lachkar, Z., Loher, D., Froelicher, T.L., Plattner, G.-K., 2012. Rapid progression of ocean acidification in the California. Curr. Syst. Sci. 337, 220–223.

Gunther, E.R., 1936. Variations in behaviour of the Perú Coastal Current: with an historical introduction. Geogr. J. 88, 37–61.

Gutiérrez, D., Bouloubassi, I., Sifeddine, A., Purca, S., Goubanova, K., Graco, M., Field, D., Méjanelle, L., Velazco, F., Lorre, A., Salvatteci, R., Quispe, D., Vargas, G., Dewitte, B., Ortlieb, L., 2011. Coastal cooling and increased productivity in the main upwelling zone off Peru since the mid-twentieth century. Geophys. Res. Lett. 38, 1–6.

Haynes, R., Barton, E.D., 1990. A poleward flow along the Atlantic coast of the

Iberian Peninsula. J. Geophys. Res. 95, 11425–11442.
Hernández-Miranda, E., Quiñones, R.A., Aedo, G., Valenzuela, A., Mermoud, N., Román, C., Yañez, F., 2010. A major fish stranding caused by a natural hypoxic event in a shallow bay of the eastern South Pacific. J. Fish. Biol. 76, 1543–1564.
Hickey, B.M., 1979. The California Current System-hypotheses and facts. Prog. Oceanogr. 4 (8), 191–279.
Hill, A.E., Hickey, B.M., Shillington, F.A., Struh, P.T., Brink, K.H., Barton, E.D., Thomas, A.C., 1998. Eastern ocean boundaries coastal segment (e). In: Robinson, A.R., Brink, H.K. (Eds.), The Sea, vol. 11, The Global Coastal Ocean: Regio- nal Studies and Syntheses. John Wiley, New York, pp. 29–67.
Hormazábal, S., Shaffer, G., Letelier, J., Ulloa, O., 2001. Local and remote forcing of sea surface temperature in the coastal upwelling system off Chile. J. Geophys. Res. 106, 16657–16671.
Hormazábal, S., Shaffer, G., Silva, N., Navarro, E., 2006. The Peru Chile undercurrent and the oxygen minimum zone variability off central Chile. Gayana 70 (1), 37–45.
Hormazábal, S., Combes, V., Morales, C.E., Correa-Ramírez, M.A., Di Lorenzo, E., Nuñez, S., 2013. Intrathermocline eddies in the coastal transition zone off central Chile (31–41°S). J. Geophys. Res. Oceans 118, 1–11.
Huyer, A., Smith, R.L., Paluszkiewicz, T., 1987. Coastal upwelling off Peru during normal and El Niño times, 1981–1984. J. Geophys. Res. 92 (C13), 14297–14307.
Iriarte, J.L., Vargas, C., Tapia, F.J., Bermúdez, R., Urrutia, R.E., 2012. Primary production and plankton carbon biomass in a river-influenced upwelling area off Concepción, Chile. Prog. Oceanogr. 92 (1), 97–109.
Large, W.G., McWilliams, J.C., Doney, S.C., 1994. Oceanic vertical mixing: a review and a model with a nonlocal boundary layer parameterization. Rev. Geophys. 32, 363–403.
Letelier, J., Pizarro, O., Núñez, S., Arcos, D., 2004. Spatial and temporal variability of thermal fronts off central Chile (33–40°S). Gayana 38, 358–362.
Leth, O., Middleton, J.F., 2004. A mechanism for enhanced upwelling off central Chile: eddy advection. J. Geophys. Res. 109, 1–17.
Leth, O., Shaffer, G., 2001. A numerical study of the seasonal variability in the circulation off central Chile. J. Geophys. Res. 106, 229–248.
Leth, O., Shaffer, G., Ulloa, O., 2004. Hydrography of the eastern South Pacific Ocean: results from the Sonne 102 cruise, May–June 1995. Deep Sea Res. II 51, 2349–2369.
Marchesiello, P., McWilliams, J.C., Shchepetkin, A., 2001. Open boundary conditions for long-term integration of regional oceanic models. Ocean Model. 3 (1–2), 1–20.
Marchesiello, P., McWilliams, J.C., Shchepetkin, A., 2003. Equilibrium structure and dynamics of the California Current System. J. Phys. Oceanogr. 33, 753–783.
Marchesiello, P., Debreu, L., Couvelard, X., 2009. Spurious diapycnal mixing in terrain-following coordinate models: the problem and a solution. Ocean Model. 26, 156–169.
Mason, E., Colas, F., Pelegrí, J.L., 2012. A Lagrangian study tracing water parcels origins in the Canary Upwelling System. Sci. Mar. 76S1, 79–94.
Mason, E., Molemaker, J., Shchepetkin, A.F., Colas, F., McWilliams, J.C., Sangrà, P., 2010. Procedures for offline grid nesting in regional ocean models. Ocean Model. 35, 1–15.
Mesias, J., Matano, R., Struh, P.T., 2001. A numerical study of the upwelling circulation off central Chile. J. Geophys. Res. 106, 611–623.
Mittelstaedt, E., 1976. On the currents along the Northwest African coast south of 221 North. Dtsch. Hydrogr. Z. 29, 97–117.
Mittelstaedt, M., 1991. The ocean boundary along the northwest African coast: circulation and oceanographic properties at the sea surface. Prog. Oceanogr. 26, 307–355.
McCreary, J.P., 1981. A linear stratified ocean model of the coastal undercurrent. Philos. Trans. R. Soc. Lond. A 302, 385–413. http://dx.doi.org/10.1098/rsta.1981.0176.
McCreary, J.P., Chao, S.-Y., 1985. Three-dimensional shelf circulation along an eastern ocean boundary. J. Mar. Res. 43 (1), 13–36.
Montero, P., Daneri, G., Cuevas, L.A., González, H.E., Jacob, B., Lizárraga, L., Menschel, E., 2007. Productivity cycles in the coastal upwelling area off Concepción: the importance of diatoms and bacterioplankton in the organic carbon flux. Prog. Oceanogr. 75, 518–530.
Montes, I., Colas, F., Capet, X., Schneider, W., 2010. On the pathways of the equatorial subsurface currents in the eastern equatorial Pacific and their contributions to the Peru-Chile Undercurrent. J. Geophys. Res. 115, 1–16.
Poleward Flows Along Eastern Ocean Boundaries, Coastal and Estuarine Studies. In: Neshyba, S.J., Mooers, C.N.K., Smith, R.L., Barber, R.T. (Eds.), 34 vols., Springer-Verlag, New York, Inc., p. 374.
Oerder, V., Colas, F., Echevin, V., Codron, F., Tam, J., Belmadani, A., 2015. Peru-Chile upwelling dynamics under climate change. J. Geophys. Res. 120, 1152–1172.
Parada, C., Colas, F., Soto-Mendoza, S., Castro, L., 2012. Effects of seasonal variability in across- and alongshore transport of anchoveta (*Engraulis ringens*) larvae on model-based pre-recruitment indices off central Chile. Prog. Oceanogr. 92 (1), 192–205.
Pauly, D., Christensen, V., 1995. Primary production required to sustain global fisher- ies. Nature 374, 255–257.
Pedlosky, J., 1974. Longshore currents, upwelling and bottom topography. J. Phys. Oceanogr. 4, 214–226.
Penven, P., Debreu, L., Marchesiello, P., McWilliams, J.C., 2006. Evaluation and application of the ROMS 1-way embedding procedure to the central California upwelling system. Ocean Model. 12, 157–187.
Penven, P., Echevin, V., Pasapera, J., Colas, F., Tam, J., 2005. Average circulation, seasonal cycle and mesoscale dynamics of the Perú Current System: a modeling approach. J. Geophys. Res. 110, 1–21.
Pierce, S.D., Smith, R.L., Kosro, P.M., Barth, J.A., Wilson, C.D., 2000. Continuity of the poleward undercurrent along the eastern boundary of the mid-latitude Pacific. Deep-Sea Res. 47, 811–829.
Pizarro, O., 1999. Low Frequency Fluctuations in the Eastern Boundary Current off South America: Remote and Local Forcing (Ph.D. thesis). Earth Sciences Centre, Göteborg, Sweeden, p. 102.
Pizarro, O., Shaffer, G., Dewitte, B., Ramos, M., 2002. Dynamics of seasonal and interannual variability of the Peru–Chile undercurrent. Geophys. Res. Lett. 29 (12), 1–4.
Quiñones, R.A., Gutiérrez, M.H., Daneri, G., Gutiérrez, D., González, H.E., Chávez, F., 2010. The Humboldt Current System. In: Liu, K.K., Atkinson, L., Quiñones, R.A., Talaue-McManus, L. (Eds.), Carbon and Nutrient Fluxes in Global Continental Margins, IGBP Series Book. Springer-Verlag, New York, pp. 44–64.
Ramos, M., Pizarro, O., Bravo, L., Dewitte, B., 2006. Seasonal variability of the permanent thermocline off northern Chile. Geophys. Res. Lett. 33, 1–6.
Renault, L., Dewitte, B., Marchesiello, P., Illig, S., Echevin, V., Cambon, G., Ramos, M., Astudillo, O., Minnis, P., Ayers, J.K., 2012. Upwelling response to atmospheric coastal jets off central Chile: a modeling study of the October 2000 event. J. Geophys. Res. 117 (C02030), 1–21.
Renault, L., Hall, A., McWilliams, J.C., 2016. Orographic shaping of US West Coast wind profiles during the upwelling season. Clym. Dinam. 46 (1), 273–289.
Ridway, K.R., Dunn, J.R., Wilkin, J.L., 2002. Ocean interpolation by four-dimensional least squares—applications to the waters around Australia. J. Atmos. Ocean. Technol. 19 (9), 1357–1375.
Risien, C.M., Chelton, D.B., 2008. A global climatology of surface wind stress field from eight years of QuiKSCAT Scatterometer Data. J. Phys. Oceanogr. 38, 2379–2413.
Rivas, D., Samelson, R.M., 2010. A numerical modeling study of the upwelling source waters along the Oregon coast during 2005. J. Phys. Oceanogr. 41, 88–112. http://dx.doi.org/10.1175/2010JPO4327.1.
Shaffer, G., Hormazábal, S., Pizarro, O., Djurfeldt, L., Salinas, S., 1999. Seasonal and interannual variability of currents and temperature over the slope off central Chile. J. Geophys. Res. 104, 951–961.
Shaffer, G., Hormazábal, S., Pizarro, O., Ramos, M., 2004. Circulation and variability in the Chile Basin. Deep Sea Res. I 51, 1367–1386.
Shaffer, G., Pizarro, O., Djurfeldt, L., Salinas, S., Rutllant, J., 1997. Circulation and low-frequency variability near the Chile coast: remotely forced fluctuations during the 1991–1992 El Niño. J. Phys. Oceanogr. 27, 217–235.
Shaffer, G., Salinas, S., Pizarro, O., Vega, A., Hormazábal, S., 1995. Currents in the deep-ocean off Chile (30°S). Deep-Sea Res. I 42, 425–436.
Schneider, W., Fuenzalida, R., Garcés, J., 2004. Corrientes marinas y masas de agua, Biología Marina y Oceanografía: Conceptos y Procesos, Vol. I. Trama Impresores S.A., Chile, pp. 177–194.
Shchepetkin, A., McWilliams, J.C., 2005. The regional oceanic modeling system (ROMS): a split-explicit, free-surface, topography-following- coordinate oceanic model. Ocean Model. 9, 347–404.
Silva, S., Fonseca, T., 1983. Geostrophic component of the northern flow off northern Chile. In: Arana, P. (Ed.), Conferencia Internacional Sobre Recursos Marinos del Pacífico, pp. 59–70.
Silva, N., Konow, D., 1975. Contribución al conocimiento de las masas de agua en el Pacífico Sudoriental. Expedición Krill. Crucero 3-4. Julio-agosto 1974. Rev. Com. Perm. Pacífico Sur. 3, pp. 63–75.
Silva, N., Neshyba, S., 1979. On the southernmost extension of the Perú-Chile Undercurrent. Deep Sea Res. 26, 1387–1393.
Silva, N., Rojas, N., Fedele, A., 2009. Water masses in the Humboldt Current System: properties, distribution, and the nitrate deficit as a chemical water mass tracer for equatorial subsurface water off Chile. Deep-Sea Res. II 56, 1004–1020.
Sobarzo, M., Bravo, L., 2009. Dinámica de las corrientes asociadas a la plataforma continental interior frente a la desembocadura del río Itata. In: Parra, O., Castilla, J.C., Romero, H., Quiñones, R.A., Camaño, A. (Eds.), La cuenca hidrográfica del Itata: Aportes científicos para su gestión sustentable. Ediciones Universidad de Concepción, Concepción, Chile, pp. 161–175.
Sobarzo, M., Bravo, L., Donoso, D., Garcés-Vargas, J., Schneider, W., 2007. Coastal upwelling and seasonal cycles that influences the water column over the continental shelf of central Chile. Prog. Oceanogr. 75, 363–382.
Sobarzo, M., Bravo, L., Moffat, C., 2010. Diurnal-period, wind-forced ocean variability on the inner shelf off Concepción, Chile. Cont. Shelf Res. 30, 2043–2056.
Soto-Mendoza, S., Parada, C., Castro, L., Colas, F., Schneider, W., 2012. Modeling transport and survival of anchoveta eggs and yolk-sac larvae in the coastal zone off central-south Chile: assessing spatial and temporal spawning parameters. Prog. Oceanogr. 92 (1), 178–191.
Struh, P.T., Mesías, J., Montecino, V., Ruttlant, J., Salinas, S., 1998. Coastal ocean circulation off western South America. Coastal Segment (6,E), The Sea, Vol. 11. John Wiley & Sons, Hoboken, pp. 273–313.
Struh, P.T., Mesias, M., James, C., 1995. Altimeter observations of the Perú-Chile Countercurrent. Geophys. Res. Lett. 22, 211–214.
Sverdrup, H.U., 1947. Wind-driven currents in a barocinic ocean with application to the equatorial currents of the eastern Pacific. Proc. Natl. Acad. Sci. USA 33, 318–326.
Sydeman, W.J., García-Reyes, M., Schoeman, D.S., Rykaczewski, R.R., Thompson, S.A., Black, B.A., Bograd, S.J., 2014. Climate change and wind intensification in coastal upwelling ecosystems. Science 345 (6192), 77–80.
Thomson, R.E., Krassovski, M.V., 2010. Poleward reach of the poleward undercurrent extension. J. Geophys. Res. 115, 1–9.
Torres, R., Barton, E.D., 2006. Onset and development of the Iberian Poleward Flow

along the Galician coast. Cont. Shelf Res. 26, 1134–1153.
Ulloa, O., Pantoja, S., 2009. The oxygen minimum zone of the eastern South Pacific. Deep Sea Res. II 56 (16), 987–991.
Vargas, C., Martínez, R., San Martín, V., Aguayo, M., Silva, N., Torres, R., 2011. Allochthonous subsidies of organic matter across a lake–river–fjord landscape in the Chilean Patagonia: implications for marine zooplankton in inner fjord areas. Cont. Shelf Res. 31, 187–201.
Yanicelli, B., Castro, L., Parada, C., Scheneider, W., Colas, F., Donoso, D., 2012. Distribution of Pleuroncodes monodon larvae over the continental shelf of south-central Chile: field and modeling evidence for partial local retention and transport. Prog. Oceanogr. 92–95, 206–227.
Wooster, W.S., Reid, J.L., 1963. Eastern boundary currents, The Sea, Vol. 2. Wiley Interscience, New York, pp. 253–280.
Wooster, W.S., Gilmartin, M., 1961. The Peru-Chile Undercurrent. J. Mar. Res. 19 (3), 97–122.
Wyrtki, K., 1967. Circulation and water masses in the eastern equatorial Pacific Ocean. Int. J. Oceanol. Limnol. 1 (2), 117–147.

4.3. Capítulo 3: Factores que controlan la variabilidad estacional de la productividad en la zona sur del Sistema de Corrientes de Humboldt (30ºS-40ºS): un enfoque de modelación

Manuscrito aceptado en revista Continental Shelf Research (https://doi.org/10.1016/j.csr.2017.08.013): Vergara, O. A., Echevín, V., Sepúlveda, H. H., Quiñones, R. A. Controlling factors of the seasonal variability of productivity in the southern Humboldt Current System (30°S-40°S): a biophysical modeling approach.

Resumen

Se evaluó la variabilidad espacial y estacional de nutrientes y clorofila en la zona sur del Sistema de Corrientes de Humboldt utilizando un modelo regional de alta resolución de circulación oceánica (ROMS) acoplado a un modelo biogeoquímico (Esquema de Interacciones Pelágicas para Estudios de Carbono y Ecosistemas, PISCES). Los nutrientes simulados y los campos de clorofila fueron validados mediante observaciones satelitales e in situ de una serie de tiempo en la plataforma continental. Los ciclos anuales de clorofila y nutrientes modelados fueron consistentes con los valores más altos observados en primavera y verano, lo cual concuerda con las observaciones de que destacan la presencia de surgencia realzada en esta época. La co-limitación del crecimiento del fitoplancton por nutrientes y luz se analizó solo para las diatomeas, ya que este fue el grupo de fitoplancton dominante en las simulaciones. Los resultados mostraron que la co-limitación, cerca de la costa, se rige en otoño e invierno por la luz, y por silicato en primavera y verano, mientras que otros nutrientes limitan fuera de la costa entre enero y abril. Se analizó el transporte de nutrientes en la capa superficial. La advección vertical reflejó aquellas áreas de alta surgencia costera las cuales estaban parcialmente compensadas por procesos horizontales relacionados con el transporte inducido por remolinos desde la costa hasta el océano abierto. Se demostró que la mezcla vertical desempeña un papel clave en la reposición de nutrientes de la capa superficial.

Continental Shelf Research xxx (2017) xxx-xxx

Contents lists available at ScienceDirect

Continental Shelf Research

journal homepage: www.elsevier.com

Controlling factors of the seasonal variability of productivity in the southern Humboldt Current System (30–40°S): A biophysical modeling approach

Odette A. Vergara[a, b], Vincent Echevín[c], Héctor Hito Sepúlveda[d], Renato A. Quiñones[a, b, *]

[a] Interdisciplinary Center for Aquaculture Research, Universidad de Concepción, O'Higgins 1695, Concepción, Chile
[b] Doctorate Program in Oceanography, Department of Oceanography, Universidad de Concepción, Casilla 160-C, Concepción, Chile
[c] Laboratoire d'Oceanographie et de Climatologie: Expérimentation et Analyse Numérique (LOCEAN), Institute Pierre-Simon Laplace (IPSL), UPMC/CNRS/IRD/MNHN, 4 Place Jussieu, Case 100, 75252 Paris cedex 05, France
[d] Geophysics Department, University of Concepción, Concepción, Chile

ARTICLE INFO

Keywords:
Biogeochemical model
Humboldt Current System
Co-limitation of nutrients
Nutrient budget
ROMS-PISCES Model
Upwelling

ABSTRACT

The spatial and seasonal variability of nutrients and chlorophyll in the southern Humboldt Current System were assessed using a high-resolution regional ocean circulation model (ROMS) coupled to a biogeochemical model (Pelagic-Interactions Scheme for carbon and Ecosystem Studies; PISCES). The simulated nutrients and chlorophyll fields were validated using satellite and *in situ* observations at a continental shelf time-series station. The annual cycles of modeled chlorophyll and nutrients were consistent with the highest values observed in spring and summer, which is in agreement with enhanced upwelling observations. Co-limitation of phytoplankton growth by nutrients and light was analyzed for diatoms, the dominant phytoplankton group in the simulations. The results showed that co-limitation, near the coast, was governed in autumn and winter by light, and by silicate in spring and summer, whereas other nutrients were limiting offshore between January and April. Nutrient transport in the surface layer was analyzed. Vertical advection reflected areas with higher coastal upwelling, and was partly offset by horizontal processes related to eddy-induced transport from the nearshore to the open ocean. Vertical mixing was shown to play a key role in replenishing the surface layer with nutrients.

1. Introduction

Phytoplankton photosynthesis plays a key role in ocean biogeochemical cycles. It is the basis of marine trophic webs (Falkowski et al., 1998) and contributes to carbon sequestering and exportation as organic matter (Eppley and Peterson, 1979). Phytoplankton growth in the ocean requires optimal light conditions (Peterson et al., 1987), nutrient availability in the euphotic zone (Diehl et al., 2002) and adequate temperature (Nicklisch et al., 2008; Thomas et al., 2012). Nutrient concentrations increase with depth (Zehr and Ward, 2002), however, nutrient input in the well-lit surface layer can be stimulated by physical mechanisms such as coastal upwelling (Chávez et al., 2003), a major process in Eastern Boundary Upwelling Systems (EBUS). These regions are characterized by intense seasonally modulated upwelling events driven by alongshore winds. These winds force offshore surface Ekman horizontal flow, which is compensated by an upward flow of cool and nutrient-rich waters (Chávez and Messié, 2009), a well-described process known as coastal upwelling (e.g. Bakun, 1996; Hill et al., 1998).

The Humboldt Current System (HCS) off the coast of Chile is highly productive with primary production rates exceeding 25.8 g C m^{-2} d^{-1} (Montero et al., 2007; Quiñones et al., 2010). Here, upwelling is driven when S-SW winds (i.e. equatorward) blow with moderate to high intensity (> 5 ms^{-1}) (Marín et al., 2003) in summer, bringing Equatorial Subsurface Water (ESSW) to the surface. This water mass is associated with low concentrations of dissolved oxygen (< 0.5 mL L^{-1}), high salinity, low temperature (Atkinson et al., 2002; Strub et al., 1998; Sobarzo et al., 2007) and high concentrations of inorganic nutrients (Silva et al., 2009).

In addition to upwelling, other regulating factors of primary productivity determine the spatial and temporal distribution of phytoplankton biomass. One is vertical mixing, which determines the mixed layer depth that can vary from a few meters to more than 100 m (Kirk, 1994). Variations in mixed layer depth affect phytoplankton dynamics by controlling nutrient and light availability (Sverdrup, 1953). Echevin et al. (2008) used model simulations to show that wind-driven seasonal

* Corresponding author at: Interdisciplinary Center for Aquaculture Research, Universidad de Concepción, O'Higgins 1695, Concepción, Chile.

https://doi.org/10.1016/j.csr.2017.08.013
Received 17 February 2017; Received in revised form 19 July 2017; Accepted 19 August 2017
Available online xxx
0278-4343/

upwelling (i.e. vertical flux of nutrients to the surface layer) in the Peruvian EBUS was not a controlling factor of seasonal surface chlorophyll variability, but that seasonal variations of the mixed layer depth-controlled chlorophyll variability due to light limitation. Other physical processes, such as horizontal and vertical advection associated with mesoscale dynamics may also play an important role. Several authors have emphasized the importance of mesoscale dynamics in nutrient and chlorophyll transport to oligotrophic zones away from the coast. Gruber et al. (2011) showed that high levels of eddy activity tend to be associated with low levels of biological production in the California EBUS, and highlighted that reductions in production and export result from eddy-induced nutrient transport from the nearshore environment to the open ocean. Resplandy et al. (2011) and José et al. (2014) used biophysical modeling to suggest that lateral eddy advection is partly responsible for nutrient provision and distribution. Mesoscale eddies in the HCS appear to contribute significantly with nutrients and chlorophyll to the coastal (< 200 km) and transition zones (up to 80°W) (Correa-Ramírez et al., 2007, 2012; Grob et al., 2003; Morales et al., 2012, 2013), while horizontal Ekman transport and Ekman pumping (i.e. large-scale vertical advection) might act synchronously to extend high concentrations of chlorophyll into the offshore area (Morales et al., 2013). In addition to the physical mechanisms that determine the distribution of nutrients and chlorophyll in the ocean, the availability of different macro and micronutrients and their role in co-limiting phytoplankton growth are also important regulating factors (Messié and Chávez, 2015).

Nutrient availability in the euphotic zone depends on various factors. In the southern Humboldt Current System off central-southern Chile (30–40°S), the injection of nutrients into the mixed layer due to upwelling is partly responsible for high reported primary production rates (Daneri et al., 2000; Montero et al., 2007). Rivers however, such as the Bio-Bio and Itata, also provide important quantities of terrestrial organic matter (Vargas et al., 2012), trace metals and nutrients (anthropic and natural) (Salamanca and Pantoja, 2009) to the inner continental shelf, which enhances the microbial food web as a consequence of the high rates of primary production, mainly provided by the pico- and nanoplankton (Iriarte et al., 2012). Depending on nutrient availability, co-limitation of nutrients occurs when two or more nutrients have been depleted simultaneously down to levels where the addition of one or several is necessary to stimulate phytoplankton growth (Moore et al., 2013).

Nutrient limitation has been reported for some EBUS (Messié and Chávez, 2015). Studies in the Peru upwelling system have shown that iron limits phytoplankton in winter (Bruland et al., 2005; Hutchins et al., 2002); while nitrate and silicate are limiting in summer (Echevin et al., 2008; Messié and Chavez, 2015). In the California EBUS, iron exerts fundamental control over nitrate and silicate drawdown (Hutchins et al., 1998). Iron limitation, for instance, generates blooms of strongly silicified and faster sinking chain-forming diatoms (Hutchins and Bruland, 1998). Iron-stressed diatoms deplete surface waters of silicic acid before they deplete nitrate, leading to the secondary silicic acid limitation of the phytoplankton community (Hutchins and Bruland, 1998).

In some EBUS with large OMZs (Oxygen Minimum Zones), phytoplankton growth has been found to be nitrogen-limited. Kuypers et al. (2005) showed that the anammox process in the Benguela EBUS is the main cause of fixed inorganic nitrogen loss. Quiñones et al. (2010) reported a nitrogen deficit compared to phosphorous in several areas of the HCS, suggesting that primary production may be limited by this element. The authors developed nutrient budgets covering the entire HCS and found $\Delta N/\Delta P$ ratios significantly lower than the expected Redfield values off Chile in three regions: 18–27°S (50 km offshore limit), 27–33°S (50 km offshore limit) and 33–42°S (120 km offshore limit).

An understanding of phytoplankton growth must integrate a number of elements, including physical processes, light and nutrient availability. Untangling the most relevant biogeochemical and physical processes that generate the spatial and temporal variability of plankton remains a major challenge that can be addressed with biophysical modeling.

A number of authors have used biophysical modeling to study biophysical relationships in EBUS focused on nutrients, plankton and primary production, such as: (i) the role of specific physical forcing like tides and storms in the cross-shore transport of nutrients, primary production and chlorophyll in the Canary EBUS (Giraud et al., 2008); (ii) the role of the residence time of nearshore waters and mesoscale activity in different EBUS and their impact on net primary production (Lachkar and Gruber, 2011); (iii) the response of nitrogen, phytoplankton, and zooplankton to circulation driven by summer winds in the HCS (Baird et al., 2007).

The objectives of this study are to (a) assess the realism of a high-resolution coupled physical-biogeochemical regional model for the HCS (30–40°S; 70–80°W) using *in situ* and satellite observations; (b) use this model to characterize the spatial and temporal variability of nutrients potentially limiting phytoplankton growth in this region; and (c) determine the main physical mechanisms (horizontal, vertical advection, vertical mixing) involved in the transport of nutrients to the euphotic layer at the seasonal scale.

2. Methods

2.1. Hydrodynamic model

The hydrodynamic model used in this study is ROMS-AGRIF (Regional Oceanic Modeling System - Adaptive Grid Refinement in FORTRAN, Schepetkin and McWilliams, 2005; Penven et al., 2006; http://www.romsagrif.org).

Simulations were carried out on a grid between 29°S and 41°S, and from 69°W to 83°W (Fig. 1), with a resolution of 7.5 km and 32 sigma levels. The initial and open boundary fields were obtained from a monthly climatology from a Peru-Chile model simulation (Colas et al., 2012) using the "Roms2Roms" offline interpolation package (Mason et al., 2010). The model configuration and atmospheric forcing were described in an earlier study that also evaluated the simulations (Vergara et al., 2016).

2.2. Biogeochemical model

The PISCES (Pelagic Interactive Scheme for Carbon and Ecosystem Studies, Aumont et al., 2003; Aumont and Bopp, 2006; Aumont et al., 2015) biogeochemical model was chosen to represent phytoplankton variability and nutrient co-limitation along the Chilean continental platform. PISCES simulates the cycles of carbon, oxygen and the main nutrients that control phytoplankton development (PO_4^{3-}, NO_3^-, NH_4^+, Si, Fe). In this model phytoplankton growth depends on external nutrient concentrations. It includes two phytoplankton classes (diatoms and nanophytoplankton) and two zooplankton classes (micro and mesozooplankton). There are three non-living compartments: semi-labile dissolved organic matter, small sinking particles and large sinking particles. A detailed description of the model structure and equations can be found in Aumont et al. (2015).

PISCES coupled to ROMS has been used for the Peru upwelling system to address questions over different time scales, such as the impact of climate change on the survival of small pelagic fish larvae (Brochier et al., 2013), the impact of intraseasonal coastal-trapped waves on the nearshore Peru ecosystem subsurface (Echevin et al., 2014), and the processes that control the seasonal cycle of chlorophyll in the northern Humboldt Current System (Echevin et al., 2008).

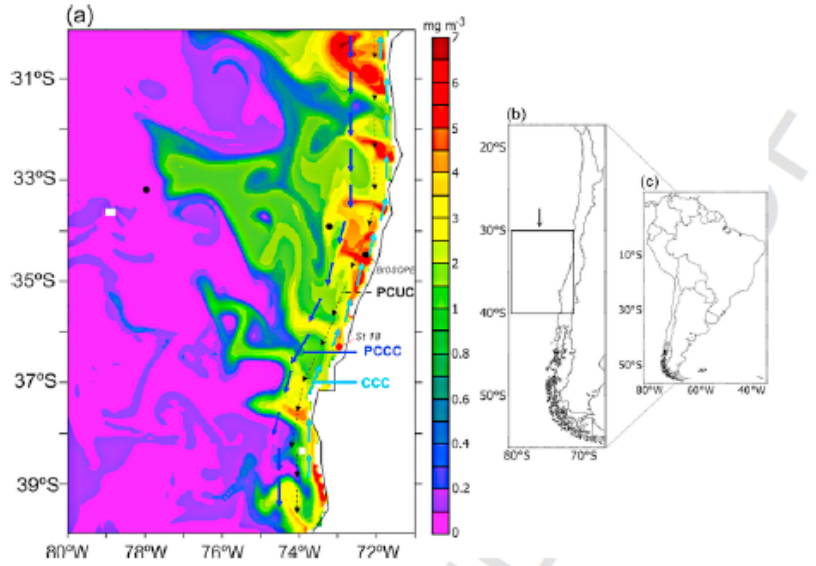

Fig. 1. (a) ROMS-PISCES model domain. Modeled surface chlorophyll (in mgChl m^{-3}, color scale) is shown (January of Year 10). The main surface (CCC, light blue arrow, and PCCC, dark blue arrow) and subsurface (PCUC, black dashed arrow) nearshore currents of the HCS are indicated. Station 18 is marked by a red dot, and the BIOSOPE stations for Fe measurements are denoted by black dots. (b) and (c) correspond to maps of Chile and South America, respectively. Rectangle in (b) indicates the location of the study area.

The biogeochemical fields of the model (nitrate, phosphate, silicate, oxygen, DIC, DOC, alkalinity) were initialized in the domain and imposed at the model's open boundaries using CARS 2009 climatology (CSIRO Atlas of Regional Seas, http://www.marine.csiro.au/~dunn/cars2009/, Ridgway et al., 2002). Due to the scarcity of data, Fe concentrations were obtained from a global climatology model (ORCA2-PISCES, Aumont et al., 2015). Iron data was also obtained from a three-dimensional atmospheric dust deposition model (Tegen and Fung, 1995) and from a time-constant depth-dependent sediment mobilization model (Moore et al., 2004).

Limitations due to light and nutrients were quantified by calculating the limiting terms in the model parameterization of primary production (Aumont et al., 2015). Primary production in the model is proportional to the limiting terms of light and nutrients. The light limitation term (L_{light}) is (1-exp (-α (Chl/C))) * PAR/(μL_{nut})), where α is the initial slope of the PI curve, Chl/C is the chlorophyll/carbon ratio, PAR is photosynthetically active radiation, and μ is the temperature-dependent development rate. PAR is computed using COADS (da Silva et al., 1994) climatological shortwave flux. When sufficient light is available this term reaches 1, and is less than 1 when light limits development. Nutrient limitation L_{nut} is equal to min $_{i=1...n}$ [$C_i/(K_i+C_i)$], where i is the index indicating a specific nutrient (PO_4^{3-}, NO_3^-, NH_4^+, Si, Fe), C_i is the concentration of the nutrient, and K_i is its saturation constant. The limiting terms were calculated for diatoms, since this group is the main contributor to total chlorophyll in the study zone. The so-called "limiting nutrient" in our study is the one (i_0) with the lowest ratio ($C_i/(K_i+C_i) \leq C_i/(K_i+C_i)$).

Runoff from Chilean rivers (e.g. the Biobio and Itata Rivers, both near 36°S) was not explicitly incorporated in the simulation. The impact of river discharge on salinity was represented owing to relaxation of climatological sea surface salinity (see Vergara et al., 2016). However, riverine nutrient input was not taken into account.

To determine the physical mechanisms that transport nutrients in the euphotic layer, advection (zonal ($-U\partial_x C$), meridional ($-V\partial_y C$) and vertical ($-W\partial_z C$)), and vertical mixing ($\partial_z(K\partial_z C)$) were computed, where U, V, W are zonal, meridional and vertical velocity terms respectively, K is the vertical diffusivity, C the nutrient concentration, and x, y, z the zonal, meridional, and vertical (oriented upward) coordinates, respectively. The transport terms were stored online and averaged every 3 days. Only the silicate transport terms were analyzed as silicate was the main limiting nutrient (see Section 3.4).

We ran ROMS/PISCES simulations for 15 years, including a 5-year spin-up period. The last 10 years of the simulations were averaged to obtain the seasonal climatology of the biological variables. The biological parameters used were similar to those listed in Echevin et al. (2014).

2.3. Data used to evaluate the model

One of the parameters estimated by ROMS is the height of the boundary layer (HBL), also named mixed layer depth (MLD). The MLD is considered as the region near its surface with vertically quasi-uniform oceanic tracers above a layer of more rapid vertical changes (Lorbacher et al., 2006). In the MLD there is little variation in salinity, temperature or density with depth (Kara et al., 2003; Pickard and Emery, 1990). The MLD is created by turbulence generated by the wind, convective cooling, breaking waves, current shear, and other physical processes and characterized by vertically uniform and intense mixing (Wijesekera and Gregg, 1996).

The parameterization of the boundary layer mixing in ROMS follows the formulation of Large et al. (1994). The boundary layer height was determined based on the dimensionless Richardson number Ri (i.e. the ratio between buoyancy and the vertical shear of horizontal velocity). The modeled mixed layer depth was compared to climatological MLD from de Boyer Montégut et al. (2004), which has a regular grid of 2 × 2° with a monthly resolution. The climatological MLD was based on individual profile estimates. The criterion selected is a threshold value of temperature or density from a near-surface value at 10 m depth (ΔT = 0.2 °C or $\Delta\sigma\theta$ = 0.03 kg m^{-3}).

Surface chlorophyll concentrations were provided by SeaWiFS satellite data (http://oceancolor.gsfc.nasa.gov/SeaWiFS/) over the 2000–

2006 period. The satellite data was compared with the model simulation.

A monthly climatology of in situ nitrate, phosphate, silicate, and chlorophyll data from Station 18, located in the central-southern Chilean shelf (36.5°S; 73.1°W; see Fig. 3a), over the 2004–2014 period was compared with the simulation. Station 18 is a time series initiated by the COPAS Oceanographic Center in 2002, located on the shelf at 88 m depth (Escribano and Schneider, 2007).

3. Results

3.1. Evaluation of mixed layer depth

The annual mean mixed layer depth (MLD) of the model was compared to the climatology in Fig. 2. The MLD was shallower nearshore than offshore due to enhanced stratification near the coast associated with nearshore upwelling of dense water (Sobarzo et al., 2007). The observed MLD was between 28 and 34 m nearshore and deeper than 50 m offshore (Fig. 2a). Near the coast, the modeled MLD ranged from 34 to 38 m and deepened offshore (> 50 m) (Fig. 2b). The greatest differences between the model and observations were found in the north of the study area (Fig. 2c). The largest discrepancies near the northern boundary could be an effect of open boundary conditions.

The modeled and observed annual MLD cycle (averaged in a 100-km band from the coast) are shown in Fig. 2d. The modeled MLD for spring and summer was about 20 m, and was deeper (~ 50–60 m) for autumn and winter. The observed MLD had similar values in summer and higher values in winter, fluctuating between 40–50 m. Although the annual cycles of the modeled MLD and the observed MLD series were similar, the model values of the MLD were deeper than those observed, mainly in autumn and winter (from May to August).

3.2. Distribution and annual cycle of surface chlorophyll

Both maps of modeled and observed surface chlorophyll showed high values near the coast in a band of approximately 100 km, decreasing gradually offshore (Fig. 3a and b). However, observed values reached concentrations close to 10 mg Chl-a m^{-3} (Fig. 3b), whereas modeled values did not exceed 3 mg Chl-a m^{-3} (Fig. 3a). The zones with the highest chlorophyll concentrations were between 34° and 37°S, and between 38° and 40°S (Fig. 3a and b).

The time-latitude plots of surface chlorophyll (averaged in a 100-km coastal band) showed that the highest concentrations were in spring and summer (Fig. 3c and d), as S-W winds favorable to upwelling predominated (Fig. 2c). The maximum values of modeled chlorophyll were 3.5 mg Chl-a m^{-3} (Fig. 3c), while observed values reached 6.5 mg Chl-a m^{-3} (Fig. 3d). The highest modeled and observed concentrations were found between ~ 33° and 37°S (Fig. 3c and d). In both the model and SeaWIFS data, a sharp change in chlorophyll concentration was found near Punta Lavapie (37.2°S), the southern limit of the Gulf of Arauco, and chlorophyll values decreased south of this latitude.

Chlorophyll values from SeaWIFS and from the simulations were compared at Station 18 (Station 18, 36.5°S; 73.1°W; see Fig. 1). The

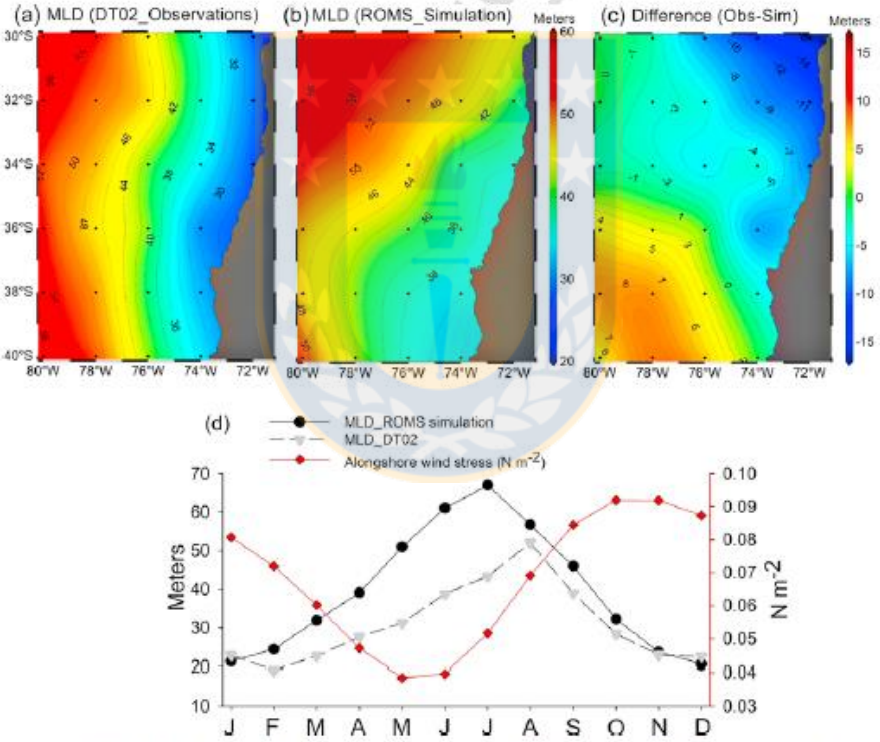

Fig. 2. Annual mean mixed layer depth (MLD, in meters) estimated by (a) de Boyer Montegut et al. (2004) climatology (2° × 2°), (b) ROMS model climatology (averaged on a 2° × 2°) and (c) differences between observations and simulation. Black dots represent the 2°x2° regular grid. (d) Annual cycle of modeled (black circles) and climatological (grey triangles) MLD (in meters) and alongshore wind stress (in N m^{-2}, red diamonds) within a band of 100 km between 30° – 38°S.

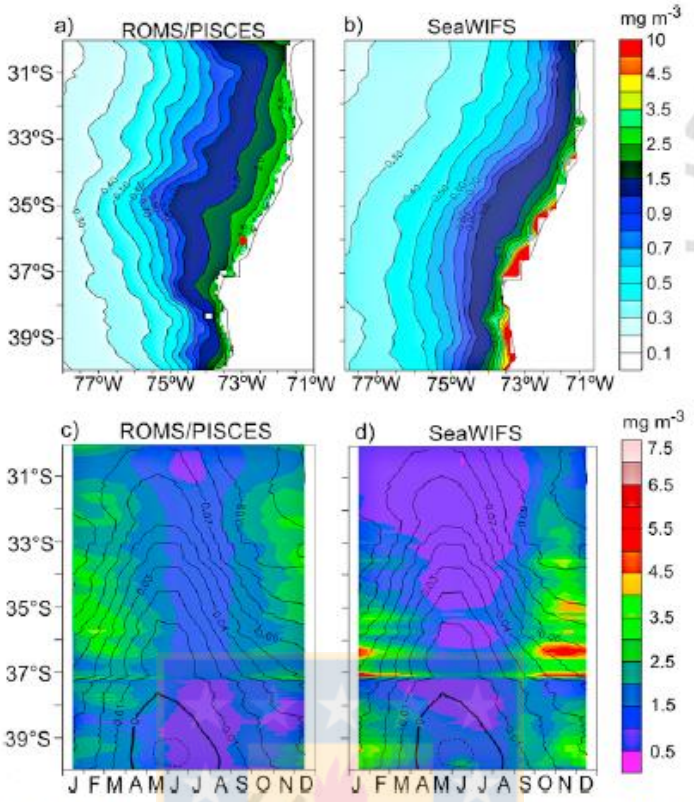

Fig. 3. Annual mean surface chlorophyll (in mg Chl-a m^{-2}) estimated by (a) the model (red circle: Station 18) and (b) SeaWIFS observations (1998–2006). Annual cycle of surface chlorophyll within a 100 km coastal band in (d) the model, and (e) SeaWIFS. Annual along-shore wind stress (in N m^{-2}) cycle is superimposed.

three datasets showed roughly similar annual cycles, with the highest concentrations in spring and summer months (Fig. 4a). Modeled chlorophyll concentrations for summer were underestimated. Chlorophyll decreased in autumn and winter in the three datasets, reaching ~ 2 mg Chl-a m^{-3}. There was, however, a time difference between the modeled minimum concentration in July-August and the observed minimum was in June-July.

We also evaluated the annual cycle of the vertical structure of chlorophyll at Station 18. The two data sets had relatively similar vertical structures, with a chlorophyll-rich (> 1 mg Chl-a m^{-3}) layer of ~ 20–30 m depth. However, modeled chlorophyll did not exceed 4 mg Chl-a m^{-3} (Fig. 4b), while it reached ~ 11 mg Chl-a m^{-3} at Station 18 (Fig. 4c). Another important difference is the progressive thickening of the modeled chlorophyll-rich layer from 20 m (March) to ~ 50 m (July), whereas observations exhibited an abrupt decrease in chlorophyll content, with values of ~ 0.2 mg m^{-3} in July and a progressive thinning of the surface chlorophyll-rich layer from ~ 30 m (January) to ~ 20 m (April).

3.3. Nutrients

The simulated phosphate, nitrate and silicate were compared to observations at Station 18 (Fig. 5). The annual cycles of the three nutrients were similar, with the highest values in spring and summer at the surface layer depth (~ 20 m), probably associated with upwelling. Discrepancies between the model and observations were found. The maximum concentration of PO_4 (~ 2.8 μM) at Station 18 (Fig. 5b) was greater than that of the model, the latter not exceeding 2.2 μM (Fig. 5a). The highest modeled nitrate values (~ 32.5 μM) were at 80 m depth (Fig. 5c), while maximum observed NO_3 was only ~ 27 μM (Fig. 5d). The high nitrate values could be due to a lack of denitrification caused by excessively high oxygen values in the model (figures not shown). Silicate concentration values for the model and Station 18 observations were similar, fluctuating between ~ 5 and 30 μM (Fig. 5e and f). The highest concentrations were found between 40 and 80 m depth. However, there was a slight increase in the silicate surface concentration at Station 18 (0–10 m) in July and August (Fig. 5f), which was not simulated by the model. This is likely due to local river nutrient discharges that were not taken into account in the model.

Although data on Fe for the study region are scarce, we used three vertical profiles of Fe measured during the BIOSOPE cruise (Blain et al., 2008; Bonnet et al., 2008) to evaluate modeled Fe concentrations (Fig. 6). The profiles were located on a cross-shore section (between 33.4° and 34.5°S) off central Chile. The offshore measurements (78.1°W) had low surface values (< 0.05 nM between 50 m and 100 m depth), in agreement with the model. Modeled subsurface values were fairly close (bias is less than 0.05 nM) to the observed values. The "nearshore" measurements (73.5°W) showed higher concentrations than offshore, with values near 0.05 nM in the surface layer and greater than 1 nM at depths between 150 m and 400 m. In contrast, the surface values of the modeled profile were slightly greater (~

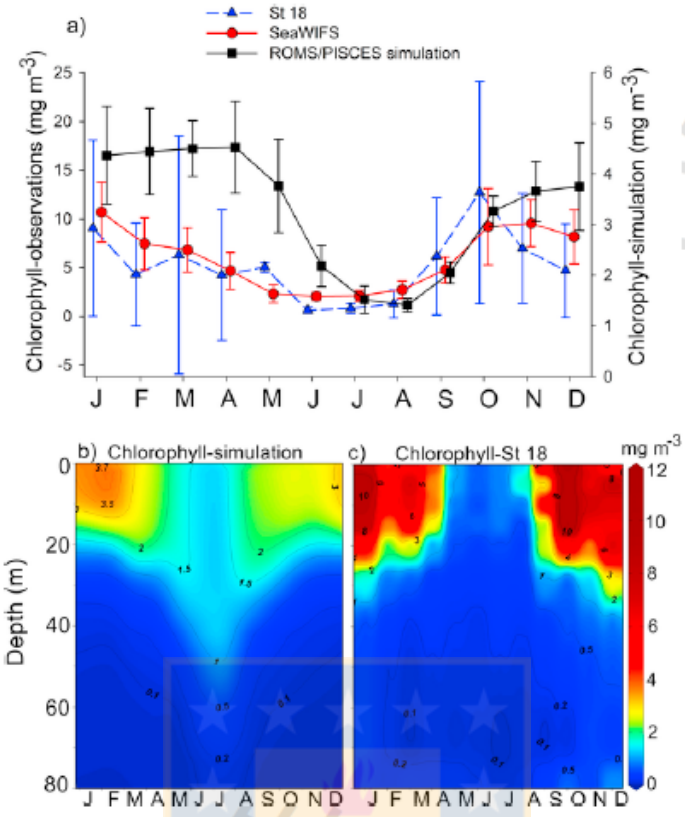

Fig. 4. Seasonal cycle of surface chlorophyll for (a) Station 18 (36.3°S; 73°W; see location in Fig. 1) *in situ* data (blue triangles), SeaWIFS satellite data (red circles) and the simulation (black squares). Seasonal cycle of chlorophyll between 0 and 80 m for (b) the model and (c) Station 18 *in situ* data.

0.07 nM) than those observed and increased moderately, reaching 1 nM at 400 m depth. The "coastal" profiles displayed the strongest discrepancies. Modeled Fe in the surface layer (0–30 m) reached 2.2 nM and decreased to 1.5 nM at ~ 80 m depth, while observed Fe between 30 m and 80 m was around 1.2–1.3 nM. Modeled Fe remained relatively unchanged (~ 1.2–1.3 nM) below 100 m depth, in contrast with observed Fe, which was over 3 nM at depths between 150 m and 300 m. While year-to-year variability of modeled Fe was strong ($\sigma \sim 1$ nM, figures not shown) between 0 and 100 m, modeled Fe at greater depths was never higher than 1.5 nM.

3.4. Co-limitation of nutrients and light for diatoms

3.4.1. Surface co-limitation

Since diatoms are the main contributor to total chlorophyll (70%) (Figure not shown), the co-limitation of nutrients was only computed for this phytoplankton group. As the differences among different simulation years of the co-limitation of nutrients and light were not significant, we chose the 12 months of a typical simulated year (Year 10) and computed co-limitation fields from 0 to 20 m depth to study seasonal variations. To highlight the presence of eddies, we superimposed the Sea Level Anomaly (SLA).

Co-limitation patterns displayed complex structures (Fig. 7). The main limiting nutrients were silicate, Fe and nitrate, with occasional small-scale patches of P limitation. Silicate and Fe were limiting mainly near the coast (~ 100 km) from January to April (Fig. 7a–d), with predominantly silicate limitation. During these same months, nitrate was limiting further from the coast, from ~ 75°W to 80°W. Light was limiting near the coast, as nutrients were more abundant nearshore due to upwelling. Light limitation occurred over a narrow band (< 100 km) in summer, which increased in winter due to decreased insolation (Hernández et al., 2012). The spatial extension of light and silicate limitation increased throughout the coastal zone from May to August (Fig. 7e–h), overlapping with nitrate limitation (May and June). Fe limitation increased from September to December, especially in November, extending away from the coast. Phosphate limitation decreased notably during these months (Fig. 7i–l).

Eddies were observed during all analyzed months, and may have transported the most important nutrients (i.e. nitrate, phosphate and silicate) from the coast to the ocean (Fig. 7). Co-limitation patterns and seasonal evolution in mesoscale eddies were apparent. Several cyclones with a predominant Fe limitation in their core occurred in summer and fall (Fig. 7a–d). In late fall and winter, nutrient limitation in the eddy cores shifted from Fe to Si (Fig. 7e–h), with the presence of ribbons of Fe and P limitation around the core (Fig. 7i), revealing a high degree of complexity.

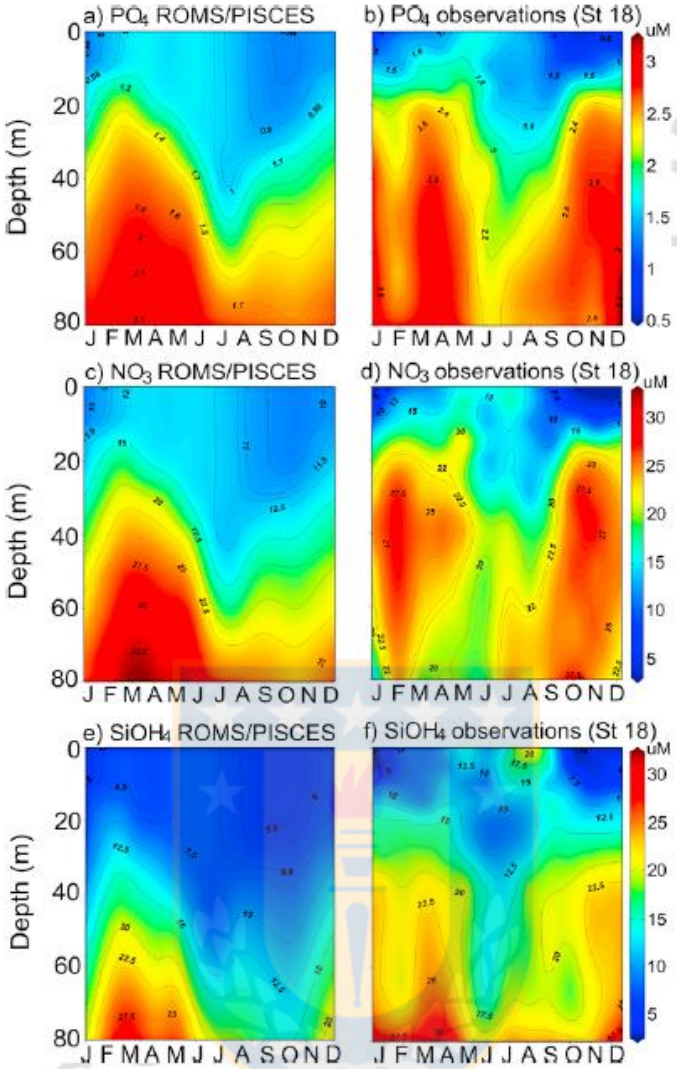

Fig. 5. Seasonal cycle of (a) Modeled phosphate, (c) nitrate and (e) silicate versus observed values (b, d, f) at Station 18. Units are µmol l^{-1}.

3.5. Silicate transport

3.5.1. Advection, mixing and silicate trends from 0 to 20 m depth

Silicon was the most important limiting nutrient for diatoms in the coastal zone (Fig. 7), which is why we analyzed the balance of this element in terms of advection and vertical mixing. We computed the silicate transport terms in the first 20 m of the water column, as the modeled maximum chlorophyll concentration was observed in the surface layer (Fig. 3b).

Mean Si concentrations fluctuated between 2 and 20 µM, with the highest values (> 10 µM) in the coastal zone between 30° and 37°S due to coastal upwelling (Fig. 8g). Si values were higher in the north of the region as the PCUC transported upwelled source waters poleward. As expected, annual mean vertical advection of Si was mainly positive near the coast due to coastal upwelling (Fig. 8a). Highest values (> 5.10^{-5} µM Si s^{-1}) were found in few areas of the northern part of the study area, from about 30° to 35°S (Fig. 8a). The horizontal advection terms displayed more complex small-scale patterns. Zonal advection was mostly negative offshore in a ~ 100 km coastal band and was positive near the coast (Fig. 8b). Meridional advection was mostly positive offshore (Fig. 8b) and negative in a narrow (< 20 km) coastal strip, which was consistent with the equatorward coastal flow (Fig. 8d) and the presence of less rich waters in the south (Fig. 8g). The signature of permanent mesoscale eddies and jets was observed between 30° and 35°S (Fig. 8d). This means that while vertical advection brought nutri-

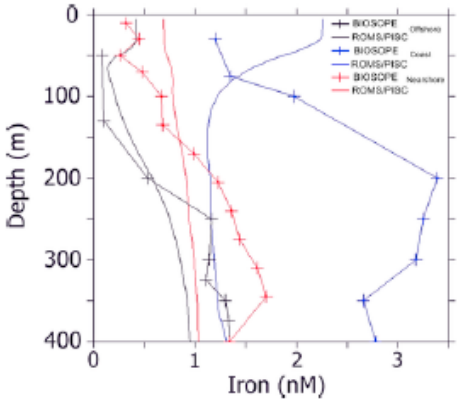

Fig. 6. Iron profiles from model simulations (lines) and BIOSOPE (lines with crosses) measurements (Blain et al., 2008; Bonnet et al., 2008) at three stations (see location in Fig. 1): "offshore" (33.36°S, 78°W; black), "nearshore" (33.8°, 73.5°W; red) and "coastal" (34.5°S; 72.4°W; blue) profiles.

ents to the coastal area, Ekman currents and enhanced offshoreward jets near 32°S, 33°S, 34°S (Fig. 8d) transported part of the high coastal nutrient load offshore (Fig. 8g), thus partly compensating for the vertical input associated with coastal upwelling (Fig. 8e). Total positive advection predominated in the study area, with highest values (~ 3–5 10^{-6} μM Si s-1) at ~ 32°, 36° and 37°S (Fig. 8e). The input of nutrients through vertical mixing was positive everywhere, and greater than through advective fluxes in the offshore regions (50 km from coast) between 30°S and 35°S (Fig. 8f).

Fig. 9 shows the sum of the physical trend, biological trend and total trend of silicate in the study zone. As expected, the physical trend was positive throughout the study zone, with highest values between 30° and 37°S (Fig. 9a). The negative biological trend (primary production is a Si sink) displayed similar patterns to those of the physical trend (Fig. 9b). The total trend was mostly positive, but values were an order of magnitude smaller than those of the physical and biological trends (Fig. 9c), indicating that the model had not reached a fully equilibrated statistical state after 15 years. Nevertheless, moderate Si drift (see also Fig. 10) suggests that a longer simulation would not significantly alter the result.

3.5.2. Cross-shore structure of currents and Si transport terms

Figs. 8 and 9 show that the zone between 31°−37°S had the highest values of advection and physical and biological trends of silicate. To study the vertical structure of Si transport in the water column, we averaged the velocity components and transport terms meridionally between 31° and 37°S (Fig. 10). Similar diagnostics were performed in Colas et al. (2012). Cross-sections are displayed between 0 and 100 m depth and 0–200 km from the coast (Fig. 10).

To highlight the relationship between Si transport and velocity patterns, vertical sections of annual mean zonal (u, Fig. 10b), meridional (v, Fig. 10d) and vertical velocity (w, Fig. 10g) are shown. The wind-driven offshoreward Ekman current associated with the coastal upwelling was reflected in negative zonal velocity (u) in the surface layer (0–15 m). The subsurface zonal velocity was positive in two areas, one close to the coast (from 10 to 50 m depth) with values > 0.5 ms^{-1}, and the other one at 100–200 km from the coast (from ~ 15–100 m depth). The positive velocity likely corresponded to the shoreward current compensating upwelling. The negative subsurface core located 60 km from the coast could have been produced by the poleward undercurrent, which was deflected slightly westward by the coastline orientation.

Meridional velocity (v) (Fig. 10d) near the coast was positive and associated with the Chile Coastal Current (CCC; Mesias et al., 2001; Strub et al., 1998; Fig. 1), which flows towards the equator. Below this current, poleward flow is associated with the PCUC (Peru-Chile Undercurrent; Huyer et al.,1991; Silva and Neshyba, 1979; Fig. 1), which was trapped on the continental platform between 40 and 100 m. The PCUC extended to 100 km offshore. The poleward flow from ~ 120–200 km was associated with the PCCC (Peru-Chile Countercurrent, Strub et al., 1995). As expected, vertical velocity (w) (Fig. 10g) was positive throughout almost the entire study section, with the highest values near the coast (> 0.5 ms^{-1}).

Zonal advection was predominantly negative in the surface layer (0–100 m) (Fig. 10e). The negative subsurface pattern was associated with the PCUC, which was southwestward due to the coastline orientation between 31° and 37°S, and thus projected zonally as a westward current transporting nutrients offshore. The surface pattern (0–10 m) of zonal advection is more complex to interpret. It was negative nearshore (< 100 km) and positive offshore (100–200 km). Note that the annual nearshore average of U was negative (Fig. 10d) and the annual mean cross-shore Si gradient ($\partial_x Si$) was positive as Si concentrations increased towards the coast (Fig. 10a). Consequently, transport associated with the mean current and mean Si gradient ($-U.\partial_x Si$) was positive (figure not shown), while total (*i.e.* eddy + mean) zonal advection was negative (Fig. 10e), suggesting that eddy fluxes play an active role by depleting the nearshore layer and enriching the offshore region (*e.g.* Gruber et al., 2011).

Meridional advection (Fig. 10c) was mainly positive, except for two zones with negative values close to the coast (~ 10 km), and between 90 and 120 km. Positive values can be associated with the undercurrent (Fig. 10b), which transports nutrient-replete waters poleward along the coast. In contrast, the equatorward coastal surface jet (Fig. 10b) transported relatively nutrient-poor Si surface waters northward (Fig. 8g), acting as a silicate sink (Fig. 10c).

Horizontal (*i.e.* zonal + meridional) advection (Fig. 10f) was negative near the coast, with values lower than -6 μM Si $month^{-1}$. Two positive zones were found, between about 100 and 200 km offshore, and near the coast at less than 60 m (Fig. 10c). Vertical advection (Fig. 10h) was mainly positive (> 6 μM Si $month^{-1}$) from the coast to 140 km offshore. Vertical mixing was a source of Si in the first 20 m depth from the coast to 200 km, with values greater than 6 μM Si $month^{-1}$ and a sink below 20 m depth (Fig. 10i). Vertical mixing was confined to the 0–50 m depth layer. It served to mix nutrient-rich subsurface waters with less rich surface waters (0 −10 m), enriching the surface waters. Total advection (Fig. 10j) was positive from the coast to 200 km offshore in the first 50 m of the water column, with transport values > 2 μM Si $month^{-1}$, and slightly negative at greater depths. The sum of all physical terms (*i.e.* advection + vertical mixing; Fig. 10k) was positive between 0 and ~ 30 m depth, with values > 2 μM Si $month^{-1}$, and slightly negative below 30 m. The total trend (physical + biological trend) (Fig. 10l) was mainly positive and weak (< 0.2 μM Si $month^{-1}$) in comparison with other terms, with slightly higher values near the coast.

3.5.3. Annual cycle of silicate balance

The annual cycles of the transport and biological terms were averaged over a coastal band of 100 km (Fig. 11a) and over an offshore band of 100 km (Fig. 11b), between 0 and 20 m depth, to study their relationships with the annual chlorophyll cycle. We considered the latitudinal zone from 31° to 37°S. Vertical mixing and vertical advection in the coastal band (Fig. 11a) were positive throughout the year and showed similar annual cycles, with higher values in spring and summer, and lower in autumn and winter, as expected from the seasonal cycle of surface winds (Fig. 2c). Horizontal advection was mainly nega-

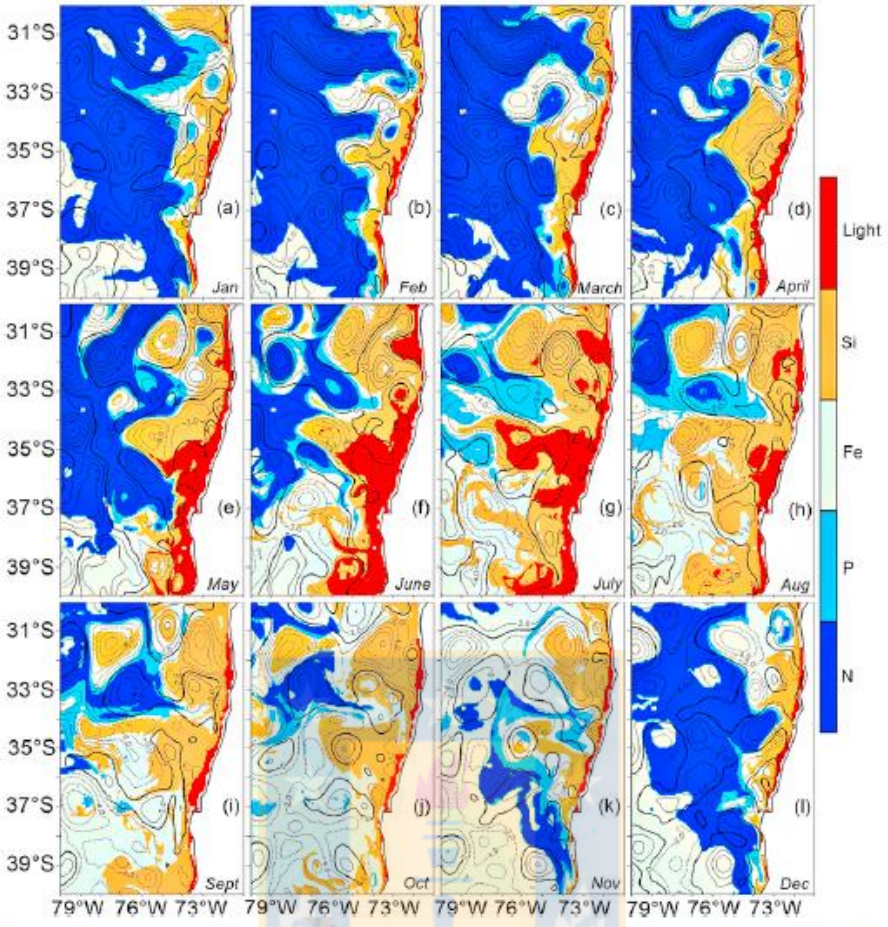

Fig. 7. Maps of surface co-limitation fields during Year 10, from January to December between 0–20 m. Colors indicate whether nutrients or light are limiting. Contours (in cm) represent the sea level anomaly.

tive, with values close to zero in autumn-winter and lower values in spring-summer (Fig. 11a). The annual cycle of total advection was similar to that of horizontal advection, but with a weaker amplitude, higher values in autumn-winter and lower values in spring-summer, and a predominance of positive values (Fig. 11a). Interestingly, vertical nutrient advection reached maximum positive values during the peak of the upwelling season (January-February), but was nevertheless offset by very strong offshore advection, possibly enhanced by eddy effects (Fig. 12) and resulting in negative values.

The total physical trend was always positive within the coastal band, with greater values in autumn-winter. The biological trend was always negative, with lower values in spring-summer ($\sim 1.5\ 10^{-6}$ µM Si s^{-1}) compared with autumn-winter ($\sim 2.5\ 10^{-6}$ µM Si s^{-1}). The total trend was weak and constant throughout the year, varying slightly with predominantly positive values ($< 0.3\ 10^{-6}$ µM Si s^{-1}).

The annual cycle of silicate balance in the oceanic offshore band (Fig. 11b) showed lower values ($< 2\ 10^{-6}$ µM Si s^{-1}) than near the coast, with different contributions from several processes. In contrast to coastal upwelling, vertical advection was negative year-round. Downwelling was likely due to anticyclonic wind stress curl (Bakun and Nelson, 1991; Aguirre et al., 2012). The highest vertical mixing values were in spring-summer and the lowest in autumn-winter, which was in agreement with the seasonal cycle of offshore wind stress intensity (Figure not shown). Negative vertical advection was partly offset by horizontal fluxes, with higher values from April to September, possibly due to enhanced eddy flux of coastally upwelled nutrients in winter (Fig. 12). In conclusion, nutrient input in the offshore band was mainly achieved through wind-driven vertical mixing in summer and horizontal advection in winter, possibly due to mesoscale eddy propagation (Correa-Ramirez et al., 2007).

In both bands, surface chlorophyll had high values in spring-summer, with greater values (> 2 mg Chl-a m^{-3}) in the coastal band than in the oceanic band (~ 1.6 mg Chl-a m^{-3}, Fig. 11). As phytoplankton growth was mainly limited by light in the coastal band (Fig. 7), surface chlorophyll was largely influenced by vertical mixing and solar radiation seasonality. Therefore, coastal chlorophyll correlated better with the vertical mixing term ($c = 0.77$, $p = 0.005$) and with (-1)*MLD ($c = 0.83$, p-value $= 0.001$) than with the total input of nutrients in the surface layer ($c = 0.54$, $p = 0.075$).

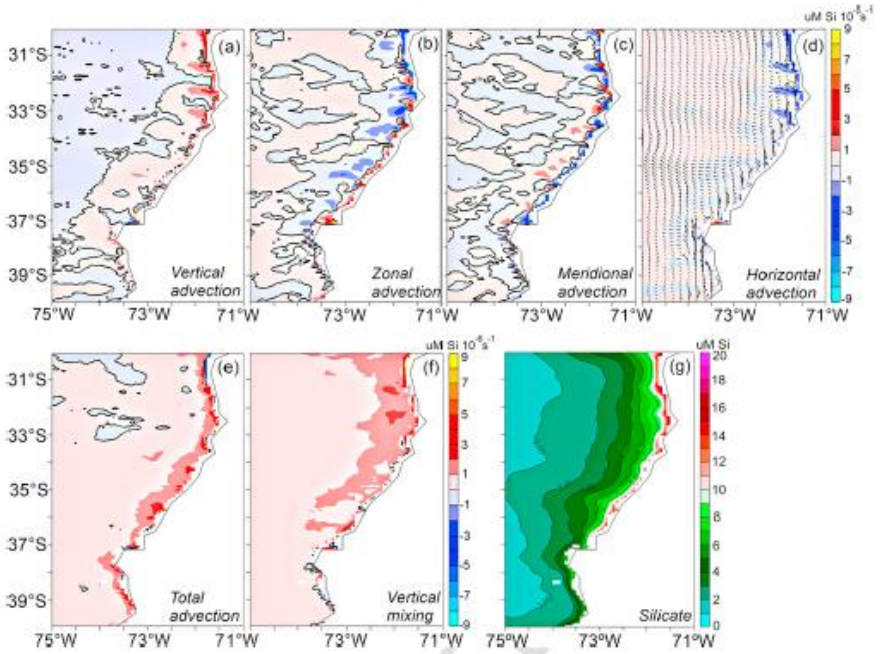

Fig. 8. Annual mean transport terms (in μmol s^{-1}) for silicate advection: vertical (a), zonal (b), meridional (c), horizontal (d), total (e), vertical mixing (f). Annual mean modeled silicate (μmol l^{-1}). All fields are averaged between 0 and 20 m.

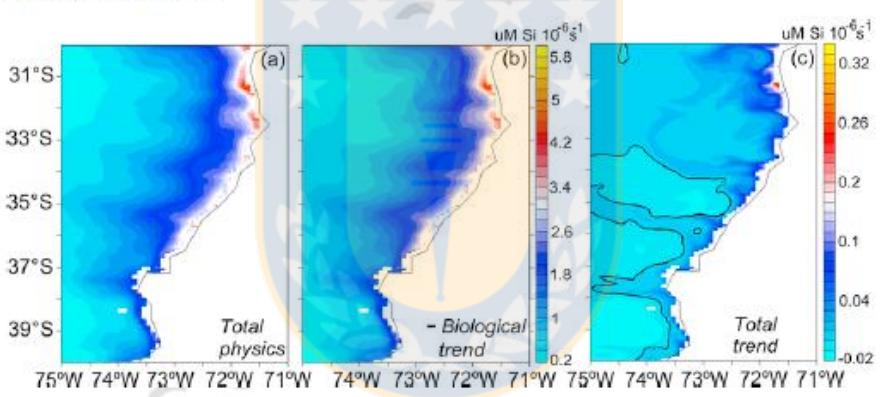

Fig. 9. Total physical trend (a), (−1)x biological trend (b) and total trend (physics + biology) for silicate (in μmol s^{-1}), between 0 and 20 m.

4. Discussion

The aim of this study was to characterize the seasonal dynamics of surface chlorophyll and its relationship to nutrient fluxes in the surface layer. Very few studies in the southern HCS have used biogeochemical-physical coupled modeling to study the relationship between hydrodynamic and biological processes. Baird et al. (2007) used a physical model (POM) (Blumberg and Mellor, 1987) coupled to an NPZ model to investigate the response of the ecosystem to the circulation driven by summer winds in central-southern Chile. These authors studied the impact of biological parameters, such as zooplankton grazing pressure, on the magnitude and spatial distribution of surface chlorophyll. The nearshore spatial resolution (~ 15 km) in Baird et al. (2007) was lower than in our simulations, thus mesoscale eddy effects might have been underestimated in their study. Moreover, they did not simulate a full seasonal cycle, and their biogeochemical model was simpler than the PISCES model. Overall, these differences make it difficult to compare their results with ours.

Our results make a significant contribution to understanding physical-biological coupling in the southern HCS. We found that the modeled surface mixed layer depth (MLD) reproduced observed seasonal variability relatively well (Fig. 2d), becoming deeper in autumn and winter, and shallower in spring and summer. The MLD appeared to be modulated mainly by alongshore wind stress in our study, but other processes not accounted for in our model, such as riverine fresh water

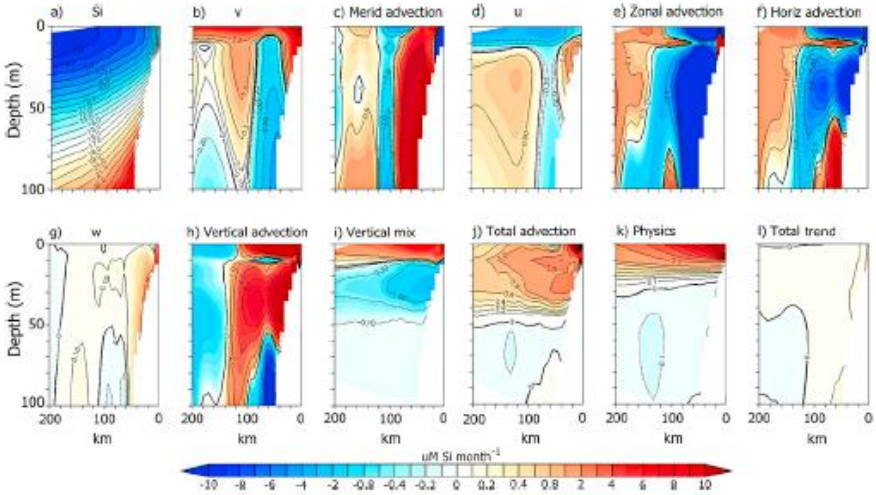

Fig. 10. Along-shore averaged (31°–37°S) sections of (a) silicate (μmol l^{-1}) and silicate transport terms (in μmol $month^{-1}$): (c) meridional advection, (e) zonal advection, (f) horizontal advection, (h) vertical advection, (i) vertical mix, (j) total advection, (k) total physical trend, and (l) total trend (physics + biology) (j) of silicate between 0 and 100 m from 31–37°S. Alongshore average of (b) zonal (u, in m s^{-1}), (d) meridional (v, in m s^{-1}) and (g) vertical (w, in m s^{-1}) velocity components.

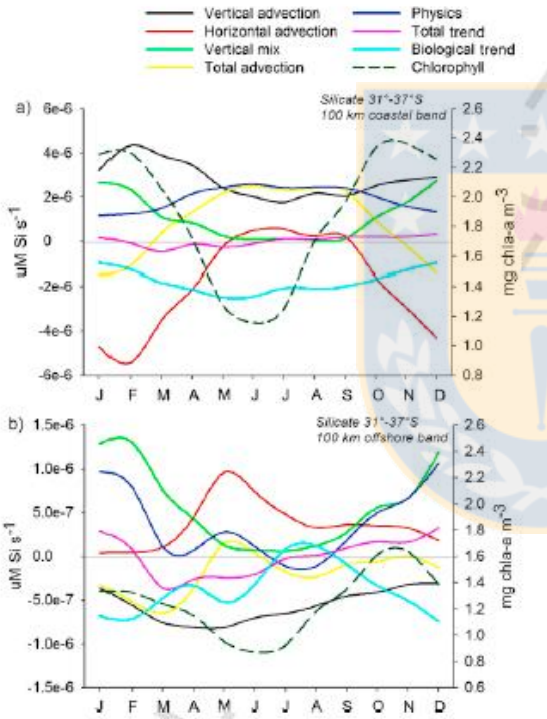

Fig. 11. Annual cycle of silicate transport terms within (a) a coastal band of 100 km, and (b) an offshore band of 100 km. Vertical advection (black), horizontal advection (red), total advection (yellow), vertical mixing (green), physical trend (blue), total trend (purple), biological trend (cyan). Surface chlorophyll (in mg Chl-a m^{-3}) is also shown (green dashed line). All fields are averaged between 0–20 m and 31°–37°S.

fluxes, may also play a role during certain periods of the year (Sobarzo et al., 2007). The nearshore modeled MLD was too deep, which could impact the simulated primary production by a too strong light limitation and decrease surface chlorophyll. Using a ½ ROMS simulation of the Pacific Ocean, Lemarié et al. (2011) computed the MLD using individual temperature profiles and the same criteria as de Boyer Montégut et al. (2004). They also obtained a positive bias (i.e. a too deep simulated MLD off the coasts of Chile, see their Fig. 5). Therefore, the differences between observed and modeled MLD could not be attributed to the different methods used. Using a high frequency (daily or 6-hourly) wind forcing may also impact the MLD, but estimating this effect is beyond the scope of the present model study.

An abrupt change in nearshore chlorophyll concentration at ~ 37°S (Gulf of Arauco) was simulated by the model and also seen in observations (Fig. 3c and d). This high chlorophyll concentration is probably an effect of the local topography. The Gulf of Arauco, an equatorward-facing gulf, favors strong upwelling events because of its geographic orientation, and thus has a high level of biological productivity (Figueroa and Moffat, 2000). This zone of complex bathymetry is also strongly influenced by the submarine canyon of the Bio-Bio River, which modifies coastal circulation and induces upwelling of water from depths greater than 200 m (Sobarzo et al., 2001, 2016). In addition, off Lavapie Point (south limit of the Gulf of Arauco), there are strong equatorward currents in the form of an upwelling jet (Atkinson et al., 2002) that could influence chlorophyll distribution.

Despite its relatively low resolution (7 km) in comparison with the bay's dimensions, our model was able to reproduce local changes in chlorophyll concentrations.

The annual chlorophyll signal near the coast (< 200 km) in this zone has been described as governed by wind stress and currents associated with westward-propagating Rossby waves (Correa-Ramírez et al., 2012). In the coastal transition zone (CTZ, west of the shelf break) increased chlorophyll concentrations are the result of nutrient advection by mesoscale eddies generated near the coast (Morales et al., 2012). Many eddies are generated in spring and summer, fertilizing offshore waters in winter (Correa-Ramírez et al., 2007). The mesoscale patterns of Fe limitation in summer, shown in Fig. 7a-d, suggest that these structures, generated near the shelf break, are rich in macronutrients like nitrate and silicate.

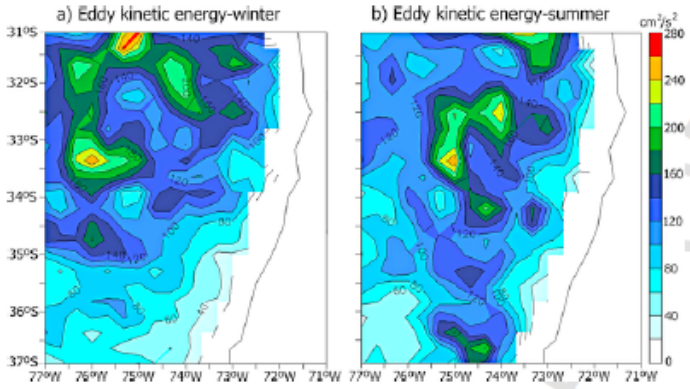

Fig. 12. Surface Eddy Kinetic Energy (in $cm^2\ s^{-2}$) during winter (a) and summer (b).

Comparison of modeled chlorophyll concentrations with *in situ* observations at Station 18 showed similar annual cycles, with high concentrations above 20 m depth in spring and summer (Fig. 4b,c). This concurs with the reports of Daneri et al. (2000) and Montero et al. (2007), where the highest chlorophyll concentrations were found between summer and the middle of autumn. Increased solar radiation is one of the main factors that trigger phytoplankton blooms in the upwelling system off central-southern Chile (Montero et al., 2007). Our results confirmed that light limitation is stronger than nutrient limitation for several months (Fig. 7). Improvements in light conditions in summer coincide with a shallower thermocline and the intensification of upwelling favorable winds in the zone (Sobarzo et al., 2007). In addition to the favorable light conditions in the system, the timing of upwelling and relaxing events is a crucial modulator of the high level of productivity in the upwelling ecosystem off central-southern Chile (Daneri et al., 2012). Relaxation of upwelling provides the required stability to produce phytoplankton blooms (Daneri et al., 2000).

The annual nitrate, phosphate, and silicate variability of the *in situ* observations at Station 18 was similar to that generated by the model (Fig. 5). The concentrations of these nutrients were high in spring-summer, coinciding with the period of winds favorable to upwelling (Sobarzo et al., 2007). High nutrient concentrations, together with low oxygen concentrations, high salinity, and low temperature, are typical of Equatorial Subsurface Waters (ESSW) (Atkinson et al., 2002; Silva et al., 2009), which are transported by the Peru-Chile Undercurrent (PCUC) along the continental shelf off Peru and Chile (Strub et al., 1998; Vergara et al., 2016). This water mass is transported to the surface in the upwelling season, fertilizing the eutrophic layer with new nutrients, allowing the existence of a highly productive ecosystem (Daneri et al., 2000; Quiñones et al., 2010).

The co-limitation of nutrients and silicate balance were only estimated for diatoms, since as noted above, diatoms were the most important contributor to total chlorophyll (~ 70%). As expected from the annual cycle of solar radiation (Sobarzo et al., 2007) in autumn and winter (April-August), light limitation extended from the very nearshore region (< 100 km) to approximately 200 km offshore (Fig. 7). Our results indicate that Fe was the offshore limiting nutrient in spring (September-November). Similar results have been reported offshore of the study region (34°S; 92°W), in the southeastern edge of the Southeast Pacific gyre (Bonnet et al., 2008). These authors found that Fe controlled photosynthetic efficiency and primary production. They reported that primary production in the southeast flank of the gyre at 92°W was co-limited by nitrogen and Fe, while in the center of the gyre nitrogen was the limiting nutrient. Blain et al. (2008) found high concentrations of Fe (1.2 nM at 30 m and 3.4 nM at 200 m; see Fig. 6) above the shelf break in the presence of low oxygen concentrations. These concentrations were roughly within the same order of magnitude as those in our simulations, but modeled Fe was much weaker at greater depth (Fig. 6), suggesting that the parameterization of Fe sources on the shelf could be improved in the model. Thus, our estimation of Fe limitation near the coast remains uncertain and more measurements are needed for a more accurate evaluation of the model. Furthermore, the modeled MLD was too deep over most of the coastal domain and, particularly, in the northern part (30–34°S; Fig. 2) in winter (Fig. 2d). This suggests that light limitation may be overestimated and could play a less important role than that shown by the model during late fall-early winter (Fig. 7e-h).

There is evidence in the literature based on carbon and nutrient box model budgets (e.g. Gordon et al., 1996) that primary production may be limited by nitrogen in the northern and central-southern Chilean HCS (Quiñones et al., 2010). Lower N/P ratios relative to the Redfield N/P ratio in upwelling ecosystems have been associated with the presence of denitrification, which plays a key role in the nitrogen cycle in the OMZ (Farías et al., 2004, 2009b; Pantoja et al., 2004; Quiñones et al., 2010).

According to the results reported by Anabalón et al. (2016), for the same study zone, our findings on Si limitation are not far from reality. They found that macro-nutrient ratios (Si/N and N/P) experienced significant temporal changes which produced important modifications in the micro-phytoplankton community structure. Anabalón et al. (2016) reported a decrease in silicate and a moderate increase in nitrate produced by land-derived processes such as a reduction in river discharge, resulting in a large reduction (up to 100%) of the mean Si/N ratios. They emphasize that changes in Si/N ratio associated with increasing nitrate in coastal waters, without large changes in Si, influence diatom growth dynamics and eventually can lead to Si-limitation. They conclude that the dominance of different diatoms species in coastal waters may affect the ambient Si/N ratios through differences in their uptake rates.

Given that silicate was the main limiting nutrient in the simulations, the different terms of silicate transport were estimated to characterize their spatial and temporal variability. Despite its limited spatial resolution (7 km), the model was able to simulate preferential zones of vertical advection, i.e. enhanced coastal upwelling near 30–32°S, 33–34°S, 35–36°S and 37–38°S (Fig. 8a). Some of these areas are strong upwelling cells referred to in the literature: Punta Lengua de Vaca (30.24°S), Curaumilla (33.1°S), Punta Nugurne (35.9°S) and Punta Lavapie (37.15°S) (Aiken et al., 2008; Figueroa and Moffat, 2000; Strub et al., 1998). Punta Lavapie (37.15°S) has received special attention since is the most intense upwelling center of the Chilean HCS

(Leth and Shaffer, 2001; Leth and Middleton, 2004; Valle-Levinson et al., 2003), and important for fishing productivity (Castillo et al., 1991; Cubillos et al., 2007; Landaeta and Castro, 2006). Greater spatial resolution is needed to better represent the dynamics of this particular region.

As expected, based on the conservation of mass balance, horizontal advection (Fig. 8d) partly balanced vertical advection. Interestingly, while coastal upwelling, and hence vertical advection was strongest in summer (Fig. 11a, black line), nutrient decrease due to horizontal advection was strong, thus the coastal region lost nutrients through advective processes. This loss was compensated by the entrainment of nutrients into the surface layer through vertical mixing (green line, Fig. 11a). Furthermore, enhanced eddy activity (related to horizontal process) tends to be associated with low levels of biological production, exerting a suppressive effect on upwelling systems (Gruber et al., 2011).

Our simulations show that in contrast to the coastal zone, offshore vertical advection was negative, with greater values in spring-summer, suggesting year-round downwelling. Using a regional physical model, Aguirre et al. (2012) described the importance of offshore upwelling/downwelling linked to Ekman pumping. They found a region offshore with anticyclonic curl associated with downwelling forced by Ekman suction. Thus, it is probable that the vertical advection offshore in our simulations is linked to Ekman suction. The latter was offset by horizontal advection, which fueled the region in autumn-winter (from April to September, Fig. 11b). These results may be related to eddy-induced nutrient transport from the nearshore environment to the open ocean (Correa-Ramirez et al., 2007).

The present model approach has some limitations. Monthly climatological winds and boundary conditions used to force the model allowed for representing the seasonal variability of the system with a fair degree of realism. Nevertheless, intraseasonal wind variability (*e.g.*, Gomez et al., 2017) and coastal trapped waves (Hormazábal et al., 2002) can modulate nearshore primary production, as occurs in the Peru EBUS (*e.g.*, Echevin et al., 2014). These fluctuations were not well represented as the climatological boundary forcing smoothed the dominant 60-day variability. Furthermore, strong episodic upwelling events that typically last one to two weeks (Leth and Middleton, 2004; Sobarzo et al., 2007) were not represented in the climatological wind forcing. Investigating the impact of physical processes not accounted for in this study on the biogeochemical ecosystem will be addressed in future work.

5. Conclusions

For the first time, an eddy-resolving three-dimensional ocean circulation model coupled to an intermediate-complexity biogeochemical model simulated the spatial and seasonal variability of nutrients and chlorophyll in the HCS off central-southern Chile (30–40°S). The annual cycles of modeled nutrients (nitrate, silicate, and phosphate) were similar to cycles observed at a coastal station (Station 18) and to satellite observations (SeaWIFS), with the highest values in spring and summer, in agreement with upwelling observations. Although modeled chlorophyll showed a spatial pattern and annual cycle similar to those of the SeaWIFS satellite data, the modeled concentrations did not exceed 4 mg Chl-a m^{-3} along the coast, while the maximum observed concentration by SeaWIFS was 10 mg m^{-3}. The modeled annual chlorophyll cycle was also similar to the cycle at Station 18, with the highest values in spring and summer in the first 20 m of the water column. However, simulated concentrations did not exceed 3.5 mg m^{-3}, while those at Station 18 reached up to 12 mg m^{-3}. The spatial distribution of the modeled mixed layer was similar to a low-resolution (2°) climatology, with lower values near the coast and higher values offshore, although the modeled mixed layer was deeper in winter than the observed mixed layer depth.

Co-limitation of phytoplankton growth by light and several nutrients was investigated using the model. Near the coast, photosynthesis was mainly governed by light during autumn and winter, and by silicate during the rest of the year. Offshore co-limitation was mainly due to nitrate in summer and autumn, and Fe during winter and spring. Occasionally Fe, nitrate and phosphate were also limiting within and around mesoscale eddies, revealing complex structures.

The spatial structure and seasonality of silicate fluxes in the surface layer (0–20 m) were characterized. Vertical advection highlighted positive areas nearshore associated with greater coastal upwelling and negative areas offshore due to Ekman suction. The strong upward flux exerted by coastal upwelling was fully offset by horizontal fluxes resulting in negative total advective flux in summer. Enhanced horizontal advection could be related to eddy-induced transport of nutrients from the nearshore region to the open ocean during the upwelling period. Upward nutrient flux through vertical mixing played a major role throughout the year, particularly in summer. This study constitutes a first step to modeling the seasonal cycle of three-dimensional coupled physical-biogeochemical processes in central-southern Chile.

Uncited references

(Dunn and Ridgway, 2002; Kamykowski and Zentara, 1990; Lemarié et al., 2012; Paulmier and Ruiz-Pino, 2009; Saito et al., 2008).

Acknowledgements

This study was funded by the Interdisciplinary Center for Aquaculture Research (INCAR; FONDAP Project N°15110027; CONICYT) and by the Programa de Investigación Marina de Excelencia (PIMEX) of the Faculty of Natural and Oceanographic Sciences (University of Concepción, Chile) funded by Celulosa Arauco y Constitución S.A. Odette Vergara was also supported by a Doctoral Scholarship from the Comisión Nacional de Investigación Científica y Tecnológica (CONICYT, Ministry of Education, Chile). We acknowledge the financial support for O. Vergara's internships at LOCEAN received from the French Embassy in Chile and the REDOC-CTA (Red Doctoral en Ciencia, Tecnología y Ambiente, University of Concepción, Chile).

References

Aguirre, C., Pizarro, O., Strub, P.T., Garreaud, R., Barth, J., 2012. Seasonal dynamics of the near-surface alongshore flow off central Chile. J. Geophys. Res. 117, 1–17.
Aiken, C., Castillo, M., Navarrete, S., 2008. A simulation of the Chilean Coastal Current and associated topographic upwelling near Valparaíso, Chile. Cont. Shelf Res. 28 (17), 2371–2381.
Anabalón, V., Morales, C.E., González, H.E., Menschel, E., Schneider, W., Hormazábal, S., Valencia, L., Escribano, R., 2016. Micro-phytoplankton community structure in the coastal upwelling zone off Concepción (central Chile): annual and inter-annual fluctuations in a highly dynamic environment. Prog. Oceanogr. 149, 174–188.
Atkinson, L.P., Valle-Levinson, A., Figueroa, D., De Pol-Holz, R., Gallardo, V.A., Schneider, W., Blanco, J.L., Schmidt, M., 2002. Oceanographic observations in Chilean coastal waters between valdivia and concepción. J. Geophys. Res. 100, 181–193.
Aumont, O., Maier-Reimer, E., Blain, S., Monfray, P., 2003. An ecosystem model of the global ocean including Fe, Si, P colimitations. Glob. Biogeochem. Cycles 17 (2), 1060.
Aumont, O., Bopp, L., 2006. Globalizing results from ocean in situ iron fertilization studies. Glob. Biogeochem. Cycles 20, https://doi.org/10.1029/2005GB002591(GB2017).
Aumont, O., Ethé, C., Tagliabue, A., Bopp, L., Gehlen, M., 2015. PISCES-v2: an ocean biogeochemical model for carbon and ecosystem studies. Geosci. Model Dev. Discuss. 8, 1375–1509.
Baird, M.E., Leth, O., Middleton, J.F., 2007. Biological response to circulation driven by mean summertime winds off central Chile: a numerical model study. J. Geophys. Res. 112, C07031. https://doi.org/10.1029/2006JC003655.
Bakun, A., 1996. Patterns in the Ocean. Ocean Processes and Marine Population Dynamics. California Sea Grant Colllege System, USA, in cooperation with Centro de Investigaciones Biológicas del Norte La Paz, Baja California Sur323.
Bakun, A., Nelson, C.S., 1991. The seasonal cycle of wind-stress curl in subtropical eastern boundary current regions. J. Phys. Oceanogr. 21, 1815–1834.
Blain, S., Bonnet, S., Guieu, C., 2008. Dissolved iron distribution in the tropical and sub tropical South Eastern Pacific. Biogeoscience 5, 269–280.

Bonnet, S., Guieu, C., Bruyant, F., Prásil, O., Van Wambeke, F., Raimbault, P., Moutin, T., Grob, C., Gorbunov, M.Y., Zehr, J.P., Masquelier, S.M., Garzarek, L., Claustre, H., 2008. Nutrient limitation of primary productivity in the Southeast Pacific (BIOSOPE cruise). Biogoscience 5, 215–225.
Blumberg, A.F., Mellor, G.L., 1987. A description of a three- dimensional coastal ocean circulation model. In: In: Heaps N. (Ed.), Three-Dimensional Coastal Ocean Models 4 AGU, Washington, D.C., pp. 1–16Coastal Estuarine Series.
Brochier, T., Echevin, V., Tam, J., Chaigneau, A., Goubanova, K., Bertrand, A., 2013. Climate change scenarios experiments predict a future reduction in small pelagic fish recruitment in the Humboldt current system. Glob. Change Biol. 19, 1841–1853.
Bruland, K.W., Rue, E.L., Smith, G.J., DiTullio, G.R., 2005. Iron, macronutrients and diatom blooms in the Peru upwelling regime: brown and blue waters of Peru. Mar. Chem. 93, 81–103.
Castillo, G., Muñoz, H., González, H., Bernal, P., 1991. Daily analysis of abundance and size variability of fish larvae in relation to oceanic water intrusions in coastal areas. Biol. Pesq. 20, 21–35.
Chávez, F.P., Ryan, J., Lluch-Cota, S.E., Ñiquen, M., 2003. From Anchovies to sardines and back: multidecadal change in the Pacific Ocean. Science 299 (5604), 217–221.
Chávez, F.P., Messié, M., 2009. A comparison of eastern boundary upwelling ecosystems, Progr. Oceanogr 83 (1–4), 80–96.
Colas, F., McWilliams, J.C., Capet, X., Kurian, J., 2012. Heat balance and eddies in the Peru-Chile current system. Clim. Dyn. 39 (1–2), 509–529.
Correa-Ramirez, M.A., Hormazábal, S., Yuras, G., 2007. Mesoscale eddies and high chlorophyll concentrations of central Chile (29–39°S). Geophys. Res. Lett. 34 (12)https://doi.org/10.1029/2007GL029541.
Correa-Ramirez, M.A., Hormazábal, S., Morales, C.E., 2012. Spatial patterns of annual and interannual surface chlorophyll-a variability in the Peru-Chile current system. Prog. Oceanogr. 92–95, 8–17.
Cubillos, L.A., Ruiz, P., Claramunt, G., Gacitúa, S., Nuñez, S., Castro, L., Riquelme, K., Alarcón, C., Oyarzún, C., Sepúlveda, A., 2007. Spawning, daily egg production, and spawning stock biomass estimationfor common sardine (Strangomera bentincki) and anchovy (Engraulis ringens) off central southern Chile in 2002. Fish. Res. 86, 228–240.
Daneri, G., Dellarossa, V., Quiñones, R., Jacob, B., Montero, P., Ulloa, O., 2000. Primary production and community respiration in the Humboldt Current System off Chile and associated oceanic areas. Mar. Ecol. Progr. Ser. 197, 41–49.
Daneri, G., Lizárraga, L., Montero, P., González, H.E., Tapia, F.J., 2012. Wind forcing and short-term variability of phytoplankton and heterotrophic bacterioplankton in the coastal zone of the Concepción upwelling system (central Chile). Prog. Oceanogr. 92–95, 92–96.
Da Silva A.M. Young C.C. Levitus S. (Eds.), 1994. Atlas of Surface Marine Data 1994, vol. 1. Algorithms and Procedures. NOAA Atlas NESDIS, vol. 6 U. S., NOAA Silver Spring, MD p 83 Technical Report
de Boyer Montégut, C., Madec, G., Fischer, A.S., Lazar, A., Iudicone, D., 2004. Mixed layer depth over the global ocean: an examination of profile data and a profile-based climatology. J. Geophys. Res. 109, C12003. https://doi.org/10.1029/2004JC002378.
Diehl, S., Berger, S., Ptacnik, R., Wild, A., 2002. Phytoplankton, light, and nutrients in a gradient of mixing depths: field experiments. Ecology 83, 399–411.
Echevin, V., Aumont, A., Ledesma, J.M., Flores, G., 2008. The seasonal cycle of surface chlorophyll in the Peruvian upwelling System: a modeling Study. Progress. Oceanogr. 79, 167–176.
Echevin, V., Albert, A., Lévy, A., Graco, M., Aumont, O., Piétri, A., Garric, G., 2014. Intraseasonal variability of nearshore productivity in the Northern Humboldt Current System: the role of coastal trapped waves. Cont. Shelf Res. 73, 14–30.
Eppley, R.W., Peterson, B.J., 1979. Particulate organic matter flux and planktonic new production in the deep ocean. Nature 282, 677–680.
Escribano, R., Schneider, W., 2007. The structure and functioning of the coastal upwelling system off central/southern Chile. Progress. Oceanogr. 75, 343–347.
Falkowski, P.G., Barber, R.T., Smetacek, V., 1998. Biogeochemical controls and feedbacks on ocean primary production. Science 281, 200–206.
Farías, L., Graco, M., Ulloa, O., 2004. Nitrogen cycling in continental shelf sediments of the upwelling ecosystem off central Chile. Deep Sea Res. Part II 51, 2491–2505.
Farías, L., Castro-González, M., Cornejo, M., Charpentier, J., Faúndez, J., Boontanon, N., Yoshida, N., 2009. Denitrification and nitrous oxide cycling within the upper oxycline of the eastern tropical South Pacific oxygen minimum zone. Limnol. Oceanogr. 1 (54), 132–144.
Figueroa, A.D., Moffat, C., 2000. On the influence of topography in the induction of coastal upwelling along the Chilean coast. Geophys. Res. Lett. 27, 3905–3908.
Giraud, X., Le Quéré, C., da Cunha, L.C., 2008. Importance of coastal nutrient supply for global ocean biogeochemistry. Glob. Biogeochem. Cycles 22, GB2025. https://doi.org/10.1029/2006GB002717.
Gomez, F.A., Spitz, Y.H., Batchelder, H.P., Correa-Ramirez, M.A., 2017. Intraseasonal patterns in coastal plankton biomass off central Chile derived from satellite observations and a biochemical model. J. Mar. Syst. https://doi.org/10.1016/j.jmarsys.2017.05.003.
Gordon D.C. Jr, Boudreau P.R., Mann K.H., 1996. LOICZ Biogeochemical Modelling Guidelines. LOICZ Reports & Studies No 5.
Gruber, N., Lachkar, Z., Frenzel, H., Marchesiello, P., Munnich, M., McWilliams, J.C., Nagai, T., Plattner, G.-K., 2011. Eddy-induced reduction of biological production in eastern boundary current system. Nat. Geosci. 4, 787–792.
Grob, C., Quiñones, R.A., Figueroa, D., 2003. Quantification of coast-ocean water transport through filaments and eddies with high chlorophyll-a content, in central-south Chile (35.5–37.5°S). Gayana 67, 55–67.
Hill, A.E., Hickey, B.M., Shillington, F.A., Strub, P.T., Brink, K.H., Barton, E.D., Thomas, A.C., 1998. Eastern Ocean boundaries. In: Robinson, A.R., Brink, K.H. (Eds.), The Sea 11, John Wiley, Hoboken, N. J, pp. 29–67.
Hernández, K., Yannicelli, B., Montecinos, A., Ramos, M., González, H.E., Daneri, G., 2012. Temporal variability of incidental solar radiation and modulating factors in a coastal upwelling area (36°S). Progress. Oceanogr. 92 (1), 18–32.
Hormazábal, S., Shaffer, G., Pizarro, O., 2002. Tropical Pacific control of intraseasonal oscillations off Chile by way of oceanic and atmospheric pathways. Geophys. Res. Lett. 29, 6.
Hutchins, D.A., Bruland, K.W., 1998. Fe-limited diatom growth and Si:N uptake ratios in a coastal upwelling regime. Nature 393, 561–564.
Hutchins, D.A., DiTullio, G.R., Zhang, Y., Bruland, K.W., 1998. An iron limitation mosaic in the California upwelling regime. Limnol. Oceanogr. 43, 1037–1054.
Hutchins, D.A., Hare, C.E., Weaber, R.S., Zhang, Y., Fire, G.F., DiTullio, G.R., Alm, M.B., Riseman, S.F., Maucher, J.M., Geesey, M.D., Trick, C.G., Smith, G.J., Rue, E.L., Conn, J., Bruland, K.W., 2002. Phytoplankton iron limitation in the Humboldt current and Peru upwelling. Limnol. Oceanogr. 47 (4), 997–1011.
Huyer, A., Knoll, M., Paluszkiewicz, T., Smith, R., 1991. The Perú undercurrent: a study in variability. Deep Sea Res. 38, 247–279.
Iriarte, J.L., Vargas, C., Tapia, F.J., Bermúdez, R., Urrutia, R.E., 2012. Primary production and plankton carbon biomass in a river-influenced upwelling area off Concepción, Chile. Progress. Oceanogr. 92 (1), 97–109.
José, Y.S., Aumont, O., Machu, E., Penven, P., Moloney, C.L., Maury, O., 2014. Influence of mesoscale eddies on biological production in the Mozambique Channel: several contrasted examples from a coupled ocean-biogeochemistry model. Deep Sea Res. II 100, 79–93.
Kara, A.B., Rochford, P.A., Hurlburt, H.E., 2003. Mixed layer depth variability over the global ocean. J. Geophys. Res. 108 (C3), 3079. https://doi.org/10.1029/2000JC000736.
Kirk, J.T.O., 1994. Light and Photosynthesis in Aquatic Ecosystems, Second ed. Cambridge University Press, Cambridge, United Kingdom, 509.
Kuypers, M.M.M., Lavik, G., Woebken, D., Schmid, M., Fuchs, B.M., Amman, R., Jorgensen, B.B., Jetten, M.S.M., 2005. Massive nitrogen loss from the Benguela upwelling system through anaerobic ammonium oxidation. PNAS 108, 6478–6483.
Lachkar, Z., Gruber, N., 2011. What controls biological production in coastal upwelling systems? Insights from a comparative modeling study. Biogeosciences 8, 2961–2976.
Landaeta, M.F., Castro, L.R., 2006. Spawning and larval survival of the Chilean hake Merluccius gayi under later summer conditions in the Gulf of Arauco, central Chile. Fish. Res. 77, 115–121.
Large, W.G., MacWilliams, J.C., Doney, S.C., 1994. Oceanic vertical mixing a review and a model with a nonlocal boundary layer parameterization. Rev. Geophys. 32, 363–403.
Leth, O., Shaffer, G., 2001. A numerical study of the seasonal variability in the circulation off central Chile. J. Geophys. Res. 106 (C10), 229–248.
Leth, O., Middleton, J.F., 2004. A mechanism for enhanced upwelling off central Chile: eddy advection. J. Geophys. Res. 109 (C12020), 1–17.
Lorbacher, K., Dommenget, D., Niiler, P.P., Kohl, A., 2006. Ocean mixed layer depth: a subsurface proxy of ocean-atmosphere variability. J. Geophys. Res. 111, C07010. https://doi.org/10.1029/2003JC002157.
Marín, V., Delgado, L., Escribano, R., 2003. Upwelling shadows at Mejillones Bay (northern Chilean coast): a remote sensing in situ analysis. Invest. Mar. Valparaíso 31 (2), 47–55.
Mason, E., Molemaker, J., Shchepetkin, A.F., Colas, F., McWilliams, J.C., Sangrà, P., 2010. Procedures for offline grid nesting in regional ocean models. Ocean Model. 35, 1–15.
Messié, M., Chávez, F., 2015. Seasonal regulation of primary production in eastern boundary upwelling systems. Prog. Oceanogr. 134, 1–18.
Montero, P., Daneri, G., Cuevas, A., González, H., Jacob, J., Lizárraga, L., Menschel, E., 2007. Productivity cycles in the upwelling area off concepción: the importance of diatoms and bacterioplankton in the organic carbon flux. Prog. Oceanogr. 75, 518–530.
Moore, J.K., Doney, S.C., Lindsay, K., 2004. Upper ocean ecosystem dynamics and iron cycling in a global three-dimensional model. Glob. Biogeochem. Cy. 18, GB4028. https://doi.org/10.1029/2004GB002220.
Moore, C.M., Mills, M.M., Arrigo, K.R., Berman-Frank, I., Bopp, L., Boyd, P.W., Galbraith, E.D., Geider, R.J., Guieu, C., Jaccard, S.L., Jickells, T.D., La Roche, J., Lenton, M., Mahowald, N.M., Marañón, E., Marinov, I., Moore, J.K., Nakatsuka, T., Oschlies, A., Saito, M.A., Thingstad, T.F., Tsuda, A., Ulloa, O., 2013. Processes and patterns of oceanic nutrient limitation. Nat. Geosci. 6, 701–710.
Morales, C.E., Hormazábal, S., Correa-Ramírez, M., Pizarro, O., Silva, N., Fernández, C., Anabalón, V., Torreblanca, M.L., 2012. Mesoscale variability and nutrient–phytoplankton distributions off central-southern Chile during the upwelling season: the influence of mesoscale eddies. Prog. Oceanogr. 104, 17–29.
Morales, C.E., Hormazábal, S., Andrade, I., Correa-Ramírez, M., 2013. Time-space variability of chlorophyll-a and associated physical variables within the region off central-Southern Chile. Remote Sens. 5, 5550–5571.
Nicklisch, A., Shatwell, T., Kohler, J., 2008. Analysis and modelling of the interactive effects of temperature and light on phytoplankton growth and relevance for the spring bloom. J. Plankton Res. 30 (1), 75–91.
Pantoja, S., Sepulveda, J., Gonzalez, H.E., 2004. Decomposition of sinking proteinaceous material during fall in oxygen minimum zone off northern Chile. Deep-Sea Res. I 51, 55–70.
Penven, P., Debreu, L., Marchesiello, P., McWilliams, J.C., 2006. Evaluation and application of the ROMS 1-way embedding procedure to the central california upwelling system. Ocean Model. 12, 157–187.

Peterson, D.H., Perry, M.J., Bencala, K.E., Talbot, M.C., 1987. Phytoplankton productivity in relation to Light Intensity: a simple equation. Estuar. Coast. Shelf Sci. 24, 813–832.
Pickard, G.L., Emery, W.J., 1990. Descriptive Physical Oceanography. Pergamon, Tarrytown, N.Y, 320.
Quiñones, R.A., Gutiérrez, M.H., Daneri, G., Gutiérrez, D.A., González, H.E., Chávez, F., 2010. Pelagic carbon fluxes in the Humboldt Current System. In: Liu, K.K., Atkinson, L., Quiñones, R.A., Talaue-McManus, L. (Eds.), Carbon and Nutrient Fluxes in Global Continental Margins: a Global Synthesis. Springer-Verlag, New York, NY, pp. 44–64.
Resplandy, L., Lévy, M., Madec, G., Pous, S., Aumont, O., Kumar, D., 2011. Contribution of mesoscale processes to nutrient budgets in the Arabian Sea. J. Geophys. Res. 116, C11007. https://doi.org/10.1029/2011JC007006.
Ridgway, K.R., Dunn, J.R., Wilkin, J.L., 2002. Ocean interpolation by four-dimensional least squares applications to the waters around Australia. J. Atmos. Ocean Technol. 19 (9), 1357–1375.
Salamanca, M., Pantoja, S., 2009. Caracterización química de la zona marina adyacente a la desembocadura del río Itata. La Cuenca del Río Itata: La cuenca hidrográfica del Itata: Aportes científicos para su gestión sustentable, pp. 177-191. Parra, O. Castilla J.C., Quiñones, H.R.A., Camaño, A (Eds.). Ediciones Universidad de Concepción, Concepción, Chile. 389 pp.
Silva, N., Neshyba, S., 1979. On the southernmost extension of the Perú-Chile Undercurrent. Deep Sea Res. 26, 1387–1393.
Sobarzo, M., Figueroa, D., Djurfeldt, L., 2001. Upwelling of subsurface water into the rim of the Biobío submarine canyon as a response to surface wind. Cont. Shelf Res. 21, 279–299.
Sobarzo, M., Saldías, G.S., Tapia, F.J., Bravo, L., Moffat, C., Largier, J.L., 2016. On subsurface cooling associated with the Biobío river Canyon (Chile). J. Geophys. Res. Oceans 121, 4568–4584.
Sobarzo, M., Bravo, L., Donoso, D., Garcés-Vargas, J., Schneider, W., 2007. Coastal upwelling and seasonal cycles that influences the water column over the continental shelf of central Chile. Progr. Oceanogr. 75, 363–382.
Strub, P.T., Mesías, J., Montecino, V., Ruttlant, J., Salinas, S., 1998. Coastal ocean circulation off Western South America. Coastal Segment (6, E). In: Robinson, A., Brink, K. (Eds.), The Sea 11, John Wiley & Sons, Hoboken, pp. 273–313.
Strub, P.T., Mesías, M., James, C., 1995. Altimeter observations of the Perú-Chile Countercurrent. Geophys. Res. Lett. 22, 211–214.
Silva, N., Rojas, N., Fedele, A., 2009. Water masses in the Humboldt Current System: properties, distribution, and the nitrate deficit as a chemical water mass tracer for equatorial subsurface water off Chile. Deep-Sea Res. Ii. 56, 1004–1020.
Schepetkin, A., McWilliams, J.C., 2005. The regional oceanic modeling system (ROMS): a split-explicit, free-surface, topography-following- coordinate oceanic model. Ocean Model. 9, 347–404.
Sverdrup, H.U., 1953. On conditions for the vernal blooming of phytoplankton. J. Cons. Int. Explor. Mer. 18, 287–295.
Tegen, I., Fung, I., 1995. Contribution to the atmospheric mineral aerosol load from land surface modification. J. Geophys. Res. 100 (D9), 18707–18726. https://doi.org/10.1029/95JD02051.
Thomas, M.K., Kremer, C.T., Klausmeier, C.A., Litchamn, E., 2012. A global pattern of thermal adaptation in marine phytoplankton. Science 338 (6110), 1085–1088. https://doi.org/10.1126/science.1224836.
Valle-Levinson, A., Atkinson, L.P., Figueroa, D., Castro, L., 2003. Flow induced by upwelling winds in an equatorward facing bay: gulf of Arauco, Chile. J. Geophys. Res. 108 (3054)https://doi.org/10.1029/2001JC001272, (C2).
Vargas, C., Contreras, P.Y., Iriarte, J.L., 2012. Relative importance of phototrophic, heterotrophic, and mixotrophic nanoflagellates in the microbial food web of a river-influenced coastal upwelling area. Aquat. Microb. Ecol. 65, 233–248.
Vergara, O.A., Echevín, V., Sepúlveda, H.H., Colas, F., 2016. Modelling the seasonal dynamics of the Peru-Chile Undercurrent off Central Chile (30–40°S). Cont. Shelf. Res. 123, 61–79.
Wijesekera, R.W., Gregg, M.C., 1996. Surface layer response to weak winds, westerly bursts, and rain squalls in the western Pacific warm pool. J. Geophys. Res. 101, 977–997.
10. J.P. Zehr, B.B. Ward, Nitrogen cycling in the Ocean: new perspectives on processes and paradigms, Appl. Environ. Microbiol. 68 (3) (2002) 1015–1024.

5. DISCUSIÓN

La zona sur del Sistema de Corrientes de Humboldt (SCH), definida en esta Tesis como un área que abarca desde 30º a 40ºS y entre 70º y 80ºW, ha sido ampliamente estudiada en sus dimensiones espaciales y temporales, profundizando en la investigación de procesos físicos, biológicos, geológicos y biogeoquímicos (ej. Levipan et al., 200; Sánchez et al., 2012; Farías et al., 2015; Sobarzo et al., 2016; Escribano et al., 2016; Cornejo et al., 2016; Schneider et al., 2017) e incluyendo entre estos, el análisis de series de tiempo (estación 18; Sobarzo et al., 2007; Escribano et al., 2012; Anabalón et al., 2016) la variabilidad interanual y espacial de procesos de mesoescala (Leth y Middleton., 2004; Correa-Ramírez et al., 2012; Hormazábal et al., 2013; Morales et al., 2013), la variabilidad interanual impuesta por el ciclo ENOS (Montecinos y Gómez, 2010; Gómez et al., 2012) y la influencia de procesos remotos en la plataforma costera del SCH centro-sur de Chile (Shaffer et al., 1997; Hormazábal et al., 2002; Pizarro et al., 2002; Middleton y Leth, 2004), entre otros. Integrar la información y las interacciones que ocurren a todo nivel, ha sido un reto permanente para los investigadores.

Entre los factores más importantes, destaca la surgencia, la cual ha sido ampliamente descrita como uno de los principales promotores de las altas tasas de producción primaria (Daneri et al., 2000; Montero et al., 2007) en el SCH. Esta alta productividad es producto, entre otros factores, del transporte a la zona fótica de Agua Ecuatorial Subsuperficial (AESS), una masa de agua caracterizada por presentar altas concentraciones de nutrientes (20–40 µM nitrato, 2.6–3 µM fosfato; 25–40 µM silicato), baja temperatura (8.5–10.5°C), baja concentración de oxígeno (4.4–44.6 µM, 2–15% saturación) y alta salinidad (34.4–34.9) (Silva et al., 2009). La AESS es transportada hacia el polo por la Corriente Subsuperficial Chile-Perú (PCUC) la cual se origina en las costas de Perú, cerca de 5°S, y fluye hasta el Golfo de Penas (48°S, Wooster y Gilmartin, 1961; Wooster y Reid, 1963; Silva y Neshyba, 1979). La variabilidad estacional del transporte de la AESS por la PCUC, junto con la descarga de los ríos presentes en la zona (ej. Biobío e Itata; Salamanca y Pantoja, 2009; Iriarte et al., 2012; Vargas et al., 2012), son factores que influyen directamente en la distribución espacio/temporal de los nutrientes en la plataforma continental. Sumado a lo anterior, dinámicas de transporte horizontal y vertical, junto con la mezcla vertical, también generan variabilidad en la distribución de nutrientes de la columna de agua (Echevin et al., 2008). Los procesos de advección, la variabilidad estacional del AESS y la descarga de los ríos, pueden inducir limitación de nutrientes

para el crecimiento del fitoplancton, el cual también se encuentra condicionado a la variabilidad estacional de la luz en la zona centro-sur de Chile (Montero et al., 2007; Daneri et al., 2012). Adicionalmente, limitación paralela o colimitación de nutrientes puede presentarse en aguas superficiales de zonas costeras las cuales al ser altamente dinámicas, son particularmente propensas a la escasez simultánea de muchos nutrientes (Saito et al., 2008). Colimitación ocurre por lo tanto, cuando dos (o más) nutrientes han sido removidos simultáneamente a niveles en los cuales, la adición de uno o de todos es requerida para estimular el crecimiento del fitoplancton (Moore et al., 2013). Concentraciones absolutas de nutrientes en la superficie del océano, o sus relaciones estequiométricas, pueden indicar el potencial de limitación existente para el crecimiento del fitoplancton en el área a estudiar (Saito et al., 2008).

Esta Tesis se ha focalizado en los tres tópicos detallados anteriormente, los cuales están íntimamente relacionados. En el Capítulo 1 se analiza la evolución temporal de la surgencia y el hundimiento en un periodo de 25 años, en el Capítulo 2 se investiga la variabilidad estacional e interanual de la PCUC y su transporte hacia el polo y en el Capítulo 3, se estudia la dinámica de advección y mezcla de nutrientes potencialmente limitantes para el crecimiento del fitoplancton.

5.1. Evolución temporal de la surgencia/hundimiento en la zona centro-sur de Chile y su posible efecto en la productividad biológica

Los resultados de esta Tesis revelaron que los eventos favorables a surgencia decrecieron en intensidad y duración durante el periodo analizado, detectándose a través de la variabilidad interanual de la intensidad y la duración promedio, una disminución de ~ $4Nm^{-2}$ día con ~8 días de duración a ~ $2Nm^{-2}$ día con ~6 días de duración los últimos años. Es posible observar estos cambios claramente a partir de 1998. A pesar de esto, la frecuencia en el número de eventos parece aumentar a partir de ese mismo año, sobre todo durante los meses de otoño-invierno. Por lo tanto, podemos decir que los eventos favorables a surgencia han disminuido en duración e intensidad, pero su frecuencia ha aumentado.

Cushman-Roisin (1994) ha construido un índice a partir de la magnitud y duración del estrés del viento favorable a surgencia denominado impulso del viento (“wind impulse”). El impulso del viento conduce a que la interfase de densidad alcance o no alcance la superficie del océano, dando lugar a una surgencia parcial o completa (Csanady, 1977). Surgencia completa, implica la formación de un frente de densidad superficial, el cual es

una zona frontal estrecha donde ocurren rápidos cambios de densidad, esto también ha sido denominado frente de surgencia (Brink, 1987). Cushman-Roisin (1994) utilizando el radio de deformación interna (R) y otros parámetros, determinó la duración y la distancia final de un frente de surgencia. El autor establece, que eventos de surgencia con una duración de 10-12 días, podrían movilizar el frente de densidad a una distancia de 5 km de la costa. Basado en esto último y en que los resultados de la presente investigación muestran que la intensidad y duración de los eventos favorables a surgencia han disminuido durante los últimos años analizados a ~ $2Nm^{-2}$ día y ~6 días, respectivamente, el frente de densidad o frente de surgencia se extendería solamente hasta ~3 km. Sin embargo, aunque estos resultados indiquen que el frente alcanzaría menos distancia que aquellos eventos más intensos y más largos presentes al inicio de la serie (~ $4Nm^{-2}$ día y ~8 días, ~4 km frente de densidad) el aumento en la frecuencia de los eventos favorables a surgencia observado en el periodo total, podrían compensar la disminución en la duración y distancia alcanzada.

La disminución en la intensidad y duración de los eventos favorables a surgencia en el SCH, puede alterar significativamente factores físicos y biogeoquímicos involucrados en producir las altas tasas de productividad primaria reportadas (Montero et al., 2007; Daneri et al., 2012). Si los eventos favorables a surgencia son menos intensos y más cortos, la cantidad de agua que arriba junto con la masa de Agua Ecuatorial Subsuperficial (AESS) rica en nutrientes hacia aguas superficiales podría verse afectada. Los resultados reportados en el Capítulo 2 de esta Tesis muestran que 20% y 14% de los flotadores virtuales lagrangianos liberados (representan a la AESS) en 33º y 37ºS en la Corriente Subsuperficial Chile-Perú (PCUC), alcanzan la superficie (Vergara et al., 2016); en consecuencia, la disminución en la intensidad de los eventos favorables a surgencia podría disminuir de manera importante el suministro de nutrientes a la zona costera afectando a la productividad biológica del sistema.

Numerosas son las investigaciones que indican cambios en los vientos favorables a surgencia las últimas décadas (ej. Sydeman et al. 2014; Varela et al., 2015). Al contrario de lo encontrado en esta Tesis, algunas de estas destacan que en zonas de borde oriental (como el SCH) el calentamiento global forzaría la intensificación de vientos favorables a surgencia durante las estaciones cálidas (primavera-verano), como consecuencia de un incremento en los gradientes de presión tierra-océano (Bakun, 1990). Otros autores han reportado que producto de una intensificación del APS y un desplazamiento hacia el sur de su núcleo (Falvey y Garreaud, 2009; Goubanova et al., 2011; Belmadani et al., 2014;

Schneider et al., 2017), los vientos costeros favorables a surgencia, se intensificarán a lo largo de las costas chilenas (Garreaud y Falvey, 2008). Si bien, las recientes inclinaciones en torno al estudio del viento en zonas de alta productividad apoyan la hipótesis del aumento de la surgencia, esta sigue siendo una postura controvertida. Investigaciones realizadas en diferentes SSBO, han presentado resultados contradictorios, los cuales indican que las estimaciones de viento desde diferentes bases de datos, pueden diferir en tendencia y variabilidad (Sydeman et al., 2014). Adicionalmente, las series de tiempo disponibles actualmente son limitadas en cuanto a su duración, calidad y extensión espacial, además, los resultados obtenidos de diferentes productos de datos en la misma área pueden variar debido a que son altamente dependientes de la longitud de la serie temporal (Varela et al., 2015).

Es necesario por lo tanto, contrastar los resultados de intensidad (Nm^{-2} día), duración y número de eventos favorables a surgencia y hudimiento obtenidos en el primer Capítulo de esta Tesis con datos satelitales de viento provenientes de productos atmosféricos de re-análisis, los cuales han sido utilizados por otros autores en la zona de estudio (Astudillo et al., 2017) y compararlos también, con otras estaciones meteorológicas a lo largo del SCH en el mismo periodo que este estudio.

En consecuencia, en base a los resultados del Capítulo 1, se rechaza la **Hipótesis 2,** la cual planteaba que la intensidad de los eventos favorables a surgencia ha aumentado durante el periodo 1988-2013.

Aunque en la zona de estudio se ha reportado que los eventos favorables a surgencia prevalecen la mayor parte del año (ej. Shaffer et al., 1997; Rutllant y Montecino, 2002; Ranh y Garreaud, 2013), los resultados de esta Tesis demuestran que el número de eventos favorables a hundimiento presentó un porcentaje no despreciable en el periodo de tiempo total analizado. El porcentaje del número de eventos favorables a surgencia y favorables a hundimiento respecto al total fue de 63% y 37%, respectivamente. Si bien, el porcentaje de número de eventos favorables a hundimiento no es bajo, el número de eventos favorables a surgencia sigue predominando en la zona de estudio.

La variabilidad interanual de la intensidad de los eventos favorables a hundimiento, reveló que esta disminuyó levemente durante el periodo analizado, desde ~ $5Nm^{-2}$ día a ~ 4 Nm^{-2} día en 2012. A pesar de esto, la correlación entre intensidad versus años analizados no fue significativa ($p>0.05$). Respecto a la duración y frecuencia de eventos favorables a hundimiento, se observó que estos no presentaron ninguna tendencia aparente ($p>0.05$), permaneciendo en ~3 eventos promedio anuales, con una duración promedio anual de ~2

días. Por lo tanto, a diferencia de los eventos favorables a surgencia, los eventos favorables a hundimiento disminuyeron levemente su intensidad en el periodo de tiempo analizado, pero su frecuencia y duración, no se vio alterada. Probablemente las condiciones o umbrales que se utilizaron en estos análisis influenciaron estos resultados, ya que se observó que la mayoría de los eventos favorables a hundimiento de alta intensidad, se producen en escalas menores a 24 horas. Para efectos de esta Tesis, se trabajó con eventos mayores a 1 día, e incluso mayores a 3 días, lo cual corresponde a escalas de tiempo en las cuales se produce alguna respuesta en el ecosistema, como ha sido reportado en el caso de la surgencia (Dugdale et al., 1990; Botsford et al., 2006; García-Reyes and Largier, 2010).

En otros sistemas de borde oriental, como el Sistema de la Corriente de California, se ha reportado que fases cálidas del El Niño Oscilación Sur, estarían asociadas con un inicio tardío de la temporada de surgencia y con una mayor intensidad del hundimiento (Bograd et al., 2009; Bylhouwer et al., 2013). Otros autores han encontrado que la variación espacial de la surgencia/hundimiento presenta tres señales dominantes de baja frecuencia en el rango de 33, 19 y 11 años, las cuales se asemejan a la periodicidad de la circulación atmosférica, del ciclo nodal lunar y de los ciclos de actividad solar (Saldívar-Lucio et al., 2016). En esta Tesis no se analizan escalas de baja frecuencia, pero la evidencia señala que debieran ser consideradas en futuras investigaciones.

Para observar las diferencias entre los eventos favorables a surgencia durante otoño-invierno versus los eventos favorables a surgencia presentes en primavera-verano, se determinó la relación entre la intensidad y el largo del evento para el total de la serie de tiempo (1988-2013). Se estableció que la correlación para ambos periodos fue similar (rho=0.81, $p<0.05$, otoño-invierno; rho=0.89, $p<0.05$, primavera-verano). El número total de eventos favorables a surgencia en otoño-invierno fue de 754 y de 767 en primavera-verano. A pesar de la similitud de estos valores, la intensidad máxima en otoño-invierno fue mucho menor que la presente en primavera-verano con ~10 Nm^{-2} día y ~25 Nm^{-2} día, respectivamente. Aunque que la intensidad en otoño-invierno no es tan alta, se ha observado que los eventos favorables a surgencia en esta época, han aumentado su frecuencia sobre todo a partir del año 1998, época en la cual se reportó uno de los eventos El Niño más intensos del siglo XX (Niño 1997-1998; Montecinos y Gómez, 2010).

En otros SSBOs, autores como Varela et al. (2010) han estudiado las respuestas biogeoquímicas y el acoplamiento bento-pelágico durante surgencia invernal, resaltando que los eventos favorables a surgencia en esta época se han vuelto recurrentes a lo largo

de la plataforma Ibérica Occidental (Álvarez et al., 2003). Estos autores reportaron la presencia de afloramientos fitoplanctónicos durante el período otoño-invierno como consecuencia de un aumento en la radiación solar, la cual coincidió con la presencia de vientos favorables de surgencia, los cuales promovieron además del ingreso de nutrientes y propiciaron la mezcla en la columna de agua. Schroeder et al. (2009) plantean que la surgencia (temprana) de invierno, incluso cuando presenta una débil magnitud o corta duración, fertiliza a la región costera central de la Corriente de California con suficientes nutrientes para asegurar una alta productividad y disponibilidad de presas que mantengan a una población reproductora de aves marinas adulta más sana, impulsando incluso, el inicio temprano de la temporada de cría. Black et al. (2011) determinaron la existencia de dos modos en la Corriente de California, uno para las condiciones de surgencia invernal y otro para la surgencia de verano. El primer modo (surgencia invernal) se caracterizó por la variabilidad de alta frecuencia asociada con el Pacífico Norte y eventos El Niño, y el segundo modo (surgencia estival) se asoció a procesos de baja frecuencia (multidecadal). La diferenciación entre estos dos conjuntos de condiciones podría ser relevante no sólo en las escalas de tiempo interanuales, sino también en relación con las tendencias a largo plazo asociadas al cambio climático global.

De acuerdo con lo encontrado en esta Tesis y lo planteado para otros SSBO, se han observado cambios en la frecuencia de los eventos favorables a surgencia en la época otoño-invierno. Si estos eventos se vuelven más frecuentes (aumentando la mezcla de la columna de agua) y si las condiciones ambientales lo permiten (aumento de luz PAR), la surgencia invernal podría generar cambios importantes en el ecosistema de la zona centro-sur de Chile. Por ejemplo, el inicio de temporada de surgencia podría adelantarse, la cual para esta área se ha establecido que comienza en septiembre o que simplemente se desarrollen grandes afloramientos fitoplanctónicos, ya que además en esta época aumenta la descarga de los ríos y nutrientes alóctonos al sistema (Salamanca y Pantoja, 2009).

A pesar que la frecuencia en el número de eventos favorables a surgencia durante otoño-invierno ha aumentado, estos eventos son mucho menos intensos que los encontrados en la época estival. Por lo tanto, se rechaza la **Hipótesis 1**, la cual planteaba que frecuencia e intensidad de vientos favorables a surgencia en la zona costera frente a Concepción (36°S) durante otoño-invierno, puede generar eventos favorables a surgencia de gran magnitud, comparables a los que se presentan en la época estival.

Para observar las diferencias entre los típicos eventos favorables a hundimiento durante otoño-invierno versus los eventos favorables a hundimiento en primavera-verano, se

determinó la relación entre la intensidad y el largo del evento para el total de la serie (1988-2013). Se estableció que la correlación para ambos periodos fue similar (rho=0.71, $p<0.05$, otoño-invierno; rho=0.64, $p<0.05$, primavera-verano). El número total de eventos favorables a hundimiento en otoño-invierno fue 523 y en primavera-verano 352. La intensidad máxima en otoño-invierno fue mayor que la presente en primavera-verano con >25 Nm^{-2} día y ~10 Nm^{-2} día, respectivamente. A pesar que la intensidad y duración de los eventos favorables a hundimiento presentes en la época estival son bajos comparados a la época invernal, se ha comprobado que la frecuencia del número de eventos en primavera-verano ha aumentado levemente a partir del año 1998, lo cual coincide con lo reportado para eventos favorables a surgencia. Futuras investigaciones deberían profundizar entre la relación del hundimiento versus eventos El Niño para la zona centro sur de Chile, ya que como se señaló con antelación, en 1998 se registró uno de los eventos Niño más fuertes reportados para SCH (1997-1998, Montecino y Gómez, 2010; Gómez et al., 2012).

Los resultados obtenidos en la presente investigación permiten rechazar la **Hipótesis 3** planteada en el Capítulo 1, la cual señala que durante primavera-verano en la zona costera frente a Concepción (36°S), la frecuencia de eventos favorables a hundimiento, puede ser tan importante como en la época invernal. Si bien estos eventos han aumentado en la época estival, nuestros resultados demuestran que su frecuencia no es tan alta como la exhibida durante otoño-invierno.

5.2. Variabilidad estacional de la Corriente Subsuperficial Chile-Perú (PCUC)

Las corrientes subsuperficiales hacia el polo como la PCUC, son frecuentes en todos los SSBO (Fonseca, 1989; Neshyba et al., 1989; Hill et al., 1998) presentándose en latitudes medias y opuestas al flujo superficial que se dirige hacia el ecuador (Pierce et al., 2000). Estas corrientes subsuperficiales usualmente alcanzan velocidades a lo largo de la costa de 0.05 a 0.2 m/s, distribuyéndose entre 150 y 300 metros de profundidad (Hickey, 1979; Gay y Chereskin, 2009; Thomson and Krassovski, 2010).

El transporte y la velocidad de la PCUC estimada en esta investigación, fueron similares a los reportados en otros estudios de modelación realizados en la misma zona de estudio (Aguirre et al., 2012). El máximo transporte detectado en las simulaciones realizadas en esta Tesis fue 0.94 Sv en 30ºS durante primavera, valor cercano a lo encontrado por otros autores a través de mediciones *in situ* en la misma latitud (1 Sv; Shaffer et al., 1997, 1999; Pizarro et al. 2002). Otro aspecto importante observado en la simulación realizada, son

los cambios latitudinales que experimenta la PCUC, tanto en su ancho (kilómetros), como en la profundización de su núcleo de mayor velocidad. Los resultados revelaron que en 30ºS se localizó la máxima velocidad latitudinal, la cual se presentó a 120 m de profundidad. En 33ºS este núcleo se observó a 218 m de profundidad, en 36ºS a 230 m y en 39ºS, alcanzó la mayor profundidad, la cual fue 260 metros. Estos resultados son coherentes a lo reportado por Leth et al. (2004), quienes también encontraron diferencias en la localización del núcleo de máxima velocidad de esta corriente a lo largo de la costa, reportando que en 28ºS la mayor velocidad se observó en 163 m, en 35ºS a 190 m y en 43ºS, la máxima velocidad se detectó en 253 m de profundidad.

La PCUC simulada, presentó cambios estacionales notorios en su transporte. En 30ºS fue 0.94 Sv durante primavera, en 33ºS el máximo valor fue 0.9 Sv durante verano, en 36ºS el más alto se presentó durante verano con 0.71 Sv y durante otoño en 39ºS se observó el máximo valor (0.48 Sv). En esta última latitud durante invierno y principios de primavera, los más bajos transportes de la PCUC, coinciden con los más bajos valores de estrés del viento. Adicionalmente, el rotor del estrés del viento entre 37º y 40ºS registró los máximos valores entre mayo y octubre, es decir durante invierno y primavera. Por lo tanto, la disminución de la intensidad de la PCUC hacia el polo, podría ser generada en parte, por la disminución del estrés del viento y el aumento del rotor del estrés del viento hacia el sur. Para determinar el vínculo entre la PCUC y el forzamiento del viento, se calcularon el transporte meridional de la corriente y el transporte de Sverdrup (1947) a partir del rotor del estrés del viento (datos SCOW). Estos cálculos se realizaron en dos bandas, de 50 km y 100 km cada una. En 30º y 36ºS, el transporte promedio de Sverdrup calculado en la banda de 50 km coincide con el transporte modelado. Los resultados sugieren que el flujo promedio de la PCUC puede ser en parte explicado por la teoría del forzamiento de Sverdrup en algunos sectores a lo largo de la costa de Chile centro-sur, pero no en toda el área de estudio. La dinámica del impacto del rotor del viento ha sido observada en otros SSBOs. Pedlosky (1974), a través de un análisis teórico, sugiere que una corriente subsuperficial en dirección al polo a lo largo de un borde oriental, se beneficiaría de un rotor del estrés del viento positivo (Hemisferio Norte). Marchesiello et al. (2003) reportaron que simulaciones regionales (ROMS) y el transporte de Sverdrup a partir del rotor del estrés del viento, fueron consistentes en el Sistema de Corrientes de California. Albert et al. (2010) mostraron que un fuerte rotor del estrés del viento favorable a surgencia en el SCH frente a Perú, indujo el arribo de la corriente

subsuperficial a la costa y genera una amplia zona costera productiva a través de la surgencia de aguas ricas en nutrientes.

La PCUC por lo tanto, es altamente influenciada por el forzamiento del viento. Los mayores transportes de esta corriente, coinciden con las épocas en las cuales se detecta la mayor intensidad de vientos favorables a surgencia, es decir, primavera y verano. Junto con esto, la disminución latitudinal del transporte concuerda con la disminución del viento hacia el sur del área de estudio. Alta intensidad del viento favorable a surgencia en la época estival, induce a que la PCUC alcance las mayores velocidades y transporte. En épocas de vientos debiles favorable a surgencia, es decir principalmente durante inverno, esta corriente adquiere bajas velocidades y bajo transporte. Así también lo reportaron Blanco et al. (2001), los cuales encontraron que esta corriente se fortalece en verano y se debilita en invierno. Fonseca (1992), destaca además, que durante verano la PCUC se localiza cerca de la costa ocupando una extensa área, contrario a lo que se observa durante invierno. Por lo tanto, si la intensidad de los vientos favorables a surgencia disminuye, tal como se muestra en el Capítulo 1, la velocidad y el transporte de esta corriente pueden verse muy afectados, debilitándose en su desplazamiento hacia el polo y afectando el arribo de la masa de AESS a la plataforma costera de la zona centro-sur de Chile.

La PCUC transporta a la AESS a lo largo de la plataforma continental del SCH (Silva and Fonseca, 1983; Strub et al., 1998), masa de agua que arriba a las costas a través de la surgencia y es responsable de las bajas concentraciones de oxígeno (Fuenzalida et al., 2009; Ulloa and Pantoja, 2009; Hernández-Miranda et al., 2010, 2017) y de las altas concentraciones de nutrientes que favorecen a la productividad primaria en la zona centro sur de Chile (promedio anual de 10–20 g Cm^{-2} $día^{-1}$, Daneri et al., 2000; Montero et al., 2007). Para determinar las trayectorias de las partículas transportadas por la PCUC y el tiempo necesario para que suban a la superficie (hasta 50 m), se liberaron flotadores virtuales en la corriente a 33° y 37° S. La mayoría de los flotadores que se desplazaron hacia el polo a lo largo de la PCUC, arribaron a superficie al sur de ambas secciones de liberación. Los porcentajes más altos de flotadores que fueron trasladados a superficie se registraron en latitudes cercanas al área de liberación. Por ejemplo, el 40% de los flotadores liberados en 33°S arribaron entre 33° y 34°S y tardaron en promedio 50 días en alcanzar 50 metros de profundidad. Del mismo modo, más del 50% de los flotadores liberados en 37°S ascendieron entre 37° y 38ºS y demoraron ~56 días en hacerlo. Sin embargo, un porcentaje significativo de flotadores cambió de dirección y terminó al norte de las secciones de liberación. Probablemente fueron transportados hacia el norte a través

de corrientes superficiales inducidas por el viento, o fueron atrapadas y transportadas por corrientes asociadas a remolinos inter-termoclina. Algunos autores han descrito la presencia de remolinos intratermoclina en el SCH (Leth y Middleton, 2004; Hormazábal et al., 2013), generados por inestabilidades baroclínicas alrededor de 37°S (Punta Lavapie). Estos remolinos, que transportan nutrientes y bajas concentraciones de oxígeno, características típicas de la AESS, también pueden transportar partículas hacia el norte, haciendo bastante complejo determinar el origen de las partículas que alcanzan la superficie durante la surgencia. Además, el porcentaje de partículas que efectivamente alcanzaron la superficie a través de la surgencia no superó el 20%. Sin embargo, no se detectaron grandes diferencias estacionales en el porcentaje promedio de partículas que arribaron a superficie, sobre todo en 33ºS, cuyos valores se sitúan alrededor de 20%. En 36ºS se observaron mayores diferencias; por ejemplo, en otoño el porcentaje fue 13.9% y en verano de 16%. El viento climatológico utilizado en el forzamiento de esta simulación, el cual no representa las frecuencias diarias y sinópticas que se han descrito como los principales componentes del estrés del viento a lo largo de la costa del centro-sur de Chile (Sobarzo et al., 2007, 2010), probablemente influyeron en estos resultados. Diferencias estacionales, mensuales y sinópticas del estrés del viento favorable a surgencia, también fueron detectadas en esta Tesis, como se ha descrito en el Capítulo1. Un próximo desafío será realizar simulaciones forzadas con viento diario y comprobar si efectivamente, ese es un factor clave en inducir tan bajas diferencias estacionales en el porcentaje de flotadores trasladados por la PCUC.

Respecto a los resultados obtenidos en el capítulo 2, se acepta la **Hipótesis 4**, la cual plantea que la corriente subsuperficial Chile-Perú (PCUC) disminuye su velocidad y transporte latitudinal (Sv) hacia el polo, presentando diferencias estacionales importantes. También se acepta la **Hipótesis 5**, la cual propone que un importante porcentaje de partículas que transporta la PCUC a lo largo de la plataforma centro-sur de Chile, son trasladadas a superficie a través de la surgencia, ya que si bien en promedio entre 20% y 14% de las partículas liberadas llegan a superficie en 33º y 36ºS, respectivamente, se observaron altos porcentajes al sur de las secciones de liberación, 40% en 33ºS y > 50% en 36ºS.

5.3. Dinámica de transporte de nutrientes potencialmente limitantes para el crecimiento del fitoplancton en la zona centro-sur de Chile

La disponibilidad de nutrientes en la zona eufótica depende de varios factores. En el SCH frente a Chile centro-sur, la inyección de nutrientes a la capa de mezcla a través de la surgencia es responsable, entre otros factores, de las altas tasas de producción primaria reportadas en esta zona (Daneri et al. 2000; Montero et al., 2007). Sin embargo, el ingreso de agua dulce proveniente de ríos (Biobío e Itata), suministran importantes cantidades de metales traza y nutrientes (Salamanca y Pantoja, 2009), así como también materia orgánica terrestre (Vargas *et al*., 2012) a la plataforma continental, contribuyendo a realzar la producción biológica de esta zona.

Los resultados observados en el Capítulo 3 de esta Tesis, han permitido reproducir el ciclo anual de los nutrientes nitrato, fosfato y silicato, los cuales presentan sus mayores concentraciones en la época estival, coincidiendo con el periodo en el que aumentan los vientos favorables a surgencia (Sobarzo et al., 2007; ver además resultados del Capítulo 1 de esta Tesis). Estas altas concentraciones de nutrientes, son típicas del AESS (Silva et al., 2009), la cual es transportada por la PCUC a lo largo de la plataforma continental de Perú y Chile (Strub et al., 1998; Vergara et al., 2016). La PCUC y su desplazamiento hacia el polo, se fortalece en primavera-verano y se debilita en invierno, proceso que es altamente influenciado por el estrés del viento y por el rotor del estrés del viento (Albert et al., 2010; Vergara et al., 2016), tal como se ha mostrado en los resultados del Capítulo 2 de esta Tesis.

El fitoplancton está constituido por un gran número de especies que se distribuyen en conjuntos espacial y temporalmente dinámicos. La disponibilidad de mecanismos físicos de transporte (que limitan la dispersión), características biológicas (ej. tasa de crecimiento, tipo funcional, requisitos físicos y químicos particulares) e interacciones bióticas (ej. competencia, depredación) determinan la presencia de distintos subconjuntos de especies. En los sistemas de surgencia, diferentes especies de fitoplancton utilizan una variedad de mecanismos o estrategias funcionales (por ejemplo, mixotrofía), que les permiten aprovechar los múltiples nichos que se generan a partir de las cambiantes condiciones de temperatura, luz, turbulencia y disponibilidad de nutrientes (Lamont et al., 2014; Vidal et al., 2017). Los factores e interacciones que determinan el crecimiento del fitoplancton son complejos, además de las características funcionales de cada especie. Destacan entre estos la profundidad de la capa de mezcla, la surgencia, la luz, la limitación por nutrientes y el transporte de nutrientes. La advección (o transporte) y mezcla de

nutrientes, son procesos físicos que explican en parte la variabilidad de la clorofila en la zona costera (Williams y Follow, 2011). Los movimientos verticales (advección vertical) juegan un rol clave en el intercambio de calor y propiedades biogeoquímicas entre la superficie y el océano profundo. En sistemas de surgencia, en áreas de frentes costeros y en remolinos de mesoescala, la velocidad vertical es fundamental y puede contribuir de manera relevante, al suministro de nutrientes en la zona eufótica (Mahadevan, 2014). En remolinos de mesoescala, tanto la advección horizontal como la vertical inducida por bombeo de Ekman y bombeo de remolinos (Klein and Lapeyre, 2009; Siegel et al., 2011; Chelton et al., 2011) determinan, entre otros factores, la distribución de la clorofila.

Al igual que con los nutrientes, la simulación ROMS/PISCES desarrollada en esta Tesis, ha permitido reproducir el ciclo anual de la clorofila, exhibiendo altas concentraciones los primeros 20 metros de la columna de agua durante primavera-verano. El incremento de los nutrientes en la capa eufótica debido a la surgencia y el arribo de la AESS, junto con el aumento de la intensidad de la radiación solar en la época estival, constituyen los principales factores que desencadenan afloramientos fitoplanctónicos en la costa de la zona centro-sur de Chile (Montero et al., 2007). La señal anual de clorofila cerca de la costa (<200 km) en esta zona, es gobernada principalmente por el estrés del viento y por corrientes asociadas a ondas de Rossby que se propagan hacia el oeste (Correa-Ramírez et al., 2012).

La co-limitación de nutrientes y luz para el crecimiento del fitoplancton, el cual es el principal responsable de la alta concentración de clorofila en el SCH (González et al., 2007; Montero et al., 2007; Morales y Anabalón, 2012), fue analizada solo para las diatomeas, ya que fueron el grupo dominante en la simulación (~70 %).

Como es de esperar, de acuerdo al ciclo anual de la radiación solar (Sobarzo et al., 2007; Rain et al., 2014) en otoño e invierno, la limitación por luz se extendió desde la región costera (<100 km) hasta ~200 km fuera de la costa. Los principales nutrientes potencialmente limitantes fueron silicato, Fe, nitrato y ocasionalmente fosfato. Silicato y Fe limitaron cerca de la costa (~100 km) desde enero hasta abril, con limitación predominante de silicato. Durante estos mismos meses, nitrato limitó fuera de la costa entre ~75°W a 80°W. Se observó además, que entre mayo y agosto, la extensión espacial en la limitación de silicato y luz incrementaron a través de la zona costera, sobreponiéndose a la limitación de nitrato durante la misma época. La limitación por Fe incrementó en primavera, especialmente durante noviembre, extendiéndose incluso fuera de la costa. Resultados similares fueron encontrados por Bonnet et al. (2008) en una

región del borde sureste del giro del Pacífico Sur localizada entre 34°S; 92°W. Estos autores encontraron que Fe controlaba la eficiencia fotosintética y la producción primaria de esta área. Ellos reportaron que la producción primaria podría estar limitada por Fe en los bordes del giro, mientras que en el centro del giro, predominó la limitación por nitrógeno.

La limitación de nutrientes ha sido reportada en algunos SBBO (Messie y Chávez, 2015). En el sistema de surgencia de Perú se ha propuesto encontrado que el hierro limita al fitoplancton en invierno (Hutchins et al., 2002; Bruland et al., 2005), mientras que silicato y nitrato serían limitantes durante verano (Echevin et al., 2008; Messié and Chávez, 2015). En el Sistema de la Corriente de California, se ha encontrado que el hierro ejerce un control fundamental sobre la disminución en la disponibilidad de nitrato y silicato (Hutchins et al., 1998). Quiñones et al. (2010) han reportado para algunas áreas del SCH, déficit de nitrógeno comparado con fósforo. Observaron que la relación $\Delta N/\Delta P$ presentó valores significativamente más bajos que los valores Redfield. Los resultados obtenidos mediante la simulación desarollada en esta tesis, son consistentes a los resultados reportados por Anabalón et al. (2016) los cuales están basados en observaciones de terreno en la misma zona de estudio. Ellos observaron un decrecimiento en silicato y un moderado incremento de nitrato producto principalmente de una disminución en la descarga de los ríos en la zona (Ríos Biobío e Itata) resultando en la reducción de razón Si/N. Un cambio en esta razón asociado a un aumento en la concentración de nitrato en la costa, sin incremento de silicato, influye directa y negativamente en el crecimiento de las diatomeas, dejando a las células limitadas por sílice.

Dado que silicato fue el principal nutriente potencialmente limitante en la simulación, los términos de transporte, fueron calculados para este nutriente. El modelo fue capaz de simular aquellas zonas con predominio de advección vertical, las cuales constituyen focos de surgencia importante, localizándose cerca de 30º-32ºS, 33º-34ºS, 35º-36ºS y 37º-38ºS. Algunas de estas zonas han sido destacadas previamente en la literatura local, por ejemplo: Punta Lengua de Vaca (30.24ºS), Curaumilla (33.1ºS), Punta Nugurne (35.9ºS) y Punta Lavapié (37.15ºS) (Figueroa and Moffat, 2000; Aiken et al., 2008; Strub et al., 1998). Punta Lavapie (37.15ºS) ha recibido especial atención ya que se ha calificado como el mayor centro de surgencia del SCH de Chile (Leth and Shaffer, 2001; Valle-Levinson et al., 2003; Leth and Middleton, 2004) y donde procesos de advección horizontal de remolinos ha sido reportada (Correa-Ramírez et al., 2012; Hormazábal et al., 2013).

Por otro lado, como se esperaba en este tipo de análisis para los términos de transporte y basado en la conservación de masa, la advección horizontal equilibró parcialmente a la advección vertical. Se observó que en verano mientras la surgencia, y por ende la advección vertical fueron altas, el decrecimiento de silicato a través de advección horizontal fue intenso. Por lo tanto, la región costera pierde nutrientes mediante procesos advectivos. Esta pérdida fue compensada por la mezcla vertical. Además, la actividad de remolinos en la zona costera, asociada a procesos de advección horizontal, se vincula a bajos niveles de producción biológica, ejerciendo efectos supresivos en sistemas de surgencia costera (Gruber et al., 2011).

A pesar que las simulaciones implementadas en el Capítulo 3, representaron adecuadamente el sistema, se observaron algunas limitaciones. Por un lado, si bien el ciclo anual de la clorofila modelado reprodujo los altos valores típicos de primavera-verano y bajos de otoño-invierno, las concentraciones reportadas, fueron notablemente más bajas que las observadas en la estación 18 y en SeaWIFS. Esto se debe en parte a la utilización de viento climatológico en el forzamiento de esta simulación, el cual como se ha mencionado previamente, no representa las frecuencias diarias y sinópticas que se han descrito como las principales componentes del estrés del viento a lo largo de la costa del centro-sur de Chile (Sobarzo et al., 2007, 2010). Diferencias estacionales, mensuales y sinópticas del estrés del viento favorable a surgencia, también fueron detectadas en esta Tesis, tal como se ha descrito en el capítulo1.

Por otra parte, las ondas atrapadas a la costa (Hormazábal et al., 2002) presentes en el SCH, pueden modular la producción primaria, tal como ha sido descrito previamente para el SCH frente Perú (Echevín et al., 2014). Estas fluctuaciones no estaban bien representadas en la simulación, ya que el forzamiento climatológico, suavizó la variabilidad de 60 días.

Entre los futuros desafíos para posteriores simulaciones, está la inclusión de la variabilidad diaria y sinóptica del viento y de los factores asociados a ondas atrapadas a la costa.

Finalmente, se acepta parcialmente la **Hipótesis 6,** la cual plantea que la advección vertical producto de la surgencia y la mezcla vertical generada principalmente por el viento se correlacionan positivamente con el ciclo anual de la clorofila en la zona centro-sur de Chile (30°-40°S; 70°-80°W), ya que si bien los términos de mezcla vertical y la capa de mezcla (MLD) se correlacionan fuertemente con la clorofila costera (rho=0.77;

$p<0.05$, mezcla vertical y $rho=0.83$, $p<0.05$, MLD), existe una baja correlación entre clorofila y la advección total ($rho=0.54$, $p>0.05$).

6.- CONCLUSIONES

1.- Los eventos favorables a surgencia entre los años 1988-2013 en la zona centro sur de Chile, han disminuido en intensidad y en duración, no así en el número de eventos, los cuales son cada vez más frecuentes, especialmente durante los meses de otoño-invierno.

2.- Los eventos favorables a hundimiento entre los años 1988-2013 en la zona centro sur de Chile han disminuido en intensidad, pero la duración y frecuencia mantuvieron valores relativamente constantes a lo largo de toda la serie, con 2 días de duración promedio anual y 3 eventos promedio anual.

3.- El porcentaje del número de eventos favorables a surgencia y favorables a hundimiento respecto al periodo total analizado es de 63% y 37%, respectivamente. Si bien, el porcentaje del número de eventos favorables a hundimiento no es despreciable, los eventos favorables a surgencia predominan en toda la serie.

4.- Respecto a la evolución temporal de los eventos favorables a surgencia entre 1988-2013 presentes en el ciclo diario, se observó que entre las 12:00 y 23:00 pm, la intensidad disminuyó notablemente, en comparación al rango entre las 00:00 y 11:00am.

5.- La velocidad y el transporte de la Corriente Subsuperficial Chile-Perú (PCUC), disminuyen hacia el polo con 0.8 Sv en 30ºS, 0.76 Sv en 33ºS, 0.76 Sv en 35ºS, 0.47 Sv en 36ºS y 0.26 Sv en 39ºS.

6.- En 33º y 39ºS se observó que la PCUC presentó máximos subsuperficiales sobre la plataforma entre 200 y 300 metros de profundidad. Estos máximos se asociaron a la Contracorriente Superficial Chile-Perú (PCCC) la cual se localizó entre 50-100 km fuera de la costa siendo particularmente intensa durante primavera y verano.

7.- El ancho promedio de la PCUC cambia hacia el sur del área de estudio, con ~50 km en 30ºS, ~100 km en 36ºS y ~30 km en 39ºS. La abrupta modificación del ancho en 36ºS puede ser resultado de alteraciones en la topografía, la presencia de una línea de costa irregular o remolinos intratermoclina.

8.- El núcleo de máxima velocidad de la PCUC se profundiza en su desplazamiento hacia el polo, detectándose a ~120 metros en 30ºS, a ~218 metros en 33ºS, a ~230 metros en 36ºS y a ~260 metros en 39ºS

9.- 20% y 14% de los flotadores lagrangianos promedio transportados por la PCUC desde 33º y 37ºS respectivamente, alcanzan la capa superficial (50 m) después de 6 meses de su liberación. La mayoría de los flotadores se desplazaron hacia el sur con la PCUC, encontrándose los porcentajes más altos en latitudes adyacentes a las zonas de liberación.

11.- Los resultados encontrados en esta tesis sugieren que cerca de la costa, el crecimiento del fitoplancton durante otoño e invierno podría estar limitado por luz principalmente y por silicato el resto del año.

12.- A través de esta tesis se sugiere que fuera de la costa la co-limitación de nutrientes podría ser principalmente por nitrato durante verano y otoño, y por hierro en invierno y primavera. Ocasionalmente hierro, nitrato y fosfato podrían ser limitantes dentro y alrededor de remolinos de mesoescala, revelando complejas estructuras.

13.- La caracterización de la estructura espacial y temporal de los flujos de silicato, reveló aquellas zonas con predominio de advección vertical positiva, las cuales constituyen áreas de surgencia importante, localizándose cerca de 30º-32ºS, 33º-34ºS, 35º-36ºS y 37º-38ºS. Algunas de estas zonas han sido destacadas previamente en la literatura local como focos de surgencia activa.

14.- Los intensos flujos verticales ejercidos por la surgencia costera, fueron totalmente compensados por los flujos horizontales, sobre todo en verano.

15.- La alta advección horizontal observada en esta simulación, podría estar relacionada con el transporte de nutrientes inducido por remolinos desde la región costera hasta el océano abierto durante el período de surgencia.

16.- La mezcla vertical fue importante durante todo el año, particularmente en verano desempeñando un rol clave en la reposición de nutrientes de la capa superficial, compensando los procesos de advección horizontal.

7.- REFERENCIAS

Aguirre, C., Pizarro, O., Strub, P. T., Garreaud, R. D. and J. Barth. 2012. Seasonal dynamics of the near-surface alongshore flow off central Chile. J. Geophys. Res., 117: 1-17.

Aguirre, C., Garreaud, R. D. and J. A. Ruttlant. 2014. Surface ocean response to synoptic-scale variability in wind stress and heat fluxes off south-central Chile. Dynamics of Atmosphere and Ocean, 65: 64-85.

Aiken, C., Castillo, M. and S. Navarrete. 2008. A simulation of the Chilean Coastal Current and associated topographic upwelling near Valparaíso, Chile. Cont. Shelf Res., 28, 2371–2381.

Aiken, C. M. 2017. A reanalysis of the Chilean ocean circulation: preliminary results for the region between 20ºS to 40ºS. Lat. Am. J. Aquat. Res., 45(1): 193-198. doi: 10.3856/vol45-issue1-fulltext-19.

Álvarez, I., de Castro, M., Prego, R., and M. Gómez-Gesteira. 2003. Hydrographic characterization of a winter-upwelling event in the Ria of Pontevedra (NW Spain). Estuar. Coast and Shelf Sciencie, 56: 869-876.

Álvarez, I., Ospina-Alvarez, N., Pazos, Y., de Castro, M., Bernardez, P., Campor, M. J., Gomez-Gesteira, J. L., Alvarez-Ossorio, M. T., Varela, M., Gómez-Gesteira, M. and R. Prego. 2009. A winter upwelling event in the Northern Galician Rias: frequency and oceanographic implications. Estuarine Coastal and Shelf Science, 82: 573–582. doi:10.1016/j.ecss.2009.02.023.

Albert, A., Echevin, V., Lévy, M. and O. Aumont. 2010. Impact of nearshore wind stress curl on coastal circulation and primary productivity in the Peru upwelling system. J. Geophys. Res., 115. 1-13.

Allen, J. S., Walstad, L. J. and P. A. Newberger. 1991. Dynamics of the coastal transition zone jet, 2, Nonlinear finite amplitude behavior. J. Geophys. Res., 96: 14995–15016.

Allen, J. S., Newberger, P. A., and J. Federiuk. 1995. Upwelling circulation on the Oregon continental shelf. Part 1: response to idealized forcing. J. Phys. Oceanogr., 25: 1843–1866.

Anabalón, V., Morales, C. E., Escribano, R. and M. A.Varas. 2007. The contribution of nano- and micro-planktonic assemblages in the surface layer (0-30 m) under different hydrographic conditions in the upwelling area off Concepción, central Chile. Progr. Oceanogr., 75: 396-414.

Anabalón, V., Morales, C. E., González, H. E., Menschel, E., Schneider, W., Hormazábal, S., Valencia, L. and R. Escribano. 2016. Micro-phytoplankton community structure in the coastal upwelling zone off Concepción (central Chile): Annual and inter-annual fluctuations in a highly dynamic environment. Progr. Oceanogr., 149 : 174-188.

Ancapichún, S. and J. Garcés-Vargas. 2015. Variability of the Southeast Pacific Subtropical Anticyclone and its impact on sea surface temperature off north- central Chile. Ciencias Marinas, 41 (1). http://dx.doi.org/10.7773/cm.v41i1.2338.

Andrade, I., Hormazábal, S., and V. Combes. 2012. Intrathermocline eddies at the Juan Fernández Archipelago, southeastern Pacific Ocean. Lat. Am. J. Aquat. Res., 42(4): 888-906.

Andrade, I., P. Sangrà, S. E. Hormazábal and M. A. Correa- Ramírez. 2014. Island mass effect in the Juan Fernández Archipelago (33°S), Southeastern Pacific. Deep-Sea Res. I, 84: 86-99.

Arcos, D. F. and N. Navarro. 1986. Análisis de un Índice de surgencia para la zona de Talcahuano Chile (Lat. 37◦S). Invest. Pesq. (Chile) 33 : 91–98.

Arcos, D., Nuñez, S., Castro, L., Navarro, N., 1987. Variabilidad vertical de clorofila en un área de surgencia frente a Chile Central. Investigacion Pesqueras (Chile) 34, 47–55.

Arcos, D. F., Nuñez, S. P. and A. Acuña. 1996. Variabilidad de pequeña escala en la zona nerítica del sistema de surgencia de Talcahuano (Chile Central): identificación y dinámica de áreas de retención larval. Gayana Oceanol. (Chile), 4: 21–58.

Aristegui, J., Barton, E. D., Alvarez-Salgado, X. A., Santos, A. M. P., Figueiras, F. G., Kifani, S., Hernandez-Leon, S., Mason, E., Machu, E. and H. Demarq. 2009. Sub-regional ecosystem variability in the Canary Current upwelling. Prog. Oceanogr., 83: 33–48. http://dx. doi.org/10.1016/j.pocean.2009.07.031.

Arntz, W. E. and E. Fahrbach. 1996. El Niño Experimento Climático de la Naturaleza. Fondo de Cultura Económica, Mexico, DF, 312.

Astudillo, O., Dewitte, B., Mallet, M., Frappart, F., Rutllant, J. A., Ramos, M., Bravo, L., Goubanova, K. and S. Illig. 2017. Surface winds off Peru-Chile: Observing closer to the coast from radar altimetry. Remote Sensing of Environment, 191: 179-196.

Aumont, O., Maier-Reimer, E., Blain, S. and P. Monfray. 2003. An ecosystem model of the global ocean including Fe, Si, P colimitations. Global Biogeochem. Cy., 17 (2), 1060.

Aumont, O. and L. Bopp. 2006. Globalizing results from ocean in situ iron fertilization studies. Global Biogeochem. Cy. 20, GB2017, doi.org/10.1029/ 2005GB002591.

Aumont, O., Ethé, C., Tagliabue, A., Bopp, L. and M. Gehlen. 2015. PISCES-v2: An ocean biogeochemical model for carbon and ecosystem studies. Geosci. Model Dev., 8: 2465–2513. doi:10.5194/gmd-8-2465-2015.

Austin, J.A. and S. Lentz. 2002: The inner shelf response towind- driven upwelling and downwelling. J. Phys.Oceanogr., 32: 2171– 2193.

Bakun, A. 1990. Global climate change and intensification of coastal upwelling. Science, 247: 198-201.

Bakun, A., and C. S. Nelson. 1991. The seasonal cycle of wind stress curl in sub-tropical eastern boundry current regions. J. Phys. Oceanogr., 21: 1815–1834.

Bakun, A., Field, D. B., Redondo-Rodríguez, A. and S. J. Weeks. 2010. Greenhouse gas, upwelling favorable winds, and the future of coastal ocean upwelling ecosystems. Global Change Biol., 16: 1213-1228.

Bakun, B., Black, B. A., Bograd, S. J., García-Reyes, M., Miller, A. J., Rykaczewski, R. R. and W. J. Sydeman. 2015. Anticipated effects of climate change on coastal upwelling ecosystems. Curr. Climate Change Report, 85–93.

Baird, M. E., Oke, P. R., Suthers, I. M. and J. H. Middleton. 2004. A plankton population model with bio-mechanical descriptions of biological processes in an idealised 2-D ocean basin, J. Mar. Syst., 50: 199–222.

Baird, M. E., Leth, O. and J. F. Middleton. 2007. Biological response to circulation driven by mean summertime winds off central Chile: A numerical model study. J. Geophys. Res. 112, C07031, doi:10.1029/2006JC003655.

Barber, R. T. and F. P.Chávez. 1983. Biological consequences of El Ninio. Science, 222: 1203– 1210.

Barber, R. T., and R. L. Smith. 1981. Coastal upwelling ecosystems. Pp. 31–68 in Analysis of Marine Ecosystems. A.R. Longhurst, ed., Academic Press, New York.

Barth, J. A., Pierce, S. D. and R. L. Smith. 2000. A separating coastal upwelling jet at Cape Blanco, Oregon and its connection to the California Current System. Deep Sea Res. Part II, 47: 783–810.

Barton, E. D., R. Torres, F. G. Figueiras, M. Gilcoto and J. L. Largier. 2016. Surface water subduction during a downwelling event in a semienclosed bay, J. Geophys. Res. Oceans, 121: 7088– 7107. doi:10.1002/2016JC011950.

Batten, M. L., Hu, C-P., Bacon, J. L. and C. S. Nelson. 1995. A Numerical Study of the Effects of Wind Forcing on the Chile Current System. J. Oceanog., 51: 585-614.

Becker, J. J., D.T. Sandwell, W. Smith, et al., 2009. Global Bathymetry and elevation data at 30 arc seconds resolution: SRTM30 PLUS. Marine Geodesy, 32:355-371.

Belmadani, A., Echevin, V., Dewitte, B. and F. Colas. 2012. Equatorially forced intraseasonal propagations along the Peru-Chile coast and their relation with the nearshore eddy activity in 1992–2000: A modeling study. J. Geophys. Res., 117: 1-20.

Belmadani, A., Echevin, V., Codron, F., Takahashi, K., and C. Junquas. 2014. What dynamics drive future wind scenarios for coastal upwelling off Peru and Chile?, Clim. Dyn., 43(7–8): 1893–1914.

Benazzouz, A., Mordane, S., Orbi, A., Chagdali, M., Hilmi, K., Atillah, A., Pelegrí, J. L. and H. Demarcq. 2014. An improved coastal upwelling index from sea surface temperature using satellite-based approach: the case of the Canary Current upwelling system. Continental Shelf Research, 81: 38–54.

Black, B. A., Schroeder, I. D., Sydeman, W. J., Bograd, S. J., Wells, B. K. and F. B. Schwing. 2011. Winter and summer upwelling modes and their relevance to climate impacts and ecological response in the California Current Ecosystem. Global Change Biology, 17: 2536–2545.

Blain, S., Bonnet, S. and C. Guieu. 2008. Dissolved iron distribution in the tropical and sub tropical South Eastern Pacific. Biogeoscience, 5: 269-280.

Blanco, J. L., Thomas, A. C., Carr, M. E. and P. T. Strub. 2001. Seasonal climatology of hydrographic conditions in the upwelling region off northern Chile. J. Geophys. Res., 106: 11451–11467.

Blanke, B., C. Roy, P. Penven, S. Speich, J. McWilliams and G. Nelson. 2002. Linking wind and interannual upwelling variability in a regional model of the southern Benguela, Geophys. Res. Lett., 29(24), 2188. doi:10.1029/2002GL015718.

Bonnet, S., Guieu, C., Bruyant, F., Prásil, O., Van Wanbeke, F., Raimbault, P., Moutin, T., Grob, C., Gorbunov, M. Y., Zehr, J. P., Masquelier, S. M., Garzarek, L. and H.

Claustre. 2008. Nutrient limitation of primary productivity in the Southeast Pacific (BIOSOPE cruise). Biogoscience, 5: 215-225.

Blumberg, A. F. and G. L. Mellor. 1987. A description of a three- dimensional coastal ocean circulation model, in Three-Dimensional Coastal Ocean Models, in: N. Heaps (Eds.), Coastal Estuarine Series. 4, AGU, Washington, D. C. pp. 1–16.

Bograd, S. J., Schroeder, I. D., Sarkar, N., Qiu, X. M., Sydeman, W.J. and F. B. Schwing. 2009. Phenology of coastal upwelling in the California Current. Geophysical Research Letters, 36, L01602.

Botsford, L. W., Lawrence, C. A., Dever, E. P., Hastings, A. and J. Largier. 2006. Effect of variable winds on biological productivity on continental shelves in coastal upwelling systems. Deep-Sea Research II, 53: 3116–3140.

Bottjer, D., and C. E. Morales. 2005. Microzooplankton grazing in a coastal embayment off Concepción, Chile, (~36°S) during non-upwelling conditions. Journal of Plankton Research (27) 4: 383, 391.

Brink, K. H. 1987. Upwelling fronts: implications and unknowns, South African Journal of Marine Science, 5:1, 3-9. DOI: 10.2989/025776187784522315.

Brochier, T., Echevin, V., Tam, J., Chaigneau, A., Goubanova, K. and A. Bertrand. 2013. Climate change scenarios experiments predict a future reduction in small pelagic fish recruitment in the Humboldt Current system. Glob. Chan. Biol., 19: 1841-1853.

Bruland, K. W., Rue, E. L. and G. J. Smith. 2001. Iron and macronutrients in California coastal upwelling regimes: implications for diatom blooms. Limnology and Oceanography, 46: 1661–1674. http://dx.doi.org/10.4319/lo.2001.46.7.1661.

Bruland, K. W., Rue, E. L., Smith, G. J. and G. R. DiTullio. 2005. Iron, macronutrients and diatom blooms in the Peru upwelling regime: brown and blue waters of Peru. Mar. Chem., 93: 81-103.

Bylhouwer, B., Ianson, D. and K. Kohfeld. 2013. Changes in the onset and intensity of wind-driven upwelling and downwelling along the North American Pacific coast, J. Geophys. Res. Oceans., 118: 2565–2580. doi:10.1002/jgrc.20194.

Cáceres, M. 1992. Vortices y filamentos observados en imagenes de satelite frente al area de surgencia de Talcahuano, Chile central, Invest. Pesq., 37: 55–66.

Capet, X. J., Marchesiello, P. and J. C. McWilliamns. 2004. Upwelling response to coastal wind profiles. Geophys. Res. Lett., 31: 1-4.

Carr, S., Capet, X., McWilliams, J. C., Pennington, J. T. and F. P.Chávez. 2008. The influence of diel vertical migration on zooplancton transport and recruitment in an up-welling region: estiamtes from a coupled behaviorial-physical model. Fish. Ocean., 17 : 1-15.

Casey, K. S., Brandon, T. B., Cornillon, P. and R. Evans. 2010. The past, present and future of the AVHRR Pathfinder SST program. In: Gower, J.F.R., Barale, V., Alberotanza, L. (Eds.), Oceanography from Space. Revisited. Springer, Netherlands.

Castillo, G., Muñoz, H., González, H. and P. Bernal. 1991. Daily analysis of abundance and size variability of fish larvae in relation to oceanic water intrusions in coastal areas. Biol. Pesq., 20: 21–35.

Castro, L. R., Quiñones, R., Arancibia, H., Figueroa, D., Roa, R., Sobrazo, M. and M. Retamal. 1997. Area de desove de la anchoveta y sardina común en la zona central. Final Research Report Project FIP 96-11. SubSecretaria de Pesca. Chile.

Castro L., Salinas, G. R. and E. Hernández. 2000. Environmental influences on winter spawning of the anchoveta Engraulis ringens off central Chile. Marine Ecology Progress Series, 197 : 247-258.

Castro-Gonzál̈éz, M. and L. Farías. 2004. N2O cycling at the core of the oxygen minimum zone off northern Chile. Marine Ecology Progress Series, 280: 1–11.

Castro-González, M., Braker, G., Farías, L. and O. Ulloa. 2005. Communities of *nirS*-type denitrifiers in the water column of the oxygen minimum zone in the eastern South Pacific. Environmental Microbiology, 7: 1298–1306. doi:10.1111/j.1462-2920.2005.00809.x.

Chaigneau, A., Dominguez, N., Eldin, G., Vasquez, L., Flores, R., Grados, C. and V. Echevin. 2013. Near-coastal circulation in the Northern Humboldt Current System from shipboard ADCP data. J. Geophys. Res. Oceans, 118: 1-16.

Chávez, F. P. and R. T. Barber. 1987. An estimate of new production in the equatorial Pacific. Deep-Sea Res, 34: 1229-1245.

Chávez, F. P. and J. R. Toggweiler. 1995. Physical estimates of global new production: The upwelling contribution, p. 313– 320. In C. P. Summerhayes et al. [eds.]. Upwelling in the ocean: modern processes and ancient records. Wiley.

Chávez, F. P., Ryan, J., Lluch-Cota, S. E. and M. Ñiquen. 2003. From Anchovies to Sardines and Back: Multidecadal Change in the Pacific Ocean. Science, 299 (5604): 217-221.

Chávez, F. P., Bertrand, A., Guevara-Carrasco, R., Soler, P. and J. Csirke. 2008. The northern Humboldt Current System: Brief history, present status and a view towards the future, Prog. Oceanogr., 79: 95–105.

Chelton, D., Schlax, M. and R. Samelson. 2011. Global observations of nonlinear mesoscale eddies, Progress in Oceanography, 91: 167-216.

Chia, F. S., Buckland-Nicks, J. and C. M. Young. 1984. Locomotion of marine invertebrate larvae: a review. Can. J. Zool., 62: 1205–1222.

Chin, E. 1970. Southeast Pacific expedition of the R.V. Anton Bruun, general account, station list, and hydrographic data. In: Anton Bruun reports. Scientific results of the Southeast Pacific expedition. EDWARD CHIN, (editor), Texas A & M University Marine Laboratory, pp. 1.3-1.86.

Churchill, J. H., Runge, J. and C. Chen, C. 2011. Processes controlling retention of spring-spawned Atlantic cod (Gadus morhua) in the western Gulf of Maine and their relationship to an index of recruitment success. Fisheries Oceanography, 20 (1): 32–46.

Claramunt, G., Cubillos, L. A., Castro, L., Hernández, C. and M. Arteaga. 2014. Variation in the spawning periods of Engraulis ringens and Strangomera bentincki off the coasts of Chile: A quantitative analysis. Fisheries Research, 160: 96–102. doi:http://dx.doi.org/10.1016/j.fishres.2013.09.010.

Clarke, A. J. 1989. Theoretical understanding of eastern ocean boundary poleward currents, , in: Neshyba, S. J., Mooers, Ch. N. K., Smith, R. L., Barber, R. T. (Eds.), Poleward Flows Along Eastern Ocean Boundaries. Springer-Verlag, New York Inc., pp. 26–39.

Clark, D. R., Widdicombe, C. E., Rees, A. P. and E. M. S. Woodward. 2016. The significance of nitrogen regeneration for new production within a filament of the Mauritanian upwelling system, Biogeosciences, 13: 2873-2888, https://doi.org/10.5194/bg-13-2873-2016.

Colas F., X. Capet, J. C. McWilliams, et al. 2008. 1997–1998 El Nino off Peru: A numerical study. Progress in Oceanography, 79:138–155. doi: http://dx.doi.org/10.1016/j. pocean.2008.10.015.

Colas, F., McWilliams, J. C., Capet, X. and J. Kurian. 2012. Heat balance and eddies in the Peru-Chile current system, Clim. Dyn., 39 (1-2): 509-529.

Cordeiro, A., Nolasco, R., Rocha, A., Ramos, A. M. and J. Dubert. 2016. Climate change in the Iberian Upwelling System: a numerical study using GCM downscaling. Climate Dynamics, 47: 451–464. doi: 10.1007/s00382-015-2848-y.

Cornejo, M., Farías, L. and M. Gallegos. 2007. Seasonal cycle of N2O vertical distribution and air sea fluxes over the continental shelf waters off central Chile (~36°S). Progress in Oceanography, 75: 383–395.

Cornejo, M. and L. Farías. 2012. Meridional variability of the vertical structure and air–sea fluxes of N_2O off central Chile (30–40ºS). Progress in Oceanography, 92(1): 33-42.

Cornejo D'Ottone, M., Bravo, L., Ramos, M., Pizarro, O., Karstensen, J., Gallegos, M., Correa-Ramirez, M., Silva, N., Farias, L. and L. Karp-Boss. 2016. Biogeochemical characteristics of a long-lived anticyclonic eddy in the eastern South Pacific Ocean, Biogeosciences, 13: 2971-2979. https://doi.org/10.5194/bg-13-2971-2016.

Correa-Ramirez, M. A., Hormazábal, S. and G. Yuras. 2007. Mesoscale eddies and high chlorophyll concentrations off central Chile (29–39°S). Geophysical Research Letters L12604. doi:10.1029/2007GL029541.

Correa-Ramírez, M. A., Hormazábal, S. and C. E. Morales. 2012. Spatial patterns of annual and interannual surface chlorophyll – a variability in the Peru-Chile Current System. Progress in Oceanography, 92-95C: 8–17.

Cropper, T. E., Hanna, E. and G. R. Bigg. 2014. Spatial and temporal seasonal trends in coastal upwelling off Northwest Africa, 1981–2012. Deep-Sea Res., 1: 94–111.

Cubillos, L., Canales, M., Hernández, A., Bucarey, D., Vilugrón, L. y L. Miranda. 1998. Poder de pesca, esfuerzo de pesca y cambios estacionales e interanuales en la abundancia relativa de *Strangomera bentincki* y *Engraulis ringens* en el área frente a Talcahuano, Chile (1990-1997). Investigaciones Marinas, Valparaíso, 26: 3-14.

Cubillos, L., Canales, M., Bucarey, D., Rojas, A y R. 1999. Época reproductiva y talla media de primera madurez sexual de *Strangomera bentincki* y *Engraulis ringens* en el período 1993-1997, zona centro-sur de Chile (1993-97). Investigaciones Marinas, Valparaíso 28, 73-85.

Cubillos, L. A., Ruiz, P., Claramunt, G., Gacitúa, S., Núñez, S., Castro, L. R., Riquelme, K., Alarcón, C., Oyarzún, C. and A. Sepúlveda. 2007. Spawning, daily egg production, and spawning stock biomass estimation for common sardine (*Strangomera bentincki*) and anchovy (*Engraulis ringens*) off central southern Chile in 2002. Fish. Res., 86: 228-240.

Cuevas, L. A., Daneri, G., Jacob, B. and P. Montero 2004. Microbial abundance and activity in the seasonal upwelling area off Concepción (~36ºS), central Chile: a comparison of upwelling and non-upwelling conditions. Deep-Sea Research II, 51: 2427–2440.

Cushman-Roisin, B., 1994. Introduction to Geophysical Fluid Dynamics. Prentice-Hall, Englewood Ciffs, NJ, 320pp.

Csanady, G. T. 1977. The coastal jet conceptual model in the dynamics of shallow seas, in The Sea, Vol. 6, Marine modelling, Goldberg, E. D., McCave, I. N., O'Brien, J. V., and Steele, J. H., Eds., Wiley, New York, 117.

Czeschel, R., Stramma, L., Schwarzkopf, F. U., Giese, B. S., Funk, A., and J. Karstensen. 2011. Middepth circulation of the eastern tropical South Pacific and its link to the oxygen minimum zone, J. Geophys. Res., 116, C01015, doi:10.1029/2010JC006565.

Daneri, G., Dellarossa, V., Quiñones, R., Jacob, B., Montero. P. and O. Ulloa. 2000. Primary production and community respiration in the Humboldt Current System off Chile and associated oceanic areas. Mar. Ecol. Prog. Ser., 197: 41-49.

Daneri, G., Lizárraga, L., Montero, P., González, H. E. and F. J. Tapia. 2012. Wind forcing and short-term variability of phytoplankton and heterotrophic bacterioplankton in the coastal zone of the Concepción upwelling system (Central Chile). Progr. Oceanogr., 92-95: 92-96.

da Silva, A.M., Young, C.C., Levitus, S. (Eds.)., 1994. Atlas of Surface Marine Data 1994, vol. 1. Algorithms and Procedures. NOAA Atlas NESDIS, vol. 6. Technical Report. U. S., NOAA, Silver, Spring, MD. pp. 83.

Dave, A. C. and M. S. Lozier. 2015. The impact of advection on stratification and chlorophyll variability in the equatorial Pacific, Geophys. Res. Lett., 42: 4523–4531. doi:10.1002/ 2015GL063290.

de Boyer Montégut, C.,. Mardec, G., Fischer, A. S., Lazar, A. and D. Iudicone. 2004. Mixed layer depth over the global ocean: An examination of profile data and a profile based climatology. J. Geophys. Res., 109, C12003, doi:101029/2004JC002378.

de Castro, M., Gómez-Gesteira, M., Alvarez, I., Cabanas, J. M. and R. Prego. 2008. Characterization of fall-winter upwelling recurrence along the Galician western coast (NW Spain) from 2000 to 2005: Dependence on atmospheric forcing. J. Marine Syst., 72: 145-158.

Demarcq, H. 2009. Trends in primary production, sea surface tempera- ture and wind in upwelling systems (1998–2007). Prog. Oceanogr., 83: 376–385, doi:10.1016/j.pocean.2009.07.022.

De Pol-Holz, R., Robinson, R.S., Hebbeln, D., Sigman, D.M. and O.Ulloa. 2009. Controls on sedimentary nitrogen isotopes along the Chile margin. Deep-Sea Research II, 56 (16): 1042-1054.

Diehl, S., Berger, S., Ptacnik, R. and A. Wild. 2002. Phytoplankton, light, and nutrients in a gradient of mixing depths: field experiments. Ecology, 83: 399–411.

Diffenbaugh, N. S., Snyder, M. A. and L. C. Sloan. 2004. Could CO2-induced land-cover feedbacks alter near-shore upwelling regimes?. PNAS, 101: 27-32.

Dugdale, R. C. 1985. The effects of varying nutrient concentration on biological production in upwelling regions. CalCOFI Report, 26: 93-96.

Dugdale, R. C., Wilkerson, F.P. and A. Morel. 1990. Realization of new production in coastal upwelling areas: a means to compare relative performance. Limnology and Oceanography, 35 (4): 822–829.

Dunn, J.R. and K. R. Ridgway. 2002. Mapping ocean properties in regions of complex topography. Deep Sea Res., 49 (3): 591–604.

Echevin, V., Colas, F., Chaigneau, A. and P. Penven. 2011. Sensitivity of the Northern Humboldt Current System nearshore modeled circulation to initial and boundary conditions. J. Geophys. Res., 116 (C07002): 1-16.

Echevin, V., Aumont, A., Ledesma, J. M. and G. Flores. 2008. The seasonal cycle of surface chlorophyll in the Peruvian upwelling System: A modeling Study. Progress in Oceanography, 79: 167-176.

Echevin, V., Albert, A., Lévy, A., Graco, M., Aumont, O., Piétri, A. and G. Garric. 2014. Intraseasonal variability of nearshore productivity in the Northern Humboldt Current System: The role of coastal trapped waves. Cont. Shelf Res., 73: 14-30.

Escribano, R. and W. Schneider. 2007. The structure and functioning of the coastal upwelling system off Central/Southern Chile, Prog. Oceanogr., 75: 343–347.

Escribano, E., Bustos-Ríos, E., Hidalgo, P. and C. E. Morales. 2016. Non-limiting food conditions for growth and production of the copepod community in a highly productive upwelling zone. Continental Shelf Research, 126: 1-14.

Espinoza-Morriberon, D., Echevin, V., Colas, F., Tam, J., Ledesma, J., Vásquez, L. and M. Graco. 2017., Impacts of El Nino events on the Peruvian upwelling system productivity, J. Geophys. Res. Oceans, 122. doi:10.1002/ 2016JC012439.

Ekman V.W. 1905. On the influence of the earth´s rotation in ocean currents, Arch. Math. Astron. Phys., 2: 1-52.

Falvey, M. and R. D., Garreaud. 2009. Regional cooling in a warming world: Recent temperature trends in the southeast Pacific and along the west coast of subtropical South America (1979–2006). J. Geophys. Res. 114. http://dx.doi.org/10.1029/2008jd010519.

Farías, L., Besoain, V. and S. García-Loyola. 2015. Presence of nitrous oxide hotspots in the coastal upwelling area off central Chile: an analysis of temporal variability based on ten years of a biogeochemical time series. Environ. Res. Lett. 10 044017, doi:10.1088/1748-9326/10/4/044017.

Farrell, T. M., Bracher, D. and J. Roughgarden. 1991. Cross-shelf transport causes recruitment to intertidal populations in central California. Limnol. Oceanogr., 36:279–288.

Fernández, C., and L. Farías. 2012. Assimilation and regeneration of inorganic nitrogen in a coastal upwelling system: ammonium and nitrate utilization. Mar. Ecol. Progr. Ser., 451: 1-14.

Figueroa, A. D. and C. Moffat. 2000. On the influence of topography in the induction of coastal upwelling along the Chilean coast. Geophysical Research Letters, 27: 3905–3908.

Figueiras, F. G., Jones, K. J., Mosquera, A. M., Alvarez-Salgado, X. A., Edwards, A. and N. MacDougall. 1994. Red tide assemblage formation in an estuarine upwelling ecosystem: Ria de Vigo. Journal of Plankton Research, 16(7): 857–878.

Fonseca, T. and M. Farías. 1987. Estudio del proceso de surgencia en la costa chilena utilizando percepción remota. Rev. Inves. Pesquera, 34: 33-46.

Fonseca, T., 1989. An overview of the Poleward Undercurrent and upwelling along the Chilean coast. In: Neshyba, S.J., Mooers, C.N.K., Smith, R.L., Barber, R.T. (Eds.), Polewards Flows Along the Eastern Ocean Boundaries. InSpring-Verlag, New York, pp. 203–228.

Foreman, M. G., Pal, G., B. and W. J. Merryfield. 2011. Trends in upwell- ing and downwelling winds along the British Columbia shelf, J. Geo- phys. Res. Oceans, 116, C10023, doi:10.1029/2011JC006995.

Fossing, H., Gallardo, V. A., Joergensen, B. B., Huttel, M., Nielsen, L. P., Schulz, H., Canfield, D. E., Foster, S., Glud, R. N., Gundersen, J. K., Kuver, J., Ramsing, N. B., Teske, A., Thamdrup, B. and O. Ulloa. 1995. Concentration and transport of nitrate by the mat-forming sulphur bacterium Thioploca. Nature, 374: 713–715.

Fuentes, M. E., Gutiérrez, M. H., Quiñones, R. A. and S. Pantoja. 2015. Effects of temperature and glucose concentration on the growth and respiration of fungal species

isolated from a highly productive coastal upwelling ecosystem. Fungal Ecol., 13: 135-149. doi.org/10.1016/j.funeco.2014.09.006.

Fuenzalida, R., Schneider, W., Garcés-Vargas, J. and L. Bravo. 2008. Satellite altimetry data reveal jet-like dynamics of the Humboldt Current. J. Geophys. Res., 113: 1-11.

Fuenzalida, R., Schneider, W., Garcés-Vargas, J., Bravo, L. and C. Lange. 2009. Vertical and horizontal extension of the oxygen minimum zone in the eastern South Pacific Ocean. Deep Sea Res. II, 56 (16): 992–1003.

Galán, A., Molina, V., Thamdrup, B., Woebken, D., Lavik, G., Kuypers, M. M. M. and O. Ulloa. 2009. Anammox bacteria and the anaerobic oxidation of mmoniumin the oxygen minimum zone off northern Chile.Deep-Sea Research II, 56 (16): 1021-1031.

Gan, J., Li, L., Wang, D. and X. Guo. 2009. Interaction of a river plume with coastal upwelling in the northeastern South China Sea. Cont. Shelf Res., 29: 728-740.

García-Reyes, M. and J. L. Largier. 2010. Observations of increased wind-driven coastal upwelling off central California. J. Geophys. Res., 115: C04011.doi:10.1029/2009JC005576.

García-Reyes, M., Largier, J. L. and W. J. Sydeman. 2014. Synoptic-scale upwelling indices and predictions of phyto- and zooplankton populations. Progr. Oceanogr., 120: 177-188.

García-Reyes, M., Lamont, T., Sydeman, W, J., Black, B. A., Rykaczewski, R. R., Thompson, S. A. and S. J. Bograd. 2017. A comparison of modes of upwelling-favorable wind variability in the Benguela and California current ecosystems. Journal of Marine System, article in press.

Garland, E. D., Zimmer, C.A. and S. J. Lentz. 2002. Larval distributions in inner-shelf waters: the roles of wind-driven cross-shelf currents and diel vertical migrations. Limnol. Oceanogr., 47: 803–817.

Garreaud, R. D., Rutllant, J. A. and H. Fuenzalida. 2002. Coastal lows along the subtropical West Coast of South America: mean structure and evolution. Monthly Weather Review, 130: 75–88.

Garreaud, R., and R. Muñoz. 2005. The low-level jet off the west coast of subtropical South America: Structure and variability. Mon. Wea. Rev., 133: 2246-2261.

Garreaud, R. and M. Falvey. 2008. The coastal winds off western sub- tropical South America in future climate scenarios, Int. J. Climatol., 29: 543–554. doi:10.1002/joc.1716.

Gay, P. S., Chereskin, T. K., 2009. Mean structure and seasonal variability of the poleward undercurrent off southern California. J. Geophs. Res. Oceans 114, 1–17.

Giacaman-Smith, J., Neira, S. and H. Arancibia. 2016. Community structure and trophic interactions in a coastal management and exploitation area for benthic resources in central Chile. Ocean & Coastal Management 119, 155-163. doi:10.1016/j.ocecoaman.2015.10.003

Gill, A.E., 1982. Atmosphere–Ocean Dynamics. Academic Press, New York p. 662.

Geider, R. J., MacIntyre, H. L. and T. M. Kana. 1997. Dynamic model of phytoplankton growth and acclimation: responses of the balanced growth rate and the chlorophyll-a: carbon ratio to light, nutrient-limitation and temperature, Mar. Ecol.-Prog. Ser., 148: 187–200.

Gómez, F., Montecinos, A., Hormazabal, S., Cubillos, L.A., Correa-Ramirez, M.A. and F. P. Chavez. 2012. Impact of spring upwelling variability off southern-central Chile on common sardine (Strangomera bentincki) recruitment. Fish. Oceanogr., 21:405–414. http://dx.doi.org/10.1111/j.1365-2419.2012.00632.x.

Gómez, F. A., Spitz, Y. H., Batchelder, H. P. and M. A. Correa-Ramirez 2017. Intraseasonal patterns in coastal plankton biomass off central Chile derived from satellite observations and a biochemical model. Journal of Marine Systems, 174: 108-118. https://doi.org/10.1016/j.jmarsys.2017.05.003.

González, H. E., Menschel, E., Aparicio, C. and C. Barria. 2007. Spatial and temporal variability of microplankton and detritus, and their export to the shelf sediments in the upwelling area off Concepción, Chile (~36°S), during 2002– 2005. Progress in Oceanography, 75: 435–451.

González, C. E., Escribano, R. and P. Hidalgo. 2015. Intra-seasonal variation of upwelling and its effects on copepod community structure off central/southern Chile (2002–2009). Hydrology, 758(1): 61-74.

Goubanova, K., Echevin, V., Dewitte, B., Codron, F., Takahashi, K., Terray, P. and M. Vrac. 2011. Statistical downscaling of sea-surface wind over the Peru–Chile upwelling region: diagnosing the impact of climate change from the IPSL-CM4 model. Clim. Dyn., 36(7–8):1365–1378. doi:10.1007/s00382-010-0824-0.

Gordon, Jr. D. C., Boudreau, P. R. Mann, K. H., Ong, J. E., Silvert, W. L., Smith, S. V., Wattayakorn. G., Wulff, F. and T. Yanagi. 1996. LOICZ (Land- Ocean Interactions in the Coastal Zone): Biogeochemical Modelling Guidelines. LOICZ Reports and Studies, 5:1-96.

Gutiérrez, M. H., Pantoja, S., Tejos, E. and R. A. Quiñones. 2011. The role of fungi in processing marine organic matter in the upwelling ecosystem off Chile. Marine Biology, 158: 205–219.

Gunther, E.R. 1936. Variations in behaviour of the Perú Coastal Current: with an historical introduction. The Geograph. J., 88: 37–61.

Grob, C., Quiñones, R. A. and D. Figueroa. 2003. Quantification of coast-ocean water transport through filaments and eddies with high chlorophyll-a content, in central-south Chile (35.5- 37.5°S). Gayana, 67: 55- 67.

Gruber, N., Lachkar, Z., Frenzel, H., Marchesiello, P., Munnich, M., McWilliams, J.C., Nagai, T. and G. K. Plattner. 2011. Eddy-induced reduction of biological production in eastern boundary current system. Nature Geoscience, 4: 787-792.

Hales, B., Takahashi, T. and L. Bandstra. 2005. Atmospheric CO2 uptake by a coastal upwelling system, Global Biogeochem. Cycles, 19, GB1009, doi:10.1029/2004GB002295.

Henson, S. A. and A. C. Thomas. 2007. Interannual variability in timing of bloom initiation in the California Current System, J. Geophys. Res., 112, C08007, doi:10.1029/2006JC003960.

Hernández, A., Cubillos, L. A. and R. A. Quiñones. 2011. Evaluación de la talla estructurada de los stocks de Ensis macha y Tagelus dombeii en el Golfo de Arauco, Chile. Revista de Biología Marina y Oceanografía, 46 (2): 157-176.

Hernández, K., Yannicelli, B., Montecinos, A., Ramos, M., González, H. E. and G. Daneri. 2012. Temporal variability of incidental solar radiation and modulating factors in a coastal upwelling area (36°S). Progress in Oceanography, 92(1): 18-32.

Hernández-Miranda, E., Quiñones, R. A., Aedo, G., Valenzuela, A., Mermoud, N., Román, C. and F. Yañez. 2010. A major fish stranding caused by a natural hypoxic event in a shallow bay of the eastern South Pacific. J. Fish Biol., 76: 1543-1564.

Hernández-Miranda, E., Veas, R., Labra, F. A., Salamanca, M. and R. A. Quiñones. 2012a. Response of the epibenthic macrofaunal community to a strong upwelling-driven hypoxic event in a shallow bay of the southern Humboldt Current System. Marine Environmental Research, 79: 16-28.

Hernández-Miranda, E., Quiñones, R. A., Aedo, G., Díaz-Cabrera, E. and J. Cisterna. 2012b. The impact of a strong natural hypoxic event on the toadfish Aphos porosus in Coliumo Bay, south-central Chile. Revista de biología marina y oceanografía, 47(3): 475-487. https://dx.doi.org/10.4067/S0718-19572012000300010.

Hernández-Miranda, E., Veas, R., Anabalón, V. and R. A. Quiñones. 2017. Short-term alteration of biotic and abiotic components of the pelagic system in a shallow bay produced by a strong natural hypoxia event. PLoS ONE, 12(7): e0179023. https://doi.org/10.1371/journal.pone.0179023.

Hickey, B.M., 1979. The California Current System-hypotheses and facts. Prog. Oceanogr., 4 (8): 191–279

Hill, A. E., Hickey, B. M., Shillington, F. A., Strub, P. T., Brink, K. H., Barton, E. D. and A. C. Thomas. 1998. Eastern ocean boundaries coastal segment (e), in: Robinson, A. R. Brink, H. K., (Eds.), The Sea, vol. 11, The Global Coastal Ocean: Regio- nal Studies and Syntheses. John Wiley, New York, pp. 29–67.

Hormazábal, S., Shaffer, G. and O. Pizarro. 2002. Tropical Pacific control of intraseasonal oscillations off Chile by way of oceanic and atmospheric pathways. Geophysical Research Letters 29(6).

Hormazábal, S., Shaffer, G. and O. Leth. 2004. Coastal transition zone off Chile, J. Geophys. Res., 109, C01021, doi:10.1029/2003JC001956.

Hormazábal, S., Shaffer, G., Silva, N. and E. Navarro. 2006. The Perú-Chile undercurrent and the oxigen minimum zone variability off central Chile. Gayana, 70 (1): 37-45. https://dx.doi.org/10.4067/S0717-65382006000300009.

Hormazábal, S., Combes, V., Morales, C. E., Correa-Ramírez, M. A., Di Lorenzo, E. and S. Nuñez. 2013. Intrathermocline eddies in the coastal transition zone off central Chile (31-41°S). J. Geophys. Res. Oceans., 118: 1-11.

Hutchins, D. A., DiTullio, G. R., Zhang, Y. and K. W. Bruland. 1998. An iron limitation mosaic in the California upwelling regime, Limnology and Oceanography, 43: 1037–1054.

Hutchins, D. A., Hare, C. E., Weaber, R. S., Zhang, Y., Fir,e, G. F., DiTullio, G. R., Alm, M. B., Riseman, S. F., Maucher, J. M., Geesey, M. D., Trick, C. G., Smith, G. J., Rue, E. L., Conn, J. and K. W. Bruland. 2002. Phytoplankton iron limitation in the Humboldt Current and Peru Upwelling. Limnology and Oceanography, 47 (4): 997-1011.

Huyer, A. 1983. Coastal upwelling in the California Current. Prog. Oceanogr., 12:259-284.

Huyer, A., Knoll, M., Paluszkiewicz, T. and R. L. Smith. 1991. The Peru Undercurrent: A study in variability. Deep-Sea Res., 38(suppl. 1): 5247–5271.

Huyer, A., Smith, R. L. and T. Paluszkiewicz. 1987. Coastal upwelling off Peru during normal and El Niño times, 1981-1984. J. Geophys. Res., 92(C13): 14297-14307.

Iles, A. C., Gouhier, T. K., Menge, B. A., Stewart, J. S., Haupt, A. J. and M. C. Lynch. 2011. Climate-driven trends and ecological implications of event-scale upwelling in the California Current System. Global Change Biol., 18(2): 783-796.

Ianson, D. and S. E. Allen. 2002. A two-dimensional nitrogen and carbon flux model in a coastal upwelling region, Global Biogeochem. Cycles, 16(1), 1011, doi:10.1029/2001GB001451.

Ianson, D.,. Feely, R. A., Sabine, C. L. and L. W. Juranek. 2009. Features of coastal upwelling regions that determine net air-sea CO2 flux, J. Oceanogr., 65: 677–687.

Iriarte, J. L. and H. E. González. 2004. Phytoplankton size structure during and after the 1997/1998 El Niño in a coastal upwelling area of the northern Humboldt Current System. Mar. Ecol. Prog. Ser., 269:83–90.

Iriarte, J. L., Vargas, C., Tapia, F. J., Bermúdez, R. and R. E. Urrutia. 2012. Primary production and plankton carbon biomass in a river-influenced upwelling area off Concepción, Chile. Progress in Oceanography, 92 (1): 97-109.

Jacob, B., Daneri, G., Quiñones, R. A. and M. Sobarzo. 2011. Community metabolism, phytoplankton size structure and heterotrophic prokaryote production in a highly productive upwelling zone off northern Chile. Marine Ecology Progress Series, 430: 23–34.

Johnson, D. R., Fonseca, T. and H. Seivers. 1980. Upwelling in the Humboldt Coastal Current near Valparaiso, Chile, J. Mar. Res., 38: 1–15.

Jury, M. R. 1985. Mesoscale variations in summer winds over the Cape Columbine – St Helena Bay region, South Africa. South African Journal of Marine Science, 3:77–88.

Kane, A., Moulin, C., Thiria, S., Bopp, L., Berrada, M., Tagliabue, A., Crépon, M., Aumont, O. and F. Badran. 2011. Improving the parameters of a global ocean biogeochemical model via variational assimilation of in situ data at five time series stations, J. Geophys. Res., 116, C06011, http://dx.doi.org/10.1029/ 2009JC006005.

Klein, P. and G. Lapeyre. 2009. The Oceanic Vertical Pump Induced by Mesoscale and Submesoscale Turbulence. Annu. Rev. Mar. Sci., 1: 351–75.

Koné, V., Aumont, O., Lévy, M. and L. Resplandy. 2009. Physical and biogeochemical controls of the phytoplankton seasonal cycle in the Indian Ocean: A modeling study, in Indian Ocean Biogeochemical Processes and Ecological Variability, Geophys. Monogr. Ser., vol. 185, edited by J. D. Wiggert et al., pp. 147–166, AGU, Washington, D. C.

Kuypers, M. M. M., Lavik, G., Woebken, D., Schmid, M., Fuchs, B. M., Amman, R., Jorgensen, B. B. and M. S. M. Jetten. 2005. Massive nitrogen loss from the Benguela upwelling system through anaerobic ammonium oxidation. PNAS, 108: 6478-6483.

Lachkar, Z. and N. Gruber. 2011. What controls biological production in coastal upwelling systems? Insights from a comparative modeling study. Biogeosciences, 8: 2961-2976.

Lamont, T., Barlow, R. G. and M. S. Kyewalyanga. 2014. Physical Drivers of Phytoplankton Production in the Southern Benguela Upwelling System. Deep Res Part 1-Oceanographic Res. Pap., 90: 1–16.

Landaeta, M. F. and L. R. Castro. 2012. Vertical distribution and gas bladder inflation/defla- tion in postlarval anchoveta Engraulis ringens during upwelling events. Journal of the Marine Biological Association of the United Kingdom, 93: 321–331. doi: 10.1017/ S0025315411001767.

Large, W. G., McWilliams, J. C. and S. C. Doney. 1994. Oceanic vertical mixing: a review and a model with a nonlocal boundary layer parameterization. Rev. Geophys., 32: 363–403.

Largier, J. L., B. Magnell, A. and C. D. Winant. 1993. Subtidal circulation over the northern California shelf, J. Geophys. Res., 98(C10): 18147–18179. doi:10.1029/93JC01074.

Lentz, S. J. 1992. The surface boundary layer in coastal upwelling regions. J. Phys. Oceanogr., 22: 1517–1539.

Lentz, S. 2004. The response of buoyant coastal plumes to upwelling-favorable winds. J. Phys.Oceanogr., 34: 2458–2469.

Leth, O. and G. Shaffer. 2001. A numerical study of the seasonal variability in the circulation off central Chile, J. Geophys. Res.,106 (C10): 229-248.

Leth, O. and J. F. Middleton. 2004. A mechanism for enhanced upwelling off central Chile: Eddy advection. J. Geophys. Res., 109: 1-17.

Leth, O., Shaffer, G. and O. Ulloa. 2004. Hydrography of the eastern South Pacific Ocean: results from the Sonne 102 cruise, May–June 1995. Deep Sea Res. II, 51: 2349–2369.

Leth, O. and J. F. Middleton, 2006. A numerical study of the upwelling circulation off central Chile: Effects of remote oceanic forcing, J. Geophys. Res., 111, C12003, doi:10.1029/2005JC003070.

Lett, C., Verley, P., Mullon, C., Parada, C., Brochier, T., Penven, P. and Blanke, B. 2008. A Lagrangian tool for modelling ichthyoplankton dynamics. Environmental Modelling & Software, 2:, 1210– 1214.

Levipán, H., Quiñones, R. and H. Urrutia. 2007. A time series of prokaryote secondary production in the oxygen minimum zone of the Humboldt Current system, off central Chile. Progress in Oceanography 75, 531–549.

Lukas, R. 1986. The termination of the Equatorial Undercurrent in the eastern Pacific, Prog. Oceanogr., 16: 63–90. doi:10.1016/0079-6611 (86)90007-8.

Mahadevan, A. 2014. Eddy effects on biogeochemistry, Nature, 506: 168–169, 2258.

McCreary, J. P. S.Y. Chao. 1985. Three-dimensional shelf circulation along an eastern ocean boundary. J. Mar. Res., 43 (1): 13–36.

Mann, K. H. and J. R. N. Lazier. 1991. Dynamics of marine ecosystems: Biological-physical interactions in the oceans. Blackwell Scientific.

Marchesiello P., McWilliams, J. C. and A. Shchepetkin. 2003. Equilibrium structure and dynamics of the California Current System. J. Phys. Oceanogr., 33: 753-783.

Marín, V, Rodriguez, L., Vallejos, L., Fuenteseca, J. and E. Oyarce. 1993. Efectos de la surgencia costera sobre la productividad primaria primaveral de Bahía Mejillones del Sur (Antofagasta, Chile). Revista Chilena de Historia Natural, 66: 479-491.

Mesias, J., Matano, P. and T. Strub. 2001. A numerical study of the upwelling circulation off central Chile. J. Geophys. Res., 106: 19611–19623.

Merryfield, W. J., Pal, B. and M. G. G. Foreman. 2009. Projected future changes in surface marine winds off the west coast of Canada, J. Geo- phys. Res., 114, C06008, doi:10.1029/2008JC005123.

Messié, M. and F. Chávez. 2015. Seasonal regulation of primary production in eastern boundary upwelling systems. Progr. Oceanogr., 134: 1-18.

Middleton, J. F. and O. K. Leth. 2004. Wind-forced setup of upwelling, geographical origins, and numerical models: The role of bottom drag, J. Geophys. Res., 109, C12019, doi:10.1029/2003JC002126.

Minas, H. J., Minas, M. and T. T. Packard. 1986. Productivity in upwelling areas deduced from hydrographic and chemical fields. Limnology and Oceanography, 31 (6): 1182–

1206.

Moffat, C. and S. Lentz. 2012. On the Response of a Buoyant Plume to Downwelling-Favorable Wind Stress. Journal of Geophysical Research, 42: 1083-1098.

Montecinos, A. and F. Gómez, F. 2010. ENSO modulation of upwelling season off southern-central Chile. Geophys. Res.Lett., 37:L02708.

Montero, P., Daneri, G., Cuevas, L. A., González, H. E., Jacob, B., Lizárraga, L. and E. Menschel. 2007. Productivity cycles in the coastal upwelling area off Concepción: the importance of diatoms and bacterioplankton in the organic carbon flux. Prog. Oceanogr., 75: 518–530.

Montecino, V., Astoreca, R., Alarcón, G., Retamal, L. and G. Pizarro. 2004. Bio-optical characteristics and primary productivity during upwelling and non-upwelling conditions in a highly productive coastal ecosystem off central Chile (36°S). Deep-sea Research Part I – Oceanographic Research Papers I, 51: 2413–2426.

Montes, I., Colas, F., Capet, X., Schneider, W., 2010. On the pathways of the equatorial subsurface currents in the eastern equatorial Pacific and their contributions to the Peru-Chile Undercurrent. J. Geophys. Res. 115, 1-16.

Morales, C. E., Gonzalez, H. E., Hormazabal, S. E., Yuras, G., Letelier, J. and L. R. Castro. 2007. The distribution of chlorophyll-a and dominant planktonic components in the coastal transition zone off Concepción, central Chile, during different oceanographic conditions. Progress in Oceanography, 75: 452–469.

Morales, C. E. and V. Anabalón. 2012. Phytoplankton biomass and microbial abundances during the spring upwelling season in the coastal area off Concepción, central- southern Chile: variability around a time series station. Prog. Oceanogr.. 92: 81– 91.

Morales, C. E., Hormazábal, S., Correa-Ramírez, M., Pizarro, O., Silva, N., Fernández, C., Anabalón, V. an M. L. Torreblanca. 2012. Mesoscale variability and nutrient–

phytoplankton distributions off central-southern Chile during the upwelling season: The influence of mesoscale eddies. Progr. Oceanogr., 104: 17-29.

Morales, C. E., Hormazábal, S., Andrade, I. and M. Correa-Ramírez. 2013. Time-Space Variability of Chlorophyll-a and Associated Physical Variables within the Region off Central-Southern Chile. Remote Sensing, 5: 5550-5571.

Moore, C. M., Mills, M. M., Arrigo, K. R., Berman-Frank, I., Bopp, L., Boyd, P. W., Galbraith, E. D., Geider, R. J., Guieu, C., Jaccard, S. L., Jickells, T. D., La Roche, J., Lenton, M., Mahowald, N. M., Marañón, E., Marinov, I., Moore, J. K., Nakatsuka, T., Oschlies, A., Saito, M. A., Thingstad, T. F., Tsuda, A. and O. Ulloa. 2013. Processes and patterns of oceanic nutrient limitation. Nature Geoscience, 6: 701–710.

Montecino, V., Strub, P. T., Tarazona, J., Chavez, F. P., Thomas, A. C. and T. Baumgartner. 2006. Bio-physical interactions off western South America. In: Robinson, A.R., Brink, K. H. (Eds.), The Sea, vol. 14A, The Global Coastal Ocean. Harvard Press Ltd., Cambridge, Mass, pp. 329–390.

Mujica, A. y O. Rojas 1980. Estudio de la reproducción, fecundidad y desove de la sardina común (Clupea strangomera bentincki) y la anchoveta (Engraulis ringens) de la zona de Talcahuano. En: Programa Perspectivas de desarrollo de las pesquerías nacionales. Subprograma Dinámica Poblacional de Sardina y Anchoveta, Zona de Talcahuano. Informe Técnico IFOP AP 80-3. CORFO.

Muñoz, R. and R. Garreaud. 2005. Dynamics of the low level jet off the west coast of subtropical South America, Mon. Weather Rev., 133: 3661–3677. doi:10.1175/MWR3074.1.

Narváez, D. A., Navarrete, S. A., Largier, J. and C. A. Vargas. 2006. Onshore advection of warm water, larval invertebrate settlement, and relaxation of upwelling off central Chile. Marine Ecology Progress Series, 309: 159–173.

Neira, S. and H. Arancibia. 2004. Trophic interactions and community structure in the upwelling system off central Chile (33–39°S), J. Exp. Mar. Biol. Ecol., 312: 349–366.

Neira, S., Moloney, C., Christensen, V., Cury, P., Shannon, L. H. Arancibia. 2014. Analysing changes in the southern Humboldt ecosystem for the period 1970–2004 by means of dynamic food web modelling. Ecological Modelling, 274: 41– 49.

Neira, S., Moloney, C., Shannon, L. J., Christensen, V., Arancibia, H. and A. Jarre. 2014. Assessing changes in the southern Humboldt in the 20th century using food web models. Ecological Modelling, 278: 52-66. doi:10.1016/j.ecolmodel.2014.01.003

Neshyba, S. J., Mooers, C. N. K., Smith, R. L., Barber, R. T. (Eds.), 1989, in: Poleward Flows Along Eastern Ocean Boundaries, Coastal and Estuarine Studies, vol. 34. Springer-Verlag New York, Inc., pp. 374.

Nicklisch, A., Shatwell, T. and J. Kohler. 2008. Analysis and modelling of the interactive effects of temperature and light on phytoplankton growth and relevance for the spring bloom. J. Plankton Res., 30 (1): 75-91.

Nixon, S. and A. Thomas. 2001. Research Note. On the size of the Peru upwelling ecosystem. Deep-Sea Res., I 48: 2521–2528.

Oerder, V., Colas, F., Echevin, V., Codron, F., Tam, J. and A. Belmadani. 2015. Peru-Chile upwelling dynamics under climate change. J. Geophys. Res., 120: 1152-1172.

Palter, J. B., Lozier, M. S. R. T. Barber. 2005. The effect of advection on the nutrient reservoir in the North Atlantic subtropical gyre. Nature, 437: 687-692.

Pantoja, S., Sepúlveda, J. H. E. González. 2004. Decomposition of sinking proteinaceous material during fall in oxygen minimum zone off northern Chile. Deep-Sea Res. I 51: 55-70.

Parada, C., Colas, F., Soto-mendoza, S. and L. Castro. 2012. Effects of seasonal variability in across- and alongshore transport of anchoveta (Engraulis ringens) larvae on model-based pre-recruitment indices off central Chile. Progress in Oceanography, 92-95C: 192-205.

Pauly, D. and V. Christensen. 1995. Primary production required to sustain global fisheries. Nature, 374: 255–257.

Pedlosky, J. 1974. Longshore currents, upwelling and bottom topography. J. Phys. Oceanogr., 4: 214–226.

Penven, P., Echevin, V., Pasapera, J., Colas, F. and J. Tam. 2005. Average circulation, seasonal cycle, and mesoscale dynamics of the Peru Current System: A modeling approach. J. Geophys. Res. 110: C10021, doi: 10.1029/2005JC002945.

Penven, P., Debreu, L., Marchesiello, P. and J. C. McWilliams. 2006. Evaluation and application of the ROMS 1-way embedding procedure to the central california upwelling system. Ocean Modelling, 12: 157–187.

Peterson, D. H., Perry, M. J., Bencala, K. E. and M. C. Talbot. 1987. Phytoplankton Productivity in Relation to Light Intensity: A Simple Equation. Estuar. Coast. Shelf Science, 24: 813-832.

Pfaff, M. C., Branch, G. M., Fisher, J. L., Hoffman, V., Ellis, A. G. and J L. Largier. 2015. Delivery of marine larvae to shore requires multiple sequential transport mechanisms. Ecology, 96(5): 1399–1410.

Pierce, S. D., Smith, R. L., Kosro, P. M., Barth, J. A. and C. D. Wilson. 2000. Continuity of the poleward undercurrent along the eastern boundary of the mid-latitude Pacific. Deep-Sea Res., 47: 811–829.

Pizarro, O., Shaffer, G., Dewitte, B. and M. Ramos. 2002. Dynamics of seasonal and interanual variability of the Peru–Chile undercurrent. Geophys. Res. Lett., 29 (12): 1-4.

Prego, R., Guzmán-Zuñiga, D., Varela, M., deCastro, M. and M. Gómez-Gesteira. 2007. Consequences of winter upwelling events on biogeochemical and phytoplankton patterns in a western Galician Ria (NW Iberian Peninsula). Estuarine Coastal Shelf Sci., 73: 409–422.

Quiñones, R. A., Hernández, A., Carrasco, P., Araya, I. y H. Muñoz.2009. Las pesquerías del sistema costero de la cuenca del río Itata. In: Parra, O., Castilla, J.C., Camaño, A., Quiñones, R., Romero, H. (Eds.), La Cuenca Hidrográfica del río Itata. Aportes Científicos para su Gestión Sustentable. Universidad de Concepción, Chile, pp. 193-211.

Quiñones, R. A., Levipán, H. and H. Urrutia. 2009. Spatial and temporal variability of planktonic archaeal abundance in the Humboldt Current System off Chile. Deep Sea Research II, 56: 1073–1082.

Quiñones, R. A., Gutiérrez, M. H., Daneri, G., Gutiérrez, D. A., González, H. E. and F. Chávez. 2010. Pelagic carbon fluxes in the Humboldt Current System. In: Liu KK, Atkinson L, Quiñones RA, Talaue-McManus L (eds) Carbon and nutrient fluxes in global continental margins: a global synthe- sis. Springer-Verlag, New York, NY, p 44–64.

Rain-Franco, A., Muñoz, C. and C. Fernández. 2014. Ammonium Production off Central Chile (36uS) by Photodegradation of Phytoplankton-Derived and Marine Dissolved Organic Matter. PLoS ONE 9(6): e100224. doi:10.1371/journal.pone.0100224.

Rahn, D. A. and R. Garreaud. 2010. Marine boundary layer over the subtropical southeast Pacific during VOCALS-REx – Part 2: Synoptic variability, Atmos. Chem. Phys., 10, 4507-4519, https://doi.org/10.5194/acp-10-4507-2010.

Rahn, D. A. and R. D. Garreaud. 2013. A synoptic climatology of the near-surface wind along the west coast of South America. Int. J. Climatol., 34 (3):780–792. http://dx.doi.org/10.1002/joc.3724.

Ramos, M., Pizarro, O., Bravo, L. and B. Dewitte. 2006. Seasonal variability of the permanent thermocline off northern Chile. Geophy. Res. Lett., 33: 1-6.

Renault, L., Dewitte, B., Falvey, M., Garreaud, R., Echevin, V. and F. Bonjean. 2009. Impact of atmospheric coastal jet off central Chile on sea surface temperature from satellite observations (2000–2007), J. Geophys. Res, 114, C08006, doi:10.1029/2008JC005083.

Renault, L., Hall, A. and J. C. McWilliams. 2016. Orographic shaping of US West Coast wind profiles during the upwelling season. Climate Dynamics, 46:273–289. DOI 10.1007/s00382-015-2583-4.

Ribeiro, A. C., Peliz, Á and A. M. P. Santos. 2005. A study of the response of the chlorophyll-a biomass to a winter upwelling event off western Iberia using SeaWiFS and in situ data. Journal of Marine Systems, 53: 87–107.

Ridway, K. R., Dunn, J. R. and J. L. Wilkin. 2002. Ocean interpolation by four-dimensional least squares—applications to the waters around Australia. J. Atmos. Ocean. Technol., 19 (9): 1357–1375.

Riquelme-Bugueño, R., Silva-Aburto, J., Escribano, E., Peterson, W. T. and W. Schneider. 2016. Growth of the Humboldt Current krill in the upwelling zone off central Chile. Journal of Marine Systems, 163: 1–11.

Risien, C.M. and D. B. Chelton. 2008. A global climatology of surface wind stress field from eight years of QuiKSCAT Scatterometer Data. J. Phys. Oceanogr,. 38: 2379–2413.

Rodriguez, J. M., Cabrero, A., Gago, J., Guevara-Fletcher, C., Herrero, M., Hernández de Rojas, A., García, A., Laíz-carrión, R., Vergara, A. R., Álvarez, P., Piñero, C. and F. Saborido-Rey. 2015. Vertical distribution and migration of fish larvae in theNW Iberian upwelling system during the winter mixing period: implications for cross-shelf distribution. Fisheries Oceanography, 24 (3): 274–290.

Rutllant, J. and V. Montecino. 2002. Multiscale upwelling forcing cycles and biological response off north-central Chile. Revista chilena de historia natural, 75 (1): 217-231. http://dx.doi.org/10.4067/S0716-078X2002000100020.

Rykaczewski, R. R., Dunne, J. P., Sydeman, W. J., García-Reyes, M., Black, B. A. and S. J. Bograd. 2015. Poleward displacement of coastal upwelling-favorable winds in the ocean's eastern boundary currents through the 21st century, Geophys. Res. Lett., 42: 6424–6431, doi:10.1002/2015GL064694.

Saavedra, N. 1980. La presión y la dirección del viento en Concepción. Tralka, 1, 153–162.

Saavedra, N. and A. Foppiano. 1992. Monthly mean pressure model for Chile. International Journal of Climatology, 12: 469-480.

Saito, M. A., Goepfert, T. J. and J. T. Ritt,. 2008. Some thoughts on the concept of colimitation: Three definitions and the importance of bioavailability. Limnol. Oceanogr., 53(1): 276–290.

Salamanca, M. y S. Pantoja, S. 2009. Caracterización química de la zona marina adyacente a la desembocadura del río Itata. La Cuenca del Río Itata: La cuenca hidrográfica del Itata: Aportes científicos para su gestión sustentable, pp. 177-191. Ed. por O. Parra, J.C. Castilla, H. R. A. Quiñones y A. Camaño. Ediciones Universidad de Concepción, Concepción, Chile. 389 pp.

Saldías, G., Sobarzo, M., Largier, J., Moffat, C. and R. Letelier. 2012. Seasonal variability of turbid river plumes off central Chile base on high-resolution MODIS imagery, Cont. Shelf Res., 123: 220-233. doi: 10.1016/j.rse.2012.03.010.

Saldívar-Lucio, R., Di Lorenzo, E., Nakamura, M., Villalobos, H., Lluch-Cota, D. and P. Del Monte-Luna. 2016. Macro-Scale Patterns in Upwelling/ Downwelling Activity at North American West Coast. PLoS ONE 11(11): e0166962. doi:10.1371/ journal.pone.0166962.

Sánchez, G. E., Lange, C. B., González, H. E., Vargas, G., Muñoz, P., Cisternas, C. and S. Pantoja. 2012. Siliceous microorganisms in the upwelling center off Concepción, Chile (36S): preservation in surface sediments and downcore fluctuations during the past ?150 years. Prog. Oceanogr., 92–95: 50–65.

Santos, A. M. P., Peliz, A., Dubert, J., Oliveira, P. B., Angelico, M. M. and P. Re. 2004. Impact of a winter upwelling event on the distribution and transport of sardine (Sardina pilchardus) eggs and larvae off western Iberia: a retention mechanism. Continental Shelf Research, 24 (14): 149–165.

Schneider, W., Donoso, D., Garcés-Vargas, J. and R. Escribano. 2017. Water-column cooling and sea surface salinity increase in the upwelling region off central-south Chile driven by a poleward displacement of the South Pacific High. Progress in Oceanography, 151: 38-48.

Schroeder, I. D., Snydeman, W. J., Sarkar, N., Thompson, S. A., Bograd, S. J. and F. B. Schwing. 2009. Winter pre-conditioning of seabird phenology in the California current, Mar. Ecol. Prog. Ser., 393: 211–223.

Shaffer, G., Hormazábal, S., Pizarro, O., Djurfeldt, L. and S. Salinas.1999. Seasonal and interannual variability of currents and temperature over the slope off central Chile. J. Geophys. Res., 104: 951–961.

Shaffer, G., Pizarro, O., Djurfeldt, L., Salinas, S. and J. Rutllant. 1997. Circulation and low-frequency variability near the Chile coast: remotely forced fluctuations during the 1991–1992 El Niño. J. Phys. Oceanogr., 27: 217–235.

Shaffer, G., Hormazábal, S., Pizarro, O. and M. Ramos. 2004. Circulation and variability in the Chile Basin. Deep Sea Res. I, 51: 1367– 1386.

Shanks, A. L., Largier, J., Brink, L., Brubaker, J. and R. Hooff. 2002. Observations on the distribution of meroplankton during a downwelling event and associated intrusion of the Chesa- peake Bay estuarine plume. J. Plankton Res., 24:391–416.

Shanks, A. L. and L. Brink. 2005. Upwelling, downwelling, and cross-shelf transport of bivalve larvae: test of a hypothesis. Mar. Ecol. Prog. Ser., 302: 1−12.

Shanks, A. L. and R. K. Shearman. 2009. Paradigm lost? Cross-shelf distributions of intertidal invertebrate larvae are unaf- fected by upwelling or downwelling. Mar. Ecol. Prog. Ser., 385: 189−204.

Shchepetkin, A. F. and J. C. McWilliams. 2003. A method for computing horizontal pressure-gradient force in an ocean model with a nonaligned vertical coordinate, J. Geophys. Res., 108(C3), 3090, doi:10.1029/ 2001JC001047.

Shchepetkin, A. F. and J. C. McWilliams. 2005. The regional ocean modeling system: a split-explicit, free-surface, topography following coordinates ocean model. Ocean Model., 9: 347-404.

Siegel, D. A., Peterson, P., McGillicuddy, D. J., Maritorena, Jr. S. and N. B. Nelson. 2011. Bio-optical footprints created by mesoscale eddies in the Sargasso Sea, Geophys. Res. Lett., 38, L13608, doi:10.1029/2011GL047660.

Sievers C. H. A. and N. Silva. 1975. Masas de agua y circulaci6n en el Ocb, ano Pacifico Sudoriental. Latitudes 18°S-33°S (Operacibn Oceanográfica MARCHILE VIII). Ciencia y Tecnologia del Mar. Contribuci6n CONA N°i, 7-67.

Silva, N. 1977. Water mass structure and circulation off southern Chile. Master Thesis, School of Oceanography, Oregon State University, USA, 83pp.

Silva, N., Rojas, N. and A. Fedele.2009. Water masses in the Humboldt Current System: Properties, distribution, and the nitrate deficit as a chemical water mass tracer for equatorial subsurface water off Chile. Deep-Sea Res. II, 56: 1004–1020.

Silva, N. and S. Neshyba. 1977. Corrientes superficiales frente a la costa austral de Chile. Ciencia y Tecnología del Mar, 3: 37–42.

Silva, N. and S. Neshyba. 1979. On the southernmost extension of the Perú-Chile Undercurrent. Deep Sea Res., 26: 1387–1393.

Silva, N. and D. Konow. 1975. Contribución al conocimiento de las masas de agua en el Pacífico Sudoriental. Expedición Krill. Crucero 3-4. Julio-agosto 1974. Rev. Com. Perm. Pacífico Sur, 3: 63- 75.

Silva, S. and T. Fonseca. 1983. Geostrophic component of the northem flow off northern Chile, in: Arana, P. (Ed.), Conferencia Internacional Sobre Recursos Marinos del Pacifico, pp. 59-70.

Smith, R. L., 1981. A comparison of the structure and variability of the flow field in three coastal upwelling regions: Oregon, Northwest Africa and Peru. In: Richards, F.A. (Ed.), Coastal Upwelling. American Geophysical Union, Washington, D.C, pp. 107–118.

Smith, R. L. 1994. The physical processes of coastal ocean upwelling sys- tems, in Upwelling in the Ocean, edited by C. P. Summerhayes et al., pp. 39–64, John Wiley, New York.

Sordo, I., Barton, E.D., Cotos, J. M. and Y. Pazos. 2001. An inshore poleward current in the NWof the Iberian Peninsula detected from satellite images, and its relation with G. catenatum and D. acuminata blooms in the Galician Rias. Est. Coast. Shelf Sci., 53: 787–799.

Sobarzo, M., Figueroa, M. and L. Djurfeldt. 2001. Upwelling of surface water into the rim of the Biobı´o submarine canyon as a response to surface winds, Cont. Shelf Res., 21: 279–299. doi:10.1016/S0278- 4343(00)00082-0.

Sobarzo, M. and L. Djurfeldt. 2004. Coastal upwelling process on a continental shelf limited by submarine canyons, Concepción, central Chile. Journal of Geophysical Research, 109.doi:10.1029/2004JC002350.

Sobarzo, M., Bravo, L., Donoso, D., Garcés-Vargas, J. and W. Schneider. 2007a. Coastal upwelling and seasonal cycles that influences the water column over the continental shelf of central Chile. Progr. Oceanogr., 75: 363-382.

Sobarzo, M., Shearman, R. K. and S. Lentz. 2007b. Near-inertial motions over the continental shelf off Concepción, central Chile. Progress in Oceanography, 75: 348–362.

Sobarzo, M., Bravo, L. and C. Moffat. 2010. Diurnal-period, wind-forced ocean variability on inner shelf of Concepción, Chile. Cont. Shelf Res., 30: 2043-2056.

Sobarzo, M., Saldías, G. S., Tapia, F. J., Bravo, L. Moffat, C. and J. L. Largier. 2016. On subsurface cooling associated with the Biobio River Canyon (Chile), J. Geophys. Res. Oceans, 121: 4568–4584, doi:10.1002/2016JC011796.

Soto-Mendoza, S., Parada, C., Castro, L., Colas, F. and W. Schneider. 2012. Modeling transport and survival of anchoveta eggs and yolk-sac larvae in the coastal zone off central-southern Chile: assessing spatial and temporal spawning parameters. Progress in Oceanography, 92-95C: 178–191.

Soto-Mendoza, S., Hernández, F., Pérez-Santos, I., Parada, C., Castro, L. and I. Montes. 2017. Connectivity of early life stages of anchovy (*Engraulis ringens*) in the inland sea of Chiloé, Northern Patagonia (41° - 46° S): a biophysical modelling approach. Marine Ecology Progress Series, Theme Section: Small Pelagic Fish. Artículo enviado.

Strub, P. T., Kosro, P. M. and A. Huyer. 1991. The nature of the cold filaments in the California Current System. Journal of Geophysical Research, 96 (C8): 14743– 14768.

Strub, P. T., Mesias, M. and C. James. 1995. Altimeter observations of the Perú-Chile Countercurrent. Geophys. Res. Lett., 22: 211–214.

Strub, P. T., Mesías, J., Montecino, V., Ruttlant, J. and S. Salinas. 1998. Coastal ocean circulation off western South America. Coastal Segment (6,E), in: Robinson, A., Brink, K. (Eds), The Sea, Vol. 11. John Wiley & Sons, Hoboken, pp. 273-313

Strub, P. T. and C. James. 2000. Altimeter-derived variability of surface velocities in the California Current System: 2. Seasonal circulation and eddy statistics. Deep-Sea Research Part II, 47: 831–870. http://dx.doi.org/10.1016/S0967- 0645(99)00129-0.

Strub, P. T., Combres, V., Shillington, F. A. and O. Pizarro. 2013. Currents and Processes along the Eastern Boundaries. Ocean Circulation and Climate 2nd Edition. Edited by Dr. Gerold Siedler, Dr. John Church, Dr. W. John Gould and Dr. Stephen M. Griffies. Academic Press. ISBN: 978-0-12-391851-2.

Sverdrup, H. U. 1947. Wind-driven currents in a baroclinic ocean with application to the equatorial currents of the eastern Pacific. Proc. Natl. Acad. Sci. U.S.A. 33, 318-326.

Sydeman, W. J., García-Reyes, M., Schoeman, D. S., Rykaczewski, R. R., Thompson, S. A., Black, B. A. and S. J. Bograd. 2014. Climate change and wind intensification in coastal upwelling ecosystems. Science, 345 (6192): 77-80.

Tapia, F. J., Navarrete, S. A., Castillo, M., Menge, B. A., Castilla, J. A., Largier, J., Wieters, E. A., Broitman, B. L., Barth, J. A. 2009. Thermal indices of upwelling effects on inner- shelf habitats. Prog. Oceanogr., 83: 278−287.

Tegen, I., and I. Fung. 1995. Contribution to the atmospheric mineral aerosol load from land surface modification. J. Geophys. Res., 100 (D9): 18707–18726. doi:10.1029/95JD02051.

Thomas, M.K., Kremer, C.T., Klausmeier, C.A., Litchamn, E. 2012. A Global Pattern of Thermal Adaptation in Marine Phytoplankton. Science 338 (6110), 1085-1088, doi: 10.1126/science.1224836.

Tomczak M, Godfrey J. S. 2003. Regional Oceanography: An Introduction. 2nd ed. Daya Publishing House, Delhi, 390 pp.

Thomson, R. E. and M. V. Krassovski. 2010. Poleward reach of the poleward undercurrent extension. J. Geophys. Res., 115: 1-9.

Tortell, P. D., Merzouk, A., Ianson, D., Pawlowicz, R. and D. Yelland. 2012. Influence of regional climate forcing on surface water pCO2, ?O2/Ar and dimethylsulfide (DMS) along the southern British Colum- bia coast, Continent. Shelf Res., 47: 119–132. doi:10.1016/ j.csr.2012.07.007.

Troncoso, V. A., Daneri, G., Cuevas, L. A., Jacob, B. and P. Montero. 2003. Bacterial carbon flow in the Humboldt Current System off Chile. Marine Ecology Progress Series, 250: 1–12.

Ulloa, O., R. Escribano, S. Hormazabal, R. Quiñones, R. González, and M. Ramos. 2001. Evolution and biological effects of the 1997–98 El Niño in the upwelling ecosystem off northern Chile, Geophys. Res. Lett., 28: 1591–1594.

Ulloa, O. S. Pantoja. 2009. The oxygen minimum zone of the eastern South Pacific. Deep Sea Res., II 56(16): 987-991.

Valle-Levinson, A., Atkinson, L. P., Figueroa, D. and L. Castro. 2003. Flow induced by upwelling winds in an equatorward facing bay: Gulf of Arauco, Chile. J. Geophy. Res. 108, 3054, doi: 10.1029/2001JC001272, C2.

Varela, M., Álvarez-Ossorio, M. T., Bode, A., Prego, R., Bernárdez, P. and C. García-Soto. 2010. The effects of a winter upwelling on biogeochemical and planktonic components in an area close to the Galician Upwelling Core: The Sound of Corcubión (NW Spain). J. Sea Res., 64: 260-272.

Varela, R., Álvarez, I., Santos, F., deCastro, M. and M. Gómez-Gesteira. 2015. Has upwelling strengthened along worldwide coasts over 1982–2010? Sci Rep., 5: 1–15.

Vargas, C. A., Martínez, R., Cuevas, L. A., Pavez, M., Cartes, C., González, H., Escribano, R. and Daneri, G. 2007. The relative importance of microbial and classical food webs in a highly productive coastal upwelling area. Limnology and Oceanography, 52: 1495–1510.

Vargas, C., Contreras, P. Y. and J. L. Iriarte. 2012. Relative importance of phototrophic, heterotrophic, and mixotrophic nanoflagellates in the microbial food web of a river-influenced coastal upwelling area. Aquat. Microb. Ecol., 65: 233–248.

Vergara, O. A., Echevín, V., Sepúlveda, H. H. and F. Colas. 2016. Modelling the seasonal dynamics of the Peru-Chile Undercurrent off Central Chile (30–40°S). Cont Shelf. Res., 123: 61-79.

Vidal, T., Calado, A. J., Moita, M. T. and M. R. Cunha. 2017. Phytoplankton dynamics in relation to seasonal variability and upwelling and relaxation patterns at the mouth of Ria de Aveiro (West Iberian Margin) over a four-year period. PLoS ONE 12(5):1-25. e0177237. https://doi.org/10.1371/journal. pone.0177237.

Wang, D., Gouhier, T. C., Menge, B. A. and A. R. Ganguly. 2015. Intensification and spatial homogenization of coastal upwelling under climate change. Nature, 518: 390–394.

Warren, B.A., 1990. Book review of Poleward flows along eastern ocean boundaries. Limnology and Oceanography, 35: 1219-1220.

Whitney, M. M. and R. W. Garvine. 2005. Wind influence on a coastal buoyant outflow, J. Geophys. Res., 110, C03014, doi:10.1029/2003JC002261.

Williams, R. G., Roussenov, V. and M. J. Follows. 2006. Nutrient streams and their induction into the mixed layer, Global Biogeochem. Cycles, 20, GB1016, doi:10.1029/2005GB002586.

Winant, C. D. 1980. Downwelling over the southern California shelf, J. Phys. Oceanogr., 10: 791–799.

Wooster, W. S. and J. L. Reid. 1963. Eastern boundary currents, in: Hill, M. (Ed.), The sea, Vol. 2, Wiley Interscience, New York, pp. 253–280.

Wooster, W.S. and M. Gilmartin. 1961. The Peru-Chile Undercurrent. J. Mar. Res., 19 (3): 97-122.

Wu, J. 1982. Wind-stress coefficients over sea surface from breeze to huricane. J. Geophys. Res., 82: 9704-9706.

Yoshida K, Mao HL (1957) A theory of upwelling of large horizontal extent. JMar Res 16:40–54.

Yannicelli, B., Letelier, J., González, J., Orensanz, L. and A. Parma. 2008. Mega scale patterns of ‘loco’ catches along the Chilean coast: from coastal oceanography to improved scientific advice for management. Eastern boundary upwelling ecosystems: integrative and comparative approaches. Las Palmas, España, Junio 2008.

Yannicelli, B., Castro, L., Parada, C., Colas, F., Schneider, W. and D. Donoso. 2012. Distribution of Pleuroncodes monodon larvae over the continental shelf of south-central Chile: field and modeling evidence for partial local retention and transport. Progress in Oceanography, 92-95C: 206–227.

Zar, J. H. 1999. Biostatistical Analysis. Fourth Edition. Prentice Hall: New Jersey, 663 pp.